

SYNTHESIS OF LIGHT-SELECTIVE POLY(ETHYLENE-CO-VINYL ACETATE)  
NANOFILMS IN SUPERCRITICAL CARBON DIOXIDE

(Spine Title: Synthesis of Light-Selective Nanofilms in Supercritical CO<sub>2</sub>)

(Thesis format: Monograph)

by

William (Zhiming) Xu

Graduate Program in Engineering Science  
Department of Chemical and Biochemical Engineering

A thesis submitted in partial fulfillment  
of the requirements for the degree of  
Doctor of Philosophy

The School of Graduate and Postdoctoral Studies  
The University of Western Ontario  
London, Ontario, Canada

© William (Zhiming) Xu 2008

THE UNIVERSITY OF WESTERN ONTARIO  
SCHOOL OF GRADUATE AND POSTDOCTORAL STUDIES

**CERTIFICATE OF EXAMINATION**

Supervisor

\_\_\_\_\_  
Dr. Paul A. Charpentier

Supervisory Committee

\_\_\_\_\_  
Dr. Ajay K. Ray

\_\_\_\_\_  
Dr. Amin S. Rizkalla

Examiners

\_\_\_\_\_  
Dr. Leonardo Simon

\_\_\_\_\_  
Dr. Zhifeng Ding

\_\_\_\_\_  
Dr. Ajay K. Ray

\_\_\_\_\_  
Dr. Don Hewson

The thesis by

**William (Zhiming) Xu**

entitled:

**Synthesis of Light-Selective Poly(Ethylene-co-Vinyl Acetate)  
Nanofilms in Supercritical Carbon Dioxide**

is accepted in partial fulfillment of the  
requirements for the degree of  
Doctor of Philosophy

Date \_\_\_\_\_

\_\_\_\_\_  
Chair of the Thesis Examination Board

## Abstract and Key Words

Due to the increased requirements of environmental protection, significant effort has been made to develop new “green” chemistry and engineering methods. Two effective approaches for “green” processes are: (1) to employ routes with fewer synthetic and separation steps, and (2) to replace volatile organic solvents with environmentally friendly solvents.

Supercritical carbon dioxide (scCO<sub>2</sub>) has emerged as such a viable “green” alternative to organic solvents for several applications including extraction, polymerization, and nanotechnology, etc. In addition, it is an enabling solvent, allowing new types of chemistry and materials to be formed. In order to effectively utilize scCO<sub>2</sub>, it is required to study its effect on the relevant chemical process. This thesis focuses on the copolymerization of ethylene and vinyl acetate in scCO<sub>2</sub>, and the application of scCO<sub>2</sub> in the synthesis of novel poly(vinyl acetate) (PVAc) and poly(ethylene-co-vinyl acetate) (PEVA) nanocomposites.

Firstly, the kinetics of the process was investigated. The thermal decomposition of the free-radical initiator diethyl peroxydicarbonate (DEPDC) was monitored by *in situ* attenuate total reflection Fourier transform infrared spectroscopy (ATR-FTIR) in heptane, and in scCO<sub>2</sub>. The rate constant and activation energy of the thermal decomposition of DEPDC in scCO<sub>2</sub> were determined, and a decomposition mechanism was proposed. Further, with a knowledge of the initiator kinetics, *in situ* ATR-FTIR was employed to monitor the initial formation of copolymers of ethylene and vinyl acetate during

polymerization in scCO<sub>2</sub>. The reactivity ratios for the copolymerization of ethylene and vinyl acetate in scCO<sub>2</sub> were determined using both the Kelen-Tudos and the non-linear least-squares methods.

The potential of scCO<sub>2</sub> was further examined to synthesize advanced and novel nanomaterials based on an understanding of the polymerization mechanism. A novel one-step synthesis route was developed for making silica-PVAc nanocomposites in scCO<sub>2</sub>, where the parallel reactions of free radical polymerization, hydrolysis/condensation, and linkage of the nanoparticles to the polymer chains, were found to take place simultaneously. This provides a new process featuring significant energy-saving, waste-reduction, and excellent distribution of nanoparticles in the polymer matrix. In addition, the incorporation of quantum dots (QDs) into a transparent polymer matrix was investigated to form light-selective nanofilms. Both CdS and CdS-ZnS core-shell QDs were synthesized, then functionalized with a methoxysilane group, and finally used to synthesize novel QD-PVAc and QD-PEVA nanocomposites in scCO<sub>2</sub>. The synthesized QD-PEVA nanofilms displayed significant absorption in the ultraviolet and violet regions of the electromagnetic spectrum, while providing a characteristic emission in the region from orange to red light. These materials have significant potential in green houses, and solar absorber films.

**Key Words:** supercritical CO<sub>2</sub>, initiator, thermal decomposition, kinetics, mechanism, ATR-FTIR, reactivity ratios, ethylene, vinyl acetate, silica, nanocomposite, one-pot synthesis, light-selective, nanofilm, quantum dots.

## Co-Authorship Statement

Chapter 3, 4, 5, and 6 encompass research studies that have been either published or submitted to peer-refereed journals. Individual contributions of the authors of each journal article are stated below.

### Chapter 3

<b>Article Title</b>	<i>In situ</i> ATR-FT-IR study of the thermal decomposition of diethyl peroxydicarbonate in supercritical carbon dioxide
<b>Authors</b>	William Z. Xu, Xinsheng Li, Paul A. Charpentier
<b>Current status</b>	Published: <i>Polymer</i> 2007, 48(5), 1219-1228
W. Xu conducted the experiments for decomposition mechanism study, analyzed all the data, wrote and revised the manuscript. The decomposition rate constant data under various conditions were contributed by X. Li. Various drafts of the paper were reviewed by P. Charpentier. This work was supervised by P. Charpentier.	

#### Chapter 4

<b>Article Title</b>	FTIR study on measuring the monomer reactivity ratios for ethylene-vinyl acetate polymerization in supercritical CO <sub>2</sub>
<b>Authors</b>	William Z. Xu, Paul A. Charpentier
<b>Current status</b>	Accepted by <i>Industrial &amp; Engineering Chemistry Research</i>
<p>W. Xu conducted the experimental work, analyzed the data, and wrote the manuscript. Several drafts of the manuscript were reviewed by P. Charpentier. This work was supervised by P. Charpentier.</p>	

#### Chapter 5

<b>Article Title</b>	A novel approach to the synthesis of SiO <sub>2</sub> -PVAc nanocomposites using a one-pot synthesis in supercritical CO <sub>2</sub>
<b>Authors</b>	Paul A. Charpentier, William Z. Xu, Xinsheng Li
<b>Current status</b>	Published: <i>Green Chemistry</i> 2007, 9(7), 768-776
<p>P. Charpentier wrote the manuscript with W. Xu. W. Xu conducted the experimental work except one experiment conducted by X. Li. W. Xu analyzed the data and revised the manuscript. The <i>in situ</i> FTIR spectra of homopolymerization of vinyl acetate in supercritical CO<sub>2</sub> were contributed by X. Li. This work was supervised by P. Charpentier.</p>	

## Chapter 6

<b>Article Title</b>	Light-selective nanofilms of quantum dot-poly(ethylene-co-vinyl acetate) synthesized using supercritical CO <sub>2</sub>
<b>Authors</b>	William Z. Xu, Paul A. Charpentier
<b>Current status</b>	Submitted to <i>Journal of Physical Chemistry</i>
<p>W. Xu conducted the experimental work, analyzed the data, and wrote the manuscript. Various drafts of the manuscript were reviewed by P. Charpentier. This work was supervised by P. Charpentier.</p>	

## **Acknowledgements**

Firstly, I would like to thank Professor Paul A. Charpentier for his continuous guidance and support throughout my graduate studies at Western. I am very grateful to him for this valuable opportunity to pursue my graduate studies under his supervision. Also, I would like to thank Professors Ajay K. Ray and Amin S. Rizkalla for their kind help and direction during my graduate studies.

Secondly, I would like to acknowledge many specialists for their assistance in sample characterization. They include Mr. Fred Pearson of the Brockhouse Institute for Materials Research, McMaster University for HRTEM, Mr. Ronald Smith and Dr. Richard B. Gardiner of the Department of Biology, UWO for TEM, Mr. Mark C. Biesinger of the Surface Science Western, UWO and Mr. Mohammad Rahbari of the Department of Chemical and Biochemical Engineering, UWO for EDX elemental analysis and mapping, Dr. Robert H. E. Hudson of the Department of Chemistry, UWO, Dr. Elizabeth Gillies of Departments of Chemistry and Chemical and Biochemical Engineering, UWO, Ms Lee-Ann Briere of the Schulich School of Medicine & Dentistry, UWO, and Dr. Alex Siemiarczuk of Photon Technology International for photoluminescence.

Thirdly, I would like to express my appreciation to the colleagues in our group: to Xinsheng Li for his cooperation on two projects, the initiator decomposition and the one-pot synthesis of SiO<sub>2</sub>-poly(vinyl acetate) nanocomposites, Kevin Burgess for his assistance in repairing high-pressure syringe pumps, SM Zahangir Khaled for his kind



help with TGA and UV experiments, Jeff Gribbon for TGA experiments, Ruohong Sui for his assistance in deconvolution of FTIR spectra, Behnez Hojjati, Vahid Raesi, Bo Chen, Jeff Wood, Shawn Dodds, Rahima Lucky, Muhammad Chowdhury, Nasrin Farhangi, Ming Jia, and Colin Ho for their friendship and help. Special thanks go to Ryan MacIver for fruitful discussions about the synthesis of quantum dots and the CdS precursor.

In addition, I wish to thank the government of Ontario and the University of Western Ontario for OGSST scholarship and the financial funding from the Canadian Natural Science and Engineering Research Council (NSERC), the Ontario Centre's of Excellence (OCE) (through the EMK program), and the Canadian Foundation for Innovation (CFI). I would also like to acknowledge Dr. Alex Henderson and Dr. Dirk Hair of AT Plastics Inc. for fruitful discussions and their providing poly(ethylene-co-vinyl acetate) samples.

Finally, I would like to express my sincere gratitude to my wife Fengyu Jin for her understanding, support, and encouragement during my graduate studies.

## Table of Contents

Title Page .....	i
Certificate of Examination .....	ii
Abstract and Key Words .....	iii
Co-Authorship Statement.....	v
Acknowledgements.....	viii
Table of Contents .....	x
List of Tables .....	xv
List of Figures .....	xvi
List of Appendices .....	xxii
List of Abbreviations, Symbols, Nomenclature.....	xxiii
Chapter 1. Introduction .....	1
1.1. Background .....	2
1.1.1. Polymerizations in Supercritical Carbon Dioxide .....	3
1.1.2. Copolymerization of Ethylene and Vinyl Acetate .....	10
1.1.3. Polymer Nanocomposites .....	15
1.1.4. Quantum Dots .....	18
1.2. Research Objectives.....	22
1.3. Thesis Structure .....	22
Chapter 2. Experimental and Characterization Methods .....	25
2.1. Outline.....	26

2.2. Experimental Setup.....	26
2.3. Characterization Methods .....	28
2.3.1. ATR-FTIR Spectroscopy .....	28
2.3.2. Ultraviolet-Visible Spectroscopy.....	30
2.3.3. Nuclear Magnetic Resonance Spectroscopy.....	31
2.3.4. Thermogravimetric Analysis .....	33
2.3.5. Transmission Electron Microscopy .....	34
2.3.6. Energy Dispersive X-Ray Spectroscopy.....	36
2.3.7. Photoluminescence .....	37
Chapter 3. <i>In Situ</i> ATR-FTIR Study of the Thermal Decomposition of Diethyl Peroxydicarbonate in Supercritical CO <sub>2</sub> .....	39
3.1. Introduction.....	41
3.2. Experimental.....	43
3.2.1. Materials .....	43
3.2.2. Preparation of DEPDC Initiator.....	44
3.2.3. Reactor and <i>In Situ</i> ATR-FTIR Measurements .....	44
3.2.4. Nuclear Magnetic Resonance .....	45
3.3. Results and Discussion .....	45
3.3.1. Assignment of Characteristic Peaks of DEPDC .....	45
3.3.2. Thermal Decomposition of DEPDC in Heptane and Supercritical CO <sub>2</sub> .....	46
3.3.3. Kinetic Measurement.....	51
3.3.4. Decomposition Mechanism of DEPDC in ScCO <sub>2</sub> .....	59
3.4. Conclusions.....	67

Chapter 4. FTIR Study on Measuring the Monomer Reactivity Ratios for Ethylene-Vinyl Acetate Polymerization in Supercritical CO <sub>2</sub> .....	68
4.1. Introduction.....	70
4.2. Experimental.....	72
4.2.1. Materials .....	72
4.2.3 Characterization.....	74
4.3. Results and Discussion .....	75
4.3.1. FTIR Analysis of Copolymerization.....	75
4.3.2. Determination of PEVA Composition by TGA and NMR Analysis.....	79
4.3.3. Determination of Reactivity Ratios .....	83
4.3.3.1. Model Comparison.....	83
4.3.3.2. Effect of Reaction Temperature and Pressure .....	88
4.3.4. Discussion.....	89
4.4. Conclusions.....	93
Chapter 5. A Novel Approach to the Synthesis of SiO <sub>2</sub> -PVAc Nanocomposites Using a One-Pot Synthesis in Supercritical CO <sub>2</sub> .....	94
5.1. Introduction.....	96
5.2. Experimental.....	98
5.2.1. Materials .....	98
5.2.2. Polymerization Procedure.....	99
5.2.3. Characterization .....	99
5.3. Results and Discussion.....	100
5.3.1. Copolymerization.....	100

5.3.2. Hydrolysis.....	103
5.3.3. One-Pot Synthesis.....	106
5.4. Conclusions.....	112
Chapter 6. Synthesis of Light-Selective Quantum Dot-Polymer Nanofilms in Supercritical CO <sub>2</sub> .....	114
6.1. Introduction.....	116
6.2. Experimental .....	118
6.2.1. Materials .....	118
6.2.2. Preparation of the Single-Molecular Precursor Bis(diethyldithiocarbamate) Cadmium (II) .....	119
6.2.3. Preparation of CdS-ZnS and CdS QDs.....	120
6.2.4. Ligand Exchange of QDs.....	121
6.2.5. Synthesis of Polymer Nanofilms .....	122
6.2.5.1. CdS-ZnS QD-PVAc Nanofilms.....	122
6.2.5.2. QD-PEVA Nanofilms .....	123
6.2.6. Characterization .....	124
6.3. Results and Discussion. ....	126
6.3.1. CdS-ZnS Core-Shell QDs.....	126
6.3.2. Ligand Exchange of the CdS-ZnS QDs .....	129
6.3.3. Synthesis of QD-Polymer Nanofilms .....	132
6.3.3.1. CdS-ZnS QD-PVAc Nanofilms.....	133
6.3.3.2. QD-PEVA Nanofilms .....	138
6.4. Conclusions.....	145

Chapter 7. Summary and Conclusions.....	146
7.1. Summary .....	147
7.2. Recommendations.....	151
Bibliography .....	152
Appendices.....	169
Curriculum Vitae .....	195

## List of Tables

<b>Table 3.1</b> Decomposition rate constants of DEPDC in heptane under N <sub>2</sub> .....	55
<b>Table 3.2</b> Decomposition rate constants of DEPDC in scCO <sub>2</sub> .....	56
<b>Table 3.3</b> Assignment of characteristic FTIR peaks used in this study <sup>110, 114, 116</sup> ....	65
<b>Table 4.1</b> Initial feed compositions for FTIR experiments under different reaction conditions.....	84
<b>Table 4.2</b> Ethylene mole fraction of copolymers determined by FTIR and <sup>1</sup> H NMR from copolymerization of ethylene and vinyl acetate in scCO <sub>2</sub> at 50°C 27.6MPa with various feed composition.....	85
<b>Table 4.3</b> Ethylene mole fraction of copolymers determined by FTIR from copolymerization of ethylene and vinyl acetate in scCO <sub>2</sub> with various feed composition.....	85
<b>Table 4.4</b> Reactivity ratios and 95% confidence intervals determined under different reaction conditions with different numerical methods.....	87
<b>Table 6.1</b> Relative atom number ratios of the CdS-ZnS QDs before and after the ligand exchange .....	131

## List of Figures

<b>Figure 1.1</b> Carbon dioxide pressure-temperature phase diagram. <sup>2</sup> .....	3
<b>Figure 1.2</b> SEM of silica aerogel powder collected using the rapid expansion of supercritical solutions process. The experimental conditions are TEOS/HAc= 1:4, T=60°C, P=41.4MPa. <sup>38</sup> .....	10
<b>Figure 1.3</b> Room temperature optical absorption spectra of CdSe nanocrystallites dispersed in hexane and ranging in size from ~1.2 to 11.5nm. <sup>79</sup> .....	19
<b>Figure 1.4</b> Room temperature optical absorption spectra of ~2-3nm diameter CdS, CdSe, and CdTe crystallites. <sup>79</sup> .....	20
<b>Figure 2.1</b> Schematic diagram of experimental setup.....	27
<b>Figure 2.2</b> Schematic diagram of multiple reflection ATR system. ....	30
<b>Figure 2.3</b> Schematic COSY spectrum for two coupled spins, A and B. ....	33
<b>Figure 2.4</b> Schematic diagram of a TEM instrument.....	35
<b>Figure 2.5</b> Schematic diagram of EDX.....	37
<b>Figure 2.6</b> Schematic diagram of PL measurements.....	38
<b>Figure 3.1</b> IR spectra of (a) DEPDC, (b) heptane, and (c) heptane+DEPDC. Spectra were collected at ambient temperature under atmospheric pressure. ....	46
<b>Figure 3.2</b> <i>In situ</i> FTIR spectra of DEPDC thermal decomposition in heptane (DEPDC concentration 2.7wt%) at 60°C. (a) at t = 0min; (b) at t = 60min; (c) at t = 480min; (d) resulting spectrum from c-a subtraction. ....	48



<b>Figure 3.3</b> <i>In situ</i> FTIR spectra of DEPDC thermal decomposition in scCO <sub>2</sub> (DEPDC concentration 3.4wt%) at T=50°C, P=20MPa. (a) at t=0min; (b) at t=860min; (c) resulting spectrum from b-a subtraction. ....	49
<b>Figure 3.4</b> <i>In situ</i> FTIR spectra of DEPDC thermal decomposition in supercritical ethylene (T=60°C, P=13.8MPa). (a) at t=0min; (b) at t=200min; (c) resulting spectrum from b-a subtraction. ....	50
<b>Figure 3.5</b> <i>In situ</i> FTIR results for absorbance versus reaction time curves for DEPDC decomposition in scCO <sub>2</sub> (T=60°C, P=20MPa, DEPDC concentration 8.8wt%). ....	51
<b>Figure 3.6</b> Kinetic measurement of DEPDC thermal decomposition in heptane at 50°C. ....	54
<b>Figure 3.7</b> Arrhenius plot of $\ln k_d$ versus $1/(RT)$ for DEPDC decomposition in scCO <sub>2</sub> and heptane. ....	55
<b>Figure 3.8</b> Comparison of rate constants for diethyl peroxydicarbonate decomposition in scCO <sub>2</sub> (◆) and heptane (*), to those reported in the literature for the solvents scCO <sub>2</sub> (■), t-butanol (△), and 2,2'-oxydiethylene bis(allyl carbonate)(○). ....	59
<b>Figure 3.9</b> FTIR spectrum of thermal decomposition products after 860min reaction in scCO <sub>2</sub> at 50°C and 20MPa then venting to atmospheric pressure. (Spectra were collected at ambient temperature under atmospheric pressure.) ....	62
<b>Figure 3.10</b> <i>In situ</i> FTIR spectra of before and after the induced explosive DEPDC decomposition in scCO <sub>2</sub> at 60°C and 20MPa (DEPDC concentration 18.4wt%). .....	64

<b>Figure 4.1</b> <i>In situ</i> FTIR spectra of copolymerization of ethylene and vinyl acetate in scCO <sub>2</sub> (the experimental conditions: T=50°C, P=27.6MPa, ethylene mole fraction in feed: 0.902).....	77
<b>Figure 4.2</b> <i>In situ</i> FTIR waterfall plot of the copolymerization of ethylene and VAc in scCO <sub>2</sub> (the experimental conditions: T=50°C, P=27.6MPa, ethylene mole fraction in feed: 0.887).....	78
<b>Figure 4.3</b> TGA plot of a PEVA sample (Ateva <sup>®</sup> 3325AC).....	79
<b>Figure 4.4</b> <sup>1</sup> H NMR spectra of a PEVA sample (Ateva <sup>®</sup> 3325AC) by use of different solvents. (a) chloroform-d at room temperature; (b) 1,2,4-trichlorobenzene at 60°C.....	81
<b>Figure 4.5</b> Comparison of VAc content of commercial PEVA samples determined from TGA and <sup>1</sup> H NMR. ....	82
<b>Figure 4.6</b> Calibration curve of absorbance ratio versus VAc content of PEVA copolymers.....	83
<b>Figure 4.7</b> Plot of mole fraction of ethylene in the copolymer, F <sub>1</sub> , versus mole fraction of ethylene in the feed, f <sub>1</sub> (copolymer compositions determined from <i>in situ</i> FTIR). The points are experimental data, while the lines are the examined model equations (the experimental conditions: T=50°C, P=27.6MPa). ....	86
<b>Figure 4.8</b> Copolymer composition versus feed composition for different reaction temperature and pressure conditions in scCO <sub>2</sub> . ....	89
<b>Figure 5.1</b> <i>In situ</i> FTIR measurement of free radical polymerization of vinyl acetate in supercritical CO <sub>2</sub> (The experimental conditions are: T=60°C, P=20.7MPa). ....	101

<b>Figure 5.2</b> <i>In situ</i> FTIR measurement of free radical copolymerization of vinyl acetate and VTMO in supercritical CO <sub>2</sub> (The experimental conditions are: T=60°C, P=16.8MPa, molar ratio: VAc:VTMO=40:1).....	103
<b>Figure 5.3</b> <i>In situ</i> FTIR measurement of hydrolysis of TEOS in the silane modified PVAc in scCO <sub>2</sub> (The experimental conditions are: T=60°C, P=16.8MPa, molar ratio: HAc:TEOS=4.3:1).....	105
<b>Figure 5.4</b> TEM image of the PVAc nanocomposite from hydrolysis of TEOS with acetic acid in presence of copolymer of vinyl acetate and VTMO in scCO <sub>2</sub> ..	106
<b>Figure 5.5</b> Parallel reactions of the copolymerization of vinyl acetate and VTMO and hydrolysis of TEOS/VTMO with acetic acid in scCO <sub>2</sub> (The experimental conditions: T=60°C, P=16.8MPa, molar ratio: VAc:VTMO:HAc:TEOS:DEPDC =40:1:43:10:1).....	108
<b>Figure 5.6</b> Parallel reactions of the copolymerization of vinyl acetate and VTMO and hydrolysis of TMOS/VTMO with acetic acid in scCO <sub>2</sub> (The experimental conditions: T=60°C, P=16.8MPa, molar ratio: VAc:VTMO:HAc:TMOS:DEPDC =40:1:43:10:1).....	109
<b>Figure 5.7</b> TEM images and particle size distribution histograms of the PVAc nanocomposites from the one-pot synthesis in scCO <sub>2</sub> using TMOS (left) / TEOS (right). .....	110
<b>Figure 5.8</b> EDX element Si-mapping of PVAc nanocomposite from the one-pot synthesis in scCO <sub>2</sub> using TMOS.....	111

**Figure 6.1** TEM images of the synthesized QDs. (a) CdS-ZnS QDs, (b) CdS QDs.  
(The experimental conditions are: for CdS-ZnS core-shell QDs, 180°C, 5min  
for core growth; for CdS QDs, 235°C, 30min). ..... 128

**Figure 6.2** HRTEM and the d-spacing images of the synthesized CdS-ZnS (left) and  
CdS (right) QDs. (The experimental conditions are: for CdS-ZnS core-shell  
QDs, 180°C, 5min for core growth; for CdS QDs, 235°C, 30min)..... 128

**Figure 6.3** FTIR spectra of the CdS-ZnS QDs before and after ligand exchange. 131

**Figure 6.4** Solubility test of the CdS-ZnS QDs before (left) and after (right) ligand  
exchange. .... 132

**Figure 6.5** *In situ* FTIR spectra of parallel reactions of the copolymerization of vinyl  
acetate and VTMO and hydrolysis of functionalized CdS-ZnS QDs/VTMO  
with acetic acid in scCO<sub>2</sub> (The experimental conditions: T=60°C, P=24.3MPa;  
materials: VAc: 0.1mol, VTMO: 0.005mol, DEPDC: 0.002mol, HAc: 0.02mol,  
CdS-ZnS QDs: 10.24g 0.51wt% toluene solution)..... 134

**Figure 6.6** Photoluminescence and UV-Vis spectra of (a) the CdS-ZnS QDs before  
and after the ligand exchange, and (b) the QDs/SiO<sub>2</sub>-PVAc and SiO<sub>2</sub>-PVAc  
nanocomposites..... 137

**Figure 6.7** Photoluminescence emission spectra of CdS-ZnS QD-PEVA nanofilms  
prepared in different reaction conditions (under 27.6MPa in scCO<sub>2</sub>. (a) 50°C 2  
hours without TOP; (b) 50°C 2 hours with TOP; (c) 50°C 20 hours with TOP;  
(d) 80°C 2 hours with TOP). ..... 140

<b>Figure 6.8</b> TEM images of (a) functionalized CdS-ZnS QDs, and CdS-ZnS QD-PEVA nanofilms prepared in different reaction conditions (under 27.6MPa in scCO <sub>2</sub> with TOP). (b) 50°C 2 hours; (c) 50°C 20 hours; (d) 80°C 2 hours.....	141
<b>Figure 6.9</b> Particle size distribution of the synthesized CdS QDs by light scattering measurement .....	142
<b>Figure 6.10</b> Photoluminescence emission spectra of CdS QDs and CdS QD-PEVA nanofilms prepared in different reaction conditions. (a) CdS QDs before ligand exchange; (b) CdS QDs after ligand exchange; (c) CdS QD-PEVA nanofilms prepared at 50°C for 2 hours without TOP; (d) CdS QD-PEVA nanofilms prepared at 50°C for 2 hours with TOP).....	143
<b>Figure 6.11</b> UV-Vis spectra of PEVA and PEVA nanofilms. (a) PEVA; (b) CdS-ZnS QD-PEVA with TOP; (c) CdS QD-PEVA with TOP; (d) CdS QD-PEVA without TOP.....	144

## List of Appendices

Appendix 1. Examination of the Linear Relationship between Absorbance and Weight of DEPDC in Heptane.....	170
Appendix 2. Matlab Program Used for the Calculation of $A_d$ and $E_a$ from $k_d \sim t$ Data.....	171
Appendix 3. NMR Spectra of the Residue from Decomposition of DEPDC in $ScCO_2$ .....	173
Appendix 4. Data Used for the Calibration of Absorbance Ratio versus VAc Content in PEVA Copolymer .....	175
Appendix 5. Linearization Methods for Determining Monomer Reactivity Ratios of Copolymerization.....	176
Appendix 6. Matlab Program Used for Determining the Monomer Reactivity Ratios of Copolymerization from $f_1 \sim F_1$ data .....	178
Appendix 7. FTIR and NMR Spectra of the Single-Molecular Precursor Bis(diethyldithiocarbamate) Cadmium (II) .....	181
Appendix 8. EDX Plots of the Core-Shell QDs before and after Ligand Exchange .....	184
Appendix 9. TEM and EDX Elemental Mapping Images of the Synthesized CdS-ZnS QD-PVAc Nanocomposite.....	185
Appendix 10. License Agreement with Elsevier Limited.....	186
Appendix 11. Copyright Permission from the Royal Society of Chemistry.....	191
Appendix 12. Copyright Permission from American Chemical Society.....	194

## List of Abbreviations, Symbols, Nomenclature

### Abbreviations

AIBN	2,2'-azobis(isobutyronitrile)
asym.	asymmetric
Abs	absorbance
ASB	anchor soluble balance
AT	acquisition time (s)
ATR	attenuate total reflection
au	arbitrary unit
ca.	circa
CdMe <sub>2</sub>	dimethylcadmium
COSY	correlation spectroscopy
CSTR	continuous-stirred-tank reactor
D1	delay time (s)
DEPDC	diethyl peroxydicarbonate
DIH	diisocyanatohexane
EDX, EDS	energy dispersive X-ray spectroscopy
Eqn.	equation
EVA	ethylene-vinyl acetate
FID	free-induction decay
FT-NMR	Fourier transform nuclear magnetic resonance

FTIR	Fourier transform infrared spectroscopy
gCOSY	gradient correlation spectroscopy
GHSQC	gradient heteronuclear single quantum coherence
GPC	gel permeation chromatography
HAc	acetic acid
HRTEM	high resolution transmission electron microscopy
HSQC	heteronuclear single quantum coherence
IR	infrared
KT	Kelen-Tudos
Me	methyl
MPTMO	3-mercaptopropyl trimethoxysilane
MW	molecular weight
NLLS	non-linear least-squares
NMR	nuclear magnetic resonance spectroscopy
NT	number of transients
PDMS	poly(dimethylsiloxane)
PEVA	poly(ethylene-co-vinyl acetate)
PL	photoluminescence
PMMA	poly(methyl methacrylate)
PPV	poly(phenylene vinylene)
PV	photovoltaic
PVAc	poly(vinyl acetate)
PW90	90° pulse width ( $\mu\text{s}$ )



QD	quantum dot
QDs	quantum dots
RF	radio frequency
rpm	revolutions per minute
scCO <sub>2</sub>	supercritical carbon dioxide
SEM	scanning electron microscope
SFE	supercritical fluid extraction
sym.	symmetric
TCB	1,2,4-trichlorobenzene
TDA	triple detector array
TEM	transmission electron microscopy
TEOS	tetraethyl orthosilicate
TGA	thermogravimetric analysis
THF	tetrahydrofuran
THPP	tris(hydroxypropyl)phosphine
TMOS	tetramethyl orthosilicate
TMS	tetramethylsilane
TOA	trioctylamine
TOP	trioctylphosphine
TOPO	trioctylphosphine oxide
TOPSe	trioctylphosphine selenide
UV	ultraviolet
UV-Vis	ultraviolet-visible spectroscopy

VAc	vinyl acetate
VOCs	volatile organic compounds
VTMO	vinyltrimethoxysilane
w/v	weight/volume

## Symbols

A	absorbance
$A_0$	initial absorbance
$A_d$	pre-exponential factor in the Arrhenius equation ( $s^{-1}$ )
C	concentration ( $mol \cdot L^{-1}$ )
$C_0$	initial concentration ( $mol \cdot L^{-1}$ )
$d_w/d_T$	weight loss rate ( $g \cdot ^\circ C^{-1}$ )
$E_a$	activation energy ( $J \cdot mol^{-1}$ )
f	monomer mole fraction in comonomer feed
F	monomer mole fraction in copolymer
G	function defined by Eqn. A-2
H	function defined by Eqn. A-3
$H_{min}$	smallest H value
$H_{max}$	largest H value
$k_{11}, k_{12}, k_{21}, k_{22}$	propagation rate constants ( $L \cdot mol^{-1} \cdot s^{-1}$ )
$k_d$	decomposition rate constant ( $s^{-1}$ )
l	path length (cm)
$[M_1], [M_2]$	monomer concentration ( $mol \cdot L^{-1}$ )

$[M_1\bullet], [M_2\bullet]$	radical concentration ( $\text{mol}\cdot\text{L}^{-1}$ )
P	pressure (Pa)
$P_c$	critical pressure (Pa)
r	monomer reactivity ratio
R	gas constant ( $8.314 \text{ J}\cdot\text{K}^{-1}\cdot\text{mol}^{-1}$ )
t	time (s)
T	temperature ( $^{\circ}\text{C}$ or K)
$T_c$	critical temperature ( $^{\circ}\text{C}$ )
$T_g$	glass transition temperature ( $^{\circ}\text{C}$ )
$T_{\text{onset}}$	weight loss onset temperature ( $^{\circ}\text{C}$ )
wt%	weight percent
x	monomer concentration ratio in feed defined by Eqn. A-4
y	monomer concentration ratio in copolymer defined by Eqn. A-5
®	registered trademark

### Greek letters

$\alpha$	an arbitrary constant, often assigned as $\alpha = \sqrt{H_m H_M}$
$\delta$	bending vibration
$\varepsilon$	molar absorptivity ( $\text{L}\cdot\text{mol}^{-1}\cdot\text{cm}^{-1}$ )
$\eta$	function defined by Eqn. A-7
$\nu$	stretching vibration
$\xi$	function defined by Eqn. A-8
$\rho$	rocking vibration

$\sigma$	standard deviation
$\langle\varphi\rangle$	average diameter of particles (nm)

### **Subscripts**

as	asymmetric
s	symmetric

## **Chapter 1. Introduction**

## 1.1. Background

A supercritical fluid is any substance at a temperature and pressure above its thermodynamic critical point. It has unique properties such as a liquid-like density (which allows for solvation of many compounds) and a gas-like diffusivity (which has important implications for reaction kinetics), and these properties are “tunable” by varying the pressure and/or temperature.<sup>1</sup> Supercritical fluids are being examined as a substitute for organic solvents in several industrial and laboratory processes. Carbon dioxide is the most commonly used supercritical fluid due to its moderate critical constants ( $T_c=31.1^\circ\text{C}$ ,  $P_c=7.38\text{MPa}$ ,<sup>2</sup> as shown in Figure 1.1), and its non-flammable and non-toxic nature. Not only is  $\text{CO}_2$  naturally occurring and abundant, it is also generated in large quantities as a byproduct in ammonia, hydrogen, and ethanol plants and in electrical power generation stations that burn fossil fuels. Moreover, as an ambient gas,  $\text{CO}_2$  can be easily recycled after use as a solvent to avoid any contribution to greenhouse effects. In recent years, supercritical  $\text{CO}_2$  ( $\text{scCO}_2$ ) has been used in extraction, dry cleaning, nano and micro particle formation, and chemical reactions including polymerizations as a reaction medium.

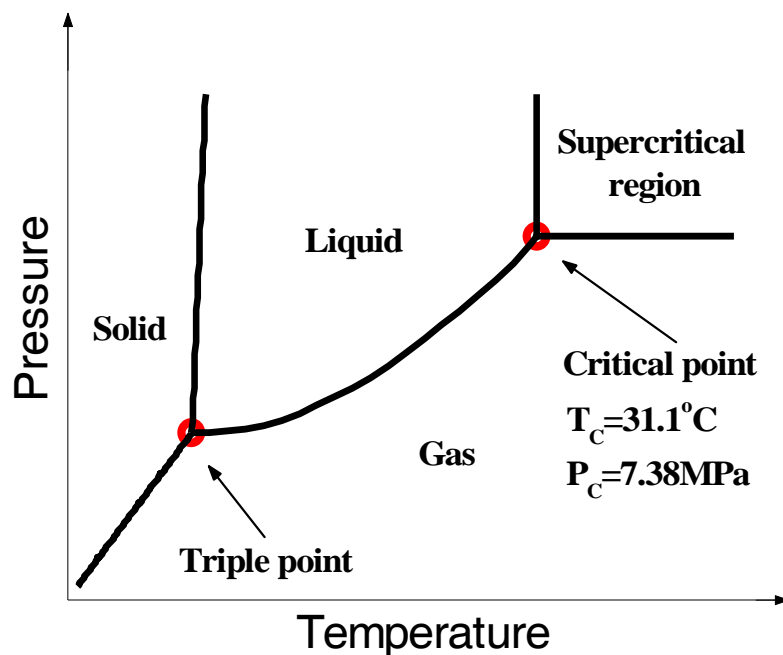


**Figure 1.1** Carbon dioxide pressure-temperature phase diagram.<sup>2</sup>

### 1.1.1. Polymerizations in Supercritical Carbon Dioxide

Polymerizations in supercritical carbon dioxide have been reviewed by DeSimone *et al*<sup>3</sup> and Mukhopadhyay *et al*<sup>4</sup>. As a solvent in polymerizations, scCO<sub>2</sub> has several advantages including excellent mass transfer and heat dissipation, small chain transfer constant, easy removal from the polymers, and facilitated removal of residual monomers.

Several important issues should be emphasized when considering scCO<sub>2</sub> as a potential polymerization solvent. Firstly, because CO<sub>2</sub> is an ambient gas, the polymers can be easily isolated from the reaction media by depressurization, resulting in dry polymer products. This feature represents potential cost and energy savings by eliminating energy-intensive drying procedures.

Secondly, solubility plays a very important role in the synthesis of polymers in scCO<sub>2</sub>. The most important limitation of utilizing CO<sub>2</sub> as an industrial solvent has been the extremely poor solubility of most non-fluorous, polar and amphiphilic materials in CO<sub>2</sub>. CO<sub>2</sub> is a good solvent for most non-polar and some polar molecules of low molar mass<sup>5</sup>, but it is a poor solvent for most high molar mass polymers under mild conditions (<100°C, <35MPa). It was reported in the literature that amorphous fluoropolymers and silicones<sup>1, 6-8</sup> showed good solubility in CO<sub>2</sub> under mild conditions. In order to expand the applications of CO<sub>2</sub>, a large amount of work has been devoted to developing inexpensive hydrocarbon-based CO<sub>2</sub>-philes, among which two typical studies were conducted by Beckman *et al*<sup>9, 10</sup> and Wallen *et al*<sup>11</sup> who synthesized poly(ether-carbonate) (known as the Beckman surfactants) and peracetylated sugars (the Wallen Sugars), respectively. Systematic studies have shown that the solubility of polymers in CO<sub>2</sub> can be affected by several factors including conformational flexibility, free volume, polymer-polymer interactions, and Lewis acid-base type interactions between CO<sub>2</sub> and polymer molecules.<sup>9, 12</sup> The interaction between the carbonyl groups of an acetate functionality and CO<sub>2</sub> is almost half as strong as the hydrogen bond interaction in a water dimer by Ab initio calculations<sup>13</sup>. In addition, the cooperative C-H...O hydrogen bond between CO<sub>2</sub> and carbonyl compounds with hydrogen atoms attached to the carbonyl carbon or the  $\alpha$ -carbon atom was found to enhance solubility of these materials in scCO<sub>2</sub>.<sup>14</sup> By using Fourier transform infrared spectroscopy (FTIR), it was found that CO<sub>2</sub> exhibited Lewis acid-base type interactions with electron-donating functional groups of polymer chains such as the carbonyl group of poly(methyl methacrylate) (PMMA).<sup>15</sup> McHugh<sup>16</sup> found that in copolymers of ethylene and methyl acrylate, increasing the methyl acrylate



content increased the copolymer solubility. The interaction of CO<sub>2</sub> and the carbonyl groups leads to an enhanced local CO<sub>2</sub> density around these functional groups.<sup>12, 17</sup> While polyethylene is insoluble in CO<sub>2</sub>, even up to 270°C and 275MPa, perfluorinated ethylene-propylene copolymer has greatly improved solubility under the same conditions.<sup>16</sup> These solubility requirements dictate the types of polymerization techniques employed in polymer synthesis. Many polymerization reactions in scCO<sub>2</sub> are conducted under heterogeneous processes due to the inherent insolubility of most polymers in scCO<sub>2</sub>.

Thirdly, the fractionation of polymers is an important area affected by polymer solubility in scCO<sub>2</sub>. Careful and controlled lowering of the density of a polymer solution allows precipitation of the highest molecular weight polymer fraction.<sup>1</sup> Krukoniš<sup>18</sup> reported that CO<sub>2</sub>-soluble synthetic oils such as poly(dimethylsiloxane) (PDMS) could be fractionated with scCO<sub>2</sub>.

Another important feature of scCO<sub>2</sub> in polymerization is CO<sub>2</sub>-induced swelling<sup>19</sup> and plasticization, which results in the lowering of the polymer's glass transition temperature ( $T_g$ )<sup>20</sup> and the depression of the polymer's melting point<sup>21</sup>. Due to the increased free volume, the swelling and plasticization allow important effects such as the removal of residual monomer from the polymer, incorporation of additives, polymer processing, formation of foams, and the synthesis of polymer composites.

Supercritical CO<sub>2</sub> has been shown to be a promising solvent in both chain-growth and step-growth polymerizations. Chain-growth routes such as free-radical polymerization of styrenics<sup>22-24</sup>, acrylates<sup>25</sup>, and methacrylates<sup>26, 27</sup>, cationic polymerization of isobutylene<sup>28</sup>, vinyl ethers<sup>29</sup>, and styrene, and transition metal-catalyzed polymerization of norbornene<sup>30</sup> and olefins<sup>31</sup>, and copolymerization of

epoxides and CO<sub>2</sub><sup>32</sup> have been reported. Step-growth reactions in CO<sub>2</sub> have produced polycarbonates<sup>33</sup>, polyamides<sup>34, 35</sup>, polyesters<sup>36</sup>, polypyrrole<sup>37</sup>, and silica gels<sup>38</sup>.

The four most widely studied free-radical heterogeneous processes are precipitation, suspension, dispersion, and emulsion. In a precipitation polymerization, an initially homogeneous mixture of monomer, initiator, and solvent becomes heterogeneous during the reaction as insoluble polymer chains aggregate to form a separate polymer phase. Powder products typically result from precipitation polymerizations. Although many common vinyl monomers exhibit high solubility in CO<sub>2</sub>, most corresponding polymers exhibit exceedingly poor solubility in CO<sub>2</sub>. As a result, the majority of early studies in this area focused on precipitation polymerization. Okubo *et al* synthesized polydivinylbiphenyl<sup>39</sup> and polyacrylonitrile<sup>40</sup> by precipitation polymerization without any colloidal stabilizer in scCO<sub>2</sub>. They found that an increase in initiator concentration led to an increase in the conversion and the degree of coagulation, but a decrease in molecular weight. At acrylonitrile concentration of 20% w/v, micron-sized, relatively monodisperse polyacrylonitrile particles with clean and uneven surfaces were produced.

In a suspension polymerization, neither the monomer nor the initiator is soluble in the continuous phase. The formed polymer is also insoluble in the continuous phase, which only acts as a dispersant and heat-dissipation agent during the polymerization. Bratton *et al*<sup>41</sup> synthesized poly(L-lactide) in scCO<sub>2</sub> by using the suspension polymerization technique.

A dispersion polymerization begins as a homogeneous mixture because of the good solubility of both the monomer and the initiator in the continuous phase. Once the growing oligomeric radicals reach a critical molecular weight, the chains are no longer

soluble in the reaction medium and phase separation takes place. At this point, the surface active stabilizing molecule adsorbs to or becomes chemically attached to the polymer colloid and prevents coagulation or agglomeration of the particles. Polymerization persists both in the continuous phase and in the growing polymer particles. The product from a dispersion polymerization exists as spherical particles, typically ranging in size from 100nm to 10 $\mu$ m. Due to the good solubility of many small organic molecules in CO<sub>2</sub>, dispersion polymerization constitutes an excellent heterogeneous method that has been developed for producing high molecular weight, CO<sub>2</sub>-insoluble, industrially important polymers.

In contrast to dispersion polymerization, the reaction mixture in an emulsion polymerization is initially heterogeneous due to the low solubility of the monomer in the continuous phase. For a reaction to take advantage of the desirable Smith-Ewart kinetics, the monomer and initiator must be segregated with the initiator preferentially dissolved in the continuous phase and not in the monomer phase. The repulsive forces, which result from the surface charges, prevent the coagulation of the growing particles and lead to a stabilized colloid. The polymer which results from an emulsion polymerization exists as spherical particles typically smaller than 1 $\mu$ m in diameter. Due to the high solubility of most vinyl monomers in CO<sub>2</sub>, emulsion polymerization in CO<sub>2</sub> probably will not be suitable for the majority of commercially important monomers.

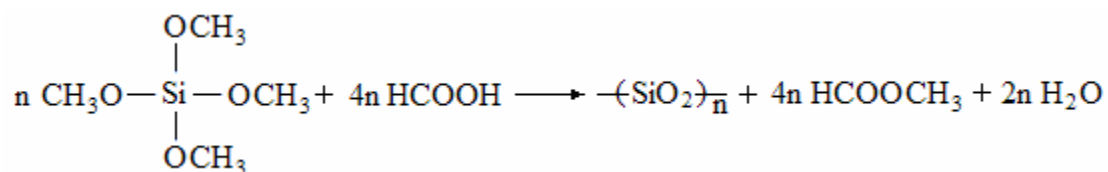
As the surfactant plays a key role in successful dispersion or emulsion polymerization, and traditional surfactants designed for emulsion and dispersion polymerizations in an aqueous or organic continuous phase are not applicable in CO<sub>2</sub>, specific surfactants are required for dispersion or emulsion polymerization in scCO<sub>2</sub>. In

general, an effective surfactant contains a CO<sub>2</sub>-philic group which is highly soluble in CO<sub>2</sub> and an anchor group which is adsorbed to the surface of the polymer particles.<sup>42</sup> In the case of different block surfactants, the anchor soluble balance (ASB) of the stabilizers is the crucial parameter affecting the efficacy of the stabilization and the kinetics of the polymerization process.<sup>27</sup> Johnston *et al*<sup>43</sup> reported that there existed significant effect of stabilizers on the particle formation stage in dispersion polymerization of methyl methacrylate in scCO<sub>2</sub>. In addition to the work and expense associated with designing and adding these surfactants or stabilizers, costly purification of the polymer synthesized from suspension, dispersion, or emulsion polymerization is often necessary for applications where clean polymer or polymer derivative is desired.<sup>44</sup>

For step-growth polymerization in scCO<sub>2</sub>, there are two significant features that make melt-phase condensation reactions performed in scCO<sub>2</sub> advantageous: easier processing and higher molecular weight materials. In order to obtain high molecular weight material, many condensation polymerizations are conducted in the melt phase in the absence of organic solvents, resulting in the high viscosity of the high molecular weight polymer. As CO<sub>2</sub> is able to plasticize the polymer melt phase, it increases the free volume of the melt and lowers the melt viscosity. As a result, good processability can be achieved. On the other hand, condensation polymerizations are driven by the removal of the small molecule condensate. Since CO<sub>2</sub> is capable of plasticizing the polymer and solubilizing the small molecule condensate, it can assist in the removal of the condensate from the reactor, resulting in better reaction kinetics.

Another remarkable application of CO<sub>2</sub> in step-growth polymerization is sol-gel polymerization. The sol-gel process is important for producing amorphous, porous

silica and polysilsesquioxane gels.<sup>45</sup> Shrinkage and cracking during the drying of monolithic sol-gels have limited their commercial applications. A promising processing route to avoid shrinkage and cracking is the avoidance of capillary forces associated with air-drying by drying above the critical temperature and critical pressure of the solvent,<sup>46, 47</sup> resulting in aerogels that retain more of the original volume of the wet gel. As CO<sub>2</sub> is a non-polar medium, sol-gel polymerization in scCO<sub>2</sub> cannot use standard formulations due to the large quantities of water needed for hydrolysis and condensation of the alkoxy silane monomers. The low miscibility of water and CO<sub>2</sub> was avoided by using the “water-free” sol-gel polymerization technique.<sup>48</sup> Alkoxy silanes react with anhydrous formic acid to give silanols that condense to give siloxane bonds necessary for creating a network polymer that will form a gel.<sup>45</sup> The alcohol produced is converted to the formate ester (Scheme 1.1). Supercritical CO<sub>2</sub> and formic acid are completely miscible at the temperatures and pressures used in the experiments. Sui<sup>38</sup> reported that formic and acetic acids gave a slow polymerization rate of silicon alkoxides and minimized the rate of the precipitation and agglomeration of the polycondensate particles. A submicron particle size range was obtained by depressurization of the sol-gel solution inside the reaction vessel, while the rapid expansion of supercritical solutions process was found to yield particles in the size range of approximately 100nm, as shown in Figure 1.2.



**Scheme 1.1** “Water-free” sol-gel polymerization technique used in scCO<sub>2</sub><sup>45</sup>

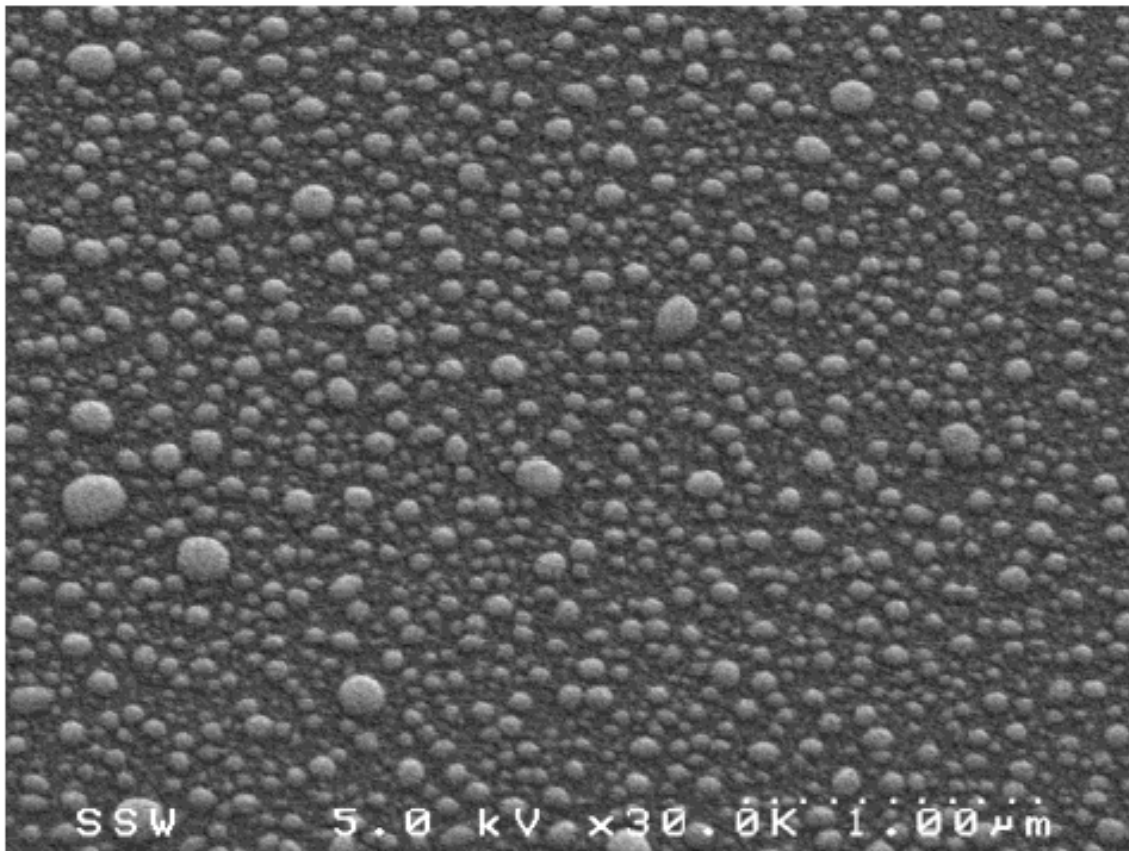


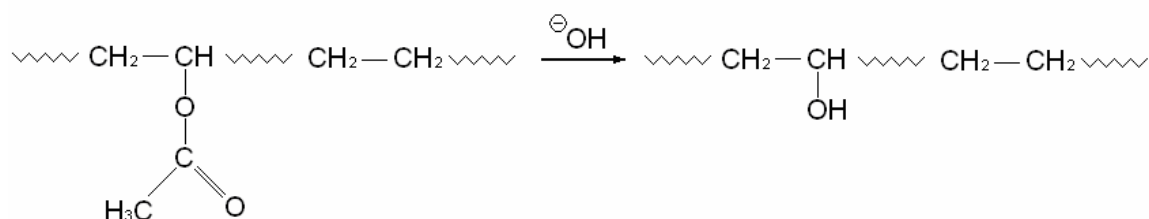
**Figure 1.2** SEM of silica aerogel powder collected using the rapid expansion of supercritical solutions process. The experimental conditions are TEOS/HAc= 1:4, T=60°C, P=41.4MPa.<sup>38</sup>

In addition, scCO<sub>2</sub> can be used as porogenic solvent to produce porous polymer materials. Wood *et al*<sup>49</sup> prepared macroporous polymer beads by suspension polymerization using supercritical CO<sub>2</sub> as the porogenic solvent. The porosity in the beads could be controlled by varying the CO<sub>2</sub> density.

### **1.1.2. Copolymerization of Ethylene and Vinyl Acetate**

Poly(ethylene-co-vinyl acetate) (PEVA) is a polyolefin copolymer as shown in Scheme 1.2. PEVA resembles polyethylene but has considerably increased flexibility with elastomeric properties. The mechanical and thermal properties of PEVA depend on the vinyl acetate content, and also on the polymerization process. As a representative

semi-crystalline random copolymer, PEVA is a typical amphoteric polymer composed of hydrophobic and hydrophilic segments, and its physical and mechanical properties are expected to vary widely with the copolymer composition. For instance, the ethylene-vinyl acetate (EVA) copolymers become completely amorphous when the VAc content exceeds 50wt%.<sup>50</sup> For low VAc content PEVA, the incorporation of VAc into the polyethylene backbone increases the polarity and clarity of the polymer films while reducing the crystallinity and stiffness.<sup>51</sup> So it is widely used in thermoplastic applications and as hot-melt adhesives, films, and surgical gloves, etc. Copolymers containing 2 ~ 18% VAc are well-recognized materials in the film industry. Medium VAc content PEVA can be used for drug release related specialty applications due to its good chemical stability, biocompatibility, and inertness. High VAc content PEVA is used in paint, adhesive, and coating applications as the incorporation of ethylene decreases the brittleness, rigidity, and hardness of poly(vinyl acetate) (PVAc). Hydrolysis of PEVA yields poly(ethylene-co-vinyl alcohol) (Scheme 1.2), which has exceptional gas barrier properties as well as oil and organic solvent resistance and is used for containers.

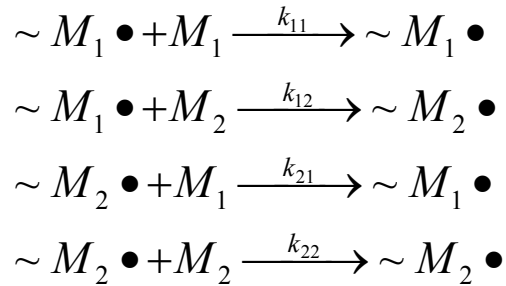


**Scheme 1.2** Hydrolysis of PEVA to form poly(ethylene-co-vinyl alcohol)

For the synthesis of PEVA, ethylene and VAc are usually copolymerized by means of free radical polymerization in continuous high-pressure reactors (upwards of

345MPa), either autoclave or tubular, followed by batch processing to remove residual monomer. Volatile organic compounds (VOCs) such as heptane are often used in a solvent based process. Hence, it is desirable to conduct the copolymerization in scCO<sub>2</sub> so as to make use of the advantages of scCO<sub>2</sub> in polymerization and to synthesize PEVA copolymer for biological and nanotechnological applications. As the VAc content has a significant effect on the properties of PEVA copolymer, it is extremely important to control the distribution of monomer sequence lengths in the copolymer chains.

By assuming that the chemical reactivity of the propagating chain in a copolymerization of monomers M<sub>1</sub> and M<sub>2</sub> is dependent on the monomer unit at the end of the chain (referred to as the first order Markov or terminal model of copolymerization<sup>52</sup>), the following four chain growth steps are possible:



**Scheme 1.3** Propagation steps of copolymerization of monomer M<sub>1</sub> and M<sub>2</sub>

From these four reactions, it can be derived

$$\frac{d[M_1]}{d[M_2]} = \frac{k_{11}[\sim M_1 \bullet][M_1] + k_{21}[\sim M_2 \bullet][M_1]}{k_{12}[\sim M_1 \bullet][M_2] + k_{22}[\sim M_2 \bullet][M_2]} \quad (1-1)$$

where [M<sub>1</sub>], [M<sub>2</sub>], [~M<sub>1</sub>•], and [~M<sub>2</sub>•] are the concentrations (mol·L<sup>-1</sup>) of M<sub>1</sub> monomer, M<sub>2</sub> monomer, ~M<sub>1</sub>• radical, and ~M<sub>2</sub>• radical, respectively, and k<sub>11</sub>, k<sub>12</sub>, k<sub>21</sub>, and k<sub>22</sub> are the propagation rate constants for ~M<sub>1</sub>• radical adding M<sub>1</sub> monomer, ~M<sub>1</sub>• radical



adding  $M_2$  monomer,  $\sim M_2\bullet$  radical adding  $M_1$  monomer, and  $\sim M_1\bullet$  radical adding  $M_2$  monomer, respectively. If a steady-state concentration is assumed for each of the reactive species  $\sim M_1\bullet$  and  $\sim M_2\bullet$  separately (i.e., their rates of interconversion are equal), the copolymerization equation (usually referred to as the Mayo-Lewis equation)<sup>53, 54</sup> can be obtained:

$$\frac{d[M_1]}{d[M_2]} = \frac{[M_1]}{[M_2]} \cdot \frac{r_1[M_1] + [M_2]}{[M_1] + r_2[M_2]} \quad (1-2)$$

where the reactivity ratios are defined in terms of the rate constants for the propagation steps as:

$$r_1 = \frac{k_{11}}{k_{12}} \quad (1-3)$$

$$r_2 = \frac{k_{22}}{k_{21}} \quad (1-4)$$

The copolymerization equation can also be expressed in terms of mole fractions instead of concentrations:

$$F_1 = \frac{r_1 f_1^2 + f_1 f_2}{r_1 f_1^2 + 2 f_1 f_2 + r_2 f_2^2} \quad (1-5)$$

where  $f_1 = 1 - f_2 = \frac{[M_1]}{[M_1] + [M_2]}$  (1-6)

$$F_1 = 1 - F_2 = \frac{d[M_1]}{d[M_1] + d[M_2]} \quad (1-7)$$

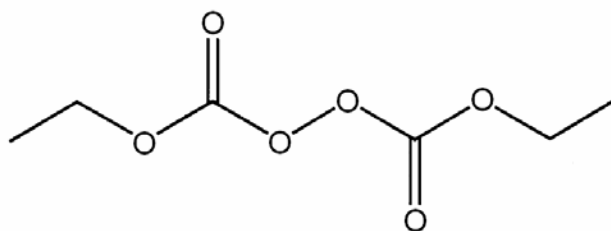
Although the above derivation of copolymerization equation involves the steady-state assumption, the same equation can also be obtained by a statistical approach without invoking steady-state conditions.<sup>55, 56</sup>

PEVA copolymer chains comprise ethylene and VAc in a distribution of sequence lengths which depend on the monomer feed ratio ( $[Ethylene]/[VAc]$ ) and the reactivity ratios ( $r_{ethylene}$  and  $r_{VAc}$ ) which reflect the inherent tendencies of a radical to react with its own monomer relative to the comonomer. In light of the copolymerization equation (Eqn. 1-2), the reactivity ratios  $r_1$  and  $r_2$  can be determined experimentally by means of measuring the copolymer composition for several different comonomer feed compositions.

The reactivity ratios for copolymerization of ethylene and VAc have been studied by several investigators including Van der Meer *et al*<sup>57, 58</sup>, German *et al*<sup>59</sup>, Erusalimskii *et al*<sup>60</sup>, Terteryan *et al*<sup>61</sup>, and Burkhart *et al*<sup>62</sup>, etc. Due to the different reaction conditions (temperature, pressure, and reaction medium) and analytical methods, the determined reactivity ratios are different, with  $r_{ethylene}$  ranging from 0.16 to 1.07 while  $r_{VAc}$  ranges from 1.00 to 3.70. Although PEVA was synthesized via dispersion polymerization in CO<sub>2</sub> by Canelas *et al*<sup>63</sup>, no study on the monomer reactivity ratios for the copolymerization of ethylene and VAc in scCO<sub>2</sub> has been reported in the literature. Hence, it is necessary to study the kinetics of the copolymerization of ethylene and VAc in scCO<sub>2</sub> in order to promote the industrial application of the “green” solvent scCO<sub>2</sub> in the production of PEVA.

As for initiators used in polymerizations in scCO<sub>2</sub>, 2,2'-azobis(isobutyronitrile) (AIBN) has been mostly employed. The decomposition kinetics of AIBN in scCO<sub>2</sub> was studied by Guan *et al*<sup>8</sup>. Other initiators, whose decomposition kinetics has been studied in dense CO<sub>2</sub> or scCO<sub>2</sub>, are bis(perfluoro-2-N-propoxypropionyl) peroxide<sup>64, 65</sup>, bis(trifluoroacetyl) peroxide<sup>65</sup>, and diethyl peroxydicarbonate (DEPDC)<sup>66</sup>. Dialkyl

peroxydicarbonates have been reported as low temperature sources of alkoxy radicals<sup>67, 68</sup> and these radicals may be formed in relatively inert media<sup>69</sup>. In this research, DEPDC (see Scheme 1.4) was selected as the initiator due to its relative ease of synthesis, its solubility in scCO<sub>2</sub>, its ability to initiate a polymerization at relatively low temperature, and previous examination of its reaction kinetics.<sup>66</sup> ScCO<sub>2</sub> has a gas-like viscosity and a very low dielectric constant, which can affect the kinetics of initiator decomposition.<sup>8, 64</sup> Understanding the kinetics of decomposition of DEPDC in scCO<sub>2</sub> is very important for the application of DEPDC in polymerizations in scCO<sub>2</sub>. On the other hand, the decomposition mechanism is also important for the applications of the synthesized copolymer PEVA. It is necessary to know what remains in the polymer chain from the decomposition of an initiator, particularly whether the remainder is toxic or degradable for applications in the biological field.



**Scheme 1.4** Structural diagram of DEPDC

### 1.1.3. Polymer Nanocomposites

Polymer nanocomposites are commonly defined as the combination of a polymer matrix resin and inclusions that have at least one dimension (i.e. length, width, or thickness) in the nanometer size range. By integrating two or more materials with complementary properties, inorganic/organic hybrids offer the potential to perform at a

level far beyond that of the constituent materials. Based on the end-use application, different types of nanoparticles are needed to provide the desired effect. The most commonly used nanoparticles in the literature include montmorillonite organoclays, carbon nanofibers, carbon nanotubes, nanosilica, nanoaluminum oxide, and nanotitanium oxide, etc.<sup>70</sup> A defining feature of polymer nanocomposites is that the small size of the fillers leads to a dramatic increase in the interfacial area as compared to traditional composites.<sup>71</sup> Due to the substantially small size and significantly high surface-to-volume ratio of nanoscale fillers, polymer nanocomposites have ultra-large interfacial area per volume, and the distances between the polymer and the filler components are extremely short. In contrast to traditional polymer composites where reinforcement is on the order of microns or above, polymer nanocomposites benefit from the synergy between filler particles and polymer chains that are on similar length scales, and the large quantity of interfacial area relative to the volume of the material.<sup>72</sup> As a result, the strong molecular interaction between the polymer and the nanoparticles gives polymer nanocomposites unique material properties. Multifunctional features attributable to polymer nanocomposites include improved mechanical properties (tensile strength, stiffness, and toughness), gas barrier properties, thermal stability, fire retardancy, chemical resistance, and charge dissipation, etc.<sup>70</sup>

There are many methods for the synthesis of polymer nanocomposites including solution intercalation, melt intercalation, roll milling, *in situ* polymerization, emulsion polymerization, and high-shear mixing.<sup>70</sup> To synthesize polymer nanocomposites, one important aspect is the incorporation of nanoparticles into the polymer matrix. Due to the large surface area per particle volume and the extremely

small size, it is difficult to overcome the inherent thermodynamic drive of nanoparticles to aggregate. Even well-dispersed nanoparticles naturally aggregate to form clusters whose size extends to length scales exceeding 1  $\mu\text{m}$ .<sup>73</sup> As a result, the major challenge for synthesizing polymer nanocomposites is learning how to disperse nanoparticles into a polymer matrix and avoid aggregation of the nanoparticles. Excellent dispersion and interfacial load transfer are usually required to achieve optimum properties of the synthesized polymer nanocomposites.

A common strategy to increase the probability of isotropic dispersion is to modify the surface of the nanoscale filler to increase favorable interactions between the nanofiller and the polymer matrix while minimizing the inter-filler attraction.<sup>72</sup> The technical approach is to bind small molecules or polymer ligands to the surface of the nanofiller. In addition, supercritical carbon dioxide can effectively swell and plasticize the amorphous region of the polymers and be released from the polymers simply by depressurization. Small molecules dissolved in  $\text{scCO}_2$  can be infused and deposited into a polymer matrix exposed to such a solution. Supercritical  $\text{CO}_2$  enhances the clay dispersion and polymer intercalation into clay nanoparticles, even when favorable intercalation between the polymer and the clay are not present, as in the case of purely hydrophobic polymers.<sup>74, 75</sup> It is challenging to synthesize polyolefin-based nanocomposites because polyolefins interact only weakly with clay surfaces. By impregnating tetraethyl orthosilicate (TEOS) into polypropylene matrix using  $\text{scCO}_2$  as a swelling agent and carrier followed by hydrolysis/condensation reaction of TEOS confined in polymer network, Sun and co-workers<sup>76</sup> synthesized silica-polypropylene nanocomposites.

In this interesting and challenging field of the synthesis of polymer nanocomposites, not only can  $\text{scCO}_2$  help disperse nanofillers into the polymer matrix and facilitate the supercritical drying step, but it can also work as a reaction medium to replace VOCs. Recent years have seen a growing tendency to develop “green” chemistry and “green” engineering. As  $\text{scCO}_2$  has shown a successful application in sol-gel polymerization to make nanoparticles, it is desirable and becomes feasible to synthesize polymer nanocomposites with fewer steps and better dispersion by using  $\text{scCO}_2$ . In this research, a one-pot technique was developed to synthesize  $\text{SiO}_2$ -PVAc nanocomposites in  $\text{scCO}_2$ . With this technique, the polymerization of VAc and the formation of spherical  $\text{SiO}_2$  nanoparticles took place simultaneously in the “green” solvent  $\text{scCO}_2$ . Excellent dispersion of the  $\text{SiO}_2$  nanoparticles into the polymer matrix was achieved by direct coupling of  $\text{SiO}_2$  nanoparticles to polymer chains while the “green” features were fully demonstrated which potentially provide a significant reduction in labor, time, cost, and waste.

#### **1.1.4. Quantum Dots**

One of the most interesting polymer nanocomposites is light-selective nanofilm. Light-selective, also called spectrally selective, refers to the ability of a film to emit and subsequently transmit desirable light while blocking out undesirable light and heat. Light-selective nanofilms can be used for greenhouse and as window films for sunlight control. Light-selective nanofilms can be obtained by incorporating organic fluorophores or inorganic fluorophores (luminescent quantum dots) into some transparent polymer matrices.

Quantum dots (QDs) are nanometer-sized semiconducting materials whose excitons are confined in all three spatial dimensions.<sup>77</sup> When the quantum dots are irradiated by light from an excitation source to reach respective energy excited states, they emit energies corresponding to the respective energy band gaps. The advantages of QDs over conventional organic fluorescent dyes include large absorption bands, narrow spectral emission bands, and photochemical stability.<sup>78</sup> Moreover, the spectral properties are tunable by varying the size (Figure 1.3) and type (Figure 1.4) of the QDs.

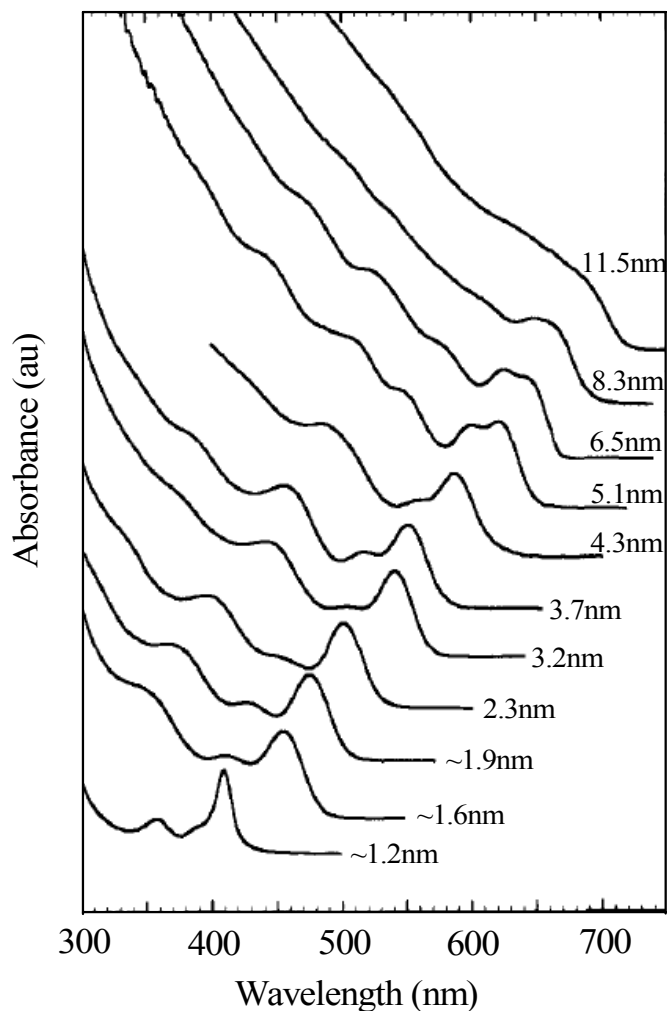


**Figure 1.3** Room temperature optical absorption spectra of CdSe nanocrystallites dispersed in hexane and ranging in size from ~1.2 to 11.5 nm.<sup>79</sup>

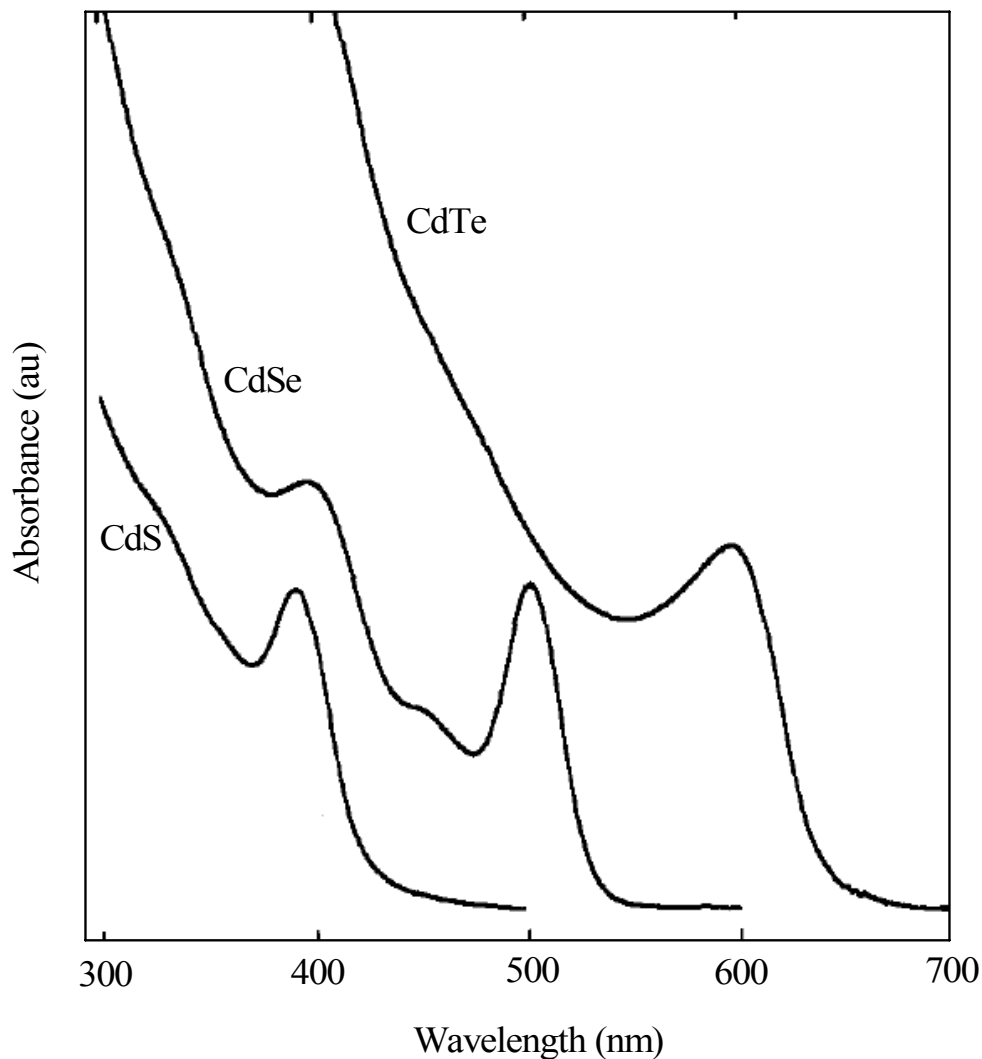
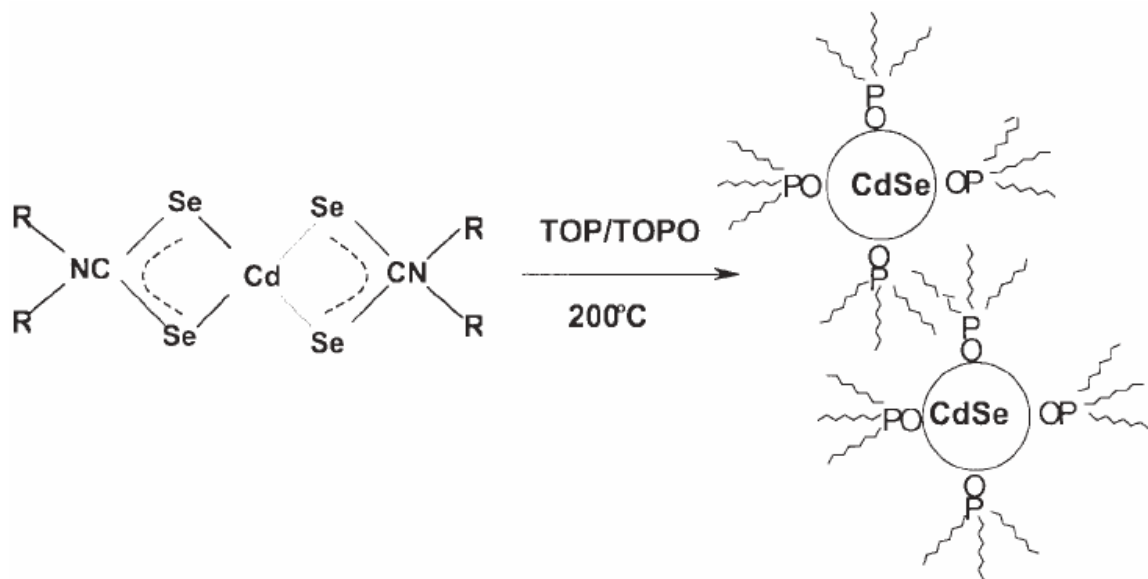


**Figure 1.4** Room temperature optical absorption spectra of  $\sim$ 2-3nm diameter CdS, CdSe, and CdTe crystallites.<sup>79</sup>

Colloidal nanocrystal QDs consist of an inorganic nanoparticle surrounded by a layer of organic ligands. The synthesis of colloidal quantum dots is based on a three-component system composed of precursors, organic surfactants, and solvents. The precursors transform into monomers when heated to a sufficiently high temperature. Once the monomers reach a high enough super saturation level, the nanocrystal growth starts with a nucleation process. Pickett and O'Brien<sup>80</sup> synthesized semiconductor



nanoparticles using single-molecular precursors that decomposed in a high boiling point coordinating solvent (Lewis base) such as trioctylphosphine oxide (TOPO), as shown in Scheme 1.5.



**Scheme 1.5** The preparation of CdSe nanoparticles capped with TOPO by using bis(dialkyldithio-carbamate) cadmium(II)<sup>80</sup>

The surface chemistry of the QDs has to be compatible with the polymer matrix in order to obtain good dispersion of the QDs throughout the matrix during the synthesis of QD-polymer nanocomposites. The synthesis of QDs is usually carried out under anaerobic condition at high temperature which is not compatible with most organic functional groups. Hence, functionalization of the surface of QDs, i.e., ligand exchange, is usually required before being incorporated into a polymer matrix. For the synthesis of QD-polymer nanocomposites, an effective ligand should contain a coordination “head” and a polymerizable “tail” in order to connect the QDs with polymer chains.<sup>81</sup>

## 1.2. Research Objectives

The objectives of this research were to conduct a comprehensive study on the copolymerization of ethylene and vinyl acetate in the “green” solvent  $\text{scCO}_2$  and the synthesis of PEVA based nanocomposites by using  $\text{scCO}_2$ . The objectives consist of the following four parts:

- (1). To study reaction kinetics and mechanism of thermal decomposition of the initiator DEPDC in  $\text{scCO}_2$ ;
- (2). To determine monomer reactivity ratios for the copolymerization of ethylene and vinyl acetate in  $\text{scCO}_2$ ;
- (3). To develop a “green” route for synthesizing  $\text{SiO}_2$ -PVAc nanocomposites by using  $\text{scCO}_2$ ;
- (4). To synthesize light-selective QD-PEVA nanofilms by using  $\text{scCO}_2$ .

## 1.3. Thesis Structure

This thesis is focused on developing a new route for synthesizing the widely commercialized copolymer, PEVA, by using the environmentally benign solvent,  $\text{scCO}_2$ . As an effort to extend the applications of PEVA synthesized using  $\text{scCO}_2$ , much work was contributed to designing a novel one-pot route to synthesize  $\text{SiO}_2$ -PVAc nanocomposites using  $\text{scCO}_2$  and inventing light-selective QD-PEVA nanofilms.

Chapter 1 provides a general review of polymerizations in  $\text{scCO}_2$ , free radical copolymerization of ethylene and vinyl acetate, polymer nanocomposites, and quantum dots. It also includes the objectives of this research.

Chapter 2 introduces the experimental setup and the major characterization methods employed in this research.

Chapter 3 presents the investigations of thermal decomposition of the initiator DEPDC in scCO<sub>2</sub>. The initiator DEPDC was first synthesized and then the kinetics and mechanism of decomposition of DEPDC were studied using high-pressure *in situ* FTIR and off-line nuclear magnetic resonance (NMR).

In Chapter 4, monomer reactivity ratios for the copolymerization of ethylene and vinyl acetate in scCO<sub>2</sub> were determined using *in situ* FTIR and compared with the results obtained from off-line <sup>1</sup>H NMR.

In Chapter 5, a one-pot route for the synthesis of SiO<sub>2</sub>-PVAc in scCO<sub>2</sub> was developed. During the synthesis, PVAc and silica nanoparticles were formed simultaneously while vinyltrimethoxysilane (VTMO) was used as a linker to attach the nanoparticles to the polymer chains. This technique features excellent dispersion of nanoparticles into the polymer matrix, and both potential energy-saving and waste-reduction improvements.

Chapter 6 describes the synthesis of light-selective QD-PEVA nanofilms in scCO<sub>2</sub>. CdS and CdS/ZnS core/shell QDs were first synthesized and then functionalized with 3-mercaptopropyl trimethoxysilane (MPTMO). A terpolymer of ethylene, vinyl acetate, and VTMO was synthesized in scCO<sub>2</sub> through free radical polymerization. The functionalized QDs were linked to PEVA chains by hydrolysis in scCO<sub>2</sub>. The synthesized QD-PEVA nanofilms showed strong absorption of short-wavelength lights and the characteristic light emission of long-wavelength lights, hence being attractive for sunlight control.

Chapter 7 provides a general conclusion of the above studies and recommendations for future work on the synthesis of PEVA and polymer nanocomposites in scCO<sub>2</sub>.

## **Chapter 2. Experimental and Characterization Methods**

## 2.1. Outline

The thermal decomposition of DEPDC, polymerization of vinyl acetate, copolymerization of ethylene and vinyl acetate, and synthesis of polymer nanocomposites were carried out in a stainless steel autoclave, with *in situ* attenuate total reflection Fourier transform infrared spectroscopy (ATR-FTIR) used for monitoring the processes.

The major instrumental analysis techniques used for characterizing the decomposition products, synthesized polymer and polymer nanocomposites, and QDs include: ATR-FTIR spectroscopy, ultraviolet-visible spectroscopy (UV-Vis), nuclear magnetic resonance spectroscopy (NMR), thermogravimetric analysis (TGA), transmission electron microscopy (TEM), energy dispersive X-ray spectroscopy (EDX), and photoluminescence (PL).

## 2.2. Experimental Setup

Figure 2.1 displays a schematic diagram of the reactor used in this research. CO<sub>2</sub> and ethylene (if required) were pumped into the reactor using syringe pumps (ISCO 260D and 100DX, respectively). Both the pumps were controlled with an ISCO (Series D) pump controller. All feed lines had check valves to prevent backflow and a rupture disk (rating at 34.5MPa) was installed in the reactor for safety protection in case of over pressurization. The reactor is a 100-mL high-pressure stainless steel autoclave (Parr Instruments) coupled with a digital pressure transducer (Ashcroft K25F) and a thermocouple (Parr-A472E2), with a turbine impeller installed to provide mixing of ingredients. The reactor was heated with a Glas-Col<sup>®</sup> heating mantle while a digital

controller (Parr 4842) was used for controlling the reaction temperature and stirring speed and displaying the reaction pressure.

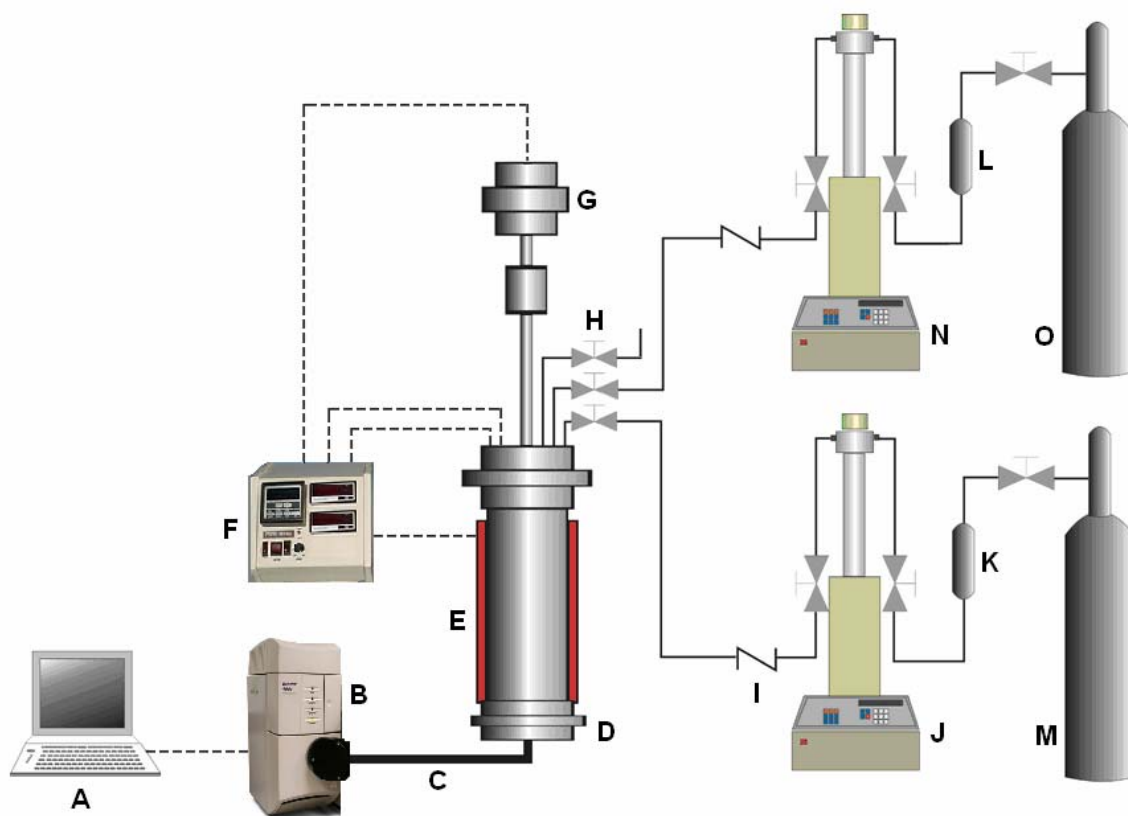


**Figure 2.1** Schematic diagram of experimental setup.

(A) Computer; (B) FTIR; (C) K4 conduit; (D) 100-mL stainless steel autoclave equipped with IR probe; (E) heating mantle; (F) Parr 4842 temperature and stirring speed controller with pressure display; (G) stirrer; (H) needle valve; (I) check valve; (J) ISCO 260D syringe pump; (K) & (L) purification columns; (M) CO<sub>2</sub> cylinder; (N) ISCO 100DX syringe pump; (O) ethylene cylinder.

*In situ* FTIR monitoring of the solution concentration in the stirred 100-mL high-pressure autoclave was performed using a high-pressure immersion probe (Sentinel-Mettler Toledo AutoChem). The DiComp ATR probe consists of a diamond wafer, a gold seal, a ZnSe support/focusing element, housed in alloy C-276. The probe was attached to an FTIR spectrometer (Mettler Toledo AutoChem ReactIR 4000) via a mirrored optical conduit, connected to a computer, supported by ReactIR 2.21 software (MTAC). This

system uses a 24-hour HgCdTe (MCT) photoconductive detector. The light source is a glow bar from which the interferometer analyzes the spectral region from 650-4000 $\text{cm}^{-1}$ . The beamsplitter inside the RIR4000 is ZnSe.

## **2.3. Characterization Methods**

### **2.3.1. ATR-FTIR Spectroscopy**

Infrared (IR) spectroscopy is one of the most common spectroscopic techniques used in chemical analysis. Infrared radiation is that part of the electromagnetic spectrum between the visible and microwave regions, spanning wavelengths from 800 to 1,000,000nm. The IR region is commonly divided into three smaller areas: near IR, mid IR, and far IR. The portion of the IR region most useful for the analysis of organic compounds is mid IR ranging from 2,500 to 16,000nm. This portion of the IR region lies in the same frequency range as a vibrating molecule. When the frequency of a specific vibration is equal to the frequency of the IR radiation directed on the molecule, the molecule absorbs the radiation which is then converted into energy for molecular vibration, by either stretching or bending. Different types of bonds, and thus different functional groups, absorb IR radiation of characteristic wavelengths. By measuring changes in transmittance (or absorption) intensity as a function of frequency, IR spectroscopy can be used to identify the chemical functional groups in the sample.

Fourier transform infrared spectroscopy (FTIR) is a measurement technique for collecting infrared spectra. Instead of recording the amount of energy absorbed when the frequency of the infrared light is varied, the IR light is guided through an interferometer. A time-domain interferogram is recorded by a detector after the light passes the sample.<sup>82</sup>



Performing a mathematical Fourier transform on the interferogram results in a frequency-domain IR spectrum identical to that from conventional (dispersive) infrared spectroscopy. Fourier transform spectrograph is more sensitive and has a much shorter sampling time than conventional spectroscopic techniques.

Attenuated total reflectance (ATR) is a sampling technique used in conjunction with infrared spectroscopy which enables samples to be examined directly in the solid or liquid state without further preparation. Traditionally, IR spectrometers have been used to analyze solids, liquids and gases by means of transmitting the IR radiation directly through the sample. Sample preparation of solid and liquid samples is very important for good spectral reproducibility. The ATR technique has revolutionized solid and liquid sample analyses through faster sampling, improved sample-to-sample reproducibility, and minimizing user-to-user spectral variation.

An ATR accessory operates by measuring the changes that occur in a totally internally reflected IR beam when the beam comes into contact with a sample (see Figure 2.2). An infrared beam is directed onto an optically dense crystal with a high refractive index at a certain angle. This internal reflectance creates an evanescent wave that extends beyond the surface of the crystal into the sample held in contact with the crystal. This evanescent wave protrudes only a few micrometers ( $0.5 \sim 5\mu\text{m}$ ) beyond the crystal surface and into the sample. Consequently, there must be good contact between the sample and the crystal surface. In regions of the infrared spectrum where the sample absorbs energy, the evanescent wave will be attenuated or altered. The attenuated energy from each evanescent wave is passed back to the IR beam, which then exits the opposite

end of the crystal and is passed to the detector in the IR spectrometer. The system then generates an infrared spectrum.

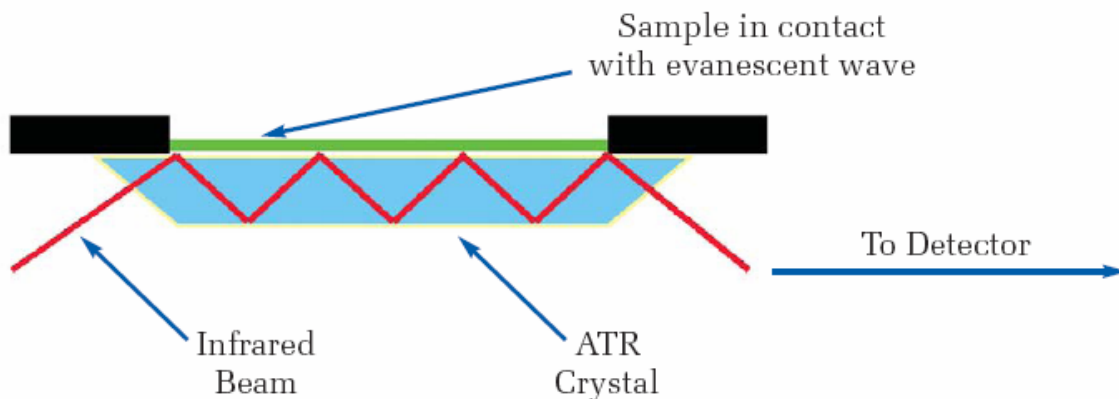


**Figure 2.2** Schematic diagram of multiple reflection ATR system.

### 2.3.2. Ultraviolet-Visible Spectroscopy

Ultraviolet-Visible spectroscopy involves the absorption of UV-Visible light. UV light is electromagnetic radiation with wavelengths ranging from 190 to 400nm and visible light has wavelengths ranging from 400 to 800nm.<sup>82</sup> UV-Visible light provides the energy to cause the promotion of an electron from a ground electronic state to an excited electronic state. UV-Vis is routinely used in the analysis of materials containing transition metal ions and highly conjugated organic compounds.

For application of UV-Vis in the analysis of semiconductors, the absorption occurs once the photon energy is sufficient to promote electrons from the valence band to the conduction band. As seen in Figures 1.3 and 1.4, the absorption peak appears in a UV-Vis spectrum at the wavelength of light that has the corresponding photon energy. The band gap of QDs can then be determined from the UV-Vis spectrum by using the de

Broglie's equation<sup>83</sup>. Hence, UV-Vis spectroscopy is widely used for measuring the band gap of semiconductors.

### **2.3.3. Nuclear Magnetic Resonance Spectroscopy**

Nuclear magnetic resonance spectroscopy is an instrumental spectroscopic technique which exploits the magnetic properties of certain nuclei to determine the structure of organic compounds. Compared with other instrumental techniques, NMR spectroscopy not only makes it possible to identify the functionality at a specific carbon atom but also allows us to determine what the neighboring carbon atoms look like.<sup>84</sup>

NMR spectroscopy is based upon the measurement of absorption of radio frequency (RF) radiation by a nucleus in a strong magnetic field. When a nucleus with a non-zero spin is placed in a magnetic field, the nuclear spin can align either in the same direction (lower energy state) or in the opposite direction (higher energy state) as the field. The energy difference between the two energy states is in the range of radio frequency. A radio frequency generator "pulses" the sample with a short burst of radio waves. Absorption of the radio frequency radiation causes the nuclear spin to realign or flip in the higher-energy direction. After absorbing energy the nuclear will re-emit RF radiation of the same frequency and return to the lower-energy state. The absorption intensity is detected by a radio frequency receiver and then an NMR spectrum is generated. In the widely used Fourier transform nuclear magnetic resonance (FT-NMR), all the excited nuclei will re-emit RF radiation at their respective resonance frequencies, creating an interference pattern in the resulting RF emission versus time, known as free-induction

decay (FID). The frequency-domain NMR spectrum is then extracted from the FID by a Fourier transform of the time-domain data.

Different nuclei resonate at different frequencies. The same nuclear in different environments flip at different frequencies. The precise resonant frequency of the energy transition is dependent on the effective magnetic field at the nuclei. This field is affected by electron shielding which is in turn dependent on the chemical environment. The electrons which surround the spinning nuclei are also charged and spinning. A spinning charge creates a magnetic field which is in opposition to the applied magnetic field. This decreases the magnitude of the applied magnetic field which reaches the nuclei. As a result, different chemical groups containing different density of valence electron show different peaks in the NMR spectra.

The most important applications for polymer chemistry and engineering are  $^1\text{H}$  and  $^{13}\text{C}$  NMR spectroscopy. The number of signals in a ( $^1\text{H}$  or  $^{13}\text{C}$ ) NMR spectrum tells us how many different kinds of (hydrogen or carbon) atoms a sample has while the intensity of the signal in the spectrum tells the quantity of the same kinds of atoms in the sample. Two-dimensional NMR spectra such as correlation spectroscopy (COSY) and heteronuclear single quantum coherence (HSQC) provide significantly more information about a molecule than the conventional (one-dimensional) NMR spectra and are especially useful in determining the structure of a molecule. Figure 2.3 shows a schematic COSY spectrum with two frequency axes of a hypothetical molecule containing just two protons, A and B, which are coupled together. A diagonal of signals (A and B) divides the spectrum in two equal halves. The dots that are not on the diagonal (X) are called cross peaks.<sup>84</sup> Cross peaks indicate pairs of protons that are coupled.

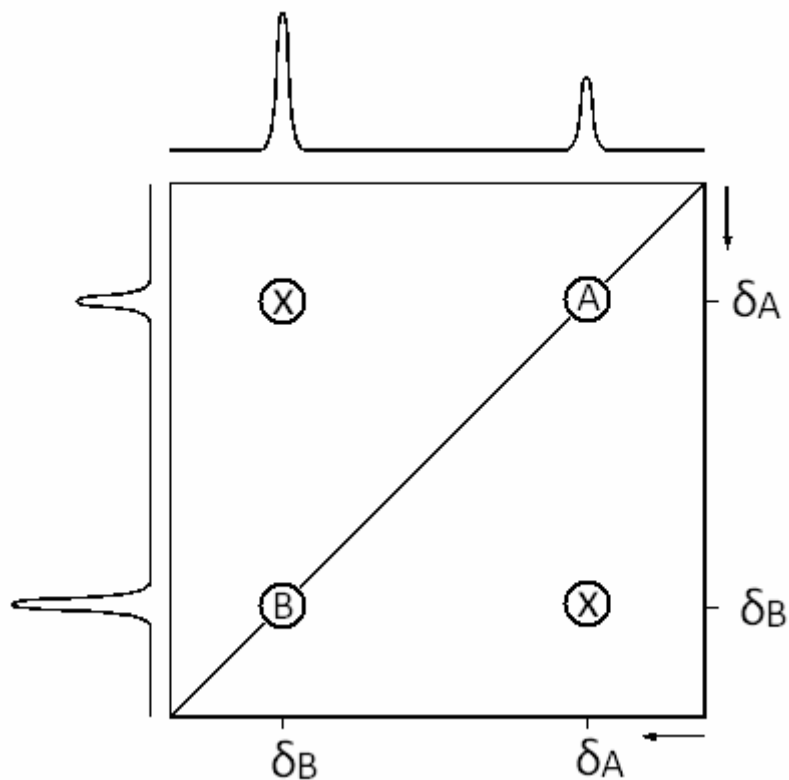


**Figure 2.3** Schematic COSY spectrum for two coupled spins, A and B.

#### 2.3.4. Thermogravimetric Analysis

Thermogravimetric analysis (TGA) is an analytical technique used to determine a material's thermal stability and composition by monitoring the weight change that occurs as a specimen is heated in air or in an inert atmosphere such as nitrogen, helium, or argon. The analyzer usually consists of a high-precision balance with a pan (generally platinum) loaded with the sample. The pan is placed in a small electrically heated oven with a thermocouple to accurately measure the temperature. The atmosphere is usually purged with an inert gas to prevent oxidation or other undesired reactions. A computer is

used to control the instrument. Analysis is carried out by raising the temperature gradually and plotting weight against temperature.

In most cases, TGA is performed with a linear temperature ramp. The maximum temperature is selected so that the specimen weight is stable at the end of the experiment, implying that all chemical reactions are completed. The decomposition temperature can be defined in many ways, including the temperature of the maximum in the weight loss rate  $(d_w/d_T)_{\max}$ , and the weight loss onset temperature ( $T_{\text{onset}}$ ). The former refers to the temperature of the maximum rate of decomposition, while the latter refers to the temperature when the decomposition just begins. However, the former can be easily determined with a derivative weight loss curve.

### **2.3.5. Transmission Electron Microscopy**

A microscope is an instrument for producing a magnified image of a small object. The resolution of a light microscope is limited by the wavelength of light, as lower wavelength light is required for one to be able to see smaller objects. The transmission electron microscope operates on the same basic principles as the light microscope, but uses electrons instead of light. As a result, TEM can be used to resolve objects to the order of a few angstroms. Although some structural features can be revealed by X-ray and neutron diffraction, direct imaging of individual nanoparticles is only possible using TEM and scanning probe microscopy.<sup>70</sup> TEM is used heavily in material science, metallurgy, and biological science.

Figure 2.4 shows a schematic diagram of a TEM instrument. An electron source at the top of the microscope emits a stream of electrons that travel through

vacuum in the column of the microscope. Instead of glass lenses focusing the light in the light microscope, the TEM uses metal apertures and electromagnetic lenses to confine and focus the electrons into a thin, focused, monochromatic beam. The electron beam then travels through an ultra thin specimen and interacts with the specimen as it passes through it. At the bottom of the microscope the unscattered electrons hit a fluorescent screen, which gives rise to a “shadow image” of the specimen with its different parts displayed in varied darkness according to their density, providing information such as structure and composition.

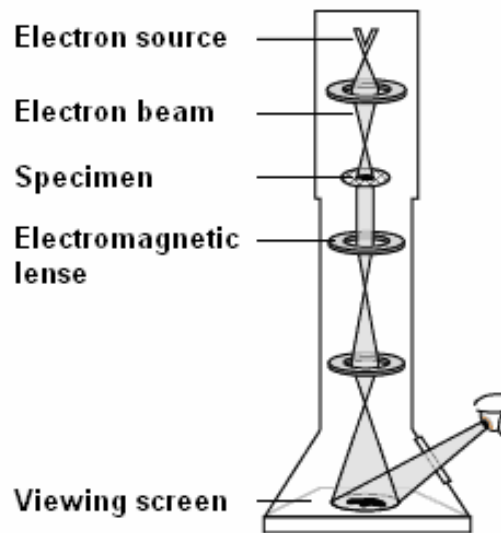


**Figure 2.4** Schematic diagram of a TEM instrument.

High resolution transmission electron microscopy (HRTEM) is an imaging mode of the TEM that allows the imaging of the crystallographic structure of a sample at an atomic scale. It is an invaluable tool to study nanocrystallites such as semiconductors. As the resolution of HRTEM has reached 0.08nm so far, the lattice fringes and d-spacing (typically a few angstroms) of nanocrystallites can be easily observed and measured.

### **2.3.6. Energy Dispersive X-Ray Spectroscopy**

Energy dispersive X-ray spectroscopy (EDX), also known as EDS, is a technique used to identify the elemental composition of a sample or small area of interest on the sample. At rest, an atom within the sample contains ground state (or unexcited) electrons in discrete energy levels or electron shells bound to the nucleus. When a sample is exposed to an electron beam inside a scanning electron microscope (SEM), the incident electron beam may excite an electron in an inner shell, causing it to be knocked out of its orbit while creating an electron hole where the electron was (Figure 2.5). An electron from an outer, higher-energy shell then fills the hole and the difference in energy between the higher-energy shell and the lower energy shell may be released in the form of an X-ray. X-rays emitted from atoms are characteristic of the elements, and the intensity distribution of the X-rays represents the thickness-projected atom densities in the sample.<sup>70</sup> By analyzing the intensity and energy of the emitted X-rays with an energy dispersive spectrometer, the elemental composition of the sample can be determined. Its characterization capabilities are due in large part to the fundamental principle that each element has a unique atomic structure allowing X-rays that are characteristic of an element's atomic structure to be identified uniquely from each other. EDX is a powerful tool for microanalysis of elemental constituents, particularly for heavier elements.



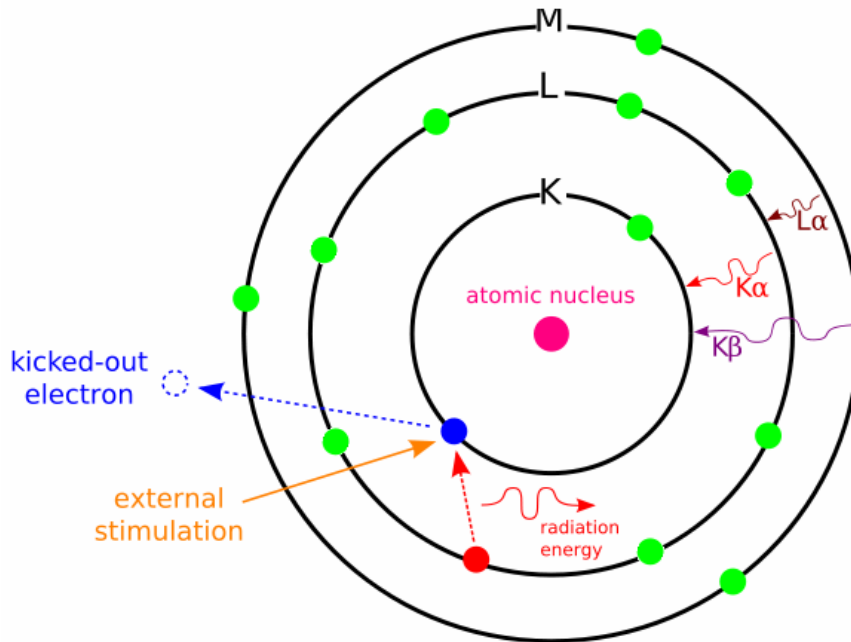


**Figure 2.5** Schematic diagram of EDX.

### 2.3.7. Photoluminescence

Photoluminescence (PL) is a process in which a substance absorbs photons and then re-radiates photons (Figure 2.6). "Photo" refers to light and "luminescence" refers to emission of light. PL is distinguished from other forms of luminescence by photo-excitation. When light is directed onto a sample, it is absorbed and imparts excess energy into the material. One way this excess energy can be dissipated by the sample is through the emission of light, or luminescence. PL spectroscopy is commonly used to probe the electronic structure of materials. The photo-excitation causes the material to jump to a higher electronic state, and then release energy, photons, as it relaxes and returns back to a lower energy level. The energy of the emitted light relates to the difference in energy levels between the two electron states involved in the transition between the excited state and the ground state.

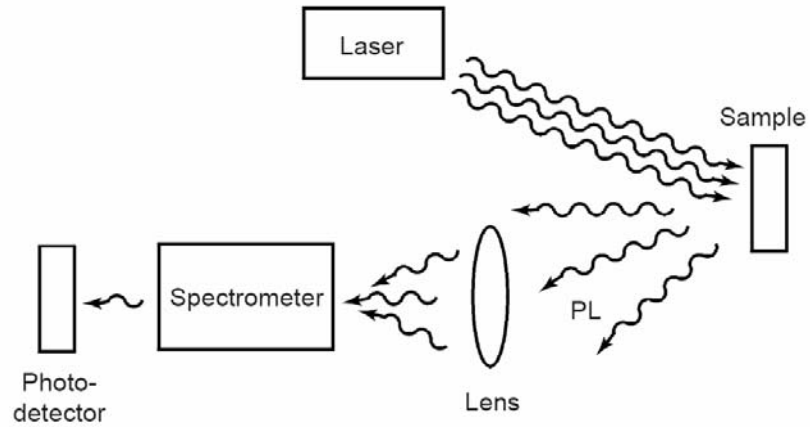


**Figure 2.6** Schematic diagram of PL measurements.

The most common radiative transition in semiconductors is between states in the conduction and valence bands, with the energy difference being known as the band gap. PL is widely used for characterization of light-emitting devices.

**Chapter 3. *In Situ* ATR-FTIR Study of the Thermal Decomposition of  
Diethyl Peroxydicarbonate in Supercritical CO<sub>2</sub>**

This chapter presents the decomposition of diethyl peroxydicarbonate (DEPDC) in the “green” solvent, scCO<sub>2</sub>. *In situ* ATR-FTIR was used to monitor the thermal decomposition of the organic free-radical initiator, DEPDC, in heptane and scCO<sub>2</sub>. The decrease in the characteristic FTIR peaks of DEPDC upon heating was utilized to examine the kinetics of the decomposition of DEPDC. The simultaneously erected FTIR peaks reflected the formation of new compounds during the decomposition. The decomposition mechanism was then proposed based on the experimental observation and analysis of the final products with FTIR and NMR. Part of this chapter is reproduced by permission of Elsevier Ltd. from the published article by the author: *In situ* ATR-FT-IR study of the thermal decomposition of diethyl peroxydicarbonate in supercritical carbon dioxide<sup>85</sup>, in *Polymer*, Copyright [2006] by Elsevier Ltd.

### 3.1. Introduction

Considerable effort has been devoted in recent years to finding environmentally-benign solvents and processes, particularly as a result of increased environmental regulations concerning the use of volatile organic compounds (VOCs)<sup>3, 6, 31, 86-88</sup>. Supercritical carbon dioxide (scCO<sub>2</sub>) has emerged as a viable “green” alternative to organic solvents for several applications, including polymer synthesis, modification, and nanotechnology<sup>89, 90</sup>. In the supercritical state, carbon dioxide can have unique properties such as liquid-like density and gas-like diffusivity, and these properties are “tunable” by varying the pressure and/or temperature<sup>1</sup>. Previously, DeSimone and coworkers have shown that scCO<sub>2</sub> is a promising alternative medium for free-radical, cationic, and step-growth polymerizations<sup>3, 86, 91</sup>. Indeed, DuPont has recently commissioned a plant to manufacture Teflon in scCO<sub>2</sub> by the use of free-radical polymerization<sup>92</sup>. The reasons for the intense industrial interest are that CO<sub>2</sub> is inert to highly electrophilic radicals (i.e., no chain transfer to solvent), inexpensive, non-toxic, non-flammable, and environmentally benign<sup>3</sup>.

In recent years, considerable attention has been attracted to investigate and study the mechanism of free radical formation and the kinetics of the decomposition of organic peroxides<sup>93-102</sup>, particularly due to their applications in organic synthesis<sup>93, 94</sup>, biological processes<sup>95, 96</sup>, polymerization<sup>97, 98</sup>, and as resin modifiers<sup>99</sup>, additives for fuel<sup>100</sup>, and explosives<sup>101</sup>. Free radical polymerization still dominates in the production of many commercial polymers such as polystyrene, polyethylene (low density), poly(ethylene-co-vinyl acetate), Teflon, and other fluorinated polymers. Due to the proven ability of scCO<sub>2</sub> in industrial continuous polymerizations, and a poor

understanding of how CO<sub>2</sub> influences reaction kinetics, a study of the chemistry of the thermal decomposition of the required organic peroxide initiators under supercritical conditions is important to understand and control the polymerizations under these conditions.

Dialkyl peroxydicarbonates (R-O-CO<sub>2</sub>)<sub>2</sub> are used as free radical initiators in many commercial processes such as the large-scale production of polymers and curing resins<sup>93, 99, 102</sup>. Compared with other classes of peroxides, the number of mechanistic studies on the decomposition of dialkyl peroxydicarbonates is relatively small, particularly in “green” solvents. According to the previous studies<sup>97, 103-107</sup>, a general decomposition mechanism of peroxydicarbonates or peroxyesters can be described as direct decomposition of the peroxides through breaking the weak O–O bond. The resulting alkoxy-carboxyl or carbonyloxy radical may either decarboxylate<sup>105-109</sup> or participate in a bimolecular reaction<sup>103, 104</sup>. In addition, solvents may have some influence on the decomposition of peroxydicarbonates as the employed solvent is seldom inert due to the high activity of the formed free radicals. Thermal decomposition of initiators in supercritical CO<sub>2</sub> has been studied by Guan *et al*<sup>8</sup>, Bunyard<sup>64</sup>, Charpentier *et al*<sup>66, 87, 88</sup> and Kadla *et al*<sup>65</sup>. It was reported that the rate constants of initiator decomposition in scCO<sub>2</sub> were different from those in other organic solvents due to its “zero-viscosity”<sup>64</sup> and low dielectric constant<sup>8</sup>. Charpentier *et al*<sup>66</sup> studied the thermal decomposition of diethyl peroxydicarbonate (DEPDC) in scCO<sub>2</sub> in a continuous-stirred-tank reactor (CSTR), wherein reaction kinetics were simulated based on a one-bond radical fission mechanism. However, this study did not harness the power of *in situ* ATR-FTIR.

Hence, the goal of this work was to study the decomposition of a previously studied initiator DEPDC in high pressure scCO<sub>2</sub> and ethylene using high pressure *in situ* ATR-FTIR, and to compare the kinetic decomposition results to previous non-FTIR techniques. Off-line NMR was used as a complementary tool for studying the decomposition mechanism. Understanding the initiator decomposition by ATR-FTIR in scCO<sub>2</sub> is the first step for analyzing more complex spectroscopic data during polymerizations to provide an understanding of the formation of ethylene-vinyl acetate polymers and inorganic/organic hybrids, the focus of the remainder of this thesis.

## **3.2. Experimental**

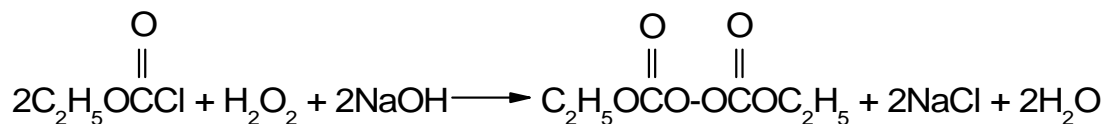
### **3.2.1. Materials**

Polymer grade ethylene (99.99%) was purchased from Matheson Gas Products Canada, and further passed through columns filled with 5Å molecular sieves and reduced 20% copper oxide/Al<sub>2</sub>O<sub>3</sub> to remove moisture and oxygen, respectively. Instrument grade CO<sub>2</sub> (from BOC Gases, 99.99%, with dip-tube) was purified by passing through columns filled with 5Å molecular sieves and reduced 20% copper oxide/Al<sub>2</sub>O<sub>3</sub> to remove moisture and oxygen, respectively. Ultra high purity N<sub>2</sub> (from BOC, 99.99%) was further purified by passing through columns filled with 5Å molecular sieves and reduced 20% copper oxide/Al<sub>2</sub>O<sub>3</sub> to remove moisture and oxygen, respectively. The initiator diethyl peroxydicarbonate (DEPDC) was home-made as described below. Heptane (Aldrich, HPLC grade) was distilled under vacuum. NaOH, 30% H<sub>2</sub>O<sub>2</sub>, ethyl chloroformate, 0.1N sodium thiosulfate solution, sodium bicarbonate, sodium sulfate, glacial acetic acid,

potassium iodine, and diethyl carbonate were purchased from Aldrich and used as received.

### 3.2.2. Preparation of DEPDC Initiator

Distilled water (100mL) was charged in a glass reactor (250mL) equipped with a magnetic agitator and a thermometer. The reactor was cooled to  $\leq 5^{\circ}\text{C}$  in an ice/water bath. Ethyl chloroformate (12mL) and 30%  $\text{H}_2\text{O}_2$  (6.64g) were added to the reactor under powerful stirring. Then NaOH solution (5N, 24mL) was introduced to the reactor dropwise. The reaction was carried out under gentle stirring for 10min with the reaction temperature controlled below  $10^{\circ}\text{C}$ . Heptane was utilized to extract the formed DEPDC from the mixture and the solution was dried over sodium sulfate. The dried solution was filtered and separated from the solvent by means of a rotary evaporator under vacuum at less than  $2^{\circ}\text{C}$ . The yield of DEPDC was measured using a standard iodimetric titration analysis technique (ASTM E298-91) to exceed 90%. \*Owing to the instability of DEPDC, highly concentrated DEPDC must be stored at very low temperature ( $-20^{\circ}\text{C}$ ). Scheme 3.1 provides the overall reaction.



**Scheme 3.1** The overall reaction of synthesis of DEPDC

### 3.2.3. Reactor and *In Situ* ATR-FTIR Measurements

The reaction was carried out in the stirred 100-mL high-pressure autoclave equipped with *In situ* ATR-FTIR, as described in Chapter 2. Spectra were recorded at a



resolution of  $2\text{cm}^{-1}$  and the absorption spectra were the results of 64 scans. *In situ* ATR-FTIR was applied to monitor the thermal decomposition of DEPDC and the product formation.

### 3.2.4. Nuclear Magnetic Resonance

Nuclear Magnetic Resonance (NMR) spectra were recorded using a Varian Inova 600 or 400.  $^1\text{H}$  and  $^{13}\text{C}$  NMR chemical shifts are reported relative to tetramethylsilane (TMS). Proton – 400.087 MHz, PW90 (90 pulse width) = 12.3  $\mu\text{s}$  (PW45 used in 1D experiment), number of transients (NT) = 8, acquisition time (AT) = 4.00 s, delay time (D1) = 1. Carbon – 100.613 MHz, PW90 = 10.4  $\mu\text{s}$  (PW 45 used in 1D), NT = 256, AT = 1.20 s, D1 = 1. gCOSY – NT=1, number of increment (NI for 2D) = 128 (linear prediction was used to give a final data set of 384 for processing), AT = 0.20 s, D1 = 1. gHSQC – NT = 4, NI = 128 (linear prediction used to 384 for processing), AT = 0.21 s, garp  $^{13}\text{C}$  decoupling used, D1= 1.

## 3.3. Results and Discussion

### 3.3.1. Assignment of Characteristic Peaks of DEPDC

In order to provide accurate data for FTIR interpretation, highly concentrated DEPDC initiator was synthesized without solvent (\*explosive). By using a standard iodimetric titration analysis technique, the concentration of the home-made DEPDC in this study was found to be greater than 97%. The two most intense absorbance peaks of DEPDC are located at 1191 and  $1794\text{cm}^{-1}$  (Figure 3.1a). The peak at  $1191\text{cm}^{-1}$  can be assigned to the C–O stretching vibration in the  $-\text{C}(\text{O})-\text{O}-$  group, while the peak

appearing at  $1794\text{cm}^{-1}$  is ascribed to the characteristic C=O stretching vibration in the  $\text{C(O)-O-O-C(O)-}$  group<sup>110, 111</sup>.

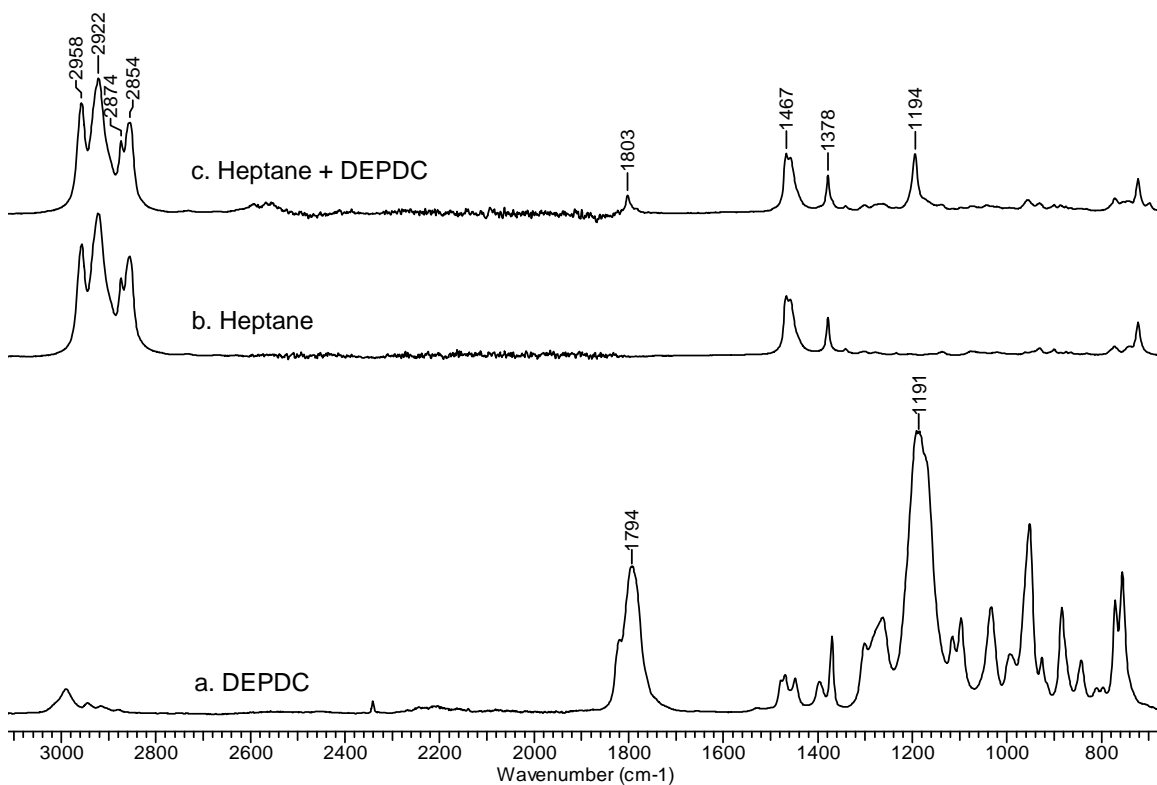


**Figure 3.1** IR spectra of (a) DEPDC, (b) heptane, and (c) heptane+DEPDC. Spectra were collected at ambient temperature under atmospheric pressure.

### 3.3.2. Thermal Decomposition of DEPDC in Heptane and Supercritical $\text{CO}_2$

In order to distinguish the characteristic peaks of DEPDC for decomposition in heptane (and later  $\text{scCO}_2$ ), the FTIR spectra of heptane and DEPDC/heptane were collected as shown in Figure 3.1b and 3.1c. The spectrum of heptane gives absorbance peaks at  $1378$ ,  $1467$ ,  $2854$ ,  $2874$ ,  $2922$ , and  $2958\text{cm}^{-1}$ . The bands appearing at  $2854$ ,  $2874$ ,  $2922$ , and  $2958\text{cm}^{-1}$  are assigned to  $\text{CH}_2$  sym.,  $\text{CH}_3$  sym.,  $\text{CH}_2$  asym., and  $\text{CH}_3$  asym. stretching vibrations, respectively, while the peaks at  $1378$ ,  $1467\text{cm}^{-1}$  are assigned to  $\text{CH}_3$  sym. bending and  $\text{CH}_3$  asym. bending/ $\text{CH}_2$  scissoring vibrations, respectively.<sup>110</sup>

In the solution of DEPDC/heptane, DEPDC showed strong absorbance peaks at 1194 and 1803 $\text{cm}^{-1}$  which slightly differ from the characteristic peaks of pure DEPDC at 1191 and 1794 $\text{cm}^{-1}$ . When the DEPDC/heptane solution was heated, the thermal decomposition of DEPDC with time was monitored and clearly observed by the decrease in peak heights at 1194 and 1803 $\text{cm}^{-1}$  (Figure 3.2 a-c). In order to clearly demonstrate the formation of decomposed products and the conversion of DEPDC, a further treatment was made by means of subtracting the spectrum measured before the reaction from the spectrum measured after the reaction (Figure 3.2d). The appearance of the positive peaks at 1262 and 1747 $\text{cm}^{-1}$  in the subtraction spectrum are ascribed to the formation of decomposed products.

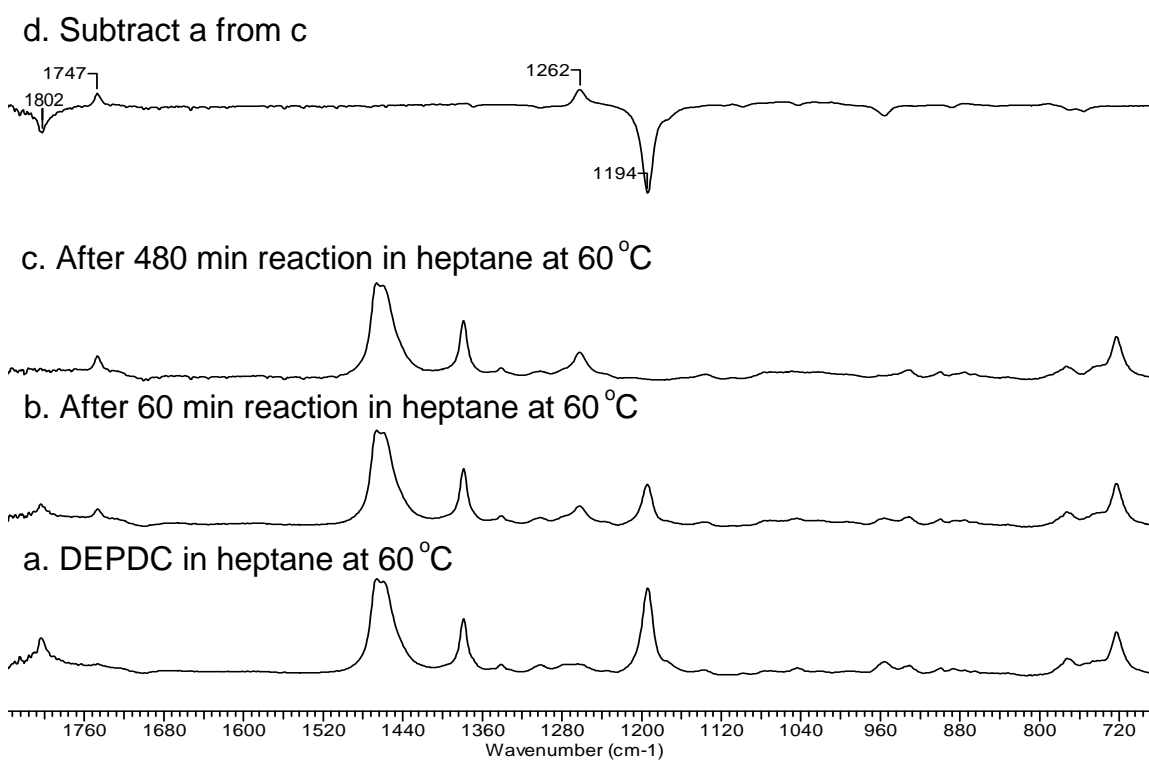


**Figure 3.2** *In situ* FTIR spectra of DEPDC thermal decomposition in heptane (DEPDC concentration 2.7wt%) at 60°C. (a) at t = 0min; (b) at t = 60min; (c) at t = 480min; (d) resulting spectrum from c-a subtraction.

Figure 3.3 shows the spectra before and after the reaction as well as the subtraction spectrum under supercritical conditions. It was found that the characteristic peaks of DEPDC in scCO<sub>2</sub> at 1803 and 1203cm<sup>-1</sup> decreased following heating time, while new peaks gradually developed at 1756 and 1250cm<sup>-1</sup>. The thermal decomposition of DEPDC was also studied in supercritical ethylene and supercritical ethylene/CO<sub>2</sub>, as DEPDC was selected as the initiator for the synthesis of ethylene-based copolymer and polymer nanocomposites in scCO<sub>2</sub>, and it is necessary to examine whether or not radical induced decomposition was significant. Figure 3.4 displays the result of FTIR spectra of the DEPDC/heptane before introducing ethylene and after the ethylene polymerization at 60°C. The subtraction result (Figure 3.4b – 3.4a) is given in Figure 3.4c. Similar to that found with heptane and scCO<sub>2</sub>, the conversion of DEPDC gives rise to negative peaks at 1193cm<sup>-1</sup> and 1803cm<sup>-1</sup>, while the new species formed from decomposition of the initiator give positive peaks at 1261 and 1747cm<sup>-1</sup>. Figure 3.5 plots the four peaks observed during DEPDC decomposition in scCO<sub>2</sub>, with two peaks decreasing from initiator decomposition and the other two peaks increasing from product formation. The intensities of characteristic peaks of DEPDC were used for kinetic analysis as discussed below.

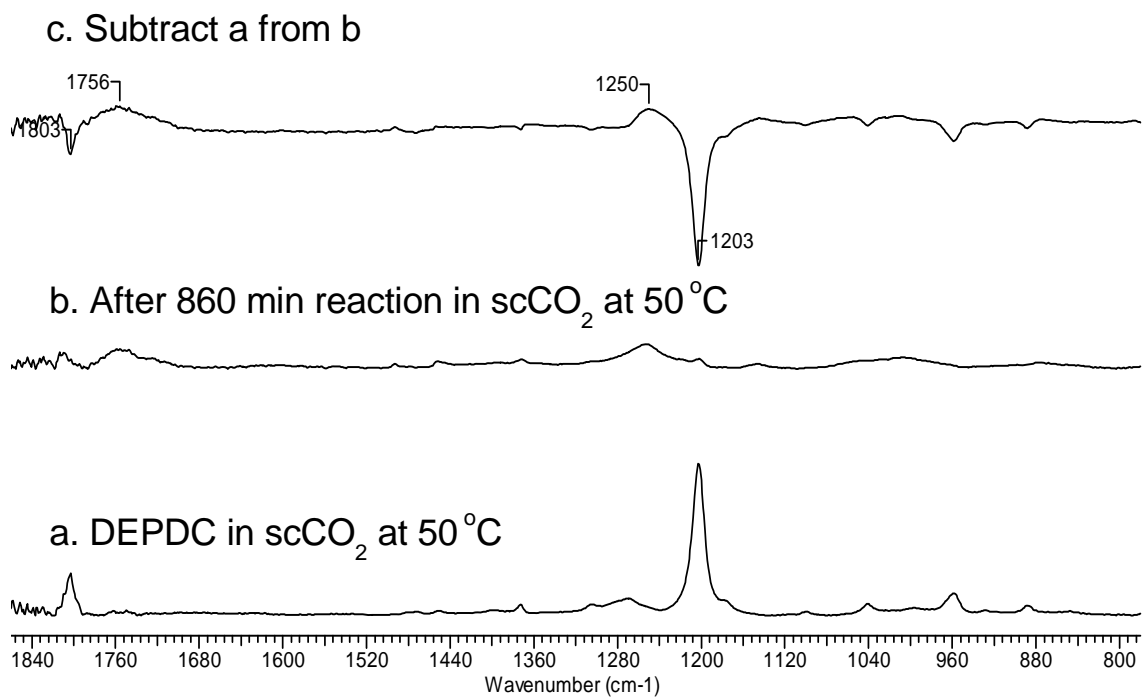


**Figure 3.3** *In situ* FTIR spectra of DEPDC thermal decomposition in scCO<sub>2</sub> (DEPDC concentration 3.4wt%) at T=50°C, P=20MPa. (a) at t=0min; (b) at t=860min; (c) resulting spectrum from b-a subtraction.

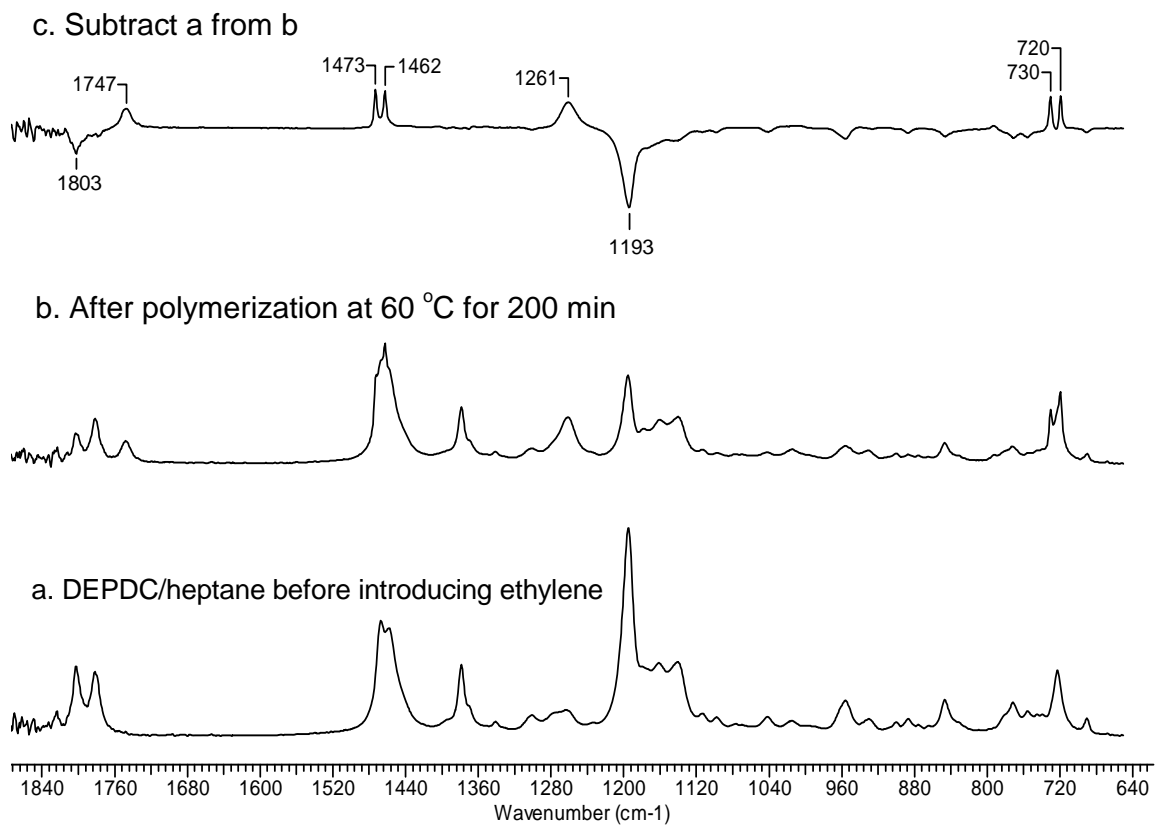


**Figure 3.4** *In situ* FTIR spectra of DEPDC thermal decomposition in supercritical ethylene ( $T=60^{\circ}\text{C}$ ,  $P=13.8\text{MPa}$ ). (a) at  $t=0\text{min}$ ; (b) at  $t=200\text{min}$ ; (c) resulting spectrum from b-a subtraction.

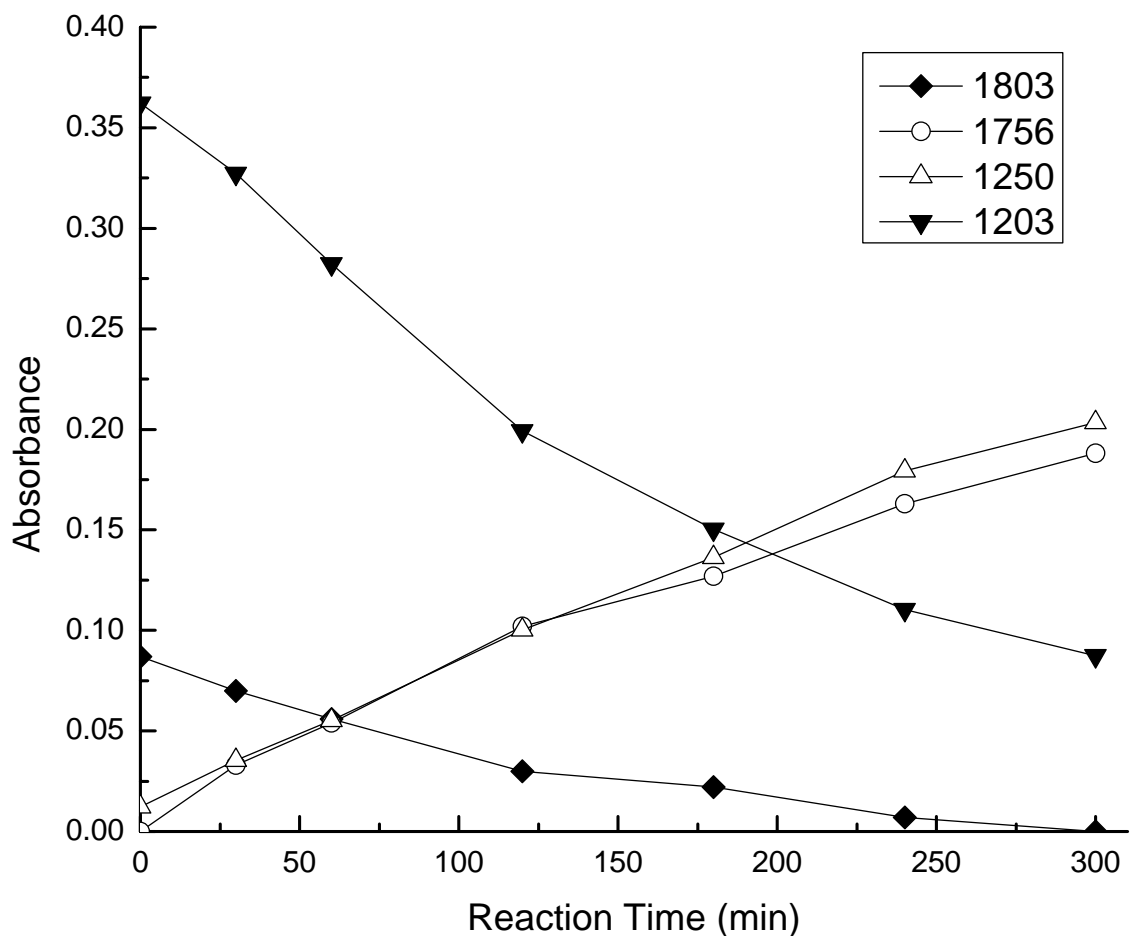


**Figure 3.5** *In situ* FTIR results for absorbance versus reaction time curves for DEPDC decomposition in scCO<sub>2</sub> (T=60°C, P=20MPa, DEPDC concentration 8.8wt%).

### 3.3.3. Kinetic Measurement

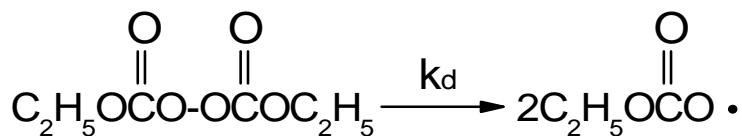
One of the advantages of using *in situ* FTIR for measuring initiator decomposition is that it provides direct measurement of the change in concentration of the reaction ingredients and products. The absorbance intensity is directly proportional to the concentration according to the Beer-Lambert law:

$$A = \varepsilon \cdot C \cdot l \quad (3-1)$$

where A is the absorbance,  $\varepsilon$  is the molar absorptivity ( $\text{L} \cdot \text{mol}^{-1} \cdot \text{cm}^{-1}$ ), C is the concentration of the compound in solution ( $\text{mol} \cdot \text{L}^{-1}$ ), and l is the path length of the

sample (cm). In order to examine the linear relationship between the absorbance intensity and the concentration, the FTIR spectra of different concentrations of DEPDC in heptane at 20°C were measured (Appendix 1). Due to the instability of DEPDC at high temperature, diethyl carbonate was used as an alternative analog to DEPDC for examining the linear relationship in scCO<sub>2</sub> (the peak at 1269cm<sup>-1</sup> was used). An excellent linear relationship was found in both studied solvents.

It is widely accepted that the decomposition of organic peroxides is via the breaking of the weak O-O single bond. Scheme 3.2 displays the formation of alkoxy-carboxyl free radicals C<sub>2</sub>H<sub>5</sub>-O-CO<sub>2</sub>• from primary dissociation of DEPDC.



**Scheme 3.2** Primary dissociation of DEPDC to form alkoxy-carboxyl free radicals

If the reaction of DEPDC decomposition is first-order,

$$\frac{dC}{dt} = -k_d C \quad (3-2)$$

where  $k_d$  is decomposition rate constant (s<sup>-1</sup>) and  $t$  is reaction time (s). By integrating equation (3-2), and taking advantage of the linear relationship:

$$\frac{C_o}{C} = \frac{A_o}{A} \quad (3-3)$$

where  $C_o$  and  $A_o$  are initial concentration and absorbance of the initiator, respectively, the following equation can be obtained:

$$\ln \frac{A_o}{A} = k_d t \quad (3-4)$$



From equation (3-4), the decomposition rate constant  $k_d$  can be determined with the experimental data absorbance  $A$  and time  $t$ . The absorbance intensities of the characteristic peaks at  $1203\text{cm}^{-1}$  in  $\text{scCO}_2$  and at  $1194\text{cm}^{-1}$  in heptane were selected for kinetic study because these peaks effectively reflected the concentration of DEPDC, provided the best signal/noise ratio, and gave no observable superposition in this spectral region.

With the experimental data ( $A_o$ ,  $A$ ,  $t$ ), a plot of  $\ln(A_o/A)$  versus  $t$  can be obtained. Figure 3.6 displays a typical plot of  $\ln(A_o/A)$  versus time for DEPDC decomposition in heptane at  $50^\circ\text{C}$  using the intensity of the characteristic peak at  $1194\text{cm}^{-1}$ . The linear plot of  $\ln(A_o/A)$  versus time is strongly in agreement with the assumed first-order unimolecular decomposition mechanism, giving the decomposition rate constant,  $k_d$ , as the slope. In order to make a comparison with the previous studies reported for DEPDC decomposition, a study was conducted on a series of experiments of DEPDC decomposition in heptane under atmospheric  $\text{N}_2$  at various temperatures between  $40$  and  $74^\circ\text{C}$ . By means of plotting  $\ln(A_o/A)$  versus  $t$ , the rate constants at different temperatures were obtained, as listed in Table 3.1. In light of the Arrhenius equation:

$$\ln k_d = \ln A_d - \frac{E_a}{RT} \quad (3-5)$$

where  $A_d$  is pre-exponential factor ( $\text{s}^{-1}$ ),  $E_a$  is activation energy ( $\text{J}\cdot\text{mol}^{-1}$ ),  $R$  is gas constant ( $\text{J}\cdot\text{K}^{-1}\cdot\text{mol}^{-1}$ ), and  $T$  is temperature (K), a plot of  $\ln k_d$  versus  $1/(RT)$  will give the activation energy as the absolute value of the slope. The plot of  $\ln k_d$  versus  $1/(RT)$  for DEPDC decomposition in heptane and  $\text{scCO}_2$  is shown in Figure 3.7. The activation energy ( $E_a$ ) and pre-exponential factor ( $A_d$ ) for thermal decomposition of DEPDC in heptane, determined from the plot with linear correlation coefficient being 0.992, are

$E_a=115$  kJ/mol and  $A_d=2.01\times 10^{14}$  s<sup>-1</sup>. The 95% confidence limits of  $E_a$  and  $A_d$  are 95 ~ 135 kJ/mol and  $1.36\times 10^{11} \sim 2.97\times 10^{17}$  s<sup>-1</sup>, respectively.

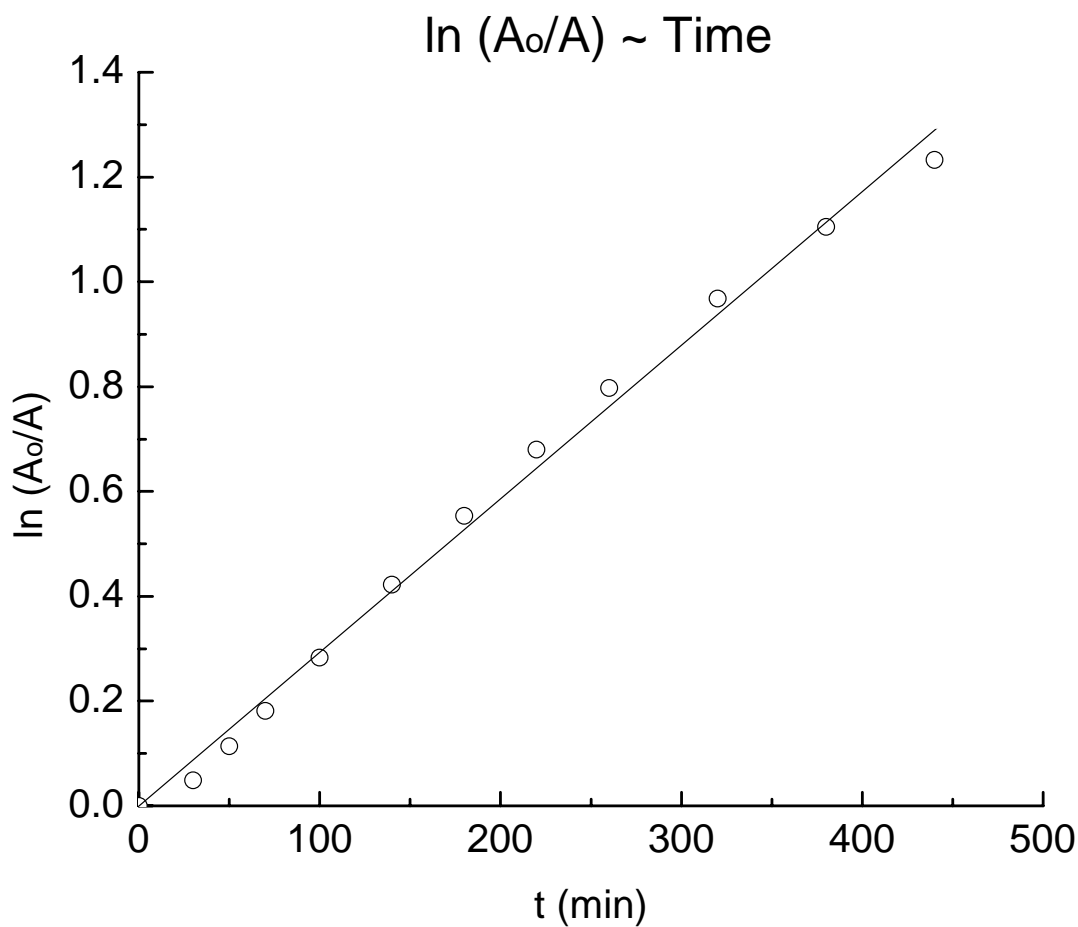


**Figure 3.6** Kinetic measurement of DEPDC thermal decomposition in heptane at 50°C.

**Table 3.1** Decomposition rate constants of DEPDC in heptane under N<sub>2</sub>

T (°C)	k <sub>d</sub> ×10 <sup>6</sup> (s <sup>-1</sup> )
40	7.8
45	29
50	48
60	180
70	520
74	740

E<sub>a</sub> = 115 kJ/mol.

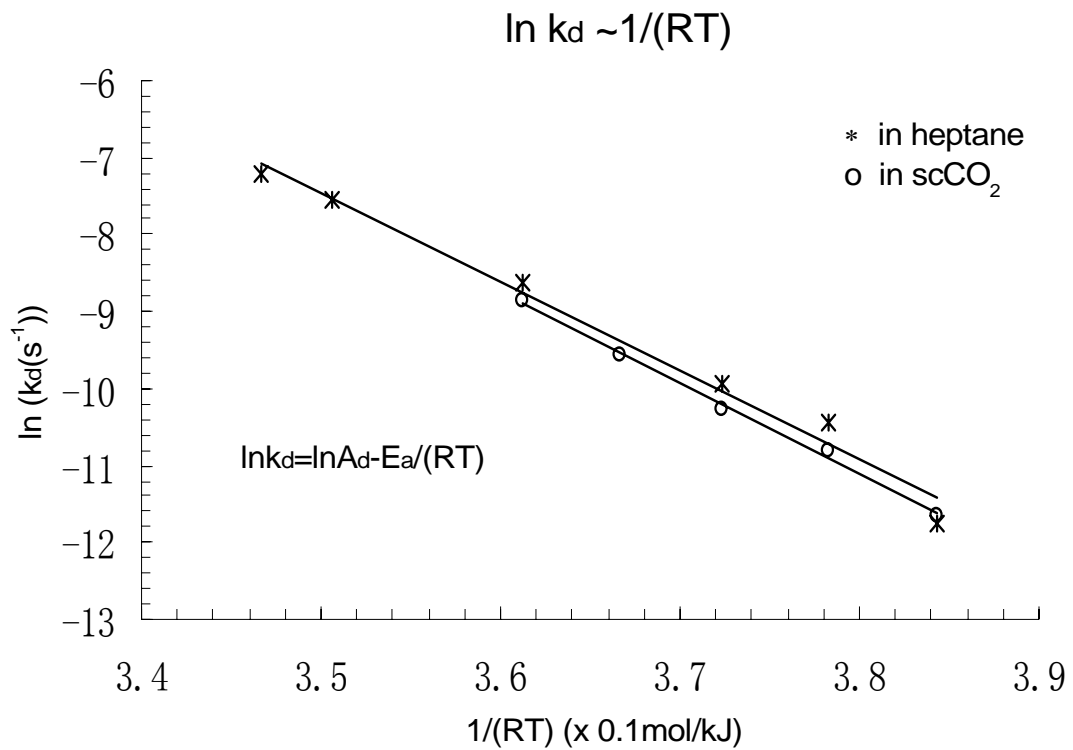


**Figure 3.7** Arrhenius plot of  $\ln k_d$  versus  $1/(RT)$  for DEPDC decomposition in scCO<sub>2</sub> and heptane.

For the decomposition of DEPDC in scCO<sub>2</sub>, the linear  $\ln(A_0/A) \sim t$  plots in the temperature range from 40 to 60°C indicate that the decomposition of DEPDC under supercritical conditions also occurred via first-order kinetics of unimolecular decomposition. The rate constants at different temperatures in scCO<sub>2</sub> are listed in Table 3.2. The activation energy ( $E_a$ ) and pre-exponential factor ( $A_d$ ) for decomposition of DEPDC in scCO<sub>2</sub>, determined from the plot with linear correlation coefficient being 0.998, are  $E_a=118$  kJ/mol and  $A_d=4.54 \times 10^{14}$  s<sup>-1</sup>. The 95% confidence limits of  $E_a$  and  $A_d$  are 106 ~ 130 kJ/mol and  $4.66 \times 10^{12} \sim 4.42 \times 10^{16}$  s<sup>-1</sup>, respectively. However, as discussed further below, if the concentration of DEPDC became high enough in pure scCO<sub>2</sub>, non-first-order kinetics and a different reaction mechanism were found.

**Table 3.2** Decomposition rate constants of DEPDC in scCO<sub>2</sub>

T(°C)	P (MPa)	$k_d \times 10^6$ (s <sup>-1</sup> )
40	10.5	8.7
45	12.1	20
50	13.7	34
55	15.2	70
60	16.8	140

CO<sub>2</sub> density = 15 mol/L.  $E_a$  = 118 kJ/mol.

As reported by Yamada *et al*<sup>97</sup>, the activation energy for the decomposition of dialkyl peroxydicarbonates is between 113 ~ 126 kJ/mol and tends to decrease with increasing alkyl group chain length. The present results obtained by *in situ* FTIR are in

good agreement with the results obtained by the conventional titration method<sup>97</sup>. However, it still looks surprising that the rate constants and the activation energy data of the decomposition of DEPDC in the two solvents are similar. This can be explained by comparing the effects of viscosity and dielectric constants for the two solvents. On the one hand, the rate constant of decomposition of organic peroxides may be increased by lowering the viscosity of the solvent. It was reported that the decomposition rate constant increased as the solvent viscosity decreased for the thermal decomposition of a series of fluorinated diacyl peroxides in scCO<sub>2</sub>.<sup>64</sup> On the other hand, the rate constant of decomposition of initiators may be decreased by lowering the dielectric constant of solvents.<sup>8</sup> A dipolar interaction between the initiator's transition state and the solvent medium exists but radical reactions are not very solvent sensitive with rates that usually span less than an order of magnitude.<sup>112</sup> Hence, the similar kinetic results in this research may be explained as scCO<sub>2</sub> has both a lower viscosity and a smaller dielectric constant than heptane.

The decomposition of DEPDC in scCO<sub>2</sub> was previously studied by Charpentier *et al*<sup>66</sup> using a CSTR in the presence of galvinoxyl as a radical scavenger in the temperature range of 65 ~ 85°C, wherein it was found the decomposition of the DEPDC was first-order and the reaction of an initiator radical with the radical scavenger is essentially instantaneous. The activation energy ( $E_a$ ) and pre-exponential factor ( $A_d$ ) for the decomposition of DEPDC in scCO<sub>2</sub> were determined as  $E_a = 132 \pm 8$  kJ/mol and  $A_d = (6.3 \pm 1.4) \times 10^{16}$  s<sup>-1</sup>. This higher  $E_a$  found using the radical scavenger technique may be due to not all the free radicals from the decomposition reacting with the radical scavenger galvinoxyl. The reactions of radicals are complex and a small number of free radicals

could be consumed in a variety of other ways without reacting with the scavenger to form the UV-detectable adduct.

The rate constants of DEPDC decomposition in both supercritical ethylene and supercritical ethylene/scCO<sub>2</sub> were measured. It was found that the decomposition rates of DEPDC under scCO<sub>2</sub> and supercritical ethylene are similar to one another, which implies that radical induced decomposition is negligible for this system. Figure 3.8 demonstrates the rate constants of DEPDC decomposition obtained from this study and from the literature using various other techniques. This figure suggests very strongly that the nature of the solvent has no significant effect on the rate constant for this initiator. Hence, high-pressure *in situ* FTIR is very useful for studying the kinetics of initiator decomposition in supercritical fluids.

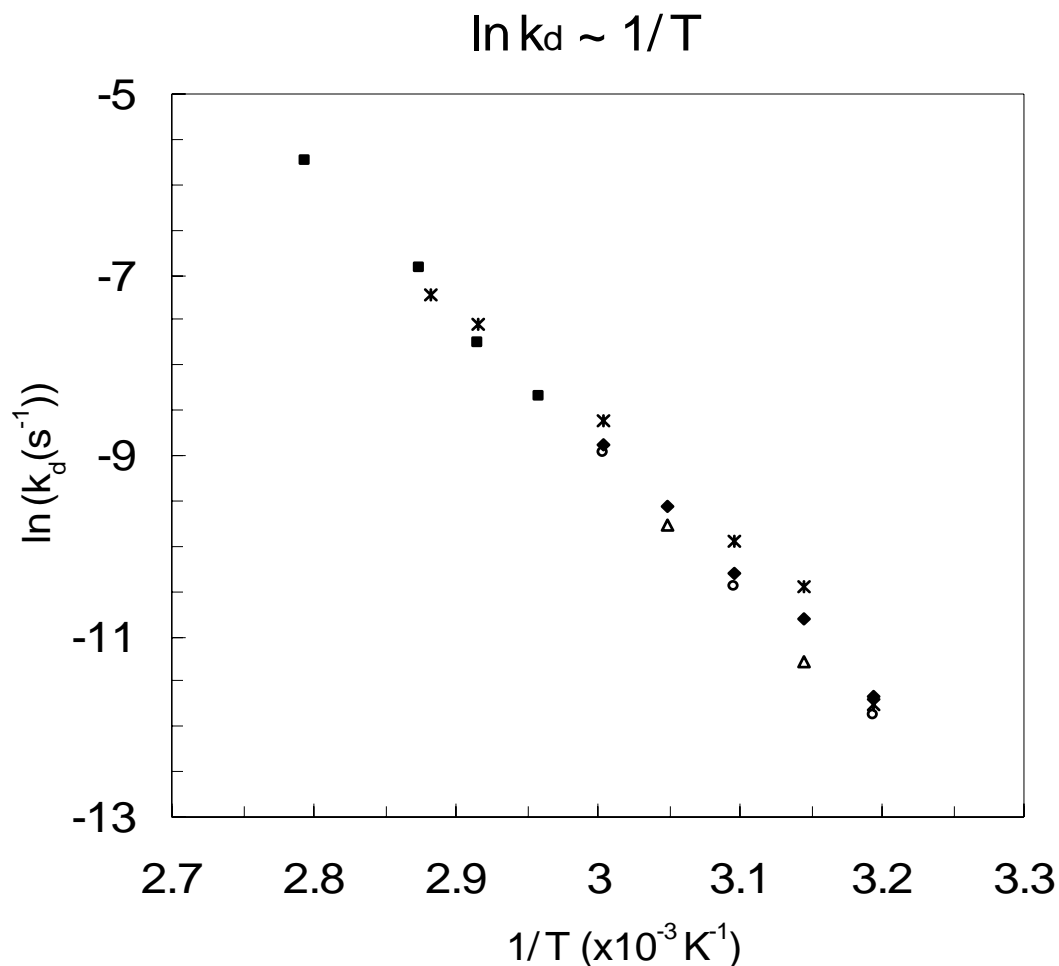


**Figure 3.8** Comparison of rate constants for diethyl peroxydicarbonate decomposition in  $\text{scCO}_2$  (◆) and heptane (\*), to those reported in the literature for the solvents  $\text{scCO}_2$  (■), t-butanol ( $\Delta$ ), and 2,2'-oxydiethylene bis(allyl carbonate) (○).

### 3.3.4. Decomposition Mechanism of DEPDC in $\text{ScCO}_2$

As described above, the thermal decomposition of low-concentration DEPDC in either  $\text{scCO}_2$  or heptane is via first-order kinetics of unimolecular decomposition. In both solvent systems studied, the FTIR spectra of the decomposed products from DEPDC show peaks in the ranges of  $1747 \sim 1756\text{cm}^{-1}$  and  $1250 \sim 1262\text{cm}^{-1}$ , which are assigned to the stretching vibrations of the C=O and C-O functional groups, respectively. Partial decarboxylation of the initially formed  $\text{C}_2\text{H}_5\text{OCO}_2\bullet$  radicals into  $\text{C}_2\text{H}_5\text{O}\bullet$  radicals and

CO<sub>2</sub> cannot be excluded from the experimental observation, but the observed growing peaks of the carboxyl group in the reaction products with reaction time (1747 and 1262cm<sup>-1</sup> in Figure 3.2 and 1756 and 1250cm<sup>-1</sup> in Figure 3.3) suggest that most of the initially formed C<sub>2</sub>H<sub>5</sub>OCO<sub>2</sub>• radicals were not decarboxylated at the relatively low temperatures under the studied experimental conditions. The free radical C<sub>2</sub>H<sub>5</sub>OCO<sub>2</sub>• is extremely reactive and able to abstract a hydrogen atom from an available source if no monomer is present to polymerize. The gradually developed absorbance peaks at 1756 and 1250cm<sup>-1</sup> during the decomposition under scCO<sub>2</sub> conditions are likely attributed to the formed molecule, monoethyl carbonate (C<sub>2</sub>H<sub>5</sub>-O-CO<sub>2</sub>H).

The extent of the decarboxylation of the free radicals strongly depends on both the structures of the free radicals and the experimental conditions. Studies on the initiator structure showed for example that CF<sub>3</sub>OCO<sub>2</sub>• decarboxylated faster than FCO<sub>2</sub>•<sup>113</sup> while carbonyloxy radicals with a tertiary α-carbon atom decarboxylated much faster than radicals with a primary α-carbon atom.<sup>105</sup> For photoinduced decomposition of peroxides using C<sub>6</sub>H<sub>5</sub>-C(O)O-OR (R=benzoyl or tert-butyl) and tert-butyl 9-methylfluorene-9-percarboxylate, decarboxylation of the benzoyloxy and 9-methylfluorenylcarbonyloxy radicals took place on the picosecond time scale.<sup>107, 109</sup> The ultrafast decarboxylation of these carbonyloxy radicals was explained by the high excess energy available after photoexcitation of the parent peroxides, and/or a fast and direct dissociation via electronically excited states. On the contrary, the alkoxy-carboxyl radicals from the thermal decomposition of dicyclohexyl peroxydicarbonate did not readily decarboxylate before entering into reactions with solvent or bimolecular disproportionation at 50°C, although the decarboxylation of alkoxy-carboxyl radicals formed from OO-t-butyl O-



cyclohexyl peroxy carbonate became significant in the 100 ~ 110°C range.<sup>103</sup> Decarboxylation of these radicals was slow relative to competing bimolecular reactions due to a high activation energy, so could be increased by higher temperatures.<sup>103</sup> Similarly, according to Buback *et al*'s photoexcitation study on 2-Me-C<sub>6</sub>H<sub>4</sub>-CO<sub>2</sub>•, intramolecular hydrogen atom migration was faster than decarboxylation at thermal energies associated with ambient temperatures, while higher energies increased the rate of decarboxylation.<sup>105</sup> Hence, the present results showing little decarboxylation for DEPDC in scCO<sub>2</sub> and hexane is expected at the relatively low temperatures studied from 40 to 74°C, and for the ethoxycarboxyl radical with a primary α-carbon atom.

To further probe the mechanism of decomposition of DEPDC in scCO<sub>2</sub>, the reactor was first cooled down to ambient temperature and then the venting was carefully carried out to atmospheric pressure during a period of approximately 30min. Figure 3.9 exhibits the spectrum of the decomposition products observed at the bottom of the reactor after the thermal decomposition of DEPDC in scCO<sub>2</sub> and subsequent venting. The two previously developed broad peaks at 1756 and 1250cm<sup>-1</sup> are no longer dominant. Instead, the newly formed peaks at 3323, 2975, 2879, 2339, 1797, 1716, 1370, 1263, 1197, 1089, 1048 and 880cm<sup>-1</sup> suggest the presence of new reaction products from decomposition. By referring to the literature and offline FTIR experimental measurements, the peaks at 3323, 2975, 2879, 1089, 1048, and 880cm<sup>-1</sup> are attributed to ethanol, which was formed from the decarboxylation of the unstable intermediate giving rise to the peaks at 1756 and 1250cm<sup>-1</sup> when CO<sub>2</sub> was vented from the reactor. The peak at 1716cm<sup>-1</sup> in Figure 3.9 can be assigned to 2,3-butanedione<sup>114</sup> while the peak at 2339cm<sup>-1</sup> indicates the existence of residual CO<sub>2</sub> and/or CO<sub>2</sub> from the conversion of residual monoethyl carbonate. It was

unavoidable to lose some volatile decomposition products during the venting process, but the major end products would remain in the reaction residue at the bottom of the reactor. This reaction residue was further analyzed using NMR ( $^1\text{H}$ ,  $^{13}\text{C}$ , gCOSY, and gHSQC) (Appendix 3), and ethanol, ethyl acetate, and 2,3-butanedione were found in the products.<sup>115</sup>

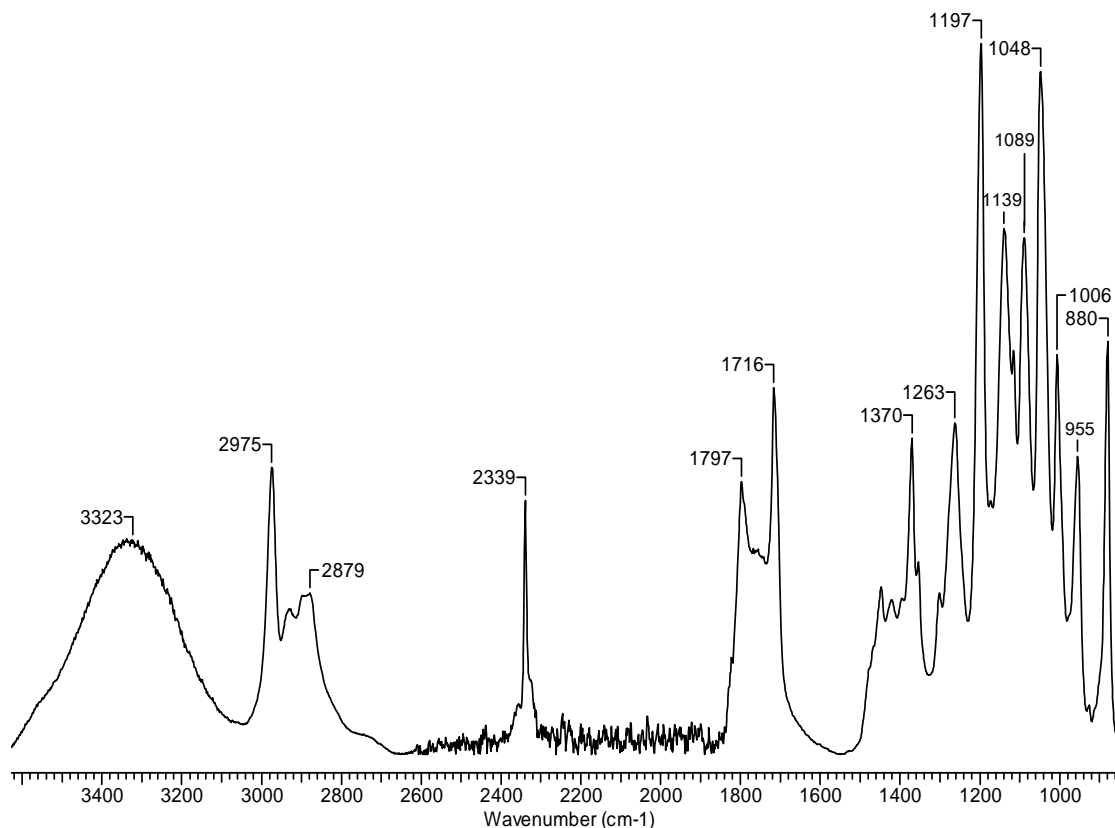


**Figure 3.9** FTIR spectrum of thermal decomposition products after 860min reaction in  $\text{scCO}_2$  at  $50^\circ\text{C}$  and 20MPa then venting to atmospheric pressure. (Spectra were collected at ambient temperature under atmospheric pressure.)

Figure 3.10a displays the spectrum of the high-purity DEPDC (without organic solvents) in a relatively high concentration in  $\text{scCO}_2$ . Heating this solution led to Figure 3.10b, which displays the IR spectrum of the induced decomposition of the initiator. This decomposition reaction was completed within a few seconds with subsequent increase in

temperature and pressure. Figure 3.10b shows new peaks at 3424, 2980, 2887, 1727, 1096, and 1044 $\text{cm}^{-1}$ . The peak at 1727 $\text{cm}^{-1}$  can be assigned to acetaldehyde while the other five peaks are ascribed to ethanol, using literature values<sup>114-116</sup>. These results are also in good agreement with the previous studies by Duynstee *et al*<sup>104</sup> who found the major products from decomposition of a similar initiator, diisopropyl peroxydicarbonate, were isopropanol, acetone and  $\text{CO}_2$ , and Van Sickle<sup>103</sup> who found the major products from decomposition of dicyclohexyl peroxydicarbonate were  $\text{CO}_2$ , cyclohexanol, and cyclohexanone. Schemes 3.3 and 3.4 summarize the likely decomposition reactions under these experimental conditions. Assignments of these absorbance peaks of DEPDC, heptane, diethyl carbonate, ethanol, and other decomposed products are given in Table 3.3 as reference. It should be mentioned that in addition to the major products discussed above, other byproducts could also be produced in small amount due to the high reactivity of the free radicals. As the free-radical mechanisms are complex, these schemes should be taken as descriptive.

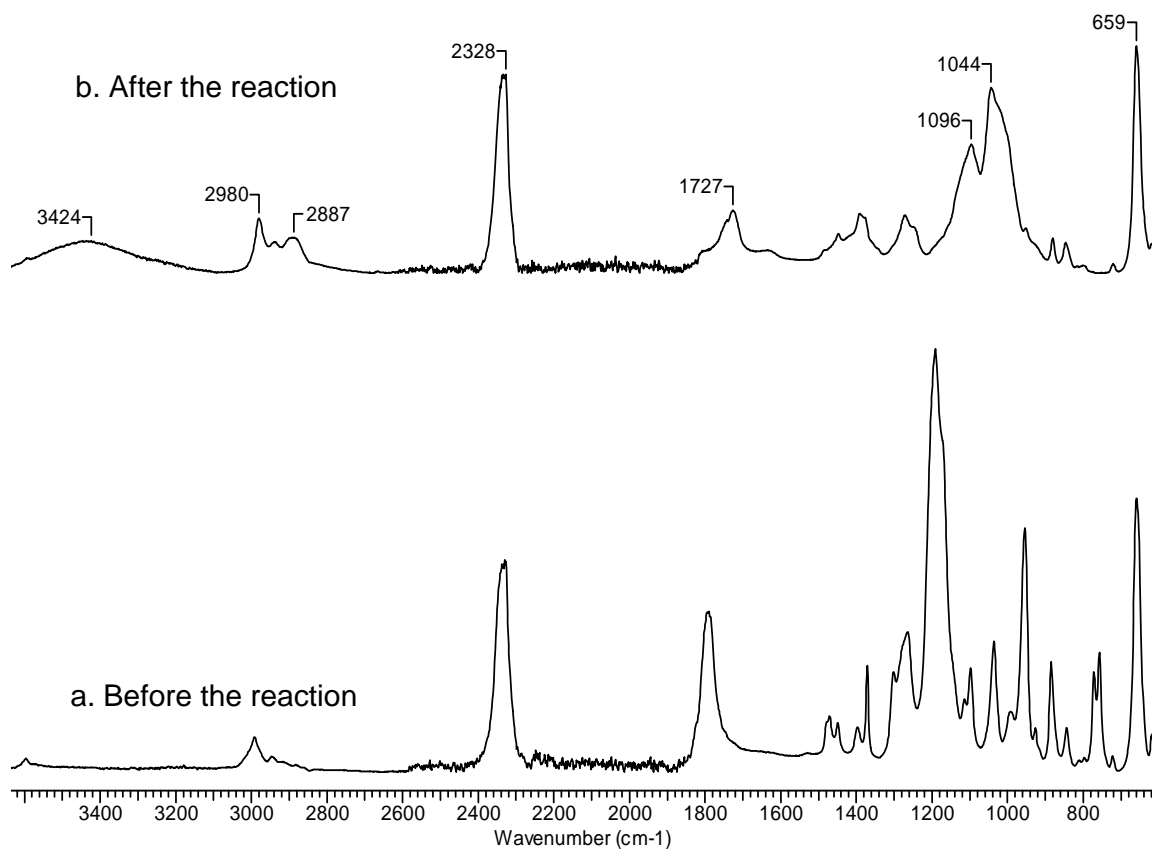
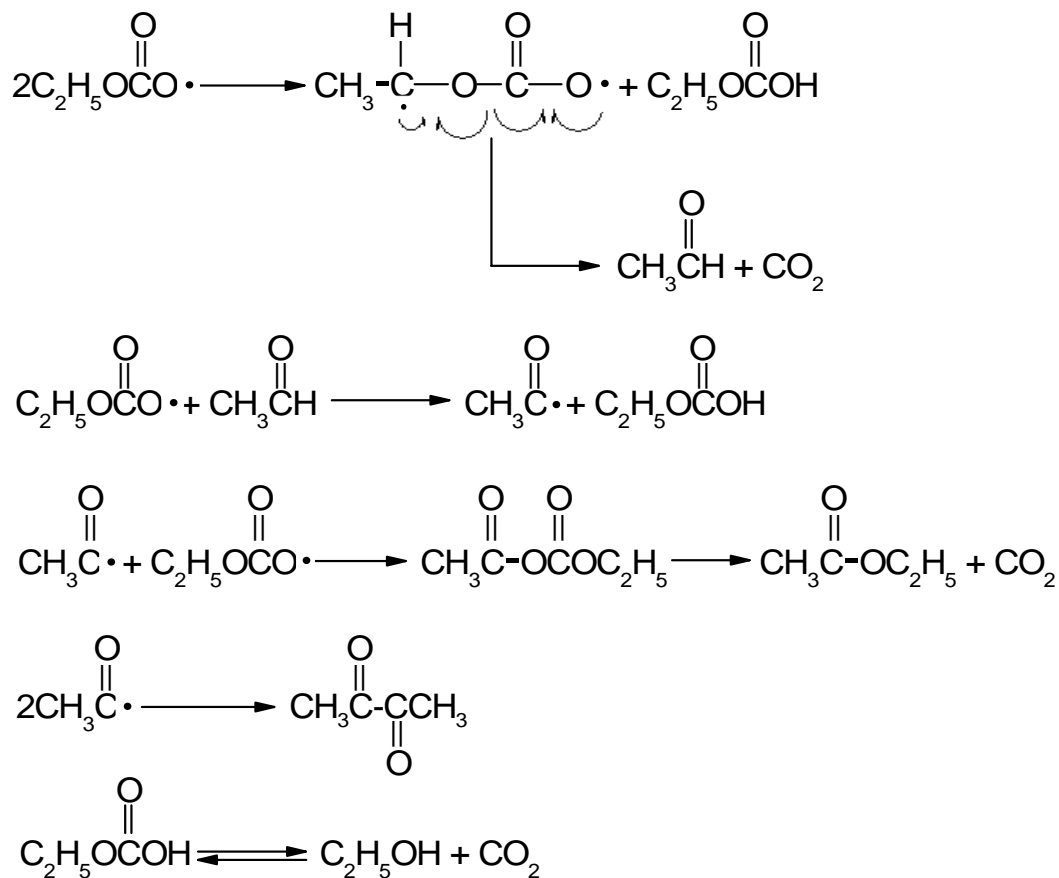


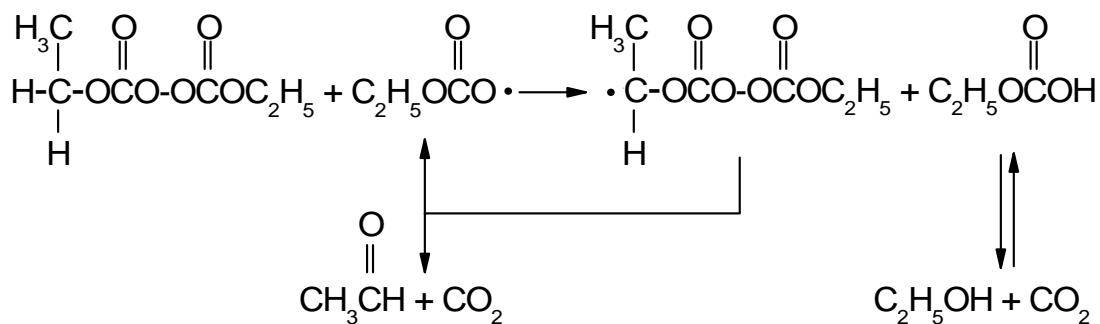
**Figure 3.10** *In situ* FTIR spectra of before and after the induced explosive DEPDC decomposition in scCO<sub>2</sub> at 60°C and 20MPa (DEPDC concentration 18.4wt%).

**Table 3.3** Assignment of characteristic FTIR peaks used in this study<sup>110, 114, 116</sup>

<b>Chemicals</b>	<b>Frequency (cm<sup>-1</sup>)</b>	<b>Assignment</b>
Heptane	2960-2850	CH <sub>3</sub> and CH <sub>2</sub> asym. & sym. stretching vibrations
	1467	CH <sub>3</sub> asym. bending / CH <sub>2</sub> scissoring vibrations
	1378	CH <sub>3</sub> sym. bending vibration (umbrella mode)
Diethyl peroxydicarbonate (DEPDC)		
	1794-1803	C=O stretching vibrations
	1191-1203	C-O stretching vibrations
Diethyl carbonate		
	1744-1751	C=O stretching vibrations
	1251-1262	O-C-O stretching vibrations
Decomposed products		
	1747	C=O stretching vibrations (in heptane)
	1756	C=O stretching vibrations (in scCO <sub>2</sub> )
	1262	O-C-O stretching vibrations (in heptane)
	1250	O-C-O stretching vibrations (in scCO <sub>2</sub> )
	3323-3424	O-H stretching vibrations (CH <sub>3</sub> CH <sub>2</sub> OH)
	2975-2980	CH <sub>3</sub> asym. stretching vibrations (CH <sub>3</sub> CH <sub>2</sub> OH)
	2879-2887	CH <sub>2</sub> asym. stretching vibrations (CH <sub>3</sub> CH <sub>2</sub> OH)
	1044-1048 & 1089-1096	C-O stretching vibrations (CH <sub>3</sub> CH <sub>2</sub> OH)
	1727	C=O stretching vibration (CH <sub>3</sub> CHO)
	1716	C=O stretching vibration (2,3-butanedione)



**Scheme 3.3** Proposed mechanism of forming monoethyl carbonate, ethanol, ethyl acetate, and 2,3-butanedione in scCO<sub>2</sub>



**Scheme 3.4** Proposed mechanism of forming ethanol and acetaldehyde for the induced decomposition of DEPDC in scCO<sub>2</sub>

### 3.4. Conclusions

This study has shown the great advantage of using *in situ* ATR-FTIR in studying the mechanism and kinetics of the thermal decomposition of diethyl peroxydicarbonate (DEPDC) in supercritical fluids (under high pressure). Two new characteristic peaks, appeared at  $1747 \sim 1756$  and  $1250 \sim 1262\text{cm}^{-1}$  simultaneously with the decomposition of DEPDC, demonstrate that the major decomposed products contain a carboxyl group and decarboxylation of the initially formed  $\text{ROCO}_2\bullet$  radicals does not occur significantly. By comparison with standard IR spectra, the two peaks are assigned to the formation of carbonates from the decomposition of DEPDC. For DEPDC decomposition in supercritical  $\text{CO}_2$ , the first formed intermediate monoethyl carbonate was decarboxylated and converted into ethanol during removal of  $\text{CO}_2$ . Through the kinetic measurements, the decomposition of DEPDC is revealed as in the first-order kinetics of unimolecular reaction regardless of the applied media. The activation energy of the thermal decomposition of DEPDC was obtained to be  $115\text{kJ/mol}$  in heptane from  $40$  to  $74^\circ\text{C}$  and  $118\text{kJ/mol}$  in  $\text{scCO}_2$  from  $40$  to  $60^\circ\text{C}$ .

**Chapter 4. FTIR Study on Measuring the Monomer Reactivity Ratios  
for Ethylene-Vinyl Acetate Polymerization in Supercritical CO<sub>2</sub>**



In this chapter, the determination of monomer reactivity ratios for copolymerization of ethylene and vinyl acetate in the “green” solvent, scCO<sub>2</sub>, is described. *In situ* ATR-FTIR was employed to monitor the copolymerization in scCO<sub>2</sub>. The FTIR spectra of the initial formation of copolymers of ethylene and vinyl acetate (VAc) were utilized for determining the reactivity ratios. Both the Kelen-Tudos and the non-linear least-squares (NLLS) methods were used to calculate the reactivity ratios. Off-line <sup>1</sup>H NMR analysis was also utilized for obtaining the copolymer composition, by which the determined reactivity ratios were compared with the ones obtained using *in situ* FTIR. The effect of polymerization temperature and pressure was examined and the solvent effect was also discussed. A version of this chapter has been accepted for publication to *Industrial & Engineering Chemistry Research*: FTIR study on measuring the monomer reactivity ratios for ethylene-vinyl acetate polymerization in supercritical CO<sub>2</sub>.<sup>117</sup>

#### 4.1. Introduction

Poly(ethylene-co-vinyl acetate) (PEVA) is a commercialized copolymer which is recognized for its flexibility, toughness, adhesion characteristics, stress-cracking resistance, and being used in a variety of applications. Some of the grades are used for hot-melt adhesives applications. PEVA is also widely used as an encapsulating resin for silicon based photovoltaic (PV) devices providing mechanical support, electrical isolation, and protection against environmental exposure.<sup>118</sup> Hydrolysis of PEVA yields poly(ethylene-co-vinyl alcohol), which can be used in a variety of containers and biomedical applications.

The thermal and mechanical properties of PEVA depend primarily on the VAc content and the polymerization process. The VAc content has a significant effect on the crystallinity, flexibility, and elastomeric properties of the copolymer with increasing VAc content leading to the PEVA copolymer becoming softer and more transparent. The copolymerization of ethylene and vinyl acetate is normally performed under high pressure, using free radicals as initiators, as vinyl acetate can effectively quench catalyst activity.<sup>119</sup> The solvent based process requires volatile organic compounds (VOCs), which are increasingly being regulated, and the very high pressure process cannot produce polymers with significant amounts of vinyl acetate. As well, the copolymerization often produces product with significant amounts of low-molecular weight highly-branched material. Hence, a new process for synthesizing this copolymer in scCO<sub>2</sub> would be highly desirable, particularly if supercritical fluid extraction (SFE) can be incorporated to remove the low MW fragments and provide better product for

emerging solar and biomedical applications. ScCO<sub>2</sub> has additional advantages as it can be rapidly and safely vented to the atmosphere or recaptured, leaving dry solvent-free polymer. This overcomes drying issues, hence significantly lowering energy requirements. Additional advantages include that polymerization in scCO<sub>2</sub> provides the ability to produce new desirable properties in the polymer, including enhanced free volume for increased loading capabilities of nanofillers<sup>120</sup> extending this commodity polymer into emerging applications.

To provide the required information for potential commercial employment, it is necessary to obtain the monomer reactivity ratios, which have not previously been measured for copolymerization of ethylene and vinyl acetate in scCO<sub>2</sub>. The reactivity ratios can be determined experimentally by using the instantaneous copolymer composition equation (Eqn. 1-2). Many analytical methods have been previously used to estimate monomer reactivity ratios, as reviewed by Penlidis and coworkers<sup>121</sup>. Fineman and Ross<sup>122</sup> developed a linearization method by rearranging the well known Mayo-Lewis equation (Eqn. 1-2), while Kelen and Tudos<sup>123</sup> modified the Fineman-Ross method by introducing an arbitrary constant in order to spread the data points more evenly. The non-linear least-squares (NLLS) method has been found to be the most statistically sound technique wherein the more useful form of the Mayo-Lewis equation (Eqn. 1-5) is employed.

In general, for measuring the reactivity ratios, copolymerizations are carried out to as low degrees of conversion as possible in a batch reactor to minimize the errors in the use of the differential equation. The copolymer composition can be determined either directly by analysis of the copolymer or indirectly by analysis of changes in the

comonomer composition. The main spectroscopic techniques that are effective for direct measurement of copolymer composition include infrared (IR), nuclear magnetic resonance (NMR) and ultraviolet (UV) spectroscopy. Among the various techniques, *in situ* Fourier transform infrared (FTIR) spectroscopy is a state-of-the-art monitoring technique which can provide real-time structural and kinetic information during a polymerization process. ATR-FTIR spectroscopy is particularly useful form of *in situ* FTIR that uses the phenomenon of total internal reflection, hence producing: (1) little to no disturbing interference from solid particles present in the solution, or generated by polymerization, and (2) a less intense solvent contribution to the overall infrared spectrum so the solvent spectra can be easily subtracted from the sample spectrum. These characteristics of a small depth of penetration with no sensitivity to solid particles constitute the technical motivation for the employment of ATR-FTIR technology as an online monitoring tool for supercritical crystallizations and polymerizations.<sup>124</sup>

In this study, the initially-formed ethylene-vinyl acetate (EVA) copolymer compositions were determined by both *in situ* ATR-FTIR and off-line <sup>1</sup>H NMR techniques. The non-linear least-squares method (using the Gauss-Newton algorithm) was employed for data analysis while the results obtained with the Kelen-Tudos method were also used for reference and comparison.

## **4.2. Experimental**

### **4.2.1. Materials**

Instrument grade CO<sub>2</sub> (99.99% purity from Praxair Canada Inc., with dip-tube) and polymer grade ethylene (99.9% purity, Praxair) were further purified by passing

through columns filled with 5Å molecular sieves and reduced 20% copper oxide/Al<sub>2</sub>O<sub>3</sub> to remove the moisture and oxygen, respectively. Argon (99.999% purity, Praxair) was used without further purification. Vinyl acetate (VAc) (>99%) purchased from Sigma-Aldrich Canada was further purified by passing through an inhibitor remover column (Aldrich) to remove hydroquinone. Deuterium chloroform from Cambridge Isotope Laboratories, Inc. and 1,2,4-trichlorobenzene (TCB) (>99%) and hydroquinone(≥99%) from Sigma-Aldrich Canada were used as received. The initiator diethyl peroxydicarbonate (DEPDC) was synthesized as previously described in Chapter 3. Several PEVA samples of varying VAc content (Ateva<sup>®</sup> 1015A, 1210, 1231, 1240A, 1525, 1807V, 1821, 1985A, 2803A, 2811, 3325AC, and 4030AC) were generously provided by AT Plastics Inc.

#### **4.2.2. Copolymerization.**

Copolymerization was conducted in the 100-mL high-pressure stainless steel autoclave coupled with a digital pressure transducer and a temperature controller. The stirring speed was controlled at 300 rpm. The comonomer vinyl acetate and the initiator DEPDC were charged into the reactor, purged with a flow of argon, and then ethylene and CO<sub>2</sub> were pumped into the autoclave. The amount of ethylene and CO<sub>2</sub> injected into the reactor was determined by measuring the pressure and volume dispensed from the syringe pumps, with the density obtained from equations of state<sup>125, 126</sup>.

The copolymerization was carried out at 50±1 or 72±1°C, and 27.6±0.3 or 13.8±0.3MPa. *In situ* ATR-FTIR was applied to monitor the solution concentration in the stirred high-pressure autoclave. Spectra were recorded at a resolution of 2cm<sup>-1</sup> and the absorption spectra were the results of 32 scans. In order to accurately measure the area under the absorbance peaks of the initially formed copolymers, spectral subtraction was

employed by subtracting the spectrum measured before the copolymerization from the spectrum measured after a few minutes of copolymerization (typically 6 ~ 10min, by taking account of maximum signal-to-noise ratio and minimum monomer conversion). Due to a small amount of overlapping of the CH<sub>2</sub> asymmetric and symmetric stretching absorbance peaks at 2929 and 2856cm<sup>-1</sup>, the peaks were further separated by a deconvolution technique using a commercial software package (ACD UVIR version 7.08, Advanced Chemistry Development Inc.). In order to obtain the most accurate results, the peak area instead of peak height was employed for calculating the peak ratios.

After ca. 30min reaction, the autoclave was cooled down to ambient temperature, and then CO<sub>2</sub> and unreacted ethylene were carefully vented leaving the formed sample in the autoclave. Subsequently, a small amount of hydroquinone was added into the autoclave to quench the polymerization, followed by drying the reaction mixture under a vacuum oven at ambient temperature for 2 days and then at 60°C for 3 days. For comparison purposes, the dried copolymers were then characterized with <sup>1</sup>H NMR.

#### **4.2.3 Characterization.**

Thermogravimetric analysis (TGA) was performed using a TA Instruments TGA Q500 with a temperature ramp from 30 to 600°C at a heating rate of 10°C/min under nitrogen atmosphere. Off-line FTIR spectra were collected with a Bruker Vector 22 spectrometer at room temperature. Spectra were recorded at a resolution of 2cm<sup>-1</sup> and the absorption spectra were the results of 32 scans. <sup>1</sup>H Nuclear magnetic resonance (NMR) spectra were recorded using a Varian Inova 600 or 400 NMR spectrometer. High VAc content (≥30wt%) PEVA samples were dissolved in deuterated chloroform and run at

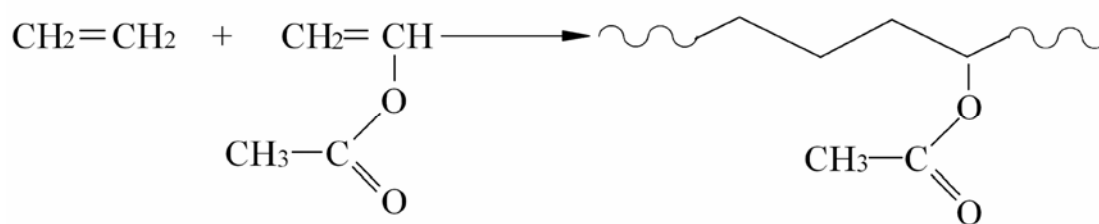
room temperature. The chemical shifts are reported relative to TMS. Frequency = 400.087 MHz, PW45 (45 pulse width) =12.3  $\mu$ s, number of transients (NT) =8, acquisition time (AT) =4.00 s, delay time (D1) =1 s. Low VAc content (<30wt%) PEVA samples were dissolved in 1,2,4-trichlorobenzene (TCB) and run at 60°C. The chemical shifts were referenced to TCB, peaks of which were previously calibrated with TMS. Frequency = 599.406 MHz, PW90 (90 pulse width) =12.1  $\mu$ s, number of transients (NT) =8, acquisition time (AT) =1.708 s, delay time (D1) =2 s. Pre-saturation frequencies: 7.22, 7.14, and 6.97ppm.

### **4.3. Results and Discussion**

#### **4.3.1. FTIR Analysis of Copolymerization**

During the copolymerization of ethylene and vinyl acetate (VAc) in scCO<sub>2</sub>, the copolymer PEVA was formed while both of the monomers, ethylene and VAc, are consumed (see Scheme 4.1). Figure 4.1 shows a plot of the *in situ* FTIR spectra of copolymerization of ethylene and vinyl acetate in scCO<sub>2</sub> from 0 to 960 minutes. Normally, while performing kinetic analysis on copolymerizations, the consumption of the monomers is monitored. However, while following this copolymerization in scCO<sub>2</sub>, the consumption of ethylene could not be monitored due to its infrared-inactive  $\nu$ C=C peak. Although the consumption of vinyl acetate could be followed from the characteristic  $\nu$ C=C peak (1648cm<sup>-1</sup>), this peak was rather small. By analyzing Figure 4.1, the absorbance intensities decreased at 1767, 1648, 1221, and 1141cm<sup>-1</sup> during the polymerization, while those at 2929, 2856, 1737, 1241 and 1020cm<sup>-1</sup> increased. The decrease in height of the peaks at 1648cm<sup>-1</sup> (due to C=C stretching vibration) and

1141 $\text{cm}^{-1}$  (due to O-C-C asymmetric stretching vibration of  $\text{CH}_3\text{C}(\text{O})\text{-O-CH=CH}_2$  molecule) indicates the conversion of vinyl acetate. That the absorbance peaks changed from 1767 to 1737 $\text{cm}^{-1}$  (due to C=O stretching vibration) and from 1221 to 1241 $\text{cm}^{-1}$  (due to C-C-O asymmetric stretching vibration) indicates the transfer of the ester groups from the monomer molecules to the polymer chains.<sup>110</sup> Hence, although the VAc monomer peaks are small, the polymer peaks are easily observed by the *in situ* FTIR data.



**Scheme 4.1** Overall reaction of synthesis of poly(ethylene-co-vinyl acetate)



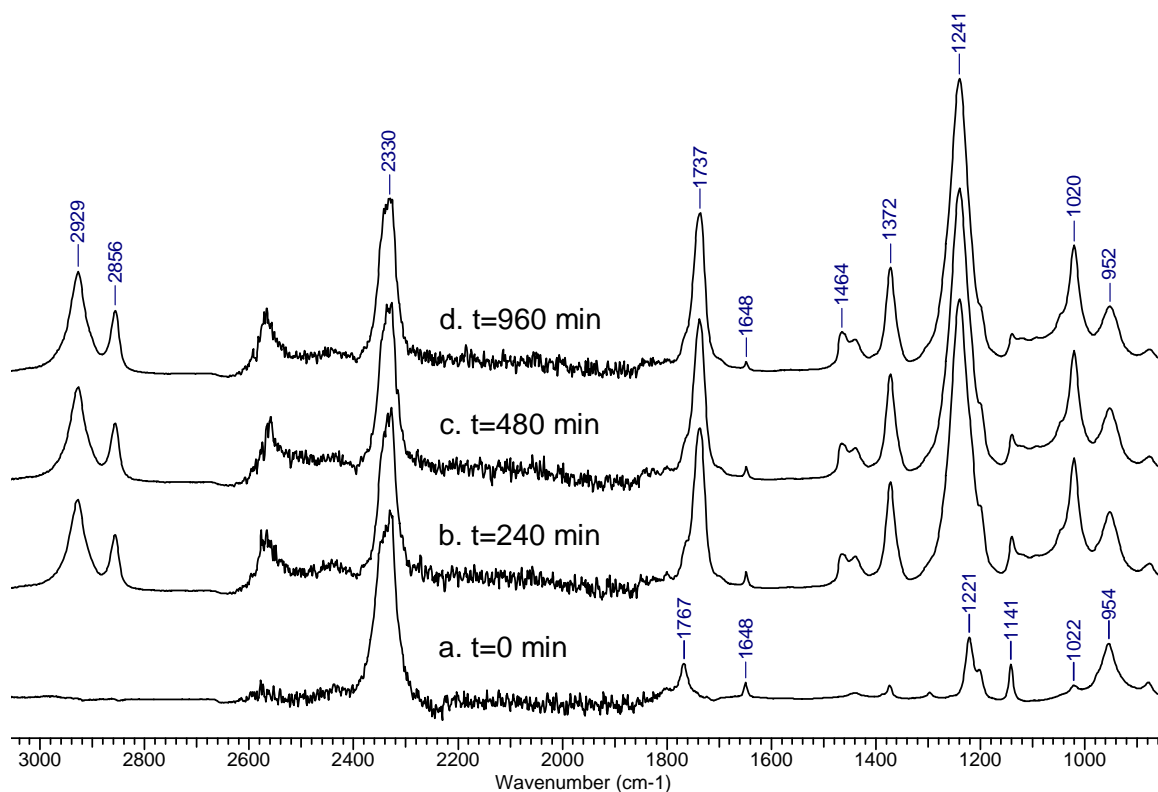


**Figure 4.1** *In situ* FTIR spectra of copolymerization of ethylene and vinyl acetate in  $scCO_2$  (the experimental conditions:  $T=50^\circ C$ ,  $P=27.6 MPa$ , ethylene mole fraction in feed: 0.902).

Figure 4.2 displays a typical *in situ* FTIR waterfall plot of the copolymerization of ethylene and VAc in  $scCO_2$  at the early stages of the copolymerization, where the reactivity ratios were determined for this study. In the experiment shown in Figure 4.2, the temperature was raised to the required reaction temperature during the first 10min heating, while the formation of copolymers is observed at ca. 4min later. The growing PEVA peaks provide useful and reliable information on the composition of the formed copolymers at low conversions, from which the reactivity ratios can be determined. The spectra of copolymers used for reactivity ratio calculation were collected at a monomer conversion of less than 2%, according to the change in area under the  $\nu C=C$  peak of vinyl

acetate ( $1648\text{cm}^{-1}$ ). As described in the introduction, low conversion is required for the successful application of the differential equation of copolymerization (Eqn. 1-2).

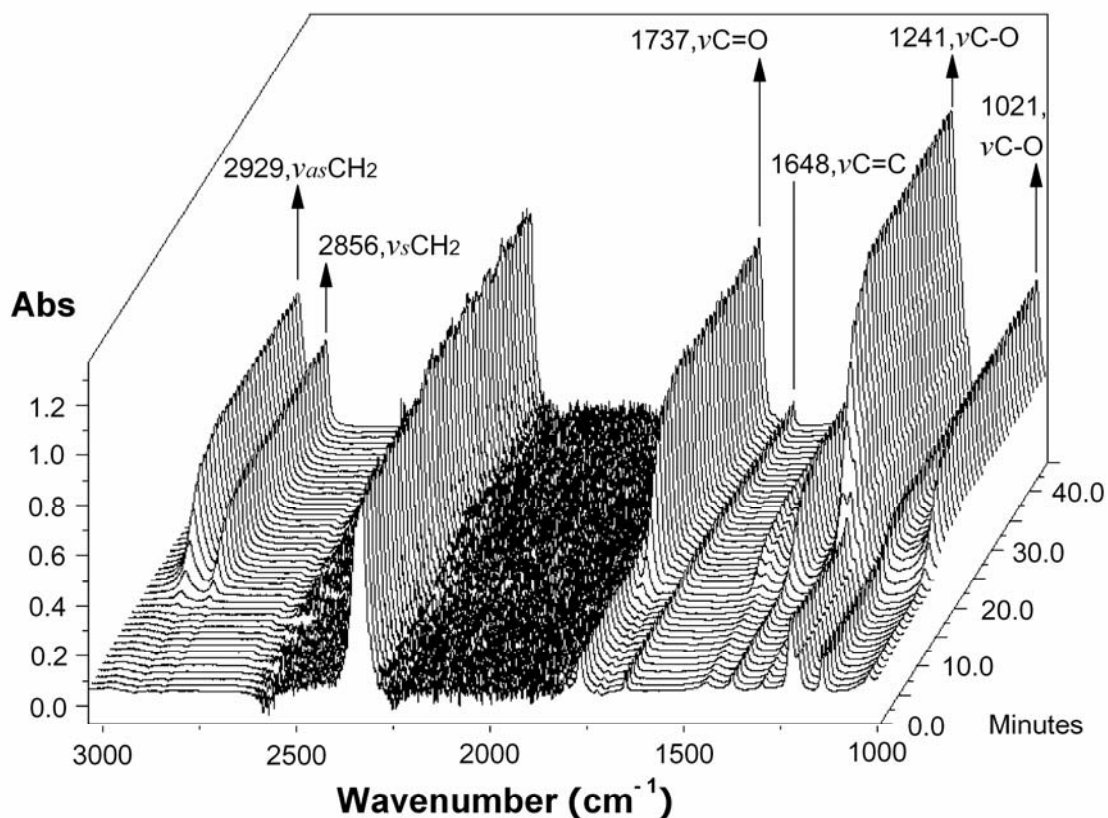


**Figure 4.2** *In situ* FTIR waterfall plot of the copolymerization of ethylene and VAc in  $\text{scCO}_2$  (the experimental conditions:  $T=50^\circ\text{C}$ ,  $P=27.6\text{MPa}$ , ethylene mole fraction in feed: 0.887).

To utilize these growing FTIR peaks during the copolymerization for measuring the reactivity ratios, a calibration curve must be established to relate the peak heights or peak areas to the composition of the formed copolymer PEVA. Pattacini *et al*<sup>127</sup> reported that there existed an excellent linear relationship between the FTIR peak ratios,  $\nu\text{C}=\text{O}(1740\text{cm}^{-1})$  or  $\nu\text{C}-\text{O}(1020\text{cm}^{-1})$  to  $\delta\text{CH}_2(1463\text{cm}^{-1})$  or  $\rho\text{CH}_2(723\text{cm}^{-1})$ , and the VAc contents for PEVA samples of low VAc content ( $\leq 11.1\text{wt}\%$ ). As well, an excellent linearity of the peak ratio  $1740\text{cm}^{-1}/1464\text{cm}^{-1}$  versus VAc content was also

observed by Williams<sup>128</sup> using TGA up to 33wt%. Figures 4.1 and 4.2 show that these peaks are clearly observable and the absorbance ratio  $1737\text{cm}^{-1}/2929\text{cm}^{-1}$  gave an excellent signal-to-noise ratio.

#### 4.3.2. Determination of PEVA Composition by TGA and NMR Analysis

To create a calibration curve for this study, so that the measured FTIR values can be related to the VAc content, several commercial PEVA samples (from AT Plastics Inc., VAc content < 42wt%) were characterized using both off-line TGA and <sup>1</sup>H NMR analysis. Figure 4.3 shows a typical TGA plot of a PEVA sample, containing two stages of weight loss at approximately 365 and 475°C, respectively. The first stage is attributed to acetic acid being evolved rapidly and quantitatively, from which the VAc content can be determined<sup>128</sup> while the residual hydrocarbon segments decompose during the second stage.<sup>129</sup>

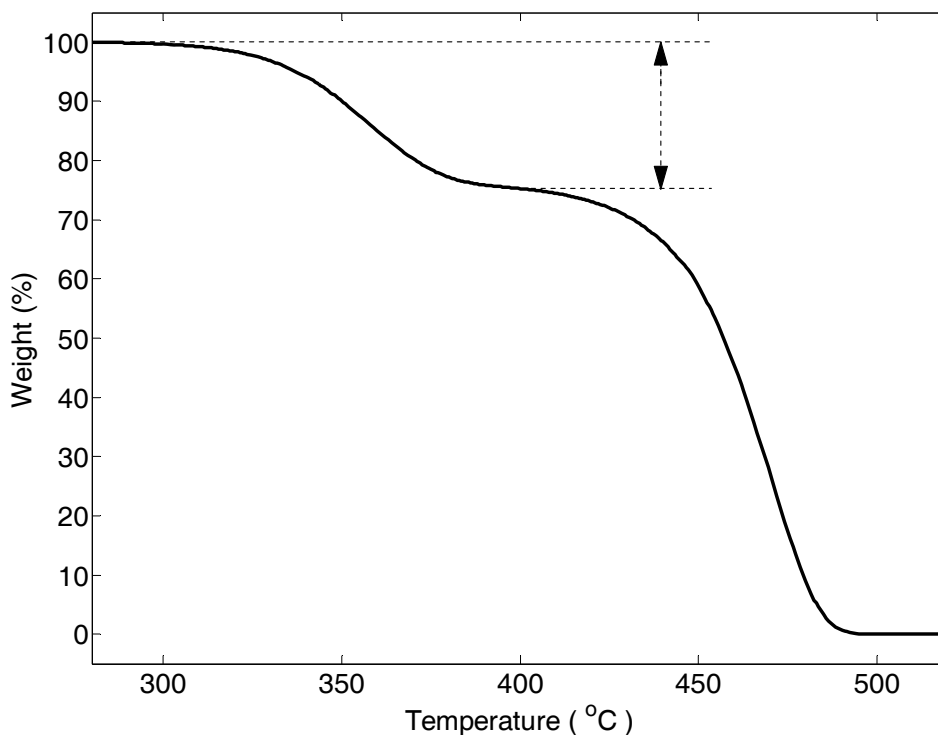


**Figure 4.3** TGA plot of a PEVA sample (Ateva<sup>®</sup> 3325AC).

In addition to TGA, NMR is considered to be an “absolute” technique for obtaining the chemical composition of copolymers. In this study,  $^1\text{H}$  NMR characterization was carried out for the commercial and home-made (VAc content: 57 ~ 98wt%) PEVA samples of high and low VAc contents, with a typical spectrum shown in Figure 4.4 for a commercial PEVA sample (Ateva<sup>®</sup> 3325AC, VAc content: ca. 34wt%). Figure 4.4a shows five major peaks appearing at 4.85(CH), 2.03(CH<sub>3</sub>-COO-), 1.49(CH<sub>2</sub>), 1.24(CH<sub>2</sub>), and 0.87ppm (CH<sub>3</sub>) using CDCl<sub>3</sub> as solvent at room temperature. When using TCB at 60 °C, the identical peaks were observed and identified (Figure 4.4b) and the obtained composition results using TCB were found to be within 5% error to those analyzed using chloroform-d. Figure 4.5 provides a comparison of the VAc contents of a series of commercial PEVA samples measured from TGA and  $^1\text{H}$  NMR, indicating that both techniques gave similar results.

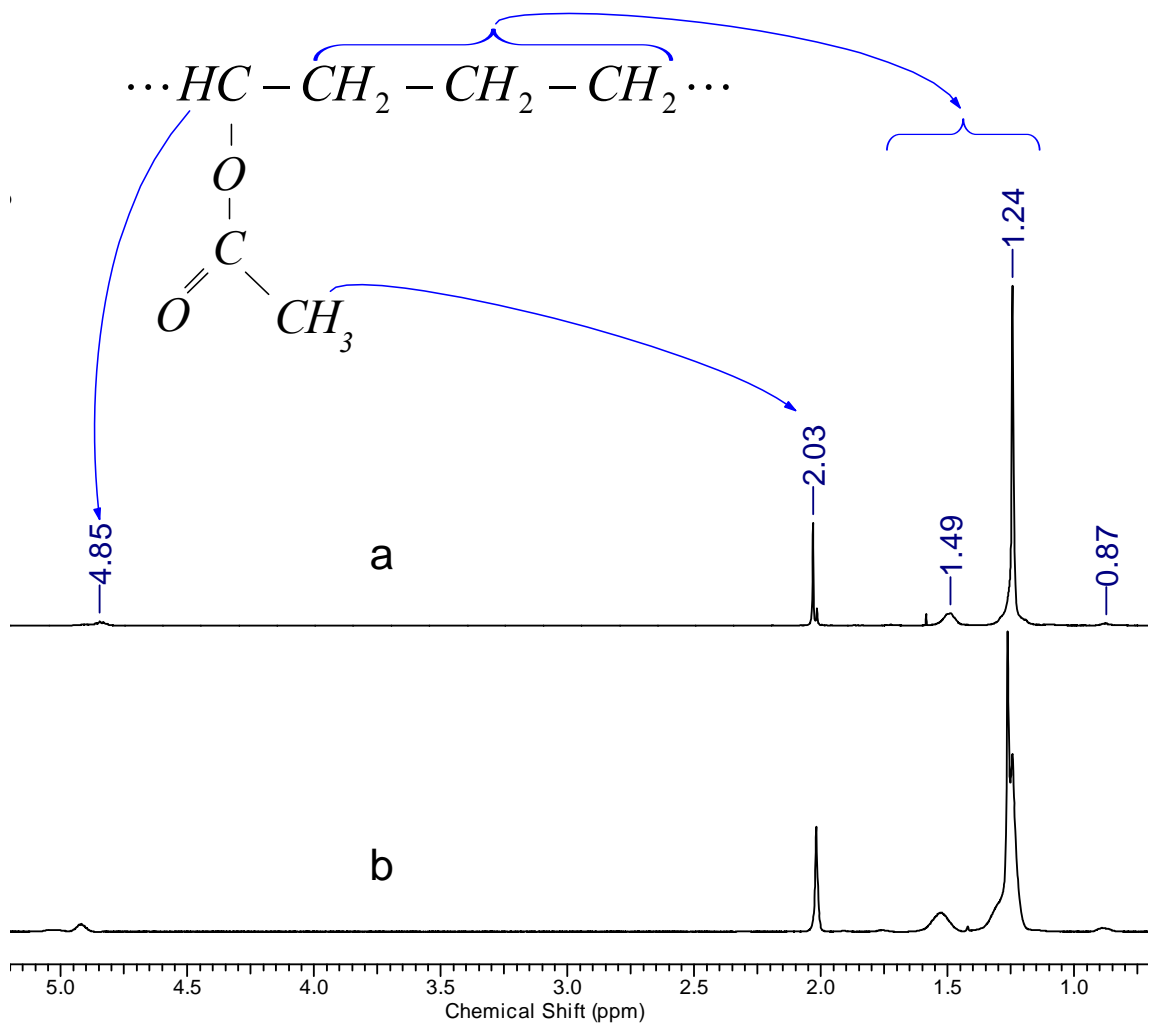


**Figure 4.4**  $^1\text{H}$  NMR spectra of a PEVA sample (Ateva<sup>®</sup> 3325AC) by use of different solvents. (a) chloroform-d at room temperature; (b) 1,2,4-trichlorobenzene at 60°C.

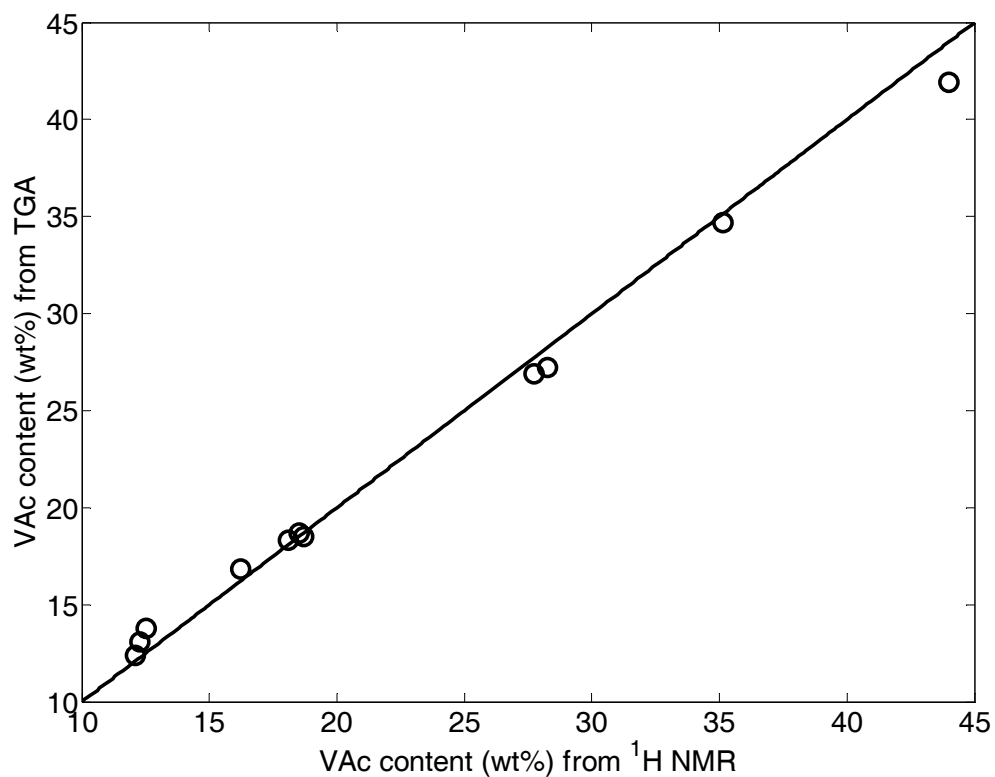


**Figure 4.5** Comparison of VAc content of commercial PEVA samples determined from TGA and <sup>1</sup>H NMR.

Using the <sup>1</sup>H NMR data and the measured values of the FTIR ratio at 1737/2929cm<sup>-1</sup>, Figure 4.6 shows the calibration curve that was established to measure the VAc content. Since the copolymer composition can be derived from the *in situ* FTIR spectra using this calibration curve, and the reactor feed compositions are known, the reactivity ratios can hence be determined.

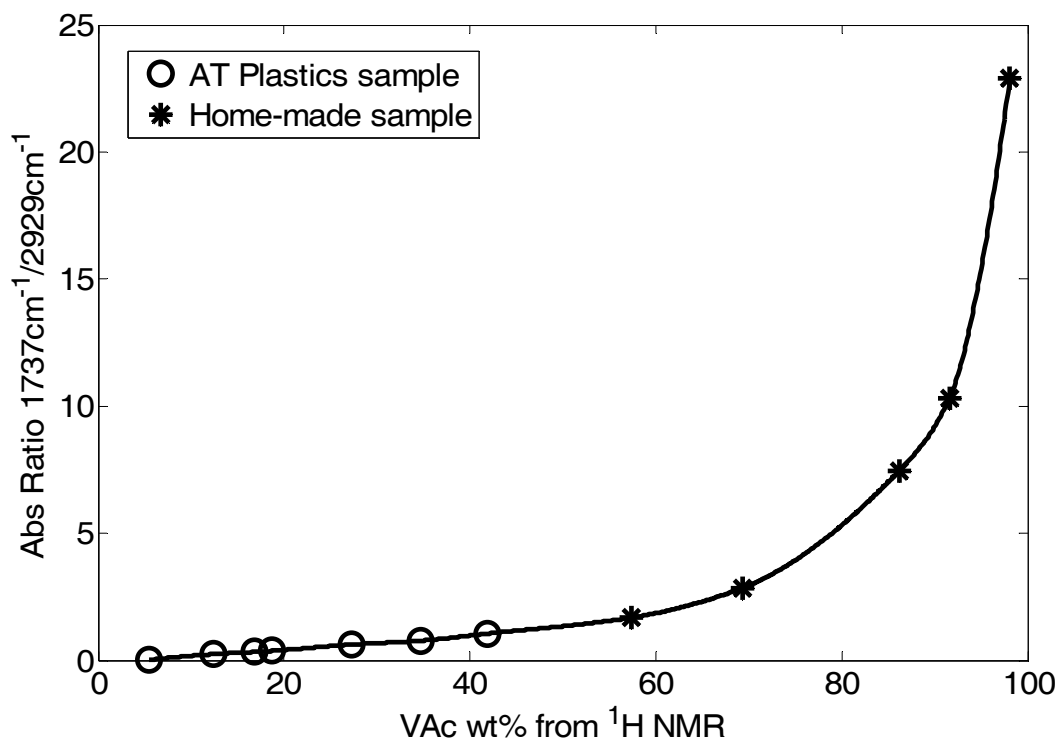


**Figure 4.6** Calibration curve of absorbance ratio versus VAc content of PEVA copolymers.

### 4.3.3. Determination of Reactivity Ratios

#### 4.3.3.1. Model Comparison

Table 4.1 provides the experimental conditions for all the ethylene-VAc copolymerizations utilized for this study. The feed compositions and the corresponding copolymer compositions are listed in Table 4.2 and 4.3.

**Table 4.1** Initial feed compositions for FTIR experiments under different reaction conditions

<b>Reaction Conditions</b>	<b>VAc (mol)</b>	<b>Ethylene (mol)</b>	<b>DEPDC (mol)</b>	<b>CO<sub>2</sub> (mol)</b>
	0.0512	0.0229	0.0035	2.30
	0.0526	0.0356	0.0046	2.28
50°C	0.0482	0.0787	0.0045	2.22
27.6MPa	0.0502	0.1562	0.0036	2.05
	0.0510	0.3998	0.0049	1.70
	0.0247	0.6061	0.0043	1.35
	0.0518	0.0259	0.0046	1.90
	0.0516	0.0569	0.0045	1.84
50°C	0.0531	0.0952	0.0046	1.77
13.8MPa	0.0509	0.2397	0.0047	1.48
	0.0233	0.2476	0.0034	1.46
	0.0516	0.0238	0.0005	2.04
	0.0523	0.0590	0.0009	1.94
72°C	0.0515	0.0925	0.0005	1.89
27.6MPa	0.0514	0.2412	0.0006	1.74
	0.0235	0.2449	0.0010	1.73



**Table 4.2** Ethylene mole fraction of copolymers determined by FTIR and  $^1\text{H}$  NMR from copolymerization of ethylene and vinyl acetate in  $\text{scCO}_2$  at  $50^\circ\text{C}$  27.6MPa with various feed composition

$f_{\text{ethylene}}$	$F_{\text{ethylene}}$ by FTIR	$F_{\text{ethylene}}$ by $^1\text{H}$ NMR
0.961	0.9526	0.934
0.887	0.8356	0.695
0.757	0.6808	0.576
0.620	0.5115	0.367
0.403	0.2521	0.160
0.309	0.2211	N/A

**Table 4.3** Ethylene mole fraction of copolymers determined by FTIR from copolymerization of ethylene and vinyl acetate in  $\text{scCO}_2$  with various feed composition

Reaction Condition	$f_{\text{ethylene}}$	$F_{\text{ethylene}}$
$50^\circ\text{C}$ 13.8MPa	0.914	0.8201
	0.825	0.6635
	0.642	0.4689
	0.524	0.3706
	0.333	0.2689
$72^\circ\text{C}$ 27.6MPa	0.912	0.8215
	0.824	0.6963
	0.642	0.5392
	0.530	0.3992
	0.316	0.2096

Figure 4.7 displays the experimental data for a set of experiments of varying  $f_1$  at 50°C and 27.6MPa in a plot of the mole fraction of ethylene in the copolymer,  $F_1$ , versus the mole fraction of ethylene in the feed,  $f_1$ . The reactivity ratios were calculated using both the NLLS and the Kelen-Tudos methods, as compared in this figure. The two methods gave very similar results (see Table 4.4), with the two fitting curves largely overlapping, with  $r_{\text{ethylene}}=0.76\pm 0.26$  and  $r_{\text{VAc}}=1.95\pm 0.65$  obtained by the NLLS method and  $r_{\text{ethylene}}=0.78$  and  $r_{\text{VAc}}=1.98$  obtained by the Kelen-Tudos method. The standard deviation values between the model and experimental data points found by using the two methods were calculated to be 0.0172 and 0.0173, respectively.

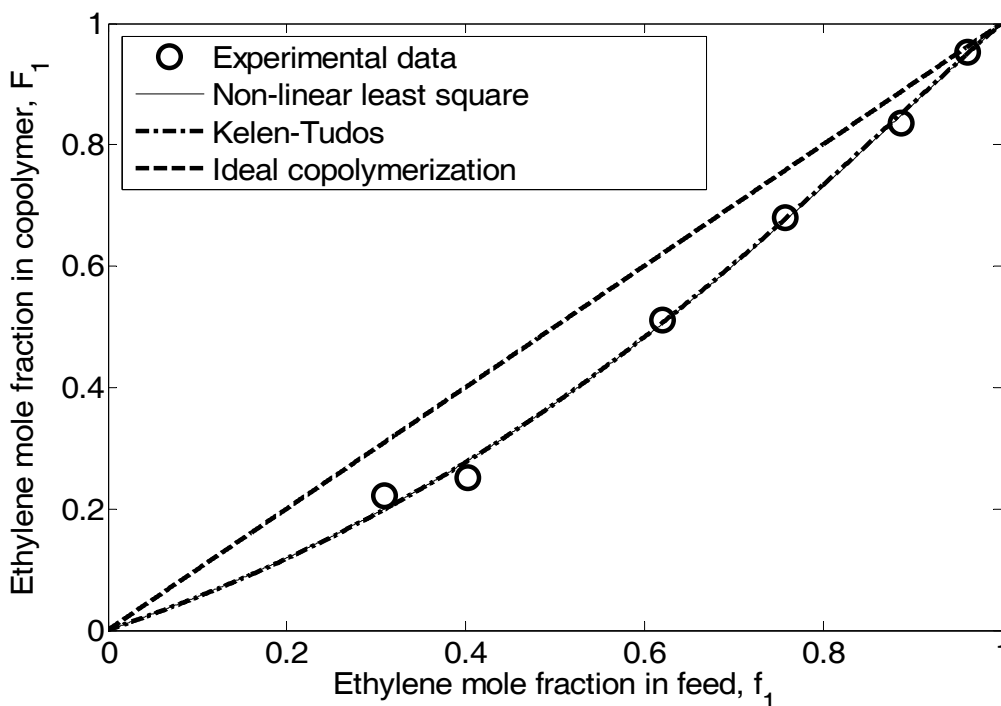


**Figure 4.7** Plot of mole fraction of ethylene in the copolymer,  $F_1$ , versus mole fraction of ethylene in the feed,  $f_1$  (copolymer compositions determined from *in situ* FTIR). The points are experimental data, while the lines are the examined model equations (the experimental conditions:  $T=50^\circ\text{C}$ ,  $P=27.6\text{MPa}$ ).

**Table 4.4** Reactivity ratios and 95% confidence intervals determined under different reaction conditions with different numerical methods

Temperature (°C)	Pressure (MPa)	Data Source	Analytical Method*	$r_{\text{ethylene}}$	$r_{\text{VAc}}$
50	27.6	<i>In situ</i> FTIR	NLLS	0.76±0.26	1.95±0.65
			KT	0.78	1.98
		Off-line <sup>1</sup> H NMR	NLLS	0.41±0.31	3.17±2.25
			KT	0.51	3.96
72	27.6	<i>In situ</i> FTIR	NLLS	0.46±0.22	1.41±0.71
			KT	0.43	1.40
50	13.8	<i>In situ</i> FTIR	NLLS	0.33±0.13	1.30±0.51
			KT	0.35	1.29

\* NLLS: Non-linear least-square; KT: Kelen-Tudos.

For comparison purposes, the formed copolymers were also characterized by offline <sup>1</sup>H NMR (see Table 4.2), with the resulting reactivity ratios listed in Table 4.4. The reactivity ratio of ethylene determined from the off-line <sup>1</sup>H NMR data is slightly smaller while that of VAc is larger in addition to the generally larger errors. The relatively large  $r_{\text{VAc}}$  and small  $r_{\text{ethylene}}$  determined by off-line <sup>1</sup>H NMR is likely due to higher monomer conversions in the experimental apparatus, as the polymerizations were normally run for 30 minutes or longer, with only the first few minutes of the FTIR data used for calculation purposes (i.e. Figure 4.2). The copolymerizations at higher conversions become heterogeneous (see Discussion) since the copolymers gave saturated

FTIR peaks after the initial stages of the reaction. These differences in the determined reactivity ratios reflect the advantages of the *in situ* FTIR method in the determination of reactivity ratios for copolymerization, as previously mentioned by Wiles *et al*<sup>130</sup>. The *in situ* method is particularly useful for high-pressure systems as it records the instantaneous composition change information, which can only be inferred using off-line measurement techniques such as NMR.

#### 4.3.3.2. Effect of Reaction Temperature and Pressure

In order to examine the effect of reaction temperature on the reactivity ratios, several experiments varying  $f_1$  were conducted at a higher temperature (72°C) and the same reaction pressure (27.6MPa) for statistical comparison. The results in Table 4.4 show that the reactivity ratios of both ethylene and VAc decrease slightly with increasing temperature from 50°C to 72°C.

Although the effect of pressure on reactivity ratios is usually negligible for most copolymerization systems, the reactivity ratios involving a gaseous comonomer (such as ethylene) appear to be pressure-dependent.<sup>131</sup> Several experiments in the copolymerization of ethylene and vinyl acetate in scCO<sub>2</sub> varying ethylene mole fraction in the feed were conducted at the same temperature (50°C) but a lower pressure (13.8MPa), for statistical comparison. As seen in Table 4.4, both  $r_{\text{ethylene}}$  and  $r_{\text{VAc}}$  increase with pressure. Figure 4.8 summarizes all the experimental data by showing a plot of copolymer composition versus feed composition for the different reaction temperature and pressure conditions examined in scCO<sub>2</sub>. It is found that the copolymer composition for the same monomer feed composition varies only slightly under the experimental conditions.

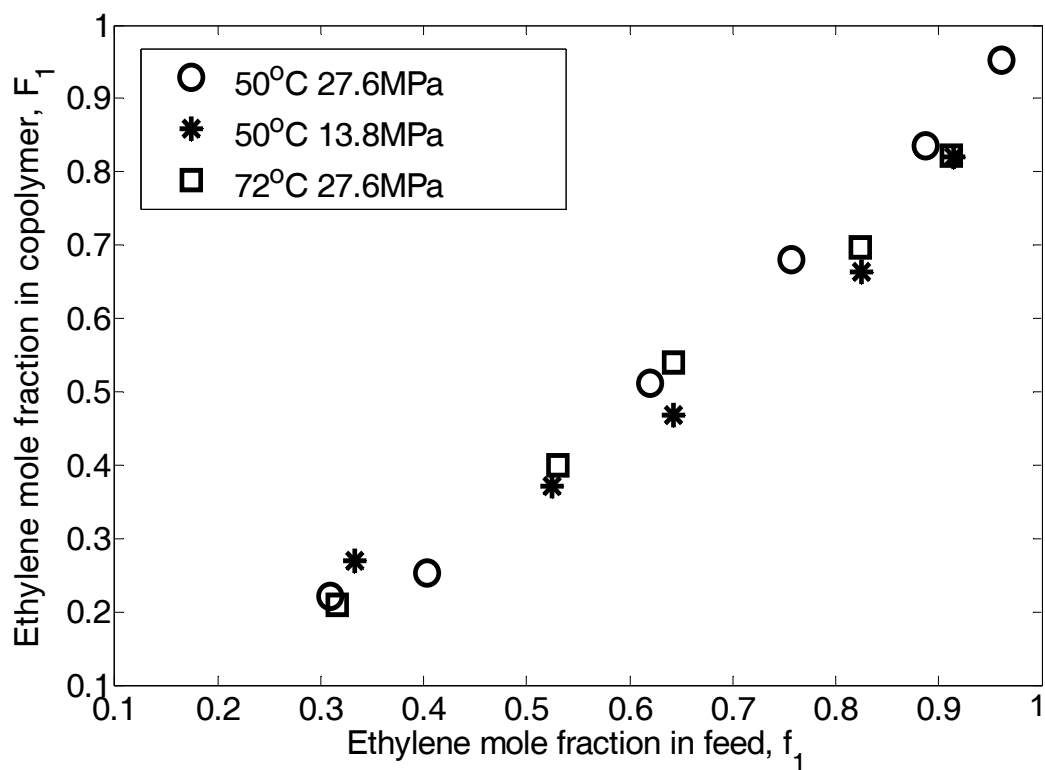


**Figure 4.8** Copolymer composition versus feed composition for different reaction temperature and pressure conditions in scCO<sub>2</sub>.

#### 4.3.4. Discussion

The monomer reactivity ratios can be theoretically calculated by means of the Q-e scheme proposed by Alfrey and Price.<sup>132</sup> From the Q-e values,<sup>133</sup> the reactivity ratios for the copolymerization of ethylene and VAc are calculated to be  $r_{\text{ethylene}}=0.59$  and  $r_{\text{VAc}}=0.72$ . By means of molecular orbital theory calculations, Filley *et al*<sup>134</sup> found that the reactivity ratios for this system were  $r_{\text{ethylene}}=0.20 \sim 0.32$  and  $r_{\text{VAc}}=0.76 \sim 0.97$  and the penultimate effect could be ignored. These theoretically-calculated results are not in good agreement with the experimentally-determined reactivity ratios found in scCO<sub>2</sub>, as listed in Table 4.4. In explanation, the reactivity ratios can be affected by the reaction

temperature, pressure, and reaction medium,<sup>52</sup> as being observed experimentally in this study.

From the literature, a weak dependence of  $r_{\text{ethylene}}$  on temperature was reported by Buback and Panten<sup>135</sup> in a study of the terpolymerization of ethylene, acrylonitrile and VAc from 170 to 240°C at 200MPa. As well, both  $r_{\text{ethylene}}$  and  $r_{\text{VAc}}$  were found to be weakly dependent on temperature from 60 to 135°C by theoretical calculations.<sup>134</sup> For the effect of pressure, Van der Meer *et al*<sup>136</sup> found that the dependence was insignificant at 62°C for the polymerization of ethylene and VAc under pressures between 3.4 and 58.8MPa using tert-butyl alcohol as solvent. However, Erusalimskii *et al*<sup>60</sup> found that the reactivity ratios of ethylene and VAc both increased significantly at 60°C when the pressure was increased from 10 to 120MPa using ethylene as the monomer/solvent. Similarly, the reactivity ratio of ethylene was also found to increase with pressure as reported by Buback and Dietzsch<sup>137</sup> for the high-pressure free-radical copolymerization of ethylene and methyl methacrylate. The present experimental results, where the pressure effect came from the increased amount of scCO<sub>2</sub>, agree rather well with these latter studies.

The reaction medium is also known to strongly affect the reactivity ratios through monomer partitioning, solubility, viscosity, and polarity.<sup>131, 134</sup> The small degree of dependence of reactivity ratios on temperature/pressure that was experimentally observed in this study might be due in part to the variation of solvent nature with these variables, as reflected by the changing density (0.854, 0.756, and 0.665g/mL at 50°C 27.6MPa, 72°C 27.6MPa, and 50°C 13.8MPa, respectively<sup>126</sup>). The effect of solvent on the copolymerization of ethylene and vinyl acetate was studied by Van der Meer *et al*<sup>57</sup> at

62°C and 3.4MPa who found that solvents of higher polarity or stronger interaction with VAc resulted in higher  $r_{\text{ethylene}}$  and lower  $r_{\text{VAc}}$  values. The present experimental results are in good agreement with this finding, with lower  $r_{\text{ethylene}}$  and higher  $r_{\text{VAc}}$  values being observed when the non-polar scCO<sub>2</sub> was used as solvent in this study. In the case of bulk copolymerization where ethylene works as the monomer/solvent, the polarity effect of non-polar ethylene could be more or less suppressed, as relatively low  $r_{\text{VAc}}$  values were observed by Raetzsch et al.<sup>138</sup> Ethylene can participate in the copolymerization while CO<sub>2</sub> cannot.

Supercritical CO<sub>2</sub> is well known to be a good solvent for most low molar mass non-polar and some polar molecules (i.e. the monomers and initiator),<sup>5</sup> but it is a poor solvent for most high molar mass polymers under mild conditions.<sup>3</sup> In general, the copolymerization of ethylene and VAc in scCO<sub>2</sub> should be considered as a precipitation polymerization, as the initially homogeneous mixture of the comonomers and initiator becomes heterogeneous during the reaction as the insoluble copolymer chains aggregate to form a separate polymer phase. Precipitation affects the copolymer composition and the monomer sequence distribution when accessibility of the reaction site is different for each monomer.<sup>139</sup> As reported by Baradie and Shoichet,<sup>140</sup> preferential solvation of one monomer in scCO<sub>2</sub> is enhanced by differences in the polarity of the solvent and the comonomers, and the polar monomer partitions from the solution phase into the polymer phase. Hence, as the copolymerization of ethylene and VAc in scCO<sub>2</sub> proceeds to higher conversions, the polar monomer VAc may be enriched at the polymerization sites, as it likely solvates the propagating macroradical chain in the non-polar scCO<sub>2</sub>. Once the polar monomer VAc has easier access to the polymerization site than the non-polar monomer

ethylene, the apparent propagating rate of VAc is enhanced while that of ethylene is weakened, leading to the observed higher  $r_{\text{VAc}}$  and lower  $r_{\text{ethylene}}$  values at higher conversions. The effect of solvent polarity on the reactivity ratios is not a phenomenon only occurring in heterogeneous polymerizations, as a similar effect was noted on the reactivity ratios in the solution copolymerization of styrene and the relatively polar monomer 2-hydroxyethyl methacrylate in nonpolar solvents.<sup>141</sup>

From cloud-point experimental data, poly(vinyl acetate) has been reported to have relatively high solubility in  $\text{scCO}_2$  by Rindfleisch *et al*<sup>16</sup> and Shen *et al*<sup>17</sup>. During the initial stages where the *in situ* FTIR results were used for determination of reactivity ratios (below 2% conversion), the copolymerization of ethylene and VAc in  $\text{scCO}_2$  was homogeneous. The ATR-FTIR probe is mainly seeing the instantaneous copolymer formed in solution, so the higher molecular weight heterogeneous material formed in later stages of the copolymerization will not be observed. Hence, the reactivity ratios determined in this study in the initial stages of copolymerization can be considered as the true reactivity ratios. Due to the enhanced polarity effect of  $\text{scCO}_2$  on the reactivity ratios in heterogeneous processes as discussed above, apparent reactivity ratios of even higher  $r_{\text{VAc}}$  and lower  $r_{\text{ethylene}}$  values should be expected at higher conversions. These measured reactivity ratios are very promising for potentially producing high content VAc copolymers in the “green” solvent,  $\text{scCO}_2$ , which are not readily achievable using the current high pressure industrial processes. Future work will further explore the mechanism of copolymerization in  $\text{scCO}_2$  and how to utilize these measured reactivity ratios studying advanced nanomaterials of PEVA for emerging applications in solar energy and biomaterials<sup>120</sup>.



#### 4.4. Conclusions

The monomer reactivity ratios of the copolymerization of ethylene and vinyl acetate in scCO<sub>2</sub> were determined using both *in situ* ATR-FTIR and off-line <sup>1</sup>H NMR analysis. The *in situ* method showed significant advantages over the off-line method for this high-pressure system. Two analytical methods including the Kelen-Tudos, and the non-linear least-squares method were applied in the determination of reactivity ratios, wherein similar results were obtained. The reactivity ratios were found to be dependent on the reaction conditions such as temperature, pressure, and the reaction medium. By comparing the results with those reported in the literature, the scCO<sub>2</sub> reaction medium was found to have significant effects on copolymerization of ethylene and VAc. The non-polar CO<sub>2</sub> was found to result in lower reactivity ratio of ethylene and higher reactivity ratio of vinyl acetate than those polar solvents studied in the literature. The determined reactivity ratios will promote the application of the “green” solvent scCO<sub>2</sub> in industrial production of copolymers of ethylene and vinyl acetate, particularly those of higher vinyl acetate content.

**Chapter 5. A Novel Approach to the Synthesis of SiO<sub>2</sub>-PVAc  
Nanocomposites Using a One-Pot Synthesis in Supercritical CO<sub>2</sub>**

In this chapter, a novel one-pot technique for the synthesis of SiO<sub>2</sub>-PVAc nanocomposites using scCO<sub>2</sub> is described. *In situ* ATR-FTIR was applied to monitor the process in scCO<sub>2</sub>, wherein the parallel reactions of free radical polymerization, hydrolysis/condensation, and linkage of silica nanoparticles to the PVAc matrix, were found to take place. Transmission electron microscopy (TEM) and EDX element Si-mapping were employed to characterize the synthesized nanocomposites, indicating excellent dispersion of nanoparticles of 10 ~ 50nm in the polymer matrix. Part of this chapter is reproduced by permission of The Royal Society of Chemistry from the published article by the author: A novel approach to the synthesis of SiO<sub>2</sub>-PVAc nanocomposites using a one-pot synthesis in supercritical CO<sub>2</sub><sup>120</sup>, in Green Chemistry, Copyright [2007] by The Royal Society of Chemistry. (<http://www.rsc.org/publishing/journals/GC/article.asp?doi=b617634h>).

## 5.1. Introduction

Significant progress has been achieved in recent years for developing new “green” chemical processes to meet the ever stringent governmental policies for environmental protection.<sup>142, 143</sup> The main criteria for developing a “green” chemical process is producing the required (or superior) materials either by a waste-free process or with a significant reduction in the amount of generated waste.<sup>144-148</sup> Generally, the development in “green” chemical processes can be divided into two scopes: reaction route alternatives<sup>144-146</sup> and solvent alternatives.<sup>6, 147-149</sup> It is widely accepted that reducing the number of synthesis steps can significantly reduce the amount of waste and energy consumption. Hence, changing the reaction route to lower the number of synthetic steps is of significant environmental and economic advantage.<sup>144</sup> As well, alternative synthesis design and approaches utilizing “green” solvents for pollution prevention are highly desirable.<sup>147-149</sup> Regulation of the use of hazardous organic solvents is becoming increasingly stringent and has spurred the development of environmentally conscious, economical reaction media.

As mentioned in Chapter 1, supercritical carbon dioxide (scCO<sub>2</sub>) has shown to be a promising alternative medium for polymerizations and continuous processes.<sup>3, 86, 150</sup> In addition to polymer synthesis, scCO<sub>2</sub> has also been developed as an enabling solvent in various chemical processes such as particle formation,<sup>151, 152</sup> extraction, coating,<sup>153</sup> cleaning,<sup>148</sup> drying, and media for organic and inorganic reactions including nanomaterials,<sup>89, 154</sup> many of which are unique with exciting properties.

Polymer nanocomposites are finding widespread industrial, household and biomedical applications in both existing and several new areas.<sup>155-157</sup> In comparison with the virgin plastics, polymer nanocomposites often have unique morphologies, physical and chemical properties, and exhibit marked improvements of fuel and gas (oxygen and CO<sub>2</sub>) barriers, flame resistance, stiffness, thermal and structural stabilities. The polymer nanocomposites normally contain fine inorganic particles or inorganic fibers well dispersed in the polymer matrix, with the particle size of the inorganic particles/fibers having a significant effect on the mechanical properties.<sup>158</sup> However, controlling the particle size at the nanometer level is a challenging project.<sup>155</sup> Of additional challenge is successful coupling of the nanoparticles to the matrix, which is highly desirable to maximize mechanical properties.<sup>155</sup> Generally, the conventional methods for synthesis of polymer composites are through complex multi-step synthetic processes, including:<sup>157, 159-168</sup> (1) formation of inorganic particles or polymer; (2) modification of the obtained inorganic particles or the polymer; and (3) introducing the inorganic particles into the polymer matrix. The most popular method is simply by mixing the two obtained parts of polymer and inorganic particles, either by melt compounding, which adds inorganic particles into a polymer melt,<sup>159-161</sup> or by a solution obtained by dissolving the polymer in an organic solvent,<sup>162-164</sup> then evacuating the solvent after mixing with the inorganic particles. In addition, usually the inorganic particles or the applied polymer requires further modification by adding a coupling agent to enhance the interaction of the inorganic part with the organic polymer for coupling to the polymer matrix.<sup>169, 170</sup> In these multi-step synthetic processes, each synthesis step consumes energy, time, labor and results in significant waste. Hence, a “green” approach to polymer nanocomposite

synthesis that provides small nanometer size particles, good distribution of the nanofillers throughout the matrix, chemical attachment of the nanofillers to the matrix, along with reducing the number of synthesis steps while using a “green” solvent, is extremely desirable.

In this research, *in situ* FTIR was applied to analyze free radical polymerization and hydrolysis in scCO<sub>2</sub>, respectively, to generate polymer nanocomposites. A novel one-step synthesis route of SiO<sub>2</sub>-PVAc polymer composites was discovered by combining parallel reactions of free radical polymerization and hydrolysis, and subsequent linkage of the particles to the polymer chain.

## **5.2. Experimental**

### **5.2.1. Materials**

Instrument grade CO<sub>2</sub> (from BOC Gases, 99.99%, with dip-tube) and ultra high purity N<sub>2</sub> (BOC, 99.99%) were further purified by passing through columns filled with 5Å molecular sieves and reduced 20% copper oxide/Al<sub>2</sub>O<sub>3</sub> to remove the moisture and oxygen, respectively. Vinyl acetate (>99%) was purchased from Aldrich Canada and distilled under vacuum. Glacial acetic acid, tetrahydrofuran (THF) (≥99.9%) (CHROMASOLV<sup>®</sup> Plus), tetraethyl orthosilicate (TEOS), tetramethyl orthosilicate (TMOS), and vinyltrimethoxysilane (VTMO) were purchased from Aldrich Canada and used as received. The initiator diethyl peroxydicarbonate (DEPDC) was synthesized as previously described in Chapter 3.

### 5.2.2. Polymerization Procedure

Synthesis was conducted in the 100-mL high-pressure stainless steel autoclave coupled with a digital pressure transducer. The stirring speed was controlled at 400 rpm. The designated chemicals were charged into the reactor, purging with a flow of nitrogen, then pumping CO<sub>2</sub> into the autoclave by means of the syringe pump (ISCO 260D). After the reaction, CO<sub>2</sub> was carefully vented leaving the formed sample in the autoclave.

*In situ* Fourier transform infrared (FTIR) was used to monitor the solution concentration in the stirred 100-mL high-pressure autoclave. Spectra were recorded at a resolution of 2cm<sup>-1</sup> and the absorption spectra were the results of 64 scans. *In situ* ATR-FTIR was applied to monitor the various chemistries studied in scCO<sub>2</sub> including: (1) thermal decomposition of DEPDC, (2) homopolymerization of vinyl acetate, (3) copolymerization of vinyl acetate and VTMO, (4) hydrolysis of silicon alkoxides in the presence of copolymer, and (5) the one-pot synthesis of nanocomposites.

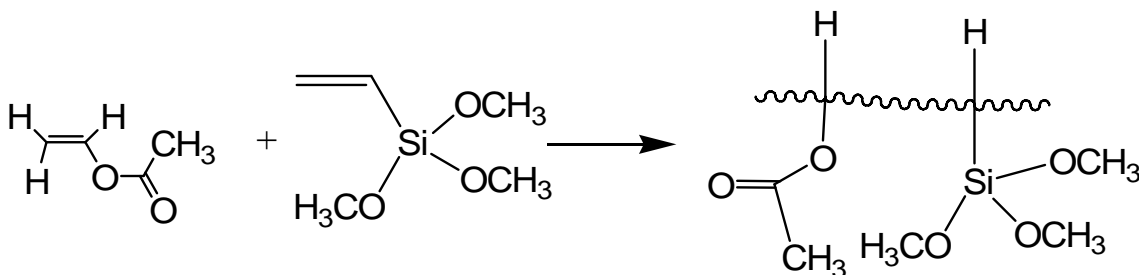
### 5.2.3. Characterization

Transmission electron microscopy (TEM) images were recorded using a Philips CM10 Transmission Electron Microscope operated at 80 kV. The specimens were previously dissolved in THF, and then placed on a copper grid covered with carbon film. EDX elemental mapping was recorded using a Hitachi S-2600N Scanning Electron Microscope.

### 5.3. Results and Discussion.

#### 5.3.1. Copolymerization

Although this one-pot process can work with essentially any vinyl monomer and silane linker that are soluble in  $scCO_2$ , vinyl acetate (VAc) was chosen as the monomer of interest because it has a relatively high solubility in  $scCO_2$ ,<sup>16, 17, 63, 171</sup> and the polymer poly (vinyl acetate) (PVAc) has widespread industrial and biomedical applications. VAc is also one of the necessary monomers for synthesis of the copolymer PEVA, as described in Chapter 4 and expanded upon in Chapter 6. Vinyltrimethoxysilane (VTMO) was applied as the second monomer for coupling to the sol-gel derived nanoparticles as well as the functionalized quantum dots which will be described in Chapter 6. A schematic diagram of the copolymerization of VAc and VTMO is shown in Scheme 5.1.



**Scheme 5.1** Copolymerization of VAc and VTMO to form copolymer

Figure 5.1 shows the FTIR spectra of the homopolymerization of vinyl acetate in  $scCO_2$ . In order to clearly identify the change of absorbance peaks in the homopolymerization and the copolymerization reactions, a transform was made in Figure 5.1f by subtracting the spectrum at reaction time  $t=0$  (Figure 5.1a) from the spectrum at reaction time  $t=300\text{min}$  (Figure 5.1e). The absorbance intensities at 1766, 1648, 1212, and  $1140\text{cm}^{-1}$  decreased during the polymerization, while those at 1729 and  $1233\text{cm}^{-1}$



increased. The decrease in height of the peaks at  $1648\text{cm}^{-1}$  (due to C=C stretching vibration) and  $1140\text{cm}^{-1}$  (due to O-C-C asymmetric stretching vibration of  $\text{CH}_3\text{C}(\text{O})\text{-O-CH=CH}_2$  molecule) indicates the conversion of vinyl acetate to poly(vinyl acetate).<sup>110</sup> That the absorbance peaks changed from  $1766$  to  $1729\text{cm}^{-1}$  (due to C=O stretching vibration) and from  $1212$  to  $1233\text{cm}^{-1}$  (due to C-C-O asymmetric stretching vibration) indicates the transfer of the ester groups from the monomer molecules to the polymer chains. Depending on the molecular weight of the polymer chains, partial solubility is expected due to the acetate functionality<sup>13</sup>, analogous to that observed with Beckman surfactants<sup>9, 10, 172</sup> or Wallen sugars<sup>11</sup>.

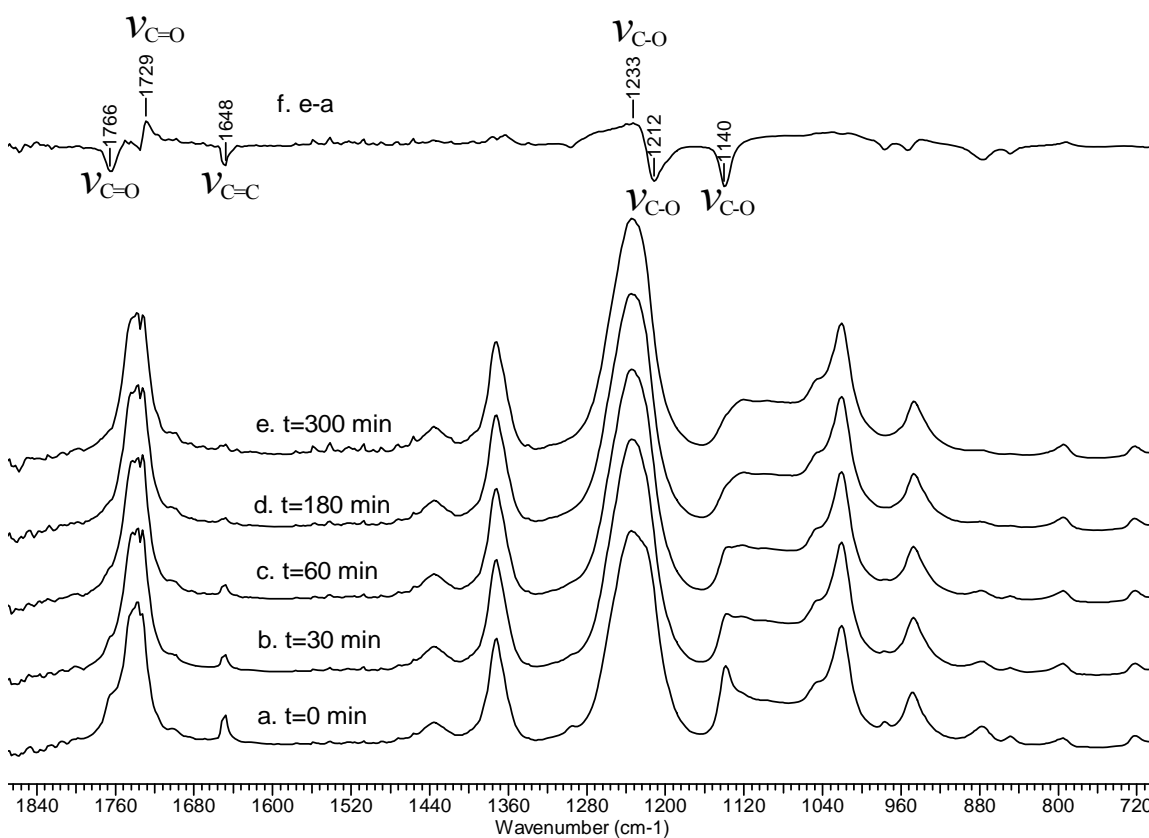


**Figure 5.1** *In situ* FTIR measurement of free radical polymerization of vinyl acetate in supercritical  $\text{CO}_2$  (The experimental conditions are:  $T=60^\circ\text{C}$ ,  $P=20.7\text{MPa}$ ).

The copolymerization of vinyl acetate and VTMO was carried out in scCO<sub>2</sub> by introducing the monomers, initiator, and CO<sub>2</sub> into the reactor, respectively. Figure 5.2 shows the FTIR spectra of a typical copolymerization at 60°C and 16.8MPa. A transform was also made in Figure 5.2f by subtracting the spectrum at reaction time t=0 (Figure 5.2a) from the spectrum at reaction time t=300min (Figure 5.2e). Similar to Figure 5.1, vinyl acetate consumption is indicated at 1764, 1649, 1214 and 1140cm<sup>-1</sup>. By contrast with the IR spectra of homopolymerization of vinyl acetate, it was found in Figure 5.2 that the previously observed peaks during homopolymerization of vinyl acetate drifted slightly and some peaks grew at 1368 and 1021cm<sup>-1</sup>, which are assigned to CH<sub>3</sub> symmetric deformation vibration and Si-O stretching vibration, respectively.<sup>173</sup> This silane modified PVAc was further applied in the next step, where hydrolysis of TMOS/TEOS was used to generate the inorganic part in the polymer composite.

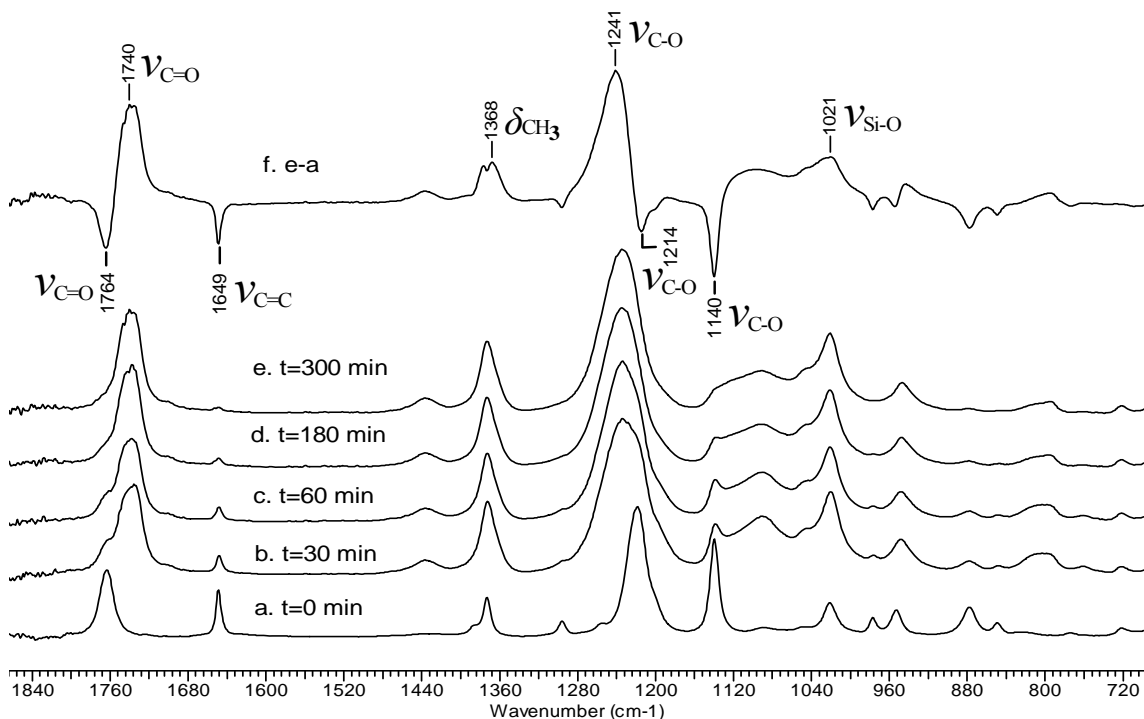


**Figure 5.2** *In situ* FTIR measurement of free radical copolymerization of vinyl acetate and VTMO in supercritical CO<sub>2</sub> (The experimental conditions are: T=60°C, P=16.8MPa, molar ratio: VAc:VTMO=40:1).

### 5.3.2. Hydrolysis

Hydrolysis using sol-gel chemistry is one of the most important methods for producing fine particles such as nanometer size inorganic particles.<sup>14, 174</sup> Supercritical CO<sub>2</sub> has been previously used to generate nanoparticles by drying the sample obtained from the sol-gel process,<sup>38, 174</sup> while previous work has shown that a direct or “one-pot” synthesis technique for the hydrolysis of metal alkoxides in scCO<sub>2</sub> was possible.<sup>38, 90</sup> It was found that a variety of liquid metal alkoxides, such as tetraethyl orthosilicate (TEOS) or tetramethyl orthosilicate (TMOS) are relatively soluble in scCO<sub>2</sub>, particularly in the presence of a polar modifier/hydrolysis agent such as acetic acid. It was also found that

both TEOS and TMOS polycondensation could be carried out at above 35°C in scCO<sub>2</sub> by using acetic acid.

Figure 5.3 demonstrates the FTIR spectra of the hydrolysis of TEOS mixed with the previously obtained copolymer of vinyl acetate and VTMO in scCO<sub>2</sub> at 60°C, in which acetic acid was added as the hydrolysis agent. It is seen that peaks grew with reaction time at 1742, 1238, 1050 and 1023cm<sup>-1</sup> but lowered at 1714 and 1292cm<sup>-1</sup>. The growing peaks at 1742 and 1238cm<sup>-1</sup> are due to the formation of acetic esters from the polycondensation reaction. The growing peak at 1050cm<sup>-1</sup> is due to the formation of Si-O-Si, while the shrinking peak at 1714 and 1292cm<sup>-1</sup> indicates the consumption of acetic acid. Figure 5.4 displays a TEM image of the formed PVAc nanocomposite. The spherical nanoparticles of various sizes are well dispersed in the polymer matrix. The particle size ranges from approximately 50-150nm.

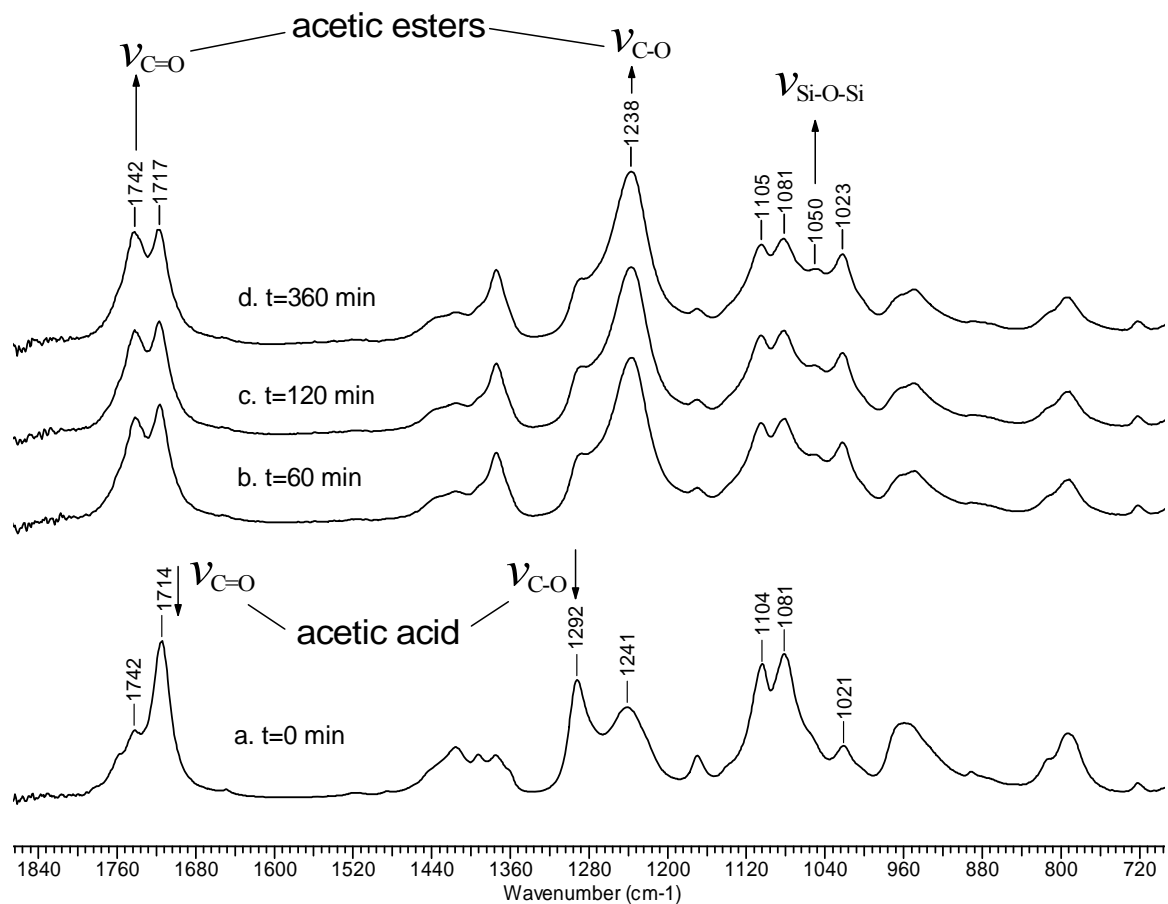


**Figure 5.3** *In situ* FTIR measurement of hydrolysis of TEOS in the silane modified PVAc in scCO<sub>2</sub> (The experimental conditions are: T=60°C, P=16.8MPa, molar ratio: HAc:TEOS=4.3:1).

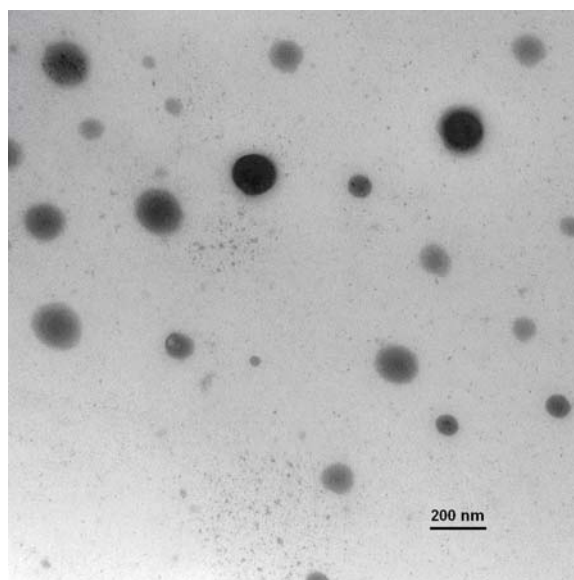


**Figure 5.4** TEM image of the PVAc nanocomposite from hydrolysis of TEOS with acetic acid in presence of copolymer of vinyl acetate and VTMO in  $scCO_2$ .

### 5.3.3. One-Pot Synthesis

The goal of this research was not only to synthesize polymer nanocomposites, but also to explore a novel “green” one-pot technique. For this purpose, all the raw materials such as vinyl acetate, VTMO, TEOS/TMOS, acetic acid, and the initiator DEPDC were introduced into the autoclave. Then the compressed  $CO_2$  was pumped into the autoclave and heated to reach the supercritical state. After 1080min reaction at  $60^\circ C$  and subsequent cooling and evacuation of  $CO_2$ , a viscous liquid was collected from the autoclave and placed in a vacuum oven. A monolith product of  $SiO_2$ -PVAc nanocomposites was then obtained. Figure 5.5 and 5.6 display the FTIR spectra from the synthesis process by using TEOS and TMOS, respectively. Both the figures show the parallel reactions of copolymerization and hydrolysis proceeding simultaneously. Figure 5.5 shows the consumption of monomer from the decreasing intensity of the peak at  $1648cm^{-1}$ , by comparing with the spectra discussed previously. The growing peaks at

1740 and 1235 $\text{cm}^{-1}$  are due to the formation of acetic esters from the polycondensation reaction, while the absorbance decrease at 1712 and 1293 $\text{cm}^{-1}$  indicates the consuming of acetic acid. The formation of oxo bonds between silicon atoms can be noticed by the widening peak in the 1052 $\text{cm}^{-1}$  region, which is similar to Figure 5.3 where TEOS nanoparticles were attached to an existing vinyl acetate-VTMO copolymer. When using TMOS as the polycondensation agent, Figure 5.6 also shows the parallel reactions occurring of copolymerization and hydrolysis. The consumption of monomer is observed from the decreasing intensity of the peak at 1649 $\text{cm}^{-1}$ , while the growing peaks at 1739 and 1236 $\text{cm}^{-1}$  are due to the formation of acetic esters from the polycondensation reaction while the absorbance decrease at 1715 and 1294 $\text{cm}^{-1}$  indicates the consuming of acetic acid. The formation of oxo bonds between silicon atoms can be noticed by the widening peak in the 1068 $\text{cm}^{-1}$  region. Figure 5.7 demonstrates the TEM images and particle size distribution histograms of the PVAc nanocomposites from the one-pot synthesis by using TMOS and TEOS, respectively. From the images, nanoparticles with a diameter of 10 ~ 50nm were well dispersed throughout the polymer matrix. The particle size distribution histograms show that the silica nanoparticles obtained when using TEOS have smaller diameter and narrower size distribution than that obtained when using TMOS precursor. This may be due to the lower reactivity of TEOS than TMOS in the sol-gel process<sup>45, 48</sup>. Low reaction rate could reduce agglomeration of particles and result in uniform and narrow distribution of particles.<sup>38</sup> Besides, these particles obtained from one-pot synthesis route are significantly smaller than those from the 2-step synthesis route discussed above. This may be due to enhanced interaction of the TEOS/TMOS alkoxide with the silane linker groups in the copolymer that forms during the one-pot synthesis,

compared to that of the two-step procedure, where the previously synthesized copolymer was placed in the reactor before subsequent hydrolysis. One can envision that as the polymer chain grows and incorporates vinyltrimethoxysilane, the silane linkage is more accessible and easier to attach to the growing nanoparticles, hence slowing down the condensation reaction and subsequently providing smaller nanoparticles. The EDX Si-mapping (Figure 5.8) also shows that the element Si was well dispersed in the material.

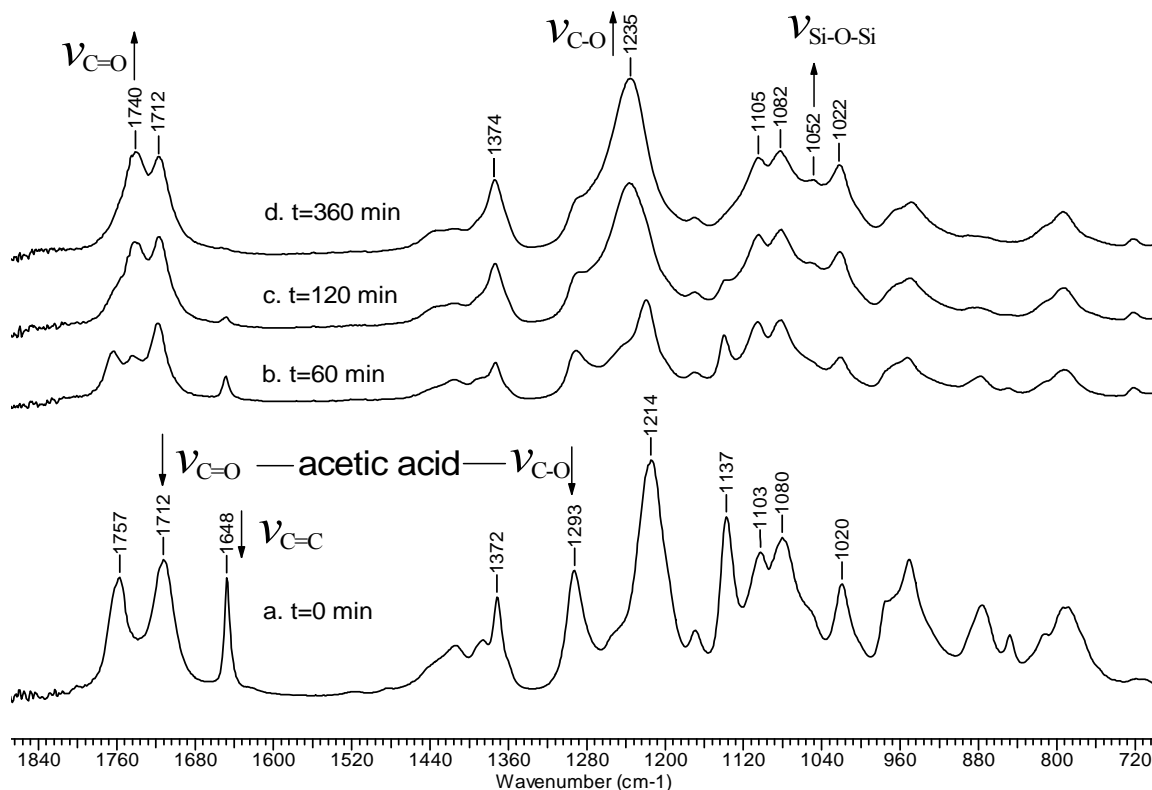


**Figure 5.5** Parallel reactions of the copolymerization of vinyl acetate and VTMO and hydrolysis of TEOS/VTMO with acetic acid in  $scCO_2$  (The experimental conditions:  $T=60^\circ C$ ,  $P=16.8MPa$ , molar ratio:  $VAc:VTMO:HAc:TEOS:DEPDC = 40:1:43:10:1$ ).



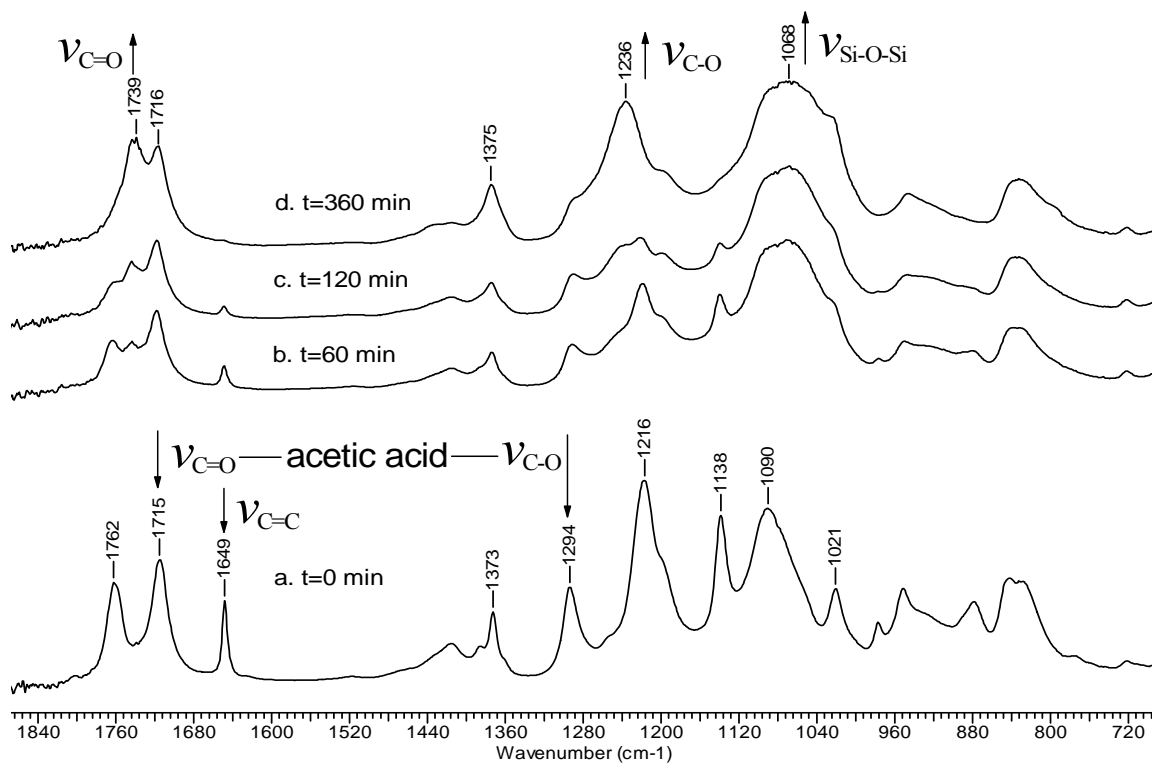


**Figure 5.6** Parallel reactions of the copolymerization of vinyl acetate and VTMO and hydrolysis of TMOS/VTMO with acetic acid in scCO<sub>2</sub> (The experimental conditions: T=60°C, P=16.8MPa, molar ratio: VAc:VTMO:HAc:TMOS:DEPDC =40:1:43:10:1).

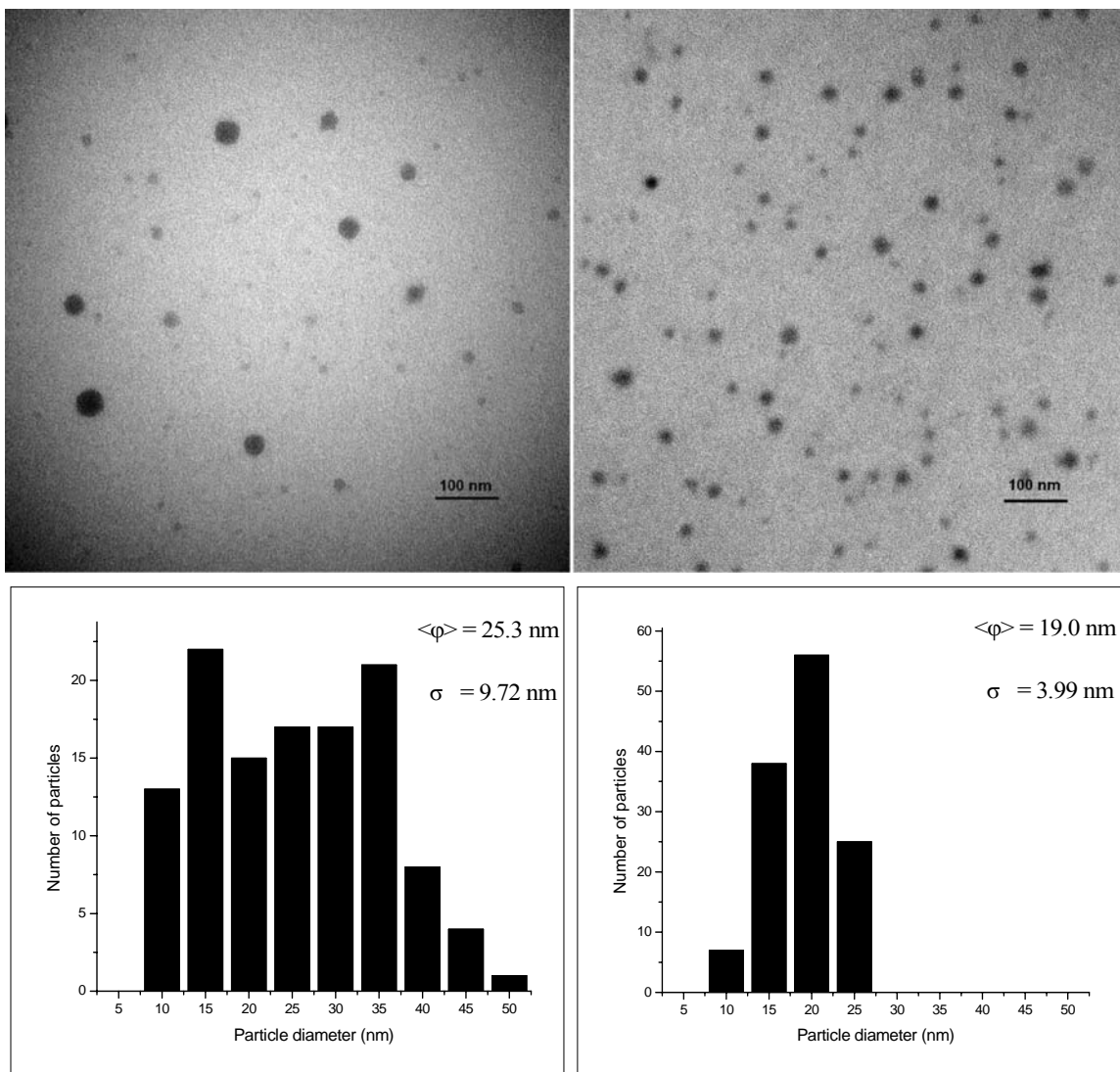


**Figure 5.7** TEM images and particle size distribution histograms of the PVAc nanocomposites from the one-pot synthesis in  $scCO_2$  using TMOS (left) / TEOS (right).

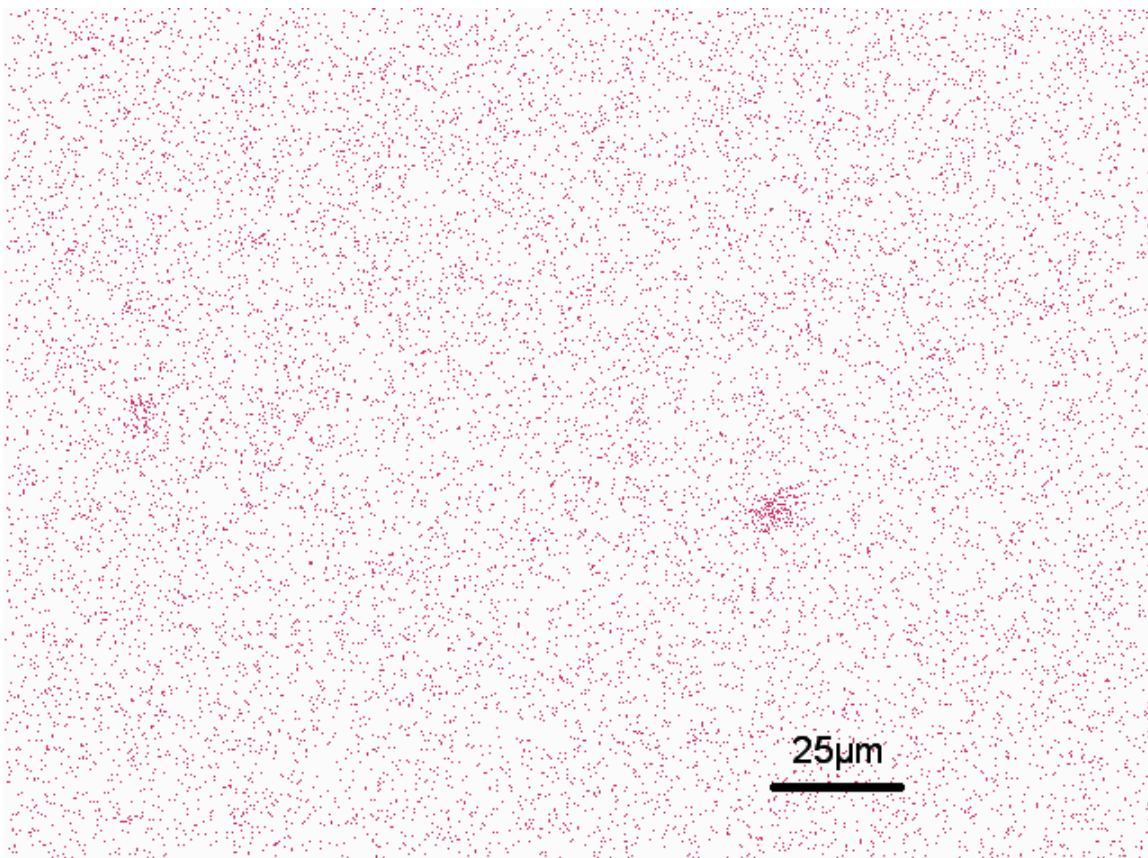


**Figure 5.8** EDX element Si-mapping of PVAc nanocomposite from the one-pot synthesis in  $scCO_2$  using TMOS.

Hence, all the FTIR evidence regarding the independent copolymerization and hydrolysis steps are found in the one-pot experiment, such as the conversion of monomers, polymer formation, consumption of acetic acid, and the formation of Si-O-Si bonding. Based on the knowledge developed on polymerization and hydrolysis, silica-PVAc nanocomposite was successfully synthesized by parallel reactions of the free radical copolymerization of vinyl acetate and VTMO and hydrolysis of TEOS/TMOS with acetic acid. This technique can be extended to other vinyl systems with solubility in  $scCO_2$ , and hydrolysis of other metal alkoxides including  $TiO_2$ ,  $ZrO_2$ , etc.

Several significant advantages of using  $\text{scCO}_2$  as a “green” solvent for both polymerization and hydrolysis over conventional methods of using aqueous or organic solvents are likely. Small nanoparticles were formed that attach directly to the polymer matrix, which is extremely challenging using existing multi-step approaches. On the one hand, due to the low heat of vaporization of  $\text{CO}_2$ , energy costs can be substantially reduced relative to water-intensive or even solvent-based processes, which often demand a large amount of energy associated with drying operations<sup>87</sup>. On the other hand, using the parallel reactions of polymerization and hydrolysis in a one-pot reactor has significant advantages over multiple-step approaches which would require more time, labor and organic solvents. In addition, this process is amendable to a continuous process, with potential coupling to supercritical fluid extraction (SFE) for resin purification. Future work will further explore the details of the one-pot mechanism in  $\text{scCO}_2$ , and how to change the synthesis conditions to form desirable nanocomposites.

#### **5.4. Conclusions**

A “green” chemical process for the synthesis of polymer nanocomposites of  $\text{SiO}_2$ -PVAc in supercritical carbon dioxide ( $\text{scCO}_2$ ) was developed. *In situ* ATR-FTIR analysis showed that the steps of polymerization, hydrolysis, and coupling occurred simultaneously in  $\text{scCO}_2$  in the autoclave. Nanoparticles in the 10 ~ 50nm range were formed, that were well distributed throughout the polymer matrix. A significant improvement has been made by reducing a complex multi-step procedure to a one-step synthesis route. As the recyclable supercritical carbon dioxide worked as solvent,

modification agent, and drying agent, this “green” process demonstrated many advantages in waste-reduction and energy-saving.

**Chapter 6. Synthesis of Light-Selective Quantum Dot-Polymer  
Nanofilms in Supercritical CO<sub>2</sub>**

This chapter presents the synthesis of light-selective quantum dot-polymer nanofilms in scCO<sub>2</sub>. Both CdS and CdS-ZnS core-shell QDs were synthesized and then functionalized with a methoxysilane group. Several characterization methods were employed to confirm the successful synthesis and functionalization of the QDs. The functionalized QDs were then incorporated into PVAc and PEVA polymer matrices using scCO<sub>2</sub> to form QD-polymer nanofilms. The light-selective properties of the synthesized nanofilms were revealed by photoluminescence and UV-Vis spectroscopy. A version of this chapter has been submitted for publication to *Journal of Physical Chemistry: Light-selective nanofilms of quantum dot-poly(ethylene-co-vinyl acetate) synthesized using supercritical CO<sub>2</sub>*.<sup>175</sup>

## 6.1. Introduction

Utilizing solar energy has been attracting considerable multidisciplinary research interest recently, as the Sun provides Earth with as much energy every hour as human civilization uses every year.<sup>176</sup> Although turning solar radiation into electricity is one option, another is finding ways to harness its heat and control the wavelengths of sunlight. Converting the undesirable higher-energy lights, e.g., UV, into desirable lower-energy lights will expand the applications of solar energy into new areas. Potentially, polymer films can be tailored for various applications such as greenhouses for controlling flowering or fruiting of plants and herbs<sup>177</sup> and window films for sunlight control with heat gain/reduction.

As a type of semiconducting nanocrystallite, quantum dots (QDs) are being intensively explored in a variety of fields such as nanobiotechnology<sup>178, 179</sup> and solar cell technology<sup>180</sup>. QDs can emit photons corresponding to their respective energy band gaps when they are excited to reach their respective excited states. The band gaps of quantum dots can be tailored by changing the type of QDs, e.g., CdS, CdSe and CdTe, and/or the size, which are tunable by controlling the reaction conditions such as time and temperature.<sup>79, 181, 182</sup>

The main method for preparing QDs is classical colloidal chemistry<sup>80</sup> where various researchers have employed organometallic and/or metal organic compounds under anaerobic conditions to synthesize QDs. For example, CdSe QDs was prepared by reacting dimethylcadmium ( $\text{CdMe}_2$ ) with trioctylphosphine selenide (TOPSe) in trioctylphosphine (TOP)/trioctylphosphine oxide (TOPO) at high temperature.<sup>79, 183</sup> Other



researchers used single-molecular precursors such as bis(diethyldithio-/diseleno-carbamato) cadmium (II) /zinc (II) for the preparation of QDs.<sup>80, 184, 185</sup> Single-molecular precursors have significant advantages of being less toxic, insensitive to air and moisture, easier to purify, and provide highly monodisperse nanoparticles, with the synthesis generally undertaken at desirable lower temperatures.<sup>80,186</sup>

In addition to the “bare” quantum dots such as CdSe and CdS, core-shell QDs have also been extensively studied due to their novel properties. Overcoating nanocrystallites with higher band gap inorganic materials has been shown to improve the photoluminescence quantum yields and photostability.<sup>187-189</sup> Particles passivated with inorganic shell structures are more robust than organically passivated dots, and have shown greater tolerance to processing conditions necessary for incorporation into solid state structures.<sup>190</sup> Some examples of core-shell quantum dot structures reported previously include CdS on CdSe<sup>189</sup>, ZnS on CdSe<sup>187, 190, 191</sup>, and ZnS on CdS<sup>192, 193</sup>, etc.

The colloidal QDs are surrounded by a layer of organic ligands in a “shell” which dictates the surface chemistry of the QDs, and therefore plays a significant role in the solubility or miscibility within a given environment.<sup>194</sup> As the high-temperature synthesis of QDs is not compatible with most organic functional groups, ligand exchange is often required for the introduction of new surface functionality to QDs. Ligand exchange with various thiol ligands has been extensively studied.<sup>195-198</sup> Compatible organic ligands with polymer matrices, such as bifunctional molecules containing a coordination “head” and a polymerizable “tail”, enable the applications of QDs in polymer composites.<sup>81</sup> Bawendi *et al*<sup>194</sup> reported a family of oligomeric phosphine ligands allowing tunable compatibility in diverse environments and flexibility for further

chemistry. In their study, tris(hydroxypropyl)phosphine (THPP) was reacted with diisocyanatohexane (DIH) to produce oligomerized THPP that was further functionalized with molecules containing an isocyanate group and an additional functional group such as methacrylate group which enabled copolymerization of QDs with many monomers.

In general, the major challenges for the successful synthesis of QD-polymer nanocomposites have been:<sup>183, 199-203</sup> (1) aggregation of the QDs due to poor miscibility of the QDs with the polymer matrix, (2) migration of the incorporated QDs when the chemical environment is changed, and (3) a significant decrease in quantum efficiency of the QDs. Supercritical carbon dioxide has been showing successful applications in fabrication of well-dispersed polymer nanocomposites.<sup>204</sup> The goal of this research was to develop a method to synthesize QD-PEVA nanofilms with a spectral emission of specific wavelengths. In this research, the one-pot technique described in Chapter 5 was extended to the synthesis of QD-PVAc nanofilms. CdS-ZnS core-shell QDs and CdS QDs were synthesized at a relatively low temperature and functionalized with a methoxysilane group. The functionalized QDs were incorporated into poly(vinyl acetate) (PVAc) and poly(ethylene-co-vinyl acetate) (PEVA) matrices by means of hydrolysis/condensation in the “green” solvent scCO<sub>2</sub>.

## **6.2. Experimental**

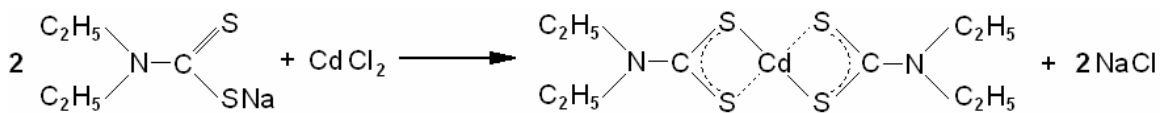
### **6.2.1. Materials**

Instrument grade CO<sub>2</sub> (99.99% purity from Praxair Canada Inc., with dip-tube), polymer grade ethylene (99.9% purity, Praxair), and ultra high purity N<sub>2</sub> (99.99%, Praxair) were further purified by passing through columns filled with 5Å molecular

sieves and reduced 20% copper oxide/ $\text{Al}_2\text{O}_3$  to remove the moisture and oxygen, respectively. Argon (99.999% purity, Praxair) was used without further purification. Vinyl acetate (VAc) (>99%) purchased from Sigma-Aldrich Canada was further purified by passing through an inhibitor remover column (Aldrich) to remove hydroquinone. (3-Mercaptopropyl)trimethoxysilane (MPTMO), vinyltrimethoxysilane (VTMO) (97%), pentane ( $\geq 99\%$ ) (DriSolv<sup>®</sup>), and cadmium chloride (tech grade, A.C.S. reagent), sodium diethyldithiocarbamate trihydrate (A.C.S. reagent), zinc diethyldithiocarbamate (98%), glacial acetic acid ( $\geq 99.99\%$ ), trioctylamine (TOA) ( $\geq 99.0\%$ ) (Fluka), trioctylphosphine (TOP) ( $\geq 90\%$ ) (Fluka), anhydrous methanol (99.8%), and toluene ( $\geq 99.9\%$ ) (CHROMASOLV<sup>®</sup> Plus) were purchased from Sigma-Aldrich Canada and used as received. Anhydrous ethyl alcohol was purchased from Commercial Alcohols, Inc., Canada and used as received. The initiator diethyl peroxydicarbonate (DEPDC) was synthesized as previously described in Chapter 3.

### **6.2.2. Preparation of the Single-Molecular Precursor Bis(diethyldithiocarbamato) Cadmium (II)**

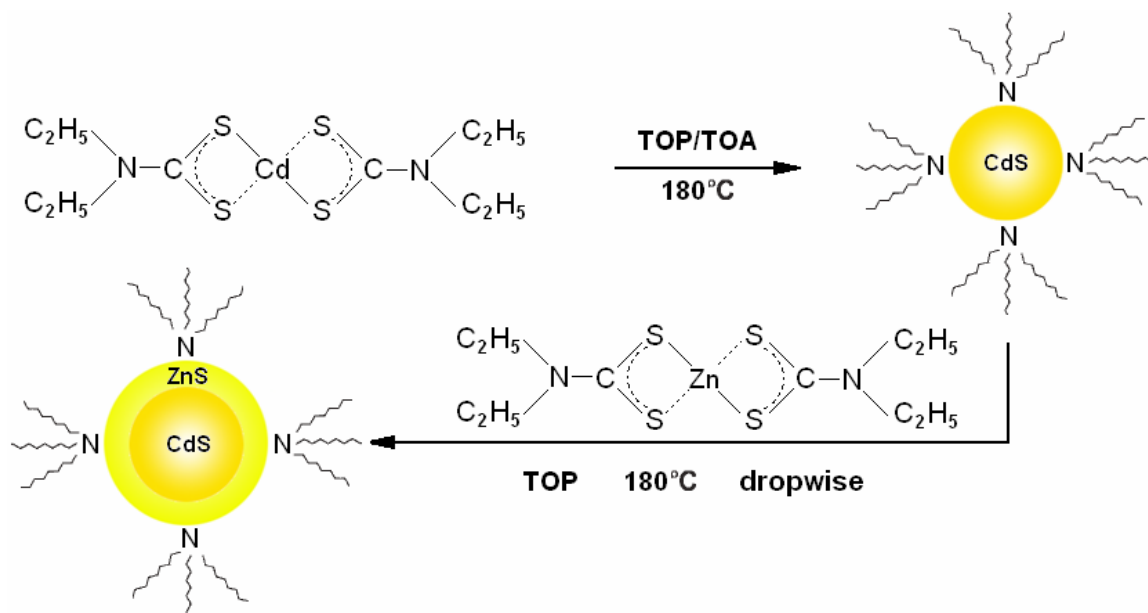
The synthesis of the single-molecular precursor  $\text{Cd}[\text{S}_2\text{CN}(\text{C}_2\text{H}_5)_2]_2$  was previously described by O'Brien and coworkers.<sup>185</sup> Stoichiometric amounts of a 0.1M aqueous solution of  $\text{NaS}_2\text{CN}(\text{C}_2\text{H}_5)_2 \cdot 3\text{H}_2\text{O}$  was reacted with 0.1M  $\text{CdCl}_2$  solution to give a white precipitate that was further filtered under vacuum and washed by means of redispersion of the precipitate into distilled water followed by vacuum filtration. Scheme 6.1 displays the reaction of synthesis of the precursor bis(diethyldithiocarbamato) Cadmium (II). The product was subsequently dried by placing in a vacuum oven at 40°C overnight.



**Scheme 6.1 The reaction of synthesis of bis(diethyldithiocarbamato) Cadmium (II)**

### 6.2.3. Preparation of CdS-ZnS and CdS QDs

A slight modification of the method reported by Yim *et al*<sup>193</sup> was used for the synthesis of CdS-ZnS core-shell QDs. 25mL TOA and a magnetic stirring bar were placed in a 100-mL three-neck flask under nitrogen equipped with a reflux condenser, a thermometer, and a thermocouple for automatic temperature control. When the temperature was stable at 180°C, a solution of 0.5g Cd[S<sub>2</sub>CN(C<sub>2</sub>H<sub>5</sub>)<sub>2</sub>]<sub>2</sub> in 9mL TOP was rapidly injected into the flask. After 5 or 10min reaction time, a solution of 0.2g Zn[S<sub>2</sub>CN(C<sub>2</sub>H<sub>5</sub>)<sub>2</sub>]<sub>2</sub> in 3mL TOP was slowly added dropwise. 5min after the completion of addition of the zinc diethyldithiocarbamate solution, the heater was removed to cool down the reaction mixture. When the temperature dropped to approximately 75°C, a large excess of methanol/ethyl alcohol was added followed by separation of the quantum dots through centrifugation. The QDs were washed with methanol, and then dispersed into toluene. The mixture of QDs in toluene was further filtered under vacuum to remove any insoluble material (poorly capped and large particles). Scheme 6.2 shows a schematic diagram of the synthesis of CdS-ZnS core-shell QDs.



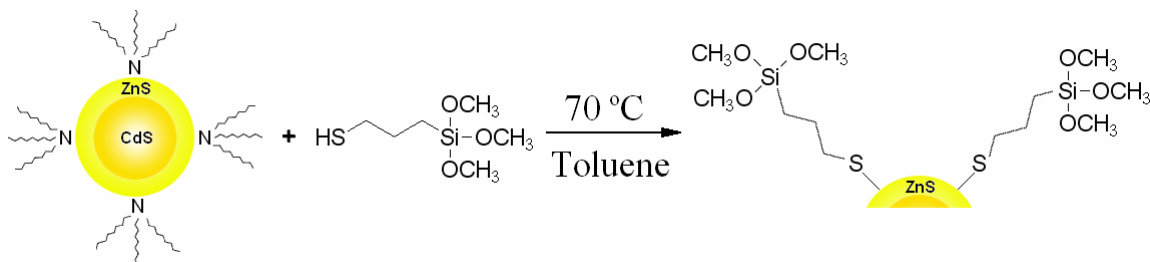
**Scheme 6.2** Schematic diagram of the synthesis of CdS-ZnS core-shell QDs

For the synthesis of CdS QDs, the procedure was carried out in the same manner as the synthesis of CdS-ZnS core-shell QDs described above, except higher temperature ( $235^\circ\text{C}$ ), longer reaction time (30min), and no addition of  $\text{Zn}[\text{S}_2\text{CN}(\text{C}_2\text{H}_5)_2]_2$ .

#### 6.2.4. Ligand Exchange of QDs

The QDs synthesized from 6.2.3 were subsequently reacted with 5mM MPTMO with stirring at  $70^\circ\text{C}$  for 24 hours under a nitrogen flow. After the reaction, the reaction mixture was cooled to ambient temperature. Then a large excess of pentane was added into the mixture followed by separation of the QDs through centrifugation. The separated quantum dots were re-dispersed into 40mL of toluene, and then 5mM MPTMO was added. The mixture was refluxed with stirring under a nitrogen flow at  $70^\circ\text{C}$  for 24 hours. This procedure was repeated several times. After centrifugation, the surface-displaced QDs were dispersed in toluene. Scheme 6.3 demonstrates a schematic diagram

of the ligand exchange of the CdS-ZnS core-shell QDs, wherein the outer organic layer TOA is replaced with MPTMO.



**Scheme 6.3** Schematic diagram of the ligand exchange of CdS-ZnS core-shell QDs

## 6.2.5. Synthesis of Polymer Nanofilms

### 6.2.5.1. CdS-ZnS QD-PVAc Nanofilms

The synthesis of CdS-ZnS QD-PVAc nanofilms was conducted in the 100-mL high-pressure stainless steel autoclave coupled with a digital pressure transducer and a temperature controller. The stirring speed was controlled at 300 rpm. The monomer vinyl acetate (0.1mol), initiator DEPDC (0.002mol), functionalized CdS-ZnS QDs (10.2407g 0.51wt% in toluene), linker VTMO (0.005mol), and hydrolysis agent acetic acid (HAc) (0.02mol) were charged into the reactor, purging with a flow of argon, followed by pumping CO<sub>2</sub> into the autoclave by means of the syringe pump (ISCO 260D). The temperature of the reactor was then raised to let the reaction take place at 60°C under 24.3MPa for 22 hours. After the reaction, CO<sub>2</sub> was carefully vented leaving the formed sample in the autoclave. The viscous liquid product was collected from the reactor and subsequently dried under vacuum at 40°C overnight.

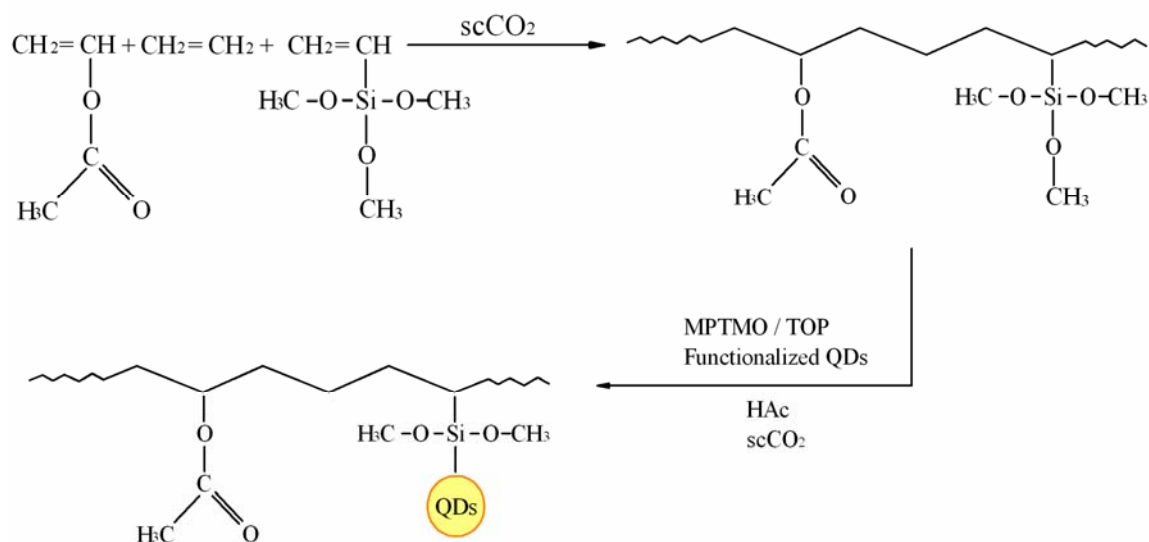
*In situ* Fourier transform infrared (FTIR) was used to monitor the reaction process in the stirred 100-mL high-pressure autoclave. Spectra were recorded at a resolution of  $2\text{cm}^{-1}$  and the absorption spectra were the results of 32 scans.

#### **6.2.5.2. QD-PEVA Nanofilms**

The synthesis of QD-PEVA nanofilms was carried out using both the above described one-step method and a two-step method. In the two-step method, the first step involved terpolymerization of ethylene, vinyl acetate, and VTMO. VAc (0.1mol), VTMO (0.005mol), and DEPDC (0.006mol) were charged into the 100-mL autoclave, purging with a flow of argon, followed by pumping ethylene (1.07mol) and  $\text{CO}_2$  into the autoclave by means of syringe pumps. The reactor was then heated to  $50^\circ\text{C}$  27.6MPa to allow the polymerization to take place for 20 hours. After the reaction,  $\text{CO}_2$  and unreacted ethylene were carefully vented leaving the formed sample in the autoclave. The solid product was collected from the reactor and subsequently dried under vacuum at  $60^\circ\text{C}$  overnight.

The formed terpolymer was then used for the synthesis of QD-PEVA nanofilms. The terpolymer (1g), QDs solution (1g 0.39wt% in toluene), HAc(0.005mol), toluene (2.2g), and MPTMO (0.04g) were introduced into the 100-mL autoclave, with TOP(0.06g) being optionally added, followed by pumping  $\text{CO}_2$  into the autoclave by the syringe pump (ISCO 260D). The reaction was carried out at  $50^\circ\text{C}$  or  $80^\circ\text{C}$  under 27.6MPa for 2 or 20 hours for the synthesis of CdS-ZnS QD-PEVA nanofilms and at  $50^\circ\text{C}$  under 27.6MPa for 2 hours for the synthesis of CdS QD-PEVA nanofilms. After the reaction,  $\text{CO}_2$  was carefully vented leaving the formed sample in the autoclave. The solid product was collected from the reactor and subsequently dried under vacuum at  $60^\circ\text{C}$  overnight.

Scheme 6.4 shows a schematic diagram of the 2-step synthesis of QD-PEVA nanofilm in  $scCO_2$ .



**Scheme 6.4** Schematic diagram of the 2-step synthesis of QD-PEVA nanofilm in  $scCO_2$

### 6.2.6. Characterization

The melting point of the synthesized single-molecular precursor bis(diethyldithiocarbamate) cadmium (II) was measured on a Barnstead Electrothermal 9100. Photoluminescence (PL) spectra were recorded on a Photon Technology International QuantaMaster™. UV-Vis absorption spectra were measured on a Cary Varian UV-VIS spectrophotometer or a Shimadzu UV-3600 UV-VIS-NIR spectrophotometer. Gel permeation chromatography (GPC) was carried out using a Viscotek GPCmax (VE2001GPC Solvent/Sample Module) & Viscotek TDA302 (Triple Detector Array). Experimental conditions were: column: GMH<sub>HR</sub>-L; mobile phase and solvent: THF; temperature: 30°C; flow rate: 1.0mL/min; injection volume: 100μL.



Energy dispersive X-ray (EDX) elemental analysis of the QDs was recorded using a Hitachi S4500 field emission scanning electron microscope with an EDAX light element. EDX system operated at 20 kV electron accelerating voltage and 30 degree tilt. The liquid QD samples were placed in a vacuum oven at 60°C overnight before the analysis. EDX elemental mapping of the nanocomposites was recorded using a Hitachi S-2600N Scanning Electron Microscope. Transmission electron microscopy (TEM) images were recorded using a Philips CM10 Transmission Electron Microscope operated at 80 kV. The specimens were previously dissolved in toluene, and then placed on a copper grid covered with carbon film. High resolution transmission electron microscopy (HRTEM) images were recorded using a JEOL 2010F FEG TEM/STEM operated at 200 kV. The images were taken with the Gatan Tridium spectrometer with a 2048 × 2048 CCD array. Nuclear magnetic resonance (NMR) spectra were recorded using a Varian Inova 600 or 400 NMR spectrometer. <sup>1</sup>H and <sup>13</sup>C NMR chemical shifts are reported relative to TMS. Proton - 400.087 MHz, PW90 (90 pulse width) =12.3 μs (PW45 used in 1D experiment), number of transients (NT) =8, acquisition time (AT) =4.00 s, delay time (D1) =1. Carbon - 100.613 MHz, PW90 =10.4 μs (PW 45 used in 1D), NT 256, AT 1.20 s, D1 =1. gCOSY - NT =1, number of increment (NI for 2D) =128 (linear prediction was used to give a final data set of 384 for processing), AT =0.20 s, D1 =1. gHSQC – NT= 4, NI =128 (linear prediction used to 384 for processing), AT =0.21 s, garp <sup>13</sup>C decoupling used, D1 =1. Dynamic Light Scattering was performed using a Malvern Zeta Sizer 3000HS<sub>A</sub>. The *In situ* ATR-FTIR was applied to monitor the various chemistries studied including: (1) the synthesized single-molecular precursor bis(diethyldithiocarbamate) cadmium (II), (2)

the CdS-ZnS QDs before and after ligand exchange, and (3) the synthesis of QD-polymer nanofilms.

### **6.3. Results and Discussion.**

#### **6.3.1. CdS-ZnS Core-Shell QDs**

The synthesized single-molecular precursor bis(diethyldithiocarbamato) cadmium (II) was characterized by means of measuring the melting point, FTIR and NMR ( $^1\text{H}$ ,  $^{13}\text{C}$ , gCOSY, and gHSQC) spectroscopy. The melting point of the precursor was measured to be  $250^\circ\text{C}$ . The FTIR spectrum of the precursor showed peaks at  $1495$  ( $\nu\text{C}=\text{N}$ ),  $1269$  ( $\nu\text{C}-\text{N}$ ),  $1070$  ( $\nu\text{C}=\text{S}$ ), and  $986\text{cm}^{-1}$  ( $\nu\text{C}-\text{S}$ ).  $^1\text{H}$  NMR of the precursor showed a triplet at  $1.33\text{ppm}$  and a quadruplet at  $3.93\text{ppm}$ ;  $^{13}\text{C}$  NMR showed two peaks at  $12.36\text{ppm}$  and  $51.16\text{ppm}$ . The gCOSY and gHSQC spectra further presented evidence of the molecular structure. All of these results indicate the successful synthesis of the single-molecular precursor bis(diethyldithiocarbamato) cadmium (II), as they are in good agreement with those reported in the literature.<sup>110, 205, 206</sup> By using zinc diethyldithiocarbamate and the synthesized single-molecular precursor bis(diethyldithiocarbamato) cadmium (II), the core-shell CdS-ZnS QDs were synthesized with the procedure mentioned above at a relatively low temperature ( $180^\circ\text{C}$ ). For the sake of ensuring that the ZnS shell was grown on the CdS core, all the bis(diethyldithiocarbamato) cadmium (II) solution was rapidly injected into the reaction flask to speed up nucleation of CdS nanocrystallites, while zinc diethyldithiocarbamate solution was slowly added dropwise to allow ZnS to grow on the CdS crystal nuclei, minimizing nucleation of ZnS crystallites.

The synthesized CdS-ZnS core-shell QDs were characterized with TEM, HRTEM, EDX, and photoluminescence. In order to compare the CdS-ZnS core-shell QDs with the “bare” CdS QDs, CdS QDs were also synthesized under similar conditions as described above to examine their crystal structure. The TEM and HRTEM images of both the synthesized “bare” CdS and core-shell CdS-ZnS QDs are displayed in Figure 6.1 and 6.2, respectively. It was found that both the “bare” and core-shell QDs presented nanocrystal structure, with a clear difference between the two types of QDs. The nanocrystal structure of the CdS QDs appears to be more uniform and regular than that of the CdS-ZnS QDs. The d-spacing of the CdS QDs was measured to be approximately 4.5Å while the CdS-ZnS QDs has a d-spacing value of approximately 3.5Å. The slight “bending” of the lattice fringes of some CdS-ZnS QDs suggests some sort of strain exists in the core-shell structure, as also observed by Bawendi and coworkers<sup>190</sup> for CdSe-ZnS QDs. The EDX plot of a CdS-ZnS/TOA sample (Appendix 8) showed the presence of sulfur, cadmium, zinc, phosphorus, oxygen, and carbon. Nitrogen was not found by EDX due to the low nitrogen concentration, and insensitivity towards nitrogen by this technique. By varying the reaction time of bis(diethyldithiocarbamate) cadmium (II) from 5min to 10min, while other reaction conditions remained unchanged, the photoluminescence emission peak shifted from 596nm to 615nm. This is due to the growing particle size of QDs with reaction time as reported in the literature.<sup>79, 186, 190</sup> The CdS-ZnS QDs were also characterized with other methods as discussed below.

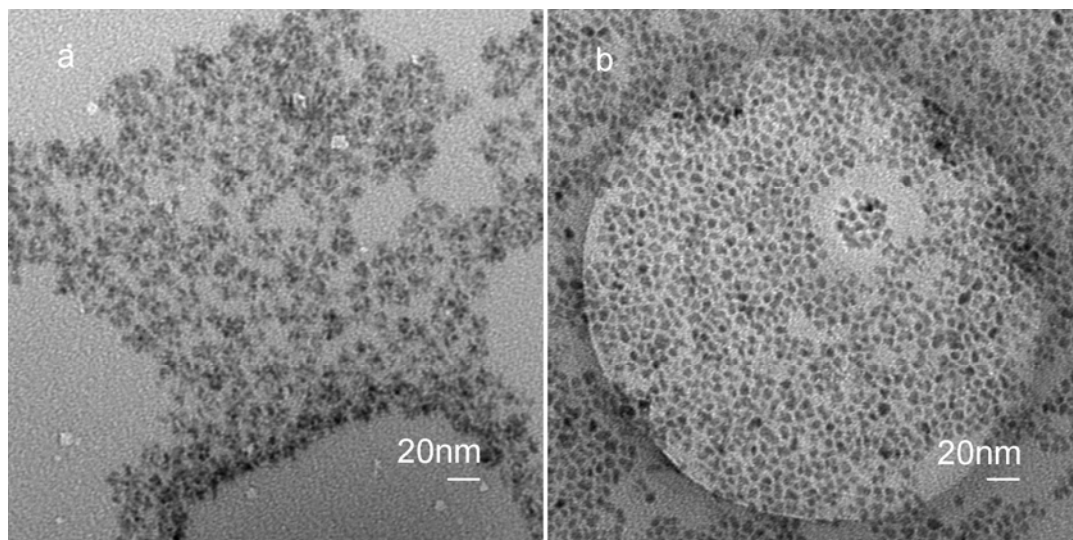


**Figure 6.1** TEM images of the synthesized QDs. (a) CdS-ZnS QDs, (b) CdS QDs. (The experimental conditions are: for CdS-ZnS core-shell QDs, 180°C, 5min for core growth; for CdS QDs, 235°C, 30min).

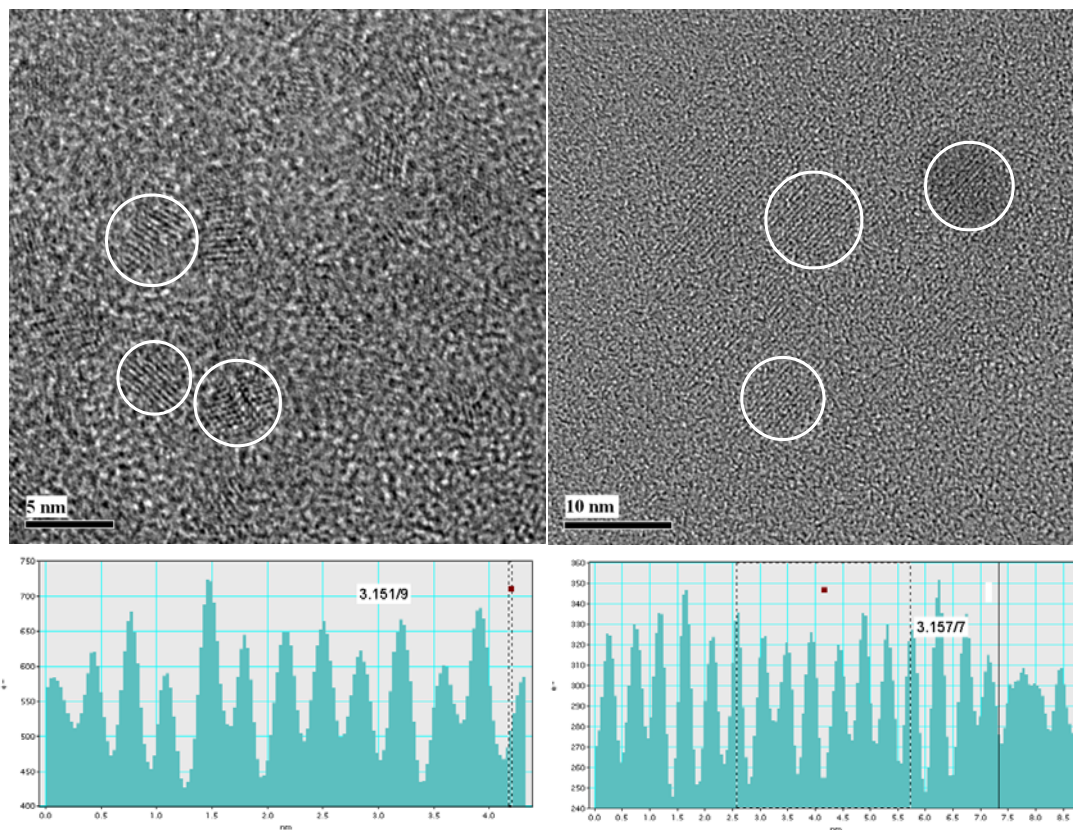


**Figure 6.2** HRTEM and the d-spacing images of the synthesized CdS-ZnS (left) and CdS (right) QDs. (The experimental conditions are: for CdS-ZnS core-shell QDs, 180°C, 5min for core growth; for CdS QDs, 235°C, 30min).

### 6.3.2. Ligand Exchange of the CdS-ZnS QDs

In order to make the QDs compatible with the polymer matrix, the surrounding organic layer has to be modified. As seen in Chapter 5, SiO<sub>2</sub>-PVAc nanocomposites were successfully synthesized in the “green” solvent scCO<sub>2</sub> by a one-pot technique where parallel reactions of free radical polymerization of vinyl acetate (VAc) and hydrolysis/condensation of tetraethyl orthosilicate (TEOS) or tetramethyl orthosilicate (TMOS) took place simultaneously, while VTMO was used as a linker to participate in both reactions so as to enhance the interaction between the silica nanoparticles and the polymer matrix.<sup>120</sup> By functionalizing the organic shell of the QDs with such functional groups as methoxysilane or ethoxysilane, it was hypothesized that the QDs could be incorporated into a polymer matrix through hydrolysis/condensation, and this step could be enabled by using scCO<sub>2</sub> as both a solvent and a drying agent. MPTMO was chosen as a candidate for the ligand exchange of the synthesized QDs as it has the required functionality with a thiol head that can coordinate with zinc or cadmium to stabilize the QDs, while the methoxysilane tail can be used for subsequent reaction to attach the QDs to the polymer chains (see Scheme 6.3).

In order to examine if the ligand exchange proceeded successfully, the QDs before and after ligand exchange were characterized with EDX elemental analysis, HRTEM, FTIR, solubility testing, photoluminescence, and UV-Vis absorption spectroscopy. Due to the limitation of EDX elemental analysis for detection of hydrogen, the poor sensitivity to nitrogen, and the interference from the employed carbon supporting film, the absolute chemical composition cannot be obtained by means of this method. However, relative ratios of the composition are available and provide important

information about the ligand exchange process. Table 6.1 displays the relative atom number ratios of the CdS-ZnS QDs before and after ligand exchange using the EDX data. It is seen that the ratios of Si/Cd and O/Cd increase significantly, while the ratio Zn/Cd drops after the ligand exchange. The increase in ratios of Si/Cd and O/Cd are consistent with MPTMO being attached to the QDs. The decrease in the Zn/Cd ratio may be due to loss of smaller zinc-enriched QDs during the repeated separation process through centrifugation. This was also evidenced by the photoluminescence spectra as discussed below. HRTEM images of the CdS-ZnS QDs after the ligand exchange show the well-preserved nanocrystallites. The FTIR spectra of the CdS-ZnS QDs before and after the ligand exchange were collected and displayed in Figure 6.3. From the spectra, the dominant peaks from the TOA alkyl groups observed at 2954 ( $\nu_{\text{as}}\text{CH}_3$ ), 2923( $\nu_{\text{as}}\text{CH}_2$ ), 2871( $\nu_{\text{s}}\text{CH}_3$ ), 2853( $\nu_{\text{s}}\text{CH}_2$ ), 1466( $\delta_{\text{s}}\text{CH}_2$  &  $\delta_{\text{as}}\text{CH}_3$ ), and 723 $\text{cm}^{-1}$  ( $\rho\text{CH}_2$ ) disappear after the ligand exchange, while new peaks are formed from the ligand exchange at 2926( $\nu_{\text{as}}\text{CH}_2$  &  $\nu_{\text{as}}\text{CH}_3$ ), 2842( $\nu_{\text{s}}\text{CH}_2$  &  $\nu_{\text{s}}\text{CH}_3$ ), 1191( $\rho\text{CH}_3$ ), 1087( $\nu_{\text{as}}\text{Si-O-C}$ ), and 813 $\text{cm}^{-1}$ ( $\nu_{\text{s}}\text{Si-O-C}$ ).<sup>110</sup> In addition, a specialized test was designed to examine the solubility difference of the QDs before and after the ligand exchange (Figure 6.4). In this test, the QDs were first dispersed in toluene, and then anhydrous methanol was added into the mixture followed by separation through centrifugation. It was found that the CdS-ZnS QDs before the ligand exchange could be easily separated from the mixture, while the QDs after the ligand exchange could hardly be separated, indicating the successful ligand exchange from the methanol-phobic TOA to methanol-philic MPTMO.

**Table 6.1** Relative atom number ratios of the CdS-ZnS QDs before and after the ligand exchange

Elements	Before ligand exchange	After ligand exchange
Si/Cd	0.03±0.01	0.32±0.01
O/Cd	0.57±0.02	1.19±0.20
Zn/Cd	0.83±0.05	0.33±0.07
S/Cd	1.46±0.03	1.42±0.02
P/Cd	0.15±0.00	0.15±0.01

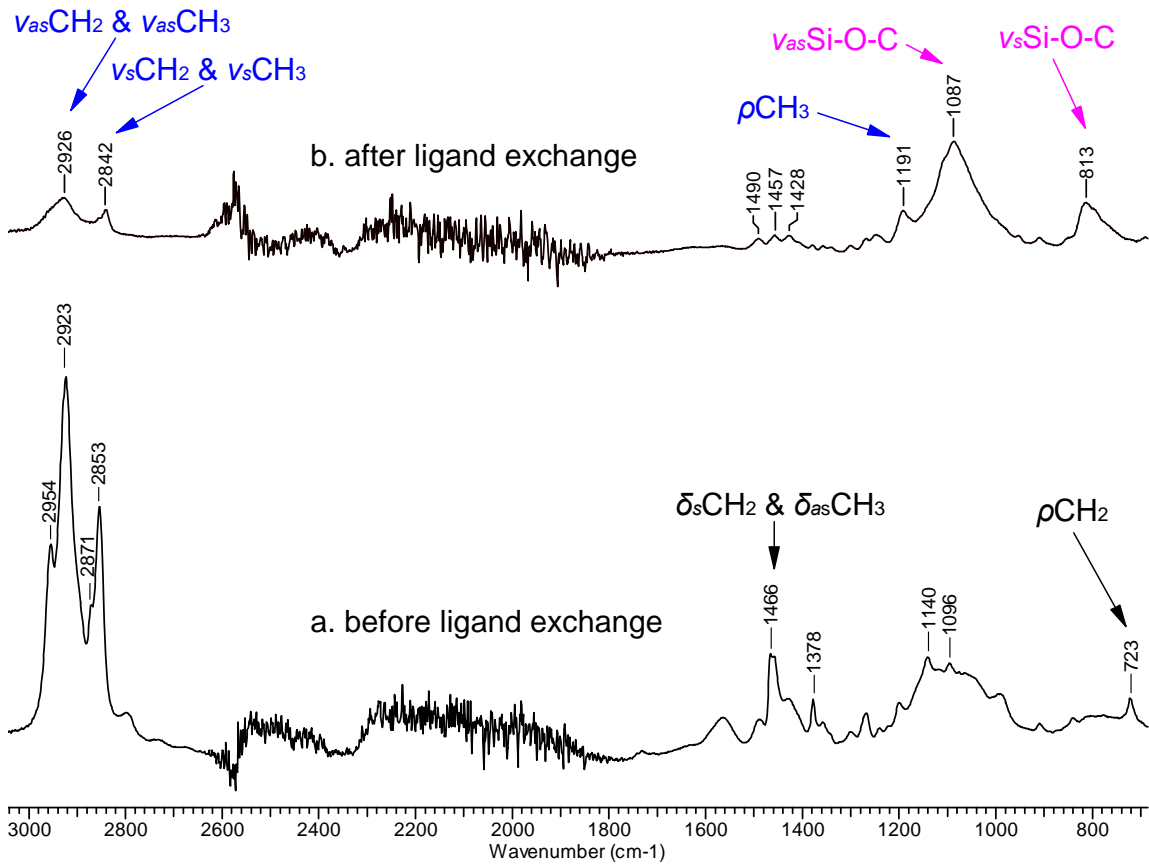


**Figure 6.3** FTIR spectra of the CdS-ZnS QDs before and after ligand exchange.

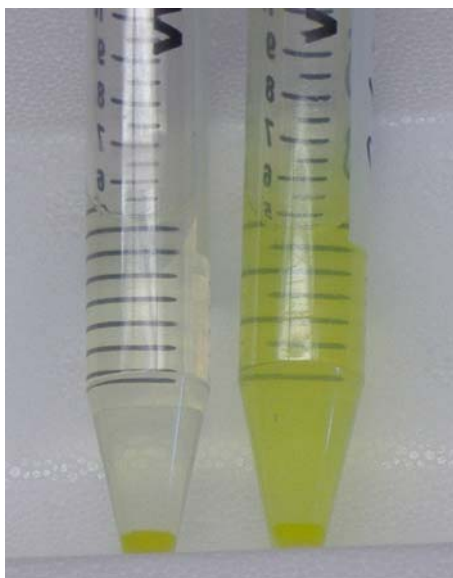


**Figure 6.4** Solubility test of the CdS-ZnS QDs before (left) and after (right) ligand exchange.

All of these results indicate the successful synthesis and ligand exchange of the CdS-ZnS core-shell QDs. The Si-O-CH<sub>3</sub> functional group in the new ligand can be employed for further incorporation of the QDs into polymer matrix through hydrolysis/condensation.

### 6.3.3. Synthesis of QD-Polymer Nanofilms

In general, the synthesis of QD-polymer nanocomposites requires at least three basic steps: (1) synthesizing polymers, (2) dissolving the synthesized polymers into solvents, (3) mixing the QDs with the polymer solution and then evaporating the solvent to form solid nanocomposites. More steps are needed in order to enhance the interaction between the QDs and the polymer chains to avoid aggregation and migration of QDs. Each step consumes energy, labor, time and chemicals, and results in significant waste. Hence, it is desirable to make nanocomposites with fewer steps, especially by incorporation of using the “green” solvent, scCO<sub>2</sub>. Due to the successful one-pot



synthesis of SiO<sub>2</sub>-PVAc nanocomposites in scCO<sub>2</sub>, as described in Chapter 5, it is necessary to examine the possibility to synthesize CdS-ZnS QD-PVAc nanofilms using a similar one-pot process.

### 6.3.3.1. CdS-ZnS QD-PVAc Nanofilms

In this process, the monomer vinyl acetate, initiator DEPDC, functionalized CdS-ZnS QDs, linker VTMO, hydrolysis agent HAc, and solvent CO<sub>2</sub> were introduced into the reactor. The reactor was then heated and maintained at 60°C for 22 hours. *In situ* FTIR was used to monitor the process of the reactions. Figure 6.5 displays the *in situ* FTIR spectra of the parallel reactions of the copolymerization of vinyl acetate and VTMO and hydrolysis of functionalized CdS-ZnS QDs/VTMO with HAc in scCO<sub>2</sub>. The decrease in peak height at 1765 (νC=O), 1650 (νC=C) and 1220cm<sup>-1</sup> (νC-O) is attributed to the consumption of the monomer vinyl acetate. The formation of oxo bonds between silicon atoms can be discerned by the widening peak in the 1045cm<sup>-1</sup> region. The gradually developed peaks at 1739 (νC=O) and 1236 (νC-O) are ascribed to the formation of new acetic esters, poly(vinyl acetate) and methyl acetate resulting from the hydrolysis/condensation reactions. The *in situ* FTIR measurement shows that the polymerization and the hydrolysis/condensation proceeded simultaneously, despite incomplete conversion, as the monomer vinyl acetate was still detectable after 22 hours reaction. The product was dried and then examined by TEM and EDX elemental mapping (Appendix 9). Relatively large nanoparticles ca. 100nm were well dispersed in the polymer matrix, which due to their relatively large size are composites of silica and the CdS-ZnS QDs. EDX elemental mapping further proved the uniform distribution of the elements Cd, Zn, S and Si in the polymer matrix.

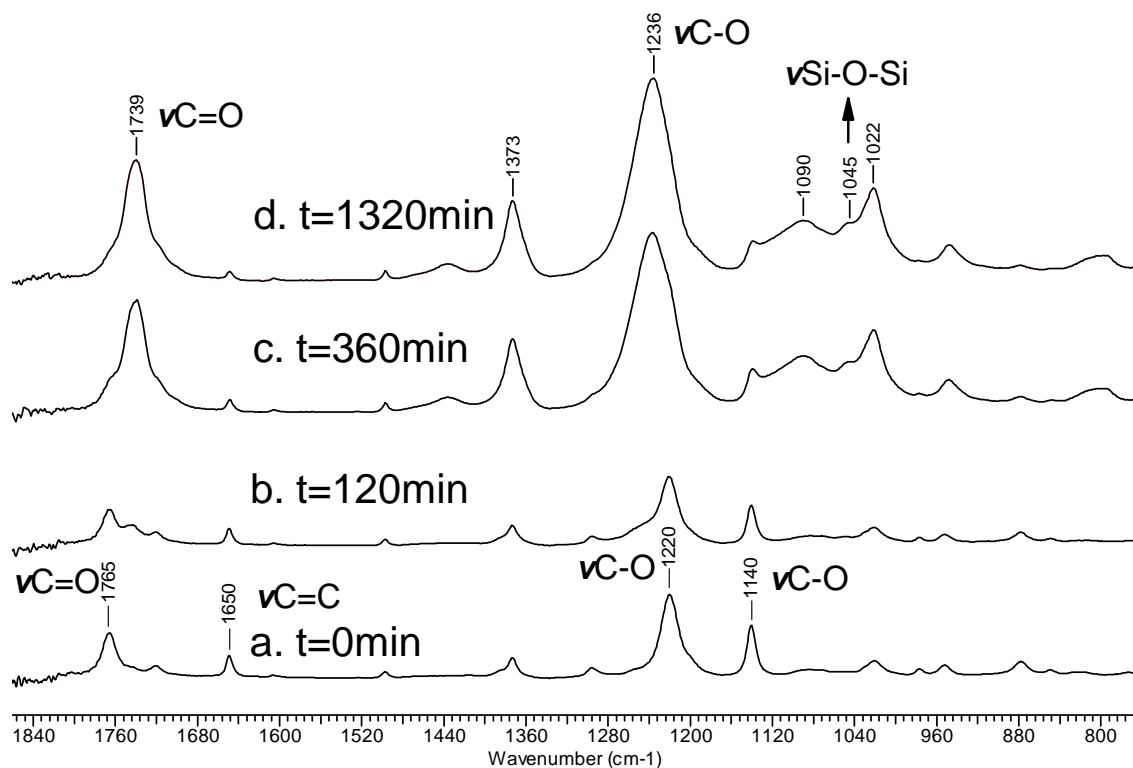


**Figure 6.5** *In situ* FTIR spectra of parallel reactions of the copolymerization of vinyl acetate and VTMO and hydrolysis of functionalized CdS-ZnS QDs/VTMO with acetic acid in scCO<sub>2</sub> (The experimental conditions: T=60°C, P=24.3MPa; materials: VAc: 0.1mol, VTMO: 0.005mol, DEPDC: 0.002mol, HAc: 0.02mol, CdS-ZnS QDs: 10.24g 0.51wt% toluene solution).

As control experiments to probe the influence of both the QDs and the SiO<sub>2</sub> nanoparticles on the synthesized PVAc nanocomposite, both a copolymer of vinyl acetate and VTMO and a silica-PVAc composite were synthesized under similar conditions in scCO<sub>2</sub>, respectively. Copolymerization of monomer vinyl acetate and VTMO in scCO<sub>2</sub> (60 °C, 24.3MPa; materials: VAc: 0.1mol, VTMO: 0.005mol, and DEPDC: 0.002mol) in the absence of QDs and HAc at 60°C for 22 hours resulted in the copolymer poly(vinyl acetate-co-VTMO). By adding HAc (0.02mol) under the similar reaction conditions, additional crosslinks among the copolymer chains were formed due to the

hydrolysis/condensation of the Si-O-CH<sub>3</sub> group in the VTMO segments of the copolymer, resulting in the SiO<sub>2</sub>-PVAc composite. TEM images of this SiO<sub>2</sub>-PVAc composite similarly showed that the silica nanoparticles were well dispersed in the sample. Gel permeation chromatography (GPC) results showed that the virgin copolymer formed in the absence of HAc had a weight-average molecular weight of ca. 27,000Da while the weight-average molecular weights of the PVAc composites with/without the QDs were at least one order of magnitude higher than that of the virgin copolymer, indicating a crosslinked structure for both the QDs/SiO<sub>2</sub>-PVAc and SiO<sub>2</sub>-PVAc nanocomposites.

The photoluminescence and UV-Vis spectra of the CdS-ZnS QDs before and after the ligand exchange were also measured, as shown in Figure 6.6a. From these spectra, the spectral properties of the CdS-ZnS QDs after the ligand exchange were maintained, although a slight red shift was observed in all the excitation, emission, and UV-Vis spectra. This red shift may be due to the loss of smaller QDs during the repeated separation process through centrifugation as mentioned above from the EDX experiments. It was found that this red shift tendency could be minimized by adding more anti-solvent, increasing the rotary speed of centrifugation, and/or extending the separation time during the centrifugation process. Figure 6.6b shows the photoluminescence and UV-Vis spectra comparing the synthesized nanocomposites with and without QDs. It is seen that by incorporating the functionalized CdS-ZnS QDs into the PVAc matrix, the nanocomposite film showed significant improvement of absorption at wavelengths from 300-500nm, especially in the UV region (below 380nm), and light emission at wavelengths from 500 to 700nm. However, the previously observed emission peak of the CdS-ZnS QDs after ligand exchange at ca. 620nm disappeared. Similar results were also observed by Skaff *et*

*al*<sup>199</sup> and Mattoussi *et al*<sup>188</sup> when they incorporated CdSe QDs into the conducting polymer poly(phenylene vinylene) (PPV). The reason for the diminishment of the characteristic peaks of QDs is attributed to both phase separation and aggregation of QDs.<sup>207, 208</sup> In order to make QD-polymer nanofilms with the retention of the initial spectral emission of the QDs, further efforts were made to stabilize the QDs in the synthesis of QD-PEVA nanofilms.

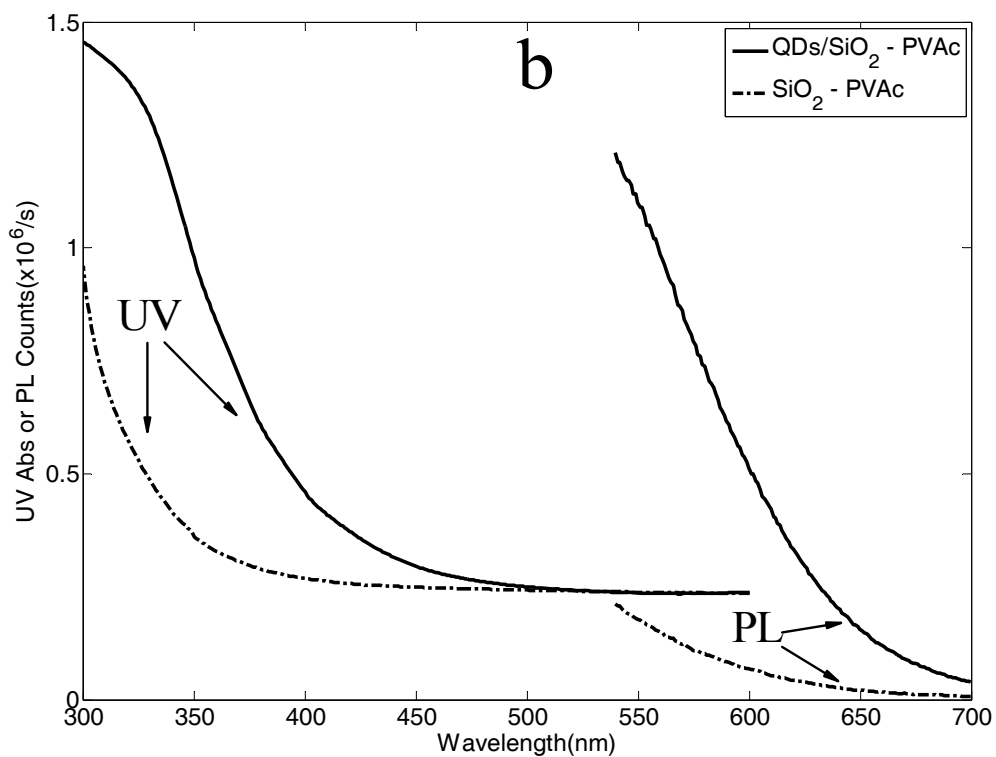
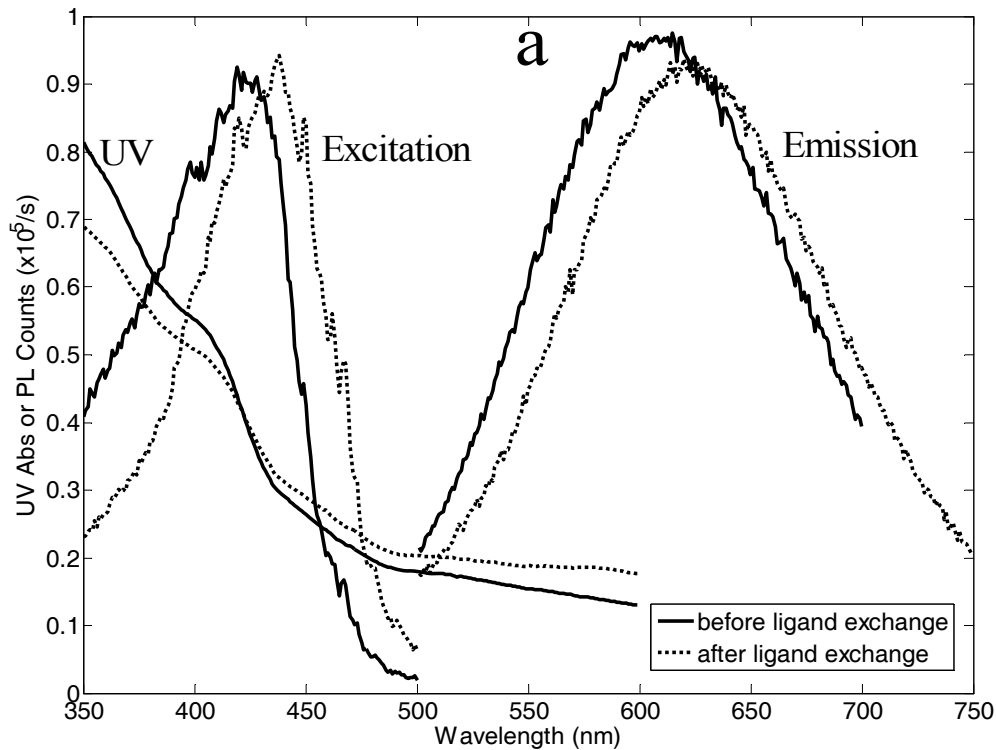


**Figure 6.6** Photoluminescence and UV-Vis spectra of (a) the CdS-ZnS QDs before and after the ligand exchange, and (b) the QDs/SiO<sub>2</sub>-PVAc and SiO<sub>2</sub>-PVAc nanocomposites.

### 6.3.3.2. QD-PEVA Nanofilms

Based on the knowledge obtained from the QD-PVAc nanocomposites, subsequent efforts were devoted to preparing and examining QD-PEVA nanocomposites, as poly(ethylene-co-vinyl acetate) (PEVA) is well-recognized in the film industry being used in various grades of film for applications including greenhouses. In order to both stabilize the QDs during the process of synthesizing the QD-PEVA nanofilms and maintaining a low crosslink density during synthesis, a small amount of the ligand MPTMO was added to the QD solution before the synthesis of nanofilms. A one-pot method including polymerization and hydrolysis was tested but did not give high molecular weight polymer with resulting poor performance attributed to the high chain transfer capability of the thiol group in the ligand MPTMO. Hence, a two-step method was subsequently developed for the synthesis including: (1) terpolymerization of ethylene, vinyl acetate, and VTMO, and (2) hydrolysis of the ligand and VTMO in the terpolymer chains with HAc (see Scheme 6.4).  $\text{scCO}_2$  was used as the reaction medium for both steps as it can effectively swell and plasticize the amorphous region of polymer to help incorporate nanoparticles into the polymer matrix<sup>76</sup>, along with facilitating both the polymerization and sol-gel chemistry steps<sup>209</sup>.

After 2 hours hydrolysis at 50°C under 27.6MPa in  $\text{scCO}_2$ , the synthesized CdS-ZnS QD-PEVA nanofilms stabilized by MPTMO with/without TOP retained the characteristic emission peak of the CdS-ZnS QDs at ca. 620nm (see Figure 6.7a and 6.7b). Extra TOP was added to examine if it would help to stabilize the QDs from agglomerating in the polymer matrix. The absorbance maximum is slightly increased when adding extra TOP from 2.5 to 3.5 ( $\times 10^6$  counts/sec), while the peak position is not

changed. In order to examine the effect of reaction temperature and time on the optical properties of PEVA nanofilms, the hydrolysis was also carried out at (1) 50°C for 20 hours and (2) 80°C for 2 hours. The resulting photoluminescence emission spectra are displayed in Figure 6.7c and 6.7d, respectively, which show that the characteristic peak of the QDs was still maintained in these synthesized PEVA nanofilms. However, the emission intensity decreased significantly by two orders of magnitude with both the extended reaction time at 50°C or increasing the reaction temperature to 80°C. This may be due to either destabilization/agglomeration of the QDs or by increased-crosslinking of the functional ligand, i.e. higher temperatures and longer reaction times would result in larger particles and higher crosslink density. This was evidenced by TEM images of the synthesized QD-PEVA nanofilms, as shown in Figure 6.8. By incorporation of the functionalized CdS-ZnS QDs of less than 10nm (Figure 6.8a) into the PEVA matrix at 50°C for 2 hours, QD-SiO<sub>2</sub> particles of 100 ~ 200nm (Figure 6.8b) were formed and well dispersed. When the reaction time was extended from 2 to 20 hours at the same temperature of 50°C, a network of particles was formed (Figure 6.8c) while increasing the reaction temperature from 50 to 80°C for the same reaction time of 2 hours resulted in significantly larger particle size of ca. 500nm (Figure 6.8d).

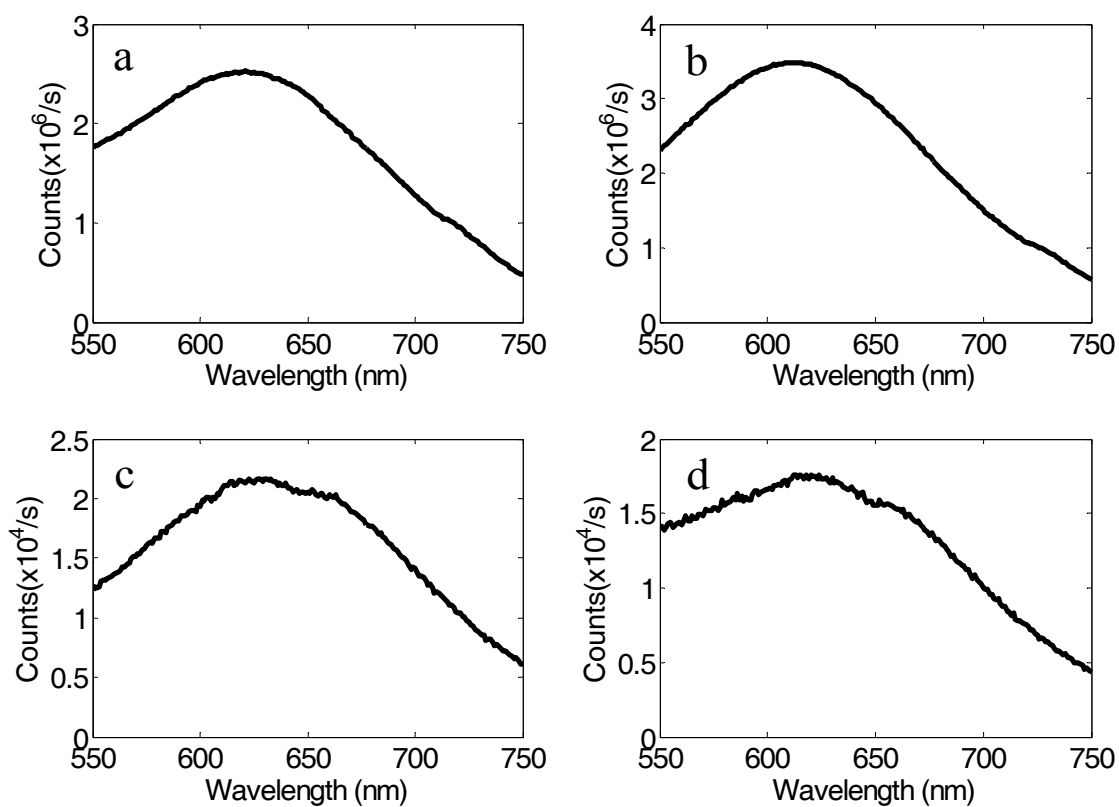


**Figure 6.7** Photoluminescence emission spectra of CdS-ZnS QD-PEVA nanofilms prepared in different reaction conditions (under 27.6MPa in scCO<sub>2</sub>). (a) 50°C 2 hours without TOP; (b) 50°C 2 hours with TOP; (c) 50°C 20 hours with TOP; (d) 80°C 2 hours with TOP).



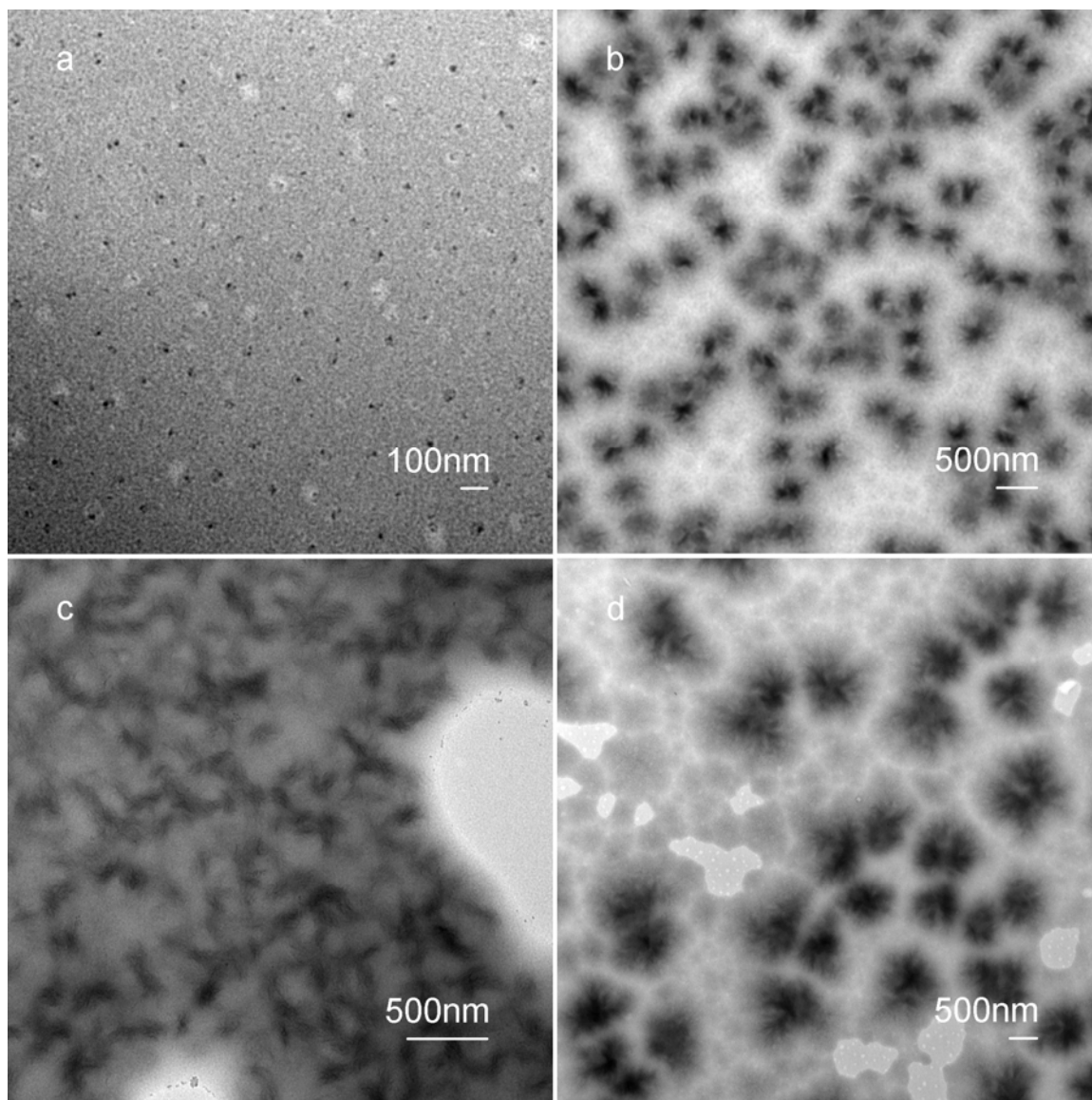


**Figure 6.8** TEM images of (a) functionalized CdS-ZnS QDs, and CdS-ZnS QD-PEVA nanofilms prepared in different reaction conditions (under 27.6MPa in scCO<sub>2</sub> with TOP). (b) 50°C 2 hours; (c) 50°C 20 hours; (d) 80°C 2 hours.

In order to examine if this two-step technique could be applied to other QD systems, “bare” CdS QDs (ca. 4.5nm) (see Figure 6.1b and 6.9) were also synthesized and functionalized under similar reaction conditions as described in the experimental section. As shown in Figure 6.10a and 6.10b, the CdS QDs had an emission peak at ca. 670 ~ 680nm. With these QDs incorporated into the PEVA matrix to form

nanocomposites, the synthesized PEVA nanofilms provided similar emission properties (Figure 6.10c). Figure 6.10d shows that similarly by adding extra TOP, the peak height was slightly increased.

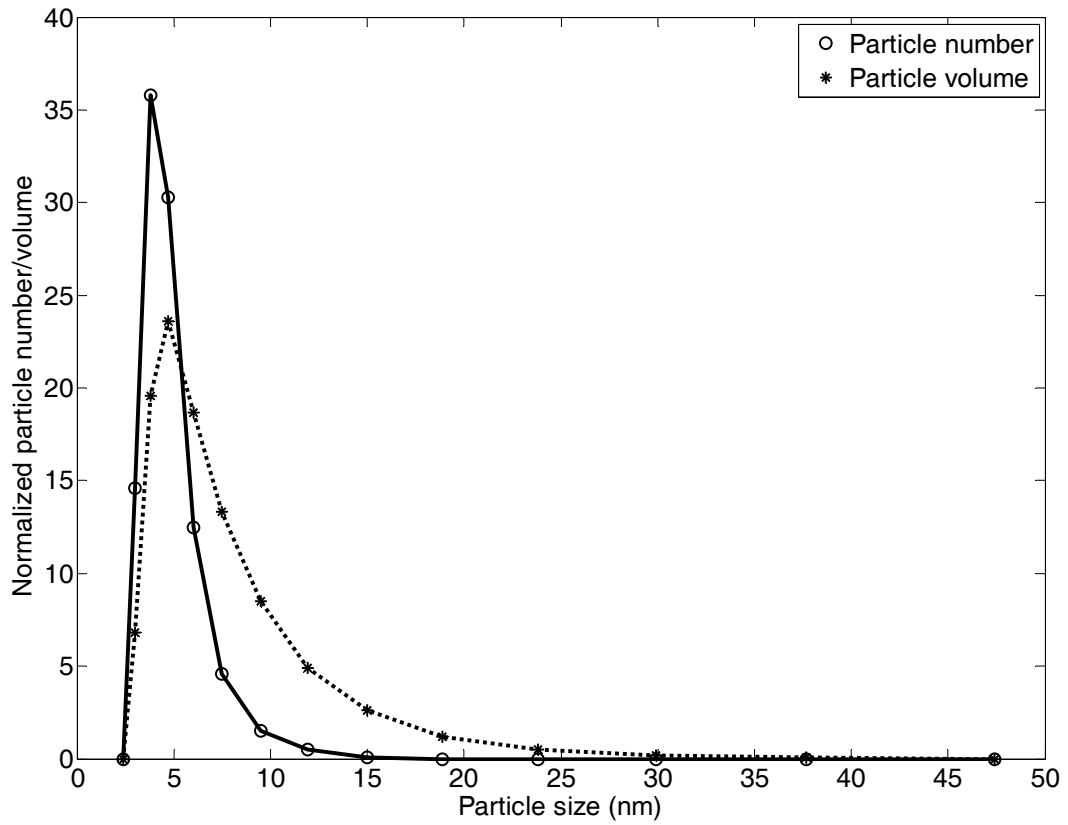


**Figure 6.9** Particle size distribution of the synthesized CdS QDs by light scattering measurement

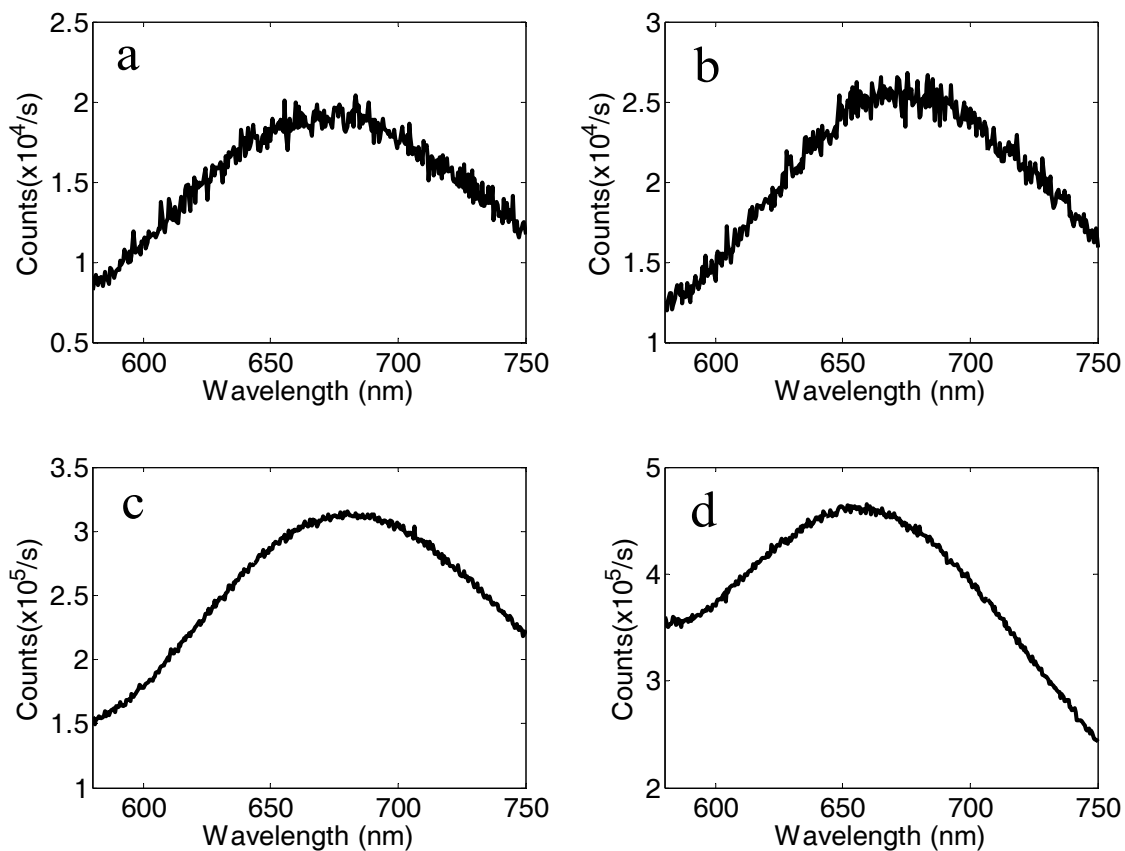


**Figure 6.10** Photoluminescence emission spectra of CdS QDs and CdS QD-PEVA nanofilms prepared in different reaction conditions. (a) CdS QDs before ligand exchange; (b) CdS QDs after ligand exchange; (c) CdS QD-PEVA nanofilms prepared at 50°C for 2 hours without TOP; (d) CdS QD-PEVA nanofilms prepared at 50°C for 2 hours with TOP).

Figure 6.11 compares the UV-Vis absorption spectra of the synthesized pure PEVA film both with and without incorporation of QDs. It is obvious that these synthesized nanofilms by means of filling CdS QDs or CdS-ZnS QDs demonstrated much stronger absorbance in the low wavelength region than the PEVA film. Along with the characteristic emission properties, these results imply potential applications of the QD-polymer nanocomposites in UV protection films and light-selective films for applications in greenhouses, etc.

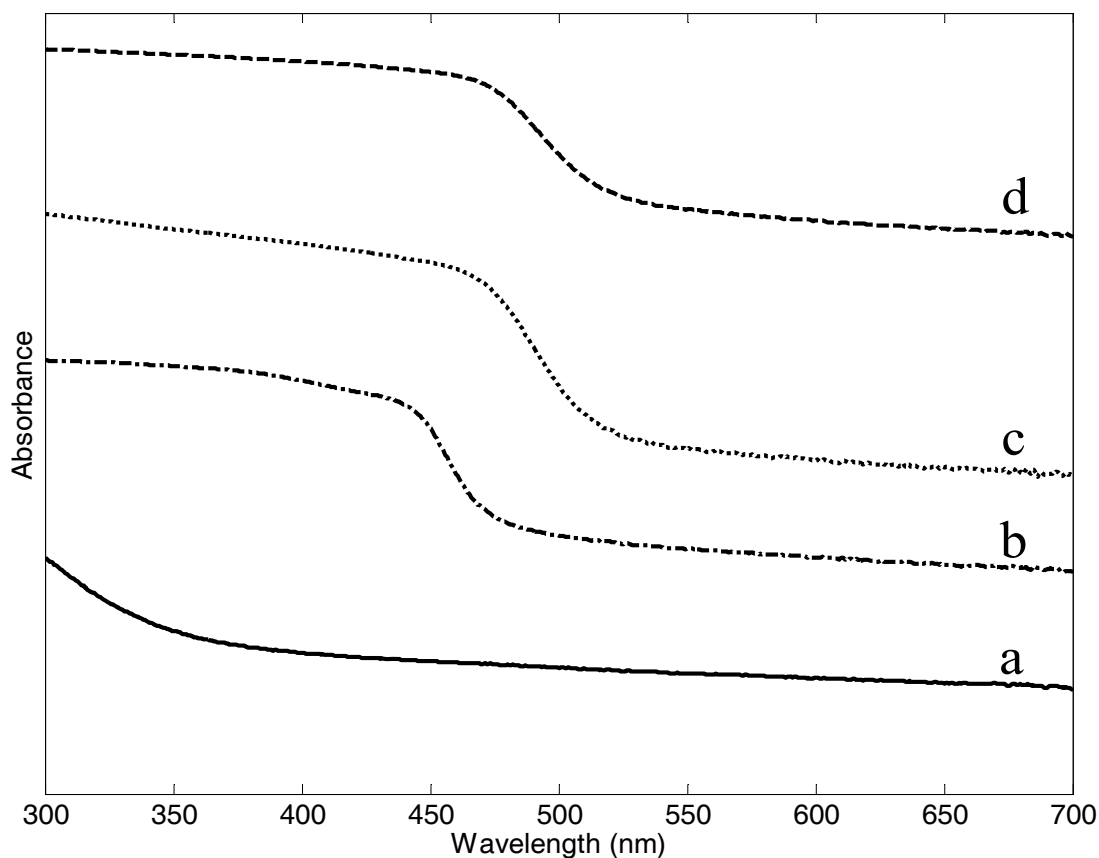


**Figure 6.11** UV-Vis spectra of PEVA and PEVA nanofilms. (a) PEVA; (b) CdS-ZnS QD-PEVA with TOP; (c) CdS QD-PEVA with TOP; (d) CdS QD-PEVA without TOP.

Hence, all the experimental results discussed above in this study provide evidence of the successful synthesis of CdS-ZnS QD-PEVA and CdS QD-PEVA nanofilms by means of terpolymerization and hydrolysis in  $scCO_2$ . The synthesized QD-PEVA nanocomposites showed significant improvement in optical absorption of low wavelength lights such as UV and violet, and characteristic emission of high wavelength lights. Several significant advantages of this technique over the conventional methods include: (1) effective light-selective absorbance and emission properties, (2) replacement of volatile organic solvents with the “green” solvent  $scCO_2$ , and (3) improved interaction between the QDs and the polymer matrices.

#### **6.4. Conclusions**

A two-step synthesis technique for the synthesis of light-selective QD-PEVA nanofilms in supercritical carbon dioxide was developed. CdS-ZnS core-shell QDs and CdS QDs were synthesized by using single-molecular precursors at relatively low temperature, 180°C. The synthesized QDs were functionalized via ligand exchange with MPTMO which enabled chemical bonding to link the QDs to PEVA chains. Stabilization of the QDs in the polymer matrix was found to be extremely important for the successful synthesis of light-selective QD-polymer nanofilms. Using an excessive amount of ligands and controlling a low crosslink density can effectively stabilize the QDs. The synthesized QD-PEVA nanofilms showed excellent optical properties of selective absorbance and emission. With this technique, QD-polymer nanofilms with various optical properties can be synthesized by tuning the band gap of the QDs.

## **Chapter 7. Summary and Conclusions**

## 7.1. Summary

With supercritical carbon dioxide (scCO<sub>2</sub>) being considered as a viable alternative to organic solvents in various chemical processes, the study of the effect of CO<sub>2</sub> on these processes becomes extremely important in order to make use of scCO<sub>2</sub>'s "green" enabling properties. ScCO<sub>2</sub> has unique physical and chemical properties such as non-polarity, low dielectric constant, low viscosity, and zero surface tension, which differentiate it from conventional organic solvents. Despite its relatively poor solvation power, scCO<sub>2</sub> is still a promising solvent for a variety of applications including polymerization, polymer modification, and polymer nanocomposites.

In this research, a comprehensive study was conducted on the copolymerization of ethylene and vinyl acetate in scCO<sub>2</sub> and the synthesis of light-selective quantum dot-poly(ethylene-co-vinyl acetate) (QD-PEVA) nanofilms using scCO<sub>2</sub>. In addition to the study of thermal decomposition of the free radical initiator diethyl peroxydicarbonate (DEPDC) in scCO<sub>2</sub> and the measurement of reactivity ratios for free radical copolymerization of ethylene and vinyl acetate in scCO<sub>2</sub>, significant efforts were made to synthesize novel PEVA nanocomposites using scCO<sub>2</sub>.

The thermal decomposition of the organic free-radical initiator, DEPDC, was studied using *in situ* attenuate total reflection Fourier transform infrared spectroscopy (ATR-FTIR) in heptane and in the "green" solvent scCO<sub>2</sub>. That the characteristic peaks of DEPDC at 1802 ~ 1803 and 1194 ~ 1203cm<sup>-1</sup> decreased significantly upon heating reflected the decomposition of DEPDC while that two new intense peaks simultaneously

appeared at 1747 and 1262 $\text{cm}^{-1}$  in heptane, and similarly at 1756 and 1250 $\text{cm}^{-1}$  in  $\text{scCO}_2$  revealed the formation of new compounds. Based on the changes in the absorbance intensity of the characteristic peaks of the initiator during the decomposition, the decomposition rate constant of DEPDC was measured experimentally. The thermal decomposition of DEPDC at low concentration in either heptane under atmospheric  $\text{N}_2$  or  $\text{scCO}_2$  under high pressure was found via the first-order kinetics of unimolecular decomposition. The activation energy of the thermal decomposition of DEPDC was found to be 115kJ/mol in heptane from 40 to 74°C and 118kJ/mol in  $\text{scCO}_2$  from 40 to 60°C. These new peaks revealed the formation of carboxyl groups contained in the decomposed products, indicating incomplete decarboxylation of the dissociated free radicals. During removal of  $\text{CO}_2$  after the reaction in  $\text{scCO}_2$ , the instable intermediate monoethyl carbonate was decarboxylated and converted into the major end product, ethanol. By using FTIR and nuclear magnetic resonance (NMR) to analyze the final decomposition products, the mechanism of thermal decomposition of DEPDC in  $\text{CO}_2$  was proposed.

An understanding of the monomer reactivity ratios is extremely useful for tailoring copolymers with desired compositions for a diversity of end-use applications. Although  $\text{scCO}_2$  did not show a significant effect on the decomposition of DEPDC, the monomer reactivity ratios were found to be affected by the “green” solvent,  $\text{scCO}_2$ . *In situ* ATR-FTIR was employed to monitor the initial formation of copolymers of ethylene and vinyl acetate (VAc) during polymerization in  $\text{scCO}_2$ . To obtain the copolymer composition, a calibration curve of absorbance ratio 1737 $\text{cm}^{-1}$ /2929 $\text{cm}^{-1}$  versus vinyl acetate content of PEVA was established, covering the range of 5 ~ 98wt%. The



reactivity ratios for copolymerization of ethylene and VAc in scCO<sub>2</sub> were determined using both the linear Kelen-Tudos and the non-linear least-squares (NLLS) methods, which gave similar results. Off-line <sup>1</sup>H NMR analysis was also utilized for obtaining the copolymer composition, by which the determined reactivity ratios were compared with the ones obtained using *in situ* FTIR, suggesting an advantage of *in situ* FTIR over off-line <sup>1</sup>H NMR in this study. The effect of reaction temperature and pressure on reactivity ratios was examined at 50 and 72°C, and 13.8 and 27.6MPa, with the lower temperature and higher pressure conditions increasing the reactivity ratios slightly.

Inorganic-polymer nanocomposites are of significant interest for emerging materials due to their improved properties, and unique combination of properties. A novel one-step synthesis route was developed for making the polymer nanocomposites silica-poly(vinyl acetate) (SiO<sub>2</sub>-PVAc) in scCO<sub>2</sub>, wherein all raw chemicals, tetraethyl orthosilicate (TEOS)/ tetramethyl orthosilicate (TMOS), vinyltrimethoxysilane (VTMO), vinyl acetate, initiator DEPDC, and hydrolysis agent acetic acid were introduced into one autoclave. *In situ* ATR-FTIR was applied to monitor the process in scCO<sub>2</sub>. It was found that the formation of polymer and nanoparticles and the linkage of nanoparticles to the polymer chains took place simultaneously. Transmission electron microscopy (TEM) and EDX element Si-mapping revealed that the SiO<sub>2</sub> nanoparticles of 10-50nm were well dispersed in PVAc matrix. This process provides a significant improvement by providing a one-step synthesis route where the potentially recyclable scCO<sub>2</sub> works as a solvent, a modification agent, and a drying agent. This “green” process has potentially many advantages in producing new and unique materials, along with waste-reduction and energy-saving properties. Production of metal-oxide polymer nanocomposites from non-

inhalable liquid precursors also has significant potential for nontoxicity in biomedical and other fields.

Polymer nanocomposites with incorporated quantum dots (QDs) have unique applications in a variety of fields. Light-selective QD-PVAc and QD-PEVA nanocomposites for application as nanofilms were synthesized and characterized. Both CdS and CdS-ZnS core-shell QDs were synthesized by means of pyrolysis of single-molecular precursors at 180°C and then functionalized with a methoxysilane group for subsequent attachment to polymer chains using sol-gel chemistry. These novel materials were examined using FTIR, EDX elemental analysis, solubility tests, photoluminescence, and UV-Vis spectroscopy for characterization of the QDs, indicating successful synthesis and functionalization. The functionalized QDs were then used to synthesize novel QD-PVAc nanocomposites via a one-pot technique and QD-PEVA nanocomposites via a two-step method in scCO<sub>2</sub> which acts as a solvent and drying agent for the sol-gel chemistry linking the QDs to the polymer chains. In the synthesis of QD-PVAc nanocomposites, the characteristic emission peak of the QDs was quenched attributed to phase separation in the nanocomposites. By stabilizing the QDs with an excessive amount of ligands and controlling the reaction conditions, light-selective QD-PEVA nanofilms were successfully synthesized using a two-step technique in scCO<sub>2</sub>. The synthesized QD-PEVA nanofilms displayed enhanced absorption in the UV and violet regions of the electromagnetic spectrum and provided a characteristic emission in the region from orange to red light. This novel synthesis route can be applied to the synthesis of other light-selective nanofilms by varying the quantum dot and polymer systems.

This research will not only promote the industrial application of scCO<sub>2</sub> in the synthesis of the widely commercialized copolymer PEVA and PEVA-based nanomaterials, but also spur research on the synthesis of various novel polymer nanocomposites using scCO<sub>2</sub>.

## **7.2. Recommendations**

Recommendations for future work are listed below.

- (1). In order to control the physical and mechanical properties and processibility of the synthesized QD-PEVA nanocomposites, it is necessary to examine the relationship among crosslink density, nanoparticle size, and reaction conditions such as temperature, pressure, concentrations, and reaction time, etc.
- (2). Research on the relationship between PEVA copolymer molecular weight and the reaction conditions is recommended, requiring a high-temperature GPC.
- (3). It would be very interesting and useful to synthesize light-selective QD-PEVA nanofilms with different emission bands covering the whole range of electromagnetic spectrum of visible light for a variety of applications.
- (4). For a certain application, other types of nanoparticles such as TiO<sub>2</sub> could be incorporated into polymer matrices via the established methods using scCO<sub>2</sub>.

## Bibliography

1. McHugh, M. A.; Krukonis, V. J., *Supercritical Fluid Extraction: Principles and Practice*. 2<sup>nd</sup> ed.; Butterworth-Heinemann: Boston, 1994.
2. Kemmere, M., Supercritical Carbon Dioxide for Sustainable Polymer Processes. In *Supercritical Carbon Dioxide in Polymer Reaction Engineering*, Kemmere, M. F.; Meyer, T., Eds. Wiley-VCH: Weinheim, 2005; pp 1-14.
3. Kendall, J. L.; Canelas, D. A.; Young, J. L.; DeSimone, J. M., Polymerizations in Supercritical Carbon Dioxide. *Chemical Reviews* **1999**, *99* (2), 543-563.
4. Ghosh, S.; Bhattacharjee, C.; Mukhopadhyay, M., Polymerisation in Supercritical Carbon Dioxide: A Review. *Indian Chemical Engineer* **2005**, *47* (4), 224-234.
5. Hyatt, J. A., Liquid and Supercritical Carbon Dioxide as Organic Solvents. *Journal of Organic Chemistry* **1984**, *49* (26), 5097-5101.
6. DeSimone, J. M.; Guan, Z.; Elsbernd, C. S., Synthesis of Fluoropolymers in Supercritical Carbon Dioxide. *Science* **1992**, *257* (5072), 945-947.
7. Hoefling, T. A.; Newman, D. A.; Enick, R. M.; Beckman, E. J., Effect of Structure on the Cloud-Point Curves of Silicone-Based Amphiphiles in Supercritical Carbon Dioxide. *Journal of Supercritical Fluids* **1993**, *6* (3), 165-171.
8. Guan, Z.; Combes, J. R.; Menciloglu, Y. Z.; DeSimone, J. M., Homogeneous Free Radical Polymerizations in Supercritical Carbon Dioxide: 2. Thermal Decomposition of 2,2'-Azobis(isobutyronitrile). *Macromolecules* **1993**, *26* (11), 2663-2669.
9. Sarbu, T.; Styranec, T.; Beckman, E. J., Non-Fluorous with Very High Solubility in Supercritical CO<sub>2</sub> down to Low Pressures. *Nature* **2000**, *405* (6783), 165-168.
10. Sarbu, T.; Styranec, T. J.; Beckman, E. J., Design and Synthesis of Low Cost, Sustainable CO<sub>2</sub>-Philes. *Industrial & Engineering Chemistry Research* **2000**, *39* (12), 4678-4683.
11. Raveendran, P.; Wallen, S. L., Sugar Acetates as Novel, Renewable CO<sub>2</sub>-Philes. *Journal of the American Chemical Society* **2002**, *124* (25), 7274-7275
12. Wick, C. D.; Siepmann, J. I.; Theodorou, D. N., Microscopic Origins for the Favorable Solvation of Carbonate Ether Copolymers in CO<sub>2</sub>. *Journal of the American Chemical Society* **2005**, *127* (35), 12338-12342.
13. Nelson, M. R.; Brokman, R. F., Ab Initio Calculations on CO<sub>2</sub> Binding to Carbonyl Groups. *Journal of Physical Chemistry A* **1998**, *102* (40), 7860-7863

14. Raveendran, P.; Wallen, S. L., Cooperative C-H...O Hydrogen Bonding in CO<sub>2</sub>-Lewis Base Complexes: Implications for Solvation in Supercritical CO<sub>2</sub>. *Journal of the American Chemical Society* **2002**, *124* (42), 12590-12599.
15. Kazarian, S. G.; Vincent, M. F.; Bright, F. V.; Liotta, C. L.; Eckert, C. A., Specific Intermolecular Interaction of Carbon Dioxide with Polymers. *Journal of the American Chemical Society* **1996**, *118* (7), 1729-1736.
16. Rindfleisch, F.; DiNoia, T. P.; McHugh, M. A., Solubility of Polymers and Copolymers in Supercritical CO<sub>2</sub>. *Journal of Physical Chemistry* **1996**, *100* (38), 15581-15587.
17. Shen, Z.; McHugh, M. A.; Xu, J.; Belardi, J.; Kilic, S.; Mesiano, A.; Bane, S.; Karnikas, C.; Beckman, E.; Enick, R., CO<sub>2</sub>-Solubility of Oligomers and Polymers That Contain the Carbonyl Group. *Polymer* **2003**, *44* (5), 1491-1498.
18. Krukonis, V., Processing of Polymers with Supercritical Fluids. *Polymer News* **1985**, *11* (1), 7-16.
19. Royer, J. R.; DeSimone, J. M.; Khan, S. A., Carbon Dioxide-Induced Swelling of Poly(dimethylsiloxane). *Macromolecules* **1999**, *32* (26), 8965-8973.
20. Wissinger, R. G.; Paulaitis, M. E., Molecular Thermodynamic Model for Sorption and Swelling in Glassy Polymer-Carbon Dioxide Systems at Elevated Pressures. *Industrial & Engineering Chemistry Research* **1991**, *30* (5), 842-851.
21. Zhang, Z.; Handa, Y. P., CO<sub>2</sub>-Assisted Melting of Semicrystalline Polymers. *Macromolecules* **1997**, *30* (26), 8505-8507.
22. Ryan, J.; Aldabbagh, F.; Zetterlund, P. B.; Okubo, M., First Nitroxide-Mediated Free Radical Dispersion Polymerizations of Styrene in Supercritical Carbon Dioxide. *Polymer* **2005**, *46* (23), 9769-9777.
23. Beuermann, S.; Buback, M.; Isemer, C.; Lacik, I.; Wahl, A., Pressure and Temperature Dependence of the Propagation Rate Coefficient of Free-Radical Styrene Polymerization in Supercritical Carbon Dioxide. *Macromolecules* **2002**, *35* (10), 3866-3869.
24. Baran, N.; Deniz, S.; Akgun, M.; Uzun, I. N.; Dincer, S., Dispersion Polymerization of Styrene in Supercritical Carbon Dioxide Using Monofunctional Perfluoropolyether and Silicone-Containing Fluoroacrylate Stabilizers. *European Polymer Journal* **2005**, *41* (5), 1159-1167.
25. Beuermann, S.; Buback, M.; Schmaltz, C., Termination Rate Coefficients of Butyl Acrylate Free-Radical Homopolymerization in Supercritical CO<sub>2</sub> and in Bulk. *Industrial & Engineering Chemistry Research* **1999**, *38* (9), 3338-3344.

26. Deniz, S.; Baran, N.; Akgun, M.; Uzun, I. N.; Dincer, S., Dispersion Polymerization of Methyl Methacrylate in Supercritical Carbon Dioxide Using a Silicone-Containing Fluoroacrylate Stabilizer. *Polymer International* **2005**, *54* (12), 1660-1668.
27. Galia, A.; Pierro, P.; Filardo, G., Dispersion Polymerization of Methyl Methacrylate in Supercritical Carbon Dioxide Stabilized with Perfluoroalkyl-Terminated Poly(ethylene glycol). *Journal of Supercritical Fluids* **2004**, *32* (1-3), 255-263.
28. Deak, G.; Pernecker, T.; Kennedy, J. P., Carbocationic Polymerization in Supercritical CO<sub>2</sub>. III. The Ceiling Temperature of and the Effect of Temperature on the Polymerization of Isobutylene. *Polymer Bulletin* **1994**, *33* (3), 259-265.
29. Clark, M. R.; DeSimone, J. M., Cationic Polymerization of Vinyl and Cyclic Ethers in Supercritical and Liquid Carbon Dioxide. *Macromolecules* **1995**, *28* (8), 3002-3004.
30. Hu, X.; Blanda, M. T.; Venumbaka, S. R.; Cassidy, P. E., Ring-Opening Metathesis Polymerization (ROMP) of Norbornene in Supercritical Carbon Dioxide Using Well-Defined Metal Carbene Catalysts. *Polymers for Advanced Technologies* **2005**, *16* (2-3), 146-149.
31. Kemmere, M.; de Vries, T.; Vorstman, M.; Keurentjes, J., A Novel Process for the Catalytic Polymerization of Olefins in Supercritical Carbon Dioxide. *Chemical Engineering Science* **2001**, *56* (13), 4197-4204.
32. Kim, I.; Yi, M. J.; Byun, S. H.; Park, D. W.; Kim, B. U.; Ha, C. S., Biodegradable Polycarbonate Synthesis by Copolymerization of Carbon Dioxide with Epoxides Using a Heterogeneous Zinc Complex. *Macromolecular Symposia* **2005**, *224* (1), 181-192.
33. Kiserow, D. J.; Shi, C.; Roberts, G. W.; Gross, S. M.; DeSimone, J. M., Solid-State Polymerization of Poly(bisphenol A carbonate) Facilitated by Supercritical Carbon Dioxide. In *ACS Symposium Series*, Brunelle, D. J.; Korn, M. R., Eds. American Chemical Society: Washington, DC, 2005; Vol. 898, pp 86-94.
34. de Gooijer, J. M.; Ellmann, J.; Moller, M.; Koning, C. E., End Group Modification of Polyamide-6 in Supercritical and Subcritical Fluids: Part 3: Amine End Group Modification with Diketene and Diketene Acetone Adduct in CO<sub>2</sub>. *Journal of Supercritical Fluids* **2004**, *31* (1), 75-87.
35. DeSimone, J. M.; Givens, R.; Ni, Y. Synthesis of Polyamides in Liquid and Supercritical Carbon Dioxide. US Patent 6025459, 1998.
36. Burke, A. L. C.; Maier, G.; DeSimone, J. M., Synthesis of Polyesters in Supercritical Carbon Dioxide. *Polymeric Materials Science and Engineering* **1996**, *74*, 248-249.

37. Yan, H.; Sato, T.; Komago, D.; Yamaguchi, A.; Oyaizu, K.; Yuasa, M.; Otake, K., Electrochemical Synthesis of a Polypyrrole Thin Film with Supercritical Carbon Dioxide as a Solvent. *Langmuir* **2005**, *21* (26), 12303-12308.
38. Sui, R.; Rizkalla, A. S.; Charpentier, P. A., Synthesis and Formation of Silica Aerogel Particles by a Novel Sol-Gel Route in Supercritical Carbon Dioxide. *Journal of Physical Chemistry B* **2004**, *108* (32), 11886-11892.
39. Okubo, M.; Fujii, S.; Maenaka, H.; Minami, H., Production of Polydivinylbiphenyl Particles by Precipitation Polymerization in Supercritical Carbon Dioxide. *Colloid & Polymer Science* **2002**, *280* (12), 1084-1090.
40. Okubo, M.; Fujii, S.; Maenaka, H.; Minami, H., Production of Polyacrylonitrile Particles by Precipitation Polymerization in Supercritical Carbon Dioxide. *Colloid & Polymer Science* **2003**, *281* (10), 964-972.
41. Bratton, D.; Brown, M.; Howdle, S. M., Suspension Polymerization of L-Lactide in Supercritical Carbon Dioxide in the Presence of a Triblock Copolymer Stabilizer. *Macromolecules* **2003**, *36* (16), 5908-5911.
42. Yates, M. Z.; Li, G.; Shim, J. J.; Maniar, S.; Johnston, K. P.; Lim, K. T.; Webber, S., Ambidextrous Surfactants for Water-Dispersible Polymer Powders from Dispersion Polymerization in Supercritical CO<sub>2</sub>. *Macromolecules* **1999**, *32* (4), 1018-1026.
43. Li, G.; Yates, M. Z.; Johnston, K. P.; Howdle, S. M., In-Situ Investigation on the Mechanism of Dispersion Polymerization in Supercritical Carbon Dioxide. *Macromolecules* **2000**, *33* (11), 4008-4014.
44. Romack, T. J.; Maury, E. E.; DeSimone, J. M., Precipitation Polymerization of Acrylic Acid in Supercritical Carbon Dioxide. *Macromolecules* **1995**, *28* (4), 912-915.
45. Loy, D. A.; Russick, E. M.; Yamanaka, S. A.; Baugher, B. M.; Shea, K. J., Direct Formation of Aerogels by Sol-Gel Polymerizations of Alkoxysilanes in Supercritical Carbon Dioxide. *Chemistry of Materials* **1997**, *9* (11), 2264-2268.
46. Fricke, J., Aerogels - A Fascinating Class of High-Performance Porous Solids. *Springer Proceedings in Physics* **1986**, *6* (Aerogels), 2-19.
47. Hrubesh, L. W., Aerogels: The World's Lightest Solids. *Chemistry & Industry* **1990**, (24), 824-827.
48. Sharp, K. G., A Two-Component, Non-Aqueous Route to Silica Gel. *Journal of Sol-Gel Science and Technology* **1994**, *2* (1-3), 35-41.
49. Wood, C. D.; Cooper, A. I., Synthesis of Macroporous Polymer Beads by Suspension Polymerization Using Supercritical Carbon Dioxide as a Pressure-Adjustable Porogen. *Macromolecules* **2001**, *34* (1), 5-8.

50. Su, Z.; Zhao, Y.; Xu, Y.; Zhang, X.; Zhu, S.; Wang, D.; Wu, J.; Han, C. C.; Xu, D., Characterization of the Sequence Distribution and Crystalline Structure of Poly(ethylene-co-vinyl acetate) Copolymers with High-Resolution NMR Spectroscopy. *Polymer* **2004**, *45* (11), 3693-3700.
51. Stael, G. C.; Tavares, M. I. B., NMR Carbon-13 High Resolution Study of Poly(ethylene-co-vinyl acetate). *Polymer Testing* **1997**, *16* (2), 193-198.
52. Odian, G., *Principles of Polymerization*. 4<sup>th</sup> ed.; John Wiley & Sons, Inc.: Hoboken, NJ, 2004; p 812.
53. Alfrey, T., Jr.; Goldfinger, G., The Mechanism of Copolymerization. *Journal of Chemical Physics* **1944**, *12*, 205-209.
54. Mayo, F. R.; Lewis, F. M., Copolymerization. I. A Basis for Comparing the Behavior of Monomers in Copolymerization; the Copolymerization of Styrene and Methyl Methacrylate. *Journal of the American Chemical Society* **1944**, *66*, 1594-1601.
55. Farina, M., Kinetic and Statistical Derivation of the Copolymerization Equation. *Makromolekulare Chemie* **1990**, *191* (11), 2795-2799.
56. Goldfinger, G.; Kane, T., Derivation of the Copolymerization Equation without Steady-State Assumptions. *Journal of Polymer Science Part A: Polymer Chemistry* **1948**, *3*, 462-463.
57. Van der Meer, R.; Aarts, M. W. A. M.; German, A. L., Effect of Solvent on the Copolymerization of Ethylene and Vinyl Acetate. *Journal of Polymer Science: Polymer Chemistry Edition* **1980**, *18* (4), 1347-1357.
58. Van der Meer, R.; German, A. L., Effect of Pressure on Free Radical Copolymerization Kinetics. II. Novel Methods of Measuring Monomer Reactivity Ratios under High-Pressure Conditions. *Journal of Polymer Science: Polymer Chemistry Edition* **1979**, *17* (2), 571-582.
59. German, A. L.; Heikens, D., Copolymerization of Ethylene and Vinyl Acetate at Low Pressure. Determination of the Kinetics by Sequential Sampling. *Journal of Polymer Science, Part A-1: Polymer Chemistry* **1971**, *9* (8), 2225-2232.
60. Erusalimskii, B. L.; Tumarkin, N. Y.; Duntov, F. I.; Lyubetskii, S. G.; Gol'denberg, A. L., Effect of Pressure on the Radical Polymerization and Copolymerization of Ethylene. *Makromolekulare Chemie* **1967**, *104* (1), 288-296.
61. Terteryan, R. A.; Dints'es, A. I.; Rysakov, M. V., Copolymerization of Ethylene with Vinyl Acetate. *Neftekhimiya* **1963**, *3* (5), 719-724.
62. Burkhart, R. D.; Zutty, N. L., Copolymerization Studies. III. Reactivity Ratios of Model Ethylene Copolymerizations and their Use in Q-e Calculations. *Journal of Polymer Science, Part A: General Papers* **1963**, *1* (4), 1137-1145.



63. Canelas, D. A.; Betts, D. E.; DeSimone, J. M.; Yates, M. Z.; Johnston, K. P., Poly(vinyl acetate) and Poly(vinyl acetate-co-ethylene) Latexes via Dispersion Polymerizations in Carbon Dioxide. *Macromolecules* **1998**, *31* (20), 6794-6805.
64. Bunyard, W. C.; Kadla, J. F.; DeSimone, J. M., Viscosity Effects on the Thermal Decomposition of Bis(perfluoro-2-*N*-propoxypropionyl) Peroxide in Dense Carbon Dioxide and Fluorinated Solvents. *Journal of the American Chemical Society* **2001**, *123* (30), 7199-7206.
65. Kadla, J. F.; DeYoung, J. P.; DeSimone, J. M., The Thermal Decomposition of Perfluoroalkyl Peroxides in Carbon Dioxide. *Polymer Preprints* **1998**, *39* (2), 835-836.
66. Charpentier, P. A.; DeSimone, J. M.; Roberts, G. W., Decomposition of Polymerisation Initiators in Supercritical CO<sub>2</sub>: A Novel Approach to Reaction Kinetics Using a CSTR. *Chemical Engineering Science* **2000**, *55* (22), 5341-5349.
67. McBay, H. C.; Tucker, O., Thermal Decomposition of Dialkyl Peroxydicarbonates in Solution. Reaction of Alkoxy Free Radicals in Pure Solvents. *Journal of Organic Chemistry* **1954**, *19*, 869-883.
68. Razuvaev, G. A.; Terman, L. M.; Petukhov, G. G., Mechanism of Thermal Decomposition of Percarbonates in Solution. *Doklady Akademii Nauk SSSR* **1961**, *136*, 628-630.
69. Moad, G.; Solomon, D. H., *The Chemistry of Radical Polymerization*. 2<sup>nd</sup> fully revised ed.; Elsevier: Oxford, UK, 2006; p 639.
70. Koo, J. H., *Polymer Nanocomposites: Processing, Characterization, and Applications*. McGraw-Hill: New York, 2006; p 272.
71. Schadler, L. S.; Brinson, L. C.; Sawyer, W. G., Polymer Nanocomposites: A Small Part of the Story. *JOM* **2007**, *59* (3), 53-60.
72. Crosby, A. J.; Lee, J.-Y., Polymer Nanocomposites: The "Nano" Effect on Mechanical Properties. *Polymer Reviews* **2007**, *47* (2), 217-229.
73. Schaefer, D. W.; Justice, R. S., How Nano Are Nanocomposites? *Macromolecules* **2007**, *40* (24), 8501-8517.
74. Herrera-Alonso, M.; Garcia-Leiner, M.; McCarthy, T. J.; Lesser, A. J., Semicrystalline Polymer Nanocomposites Using Chemically Designed Compatibilizers and Supercritical CO<sub>2</sub>-Assisted Polymer Processing. *PMSE Preprints* **2004**, *91*, 921-922.
75. Garcia-Leiner, M.; Lesser, A. J., Polymer Nanocomposites Prepared by Supercritical Carbon Dioxide-Assisted Polymer Processing. *Polymer Preprints* **2004**, *45* (1), 520-521.

76. Sun, D.; Zhang, R.; Liu, Z.; Huang, Y.; Wang, Y.; He, J.; Han, B.; Yang, G., Polypropylene/Silica Nanocomposites Prepared by In-Situ Sol-Gel Reaction with the Aid of CO<sub>2</sub>. *Macromolecules* **2005**, *38* (13), 5617-5624.
77. Norris, D. J. Measurement and Assignment of the Size-Dependent Optical Spectrum in Cadmium Selenide (CdSe) Quantum Dots. Massachusetts Institute of Technology, Cambridge, MA, USA, 1995.
78. Yang, H.; Holloway, P. H.; Santra, S., Water-Soluble Silica-Overcoated CdS:Mn/ZnS Semiconductor Quantum Dots. *Journal of Chemical Physics* **2004**, *121* (15), 7421-7426.
79. Murray, C. B.; Norris, D. J.; Bawendi, M. G., Synthesis and Characterization of Nearly Monodisperse CdE (E = Sulfur, Selenium, Tellurium) Semiconductor Nanocrystallites. *Journal of the American Chemical Society* **1993**, *115* (19), 8706-8715.
80. Pickett, N. L.; Brien, P. O., Syntheses of Semiconductor Nanoparticles Using Single-Molecular Precursors. *Chemical Record* **2001**, *1* (6), 467-479.
81. Skaff, H.; Ilker, M. F.; Coughlin, E. B.; Emrick, T., Preparation of Cadmium Selenide-Polyolefin Composites from Functional Phosphine Oxides and Ruthenium-Based Metathesis. *Journal of the American Chemical Society* **2002**, *124* (20), 5729-5733.
82. Pavia, D. L.; Lampman, G. M.; Kriz, G. S.; Vyvyan, J. R., *Introduction to spectroscopy*. 4<sup>th</sup> ed.; Brooks/Cole, Cengage Learning: Belmont, CA, 2009.
83. Brillouin, L., The Electrons in Metals and the Classification of the Corresponding Waves of de Broglie. *Compt. rend.* **1930**, *191*, 292-294.
84. Bruice, P. Y., *Organic Chemistry*. 4<sup>th</sup> ed.; Prentice Hall: Upper Saddle River, NJ, 2004.
85. Xu, W. Z.; Li, X.; Charpentier, P. A., In Situ ATR-FT-IR Study of the Thermal Decomposition of Diethyl Peroxydicarbonate in Supercritical Carbon Dioxide. *Polymer* **2007**, *48* (5), 1219-1228.
86. Young, J. L.; DeSimone, J. M., Synthesis and Characterization of Polymers: From Polymeric Micelles to Step-Growth Polymerizations. In *Green Chemistry Using Liquid and Supercritical Carbon Dioxide*, DeSimone, J. M.; Tumas, W., Eds. Oxford University Press: Oxford, 2003; pp 149-163.
87. Charpentier, P. A.; DeSimone, J. M.; Roberts, G. W., Continuous Polymerizations in Supercritical Carbon Dioxide. In *Clean Solvents*, Abraham, M. A.; Moens, L., Eds. ACS Symposium Series: Washington, DC, 2002; Vol. 819, pp 113-135.
88. Charpentier, P. A.; DeSimone, J. M.; Roberts, G. W., Continuous Precipitation Polymerization of Vinylidene Fluoride in Supercritical Carbon Dioxide: Modeling of the

Rate of Polymerization. *Industrial & Engineering Chemistry Research* **2000**, *39* (12), 4588-4596.

89. Johnston, K. P.; Shah, P. S., Materials Science: Making Nanoscale Materials with Supercritical Fluids. *Science* **2004**, *303* (5657), 482-483.

90. Sui, R.; Rizkalla, A. S.; Charpentier, P. A., Formation of Titania Nanofibers: A Direct Sol-Gel Route in Supercritical CO<sub>2</sub>. *Langmuir* **2005**, *21* (14), 6150-6153.

91. DeSimone, J. M.; Maury, E. E.; Lemert, R. M.; Combes, J. R., Near-and Supercritical Fluid Solvents for Living Anionic Polymerizations. *Makromolekulare Chemie, Macromolecular Symposia* **1993**, *67*, 251-260.

92. Going Supercritical at DuPont. *Chemical Week* **2002**, *164* (13), 24.

93. Gill, G. B., Synthetic Use of Free Radicals. In *Modern Reactions in Organic Synthesis*, Timmons, C. J., Ed. Van Nostrand Reinhold Company: London, 1970; pp 90-154.

94. Cohen, S. G.; Sparrow, D. B., Reactions of Diisopropyl Peroxydicarbonate. *Journal of the American Chemical Society* **1950**, *72* (1), 611-614.

95. Oldfield, F. F.; Yasuda, H. K., ESR Study of MMA Polymerization by a Peroxide/Amine System: Bone Cement Formation. *Journal of Biomedical Materials Research* **1999**, *44* (4), 436-445.

96. Spantulescu, M. D.; Jain, R. P.; Derksen, D. J.; Vederas, J. C., Photolysis of Diacyl Peroxides: A Radical-Based Approach for the Synthesis of Functionalized Amino Acids. *Organic Letters* **2003**, *5* (16), 2963.

97. Yamada, M.; Kitagawa, K.; Komai, T., Thermal Decomposition of Di-alkylperoxydicarbonates and their Initiating Activities for Radical Polymerization. *Plastics Industry News* **1971**, *17* (9), 131-138.

98. Beristain, M. F.; Bucio, E.; Burillo, G.; Muñoz, E.; Ogawa, T., Study on the Interaction of Diarylbutadiynes with Free Radicals: Interaction with Propagating Radicals of Some Vinyl Monomers. *Polymer Bulletin* **1999**, *43* (4/5), 357-364.

99. Perez, C. J.; Cassano, G. A.; Valles, E. M.; Failla, M. D.; Quinzani, L. M., Rheological Study of Linear High Density Polyethylenes Modified with Organic Peroxide. *Polymer* **2002**, *43* (9), 2711-2720.

100. Danilov, A. M.; Mitusova, T. N.; Kovalev, V. A.; Churzin, A. N., Organic Peroxides-Cetane-Increasing Additives for Diesel Fuels. *Chemistry and Technology of Fuels and Oils* **2003**, *39* (6), 330-333.

101. Hara, Y.; Notomi, Y.; Nakamura, H.; Shimizu, M.; Jinnouchi, T., Thermal Decomposition of Organic Peroxides. V. Thermal Decomposition of Peroxydicarbonates. *Kogyo Kayaku* **1992**, *53* (3), 254-260.
102. O'Driscoll, K. F., Organic Peroxides in Vinyl Polymerization. In *Organic Peroxides*, Swern, D., Ed. Wiley-Interscience: New York, 1970; p 609.
103. Van Sickle, D. E., Decomposition of Dicyclohexyl Peroxydicarbonate and OO-tert-butyl O-cyclohexyl Peroxycarbonate. *Journal of Organic Chemistry* **1969**, *34* (11), 3446-3451.
104. Duynstee, E. F. J.; Esser, M. L.; Schellekens, R., Thermal Decomposition of Diisopropyl Peroxydicarbonate. *European Polymer Journal* **1980**, *16* (12), 1127-1134.
105. Buback, M.; Kling, M.; Schmatz, S.; Schroeder, J., Photo-induced decomposition of organic peroxides: Ultrafast formation and decarboxylation of carbonyloxy radicals. *Physical Chemistry Chemical Physics* **2004**, *6* (24), 5441-5455.
106. Abel, B.; Assmann, J.; Botschwina, P.; Buback, M.; Kling, M.; Oswald, R.; Schmatz, S.; Schroeder, J.; Witte, T., Experimental and Theoretical Investigations of the Ultrafast Photoinduced Decomposition of Organic Peroxides in Solution: Formation and Decarboxylation of Benzoyloxy Radicals. *Journal of Physical Chemistry A* **2003**, *107* (26), 5157-5167.
107. Abel, B.; Buback, M.; Kling, M.; Schmatz, S.; Schroeder, J., A Seemingly Well Understood Light-Induced Peroxide Decarboxylation Reaction Reinvestigated with Femtosecond Time Resolution. *Journal of the American Chemical Society* **2003**, *125* (43), 13274-13278.
108. Abel, B.; Assmann, J.; Buback, M.; Grimm, C.; Kling, M.; Schmatz, S.; Schroeder, J.; Witte, T., Ultrafast Decarboxylation of Carbonyloxy Radicals: Influence of Molecular Structure. *Journal of Physical Chemistry A* **2003**, *107* (45), 9499-9510.
109. Aschenbrucker, J.; Buback, M.; Ernsting, N. P.; Schroeder, J.; Steegmuller, U., Peroxyester Decarboxylation Studied by Picosecond Transient IR Spectroscopy. *Journal of Physical Chemistry B* **1998**, *102* (29), 5552-5555.
110. Socrates, G., *Infrared and Raman Characteristic Group Frequencies: Tables and Charts*. 3<sup>rd</sup> ed.; John Wiley & Sons Ltd: Chichester, 2001; p 347.
111. Vacque, V.; Sombret, B.; Huvenne, J.; Legrand, P.; Suc, S., Characterization of the O-O Peroxide Bond by Vibrational Spectroscopy. *Spectrochimica Acta, Part A: Molecular and Biomolecular Spectroscopy* **1997**, *53A* (1), 55-56.
112. Reichardt, C., *Solvents and Solvent Effects in Organic Chemistry*. 3<sup>rd</sup> updated and enl. ed.; Wiley-VCH: Weinheim, 2003; p 629.

113. Paci, M. A. B.; Arguello, G. A.; Garcia, P.; Willner, H., Thermal Decomposition of the Perfluorinated Peroxides  $\text{CF}_3\text{OC}(\text{O})\text{OOC}(\text{O})\text{F}$  and  $\text{CF}_3\text{OC}(\text{O})\text{OOCF}_3$ . *Journal of Physical Chemistry A* **2005**, *109* (33), 7481-7488.
114. Pavia, D. L.; Lampman, G. M.; Kriz, G. S., *Introduction to Spectroscopy: A Guide for Students of Organic Chemistry*. 3<sup>rd</sup> ed.; Harcourt, Inc.: Fort Worth, 2001; p 579.
115. From SIGMA-ALDRICH websites, standard  $^1\text{H}$ ,  $^{13}\text{C}$  NMR spectra of ethyl acetate, 2,3-butanedione, diethyl carbonate, acetaldehyde, and ethanol were used and compared with the spectra from DEPDC decomposition in present study.
116. From NIST websites, standard IR spectra of ethyl acetate, 2,3-butanedione, diethyl carbonate, dimethyl carbonate, acetic acid, acetaldehyde, and ethanol were used and compared with the spectra from DEPDC decomposition in present study.
117. Xu, W. Z.; Charpentier, P. A., FTIR Study on Measuring the Monomer Reactivity Ratios for Ethylene-Vinyl Acetate Polymerization in Supercritical  $\text{CO}_2$ . *Industrial & Engineering Chemistry Research* **2008**, *Accepted*.
118. Gast, M.; Koentges, M.; Brendel, R., Lead-Free On-Laminate Laser Soldering: A New Module Assembling Concept. *Progress in Photovoltaics* **2008**, *16* (2), 151-157.
119. Williams, B. S.; Leatherman, M. D.; White, P. S.; Brookhart, M., Reactions of Vinyl Acetate and Vinyl Trifluoroacetate with Cationic Diimine Pd(II) and Ni(II) Alkyl Complexes: Identification of Problems Connected with Copolymerizations of These Monomers with Ethylene. *Journal of the American Chemical Society* **2005**, *127* (14), 5132-5146.
120. Charpentier, P. A.; Xu, W. Z.; Li, X., A Novel Approach to the Synthesis of  $\text{SiO}_2$ -PVAc Nanocomposites Using a One-Pot Synthesis in Supercritical  $\text{CO}_2$ . *Green Chemistry* **2007**, *9* (7), 768-776.
121. Polic, A. L.; Duever, T. A.; Penlidis, A., Case Studies and Literature Review on the Estimation of Copolymerization Reactivity Ratios. *Journal of Polymer Science, Part A: Polymer Chemistry* **1998**, *36* (5), 813-822.
122. Fineman, M.; Ross, S. D., Linear Method for Determining Monomer Reactivity Ratios in Copolymerization. *Journal of Polymer Science* **1950**, *5* (2), 259-262.
123. Kelen, T.; Tudos, F., Analysis of the Linear Methods for Determining Copolymerization Reactivity Ratios. I. New Improved Linear Graphic Method. *Journal of Macromolecular Science, Chemistry* **1975**, *A9* (1), 1-27.
124. Feng, L.; Berglund, K. A., ATR-FTIR for Determining Optimal Cooling Curves for Batch Crystallization of Succinic Acid. *Crystal Growth & Design* **2002**, *2* (5), 449-452.

125. Smukala, J.; Span, R.; Wagner, W., New Equation of State for Ethylene Covering the Fluid Region for Temperatures from the Melting Line to 450K at Pressures up to 300MPa. *Journal of Physical and Chemical Reference Data* **2000**, *29* (5), 1053-1121.
126. Span, R.; Wagner, W., A New Equation of State for Carbon Dioxide Covering the Fluid Region from the Triple-Point Temperature to 1100 K at Pressures up to 800 MPa. *Journal of Physical and Chemical Reference Data* **1996**, *25* (6), 1509-1596.
127. Pattacini, S. C.; Porro, T. J.; Pavlik, J., Quantitative Analysis for Vinyl Acetate in Polyethylene Copolymers Using FTIR. *American Laboratory* **1991**, *23* (9), 38, 40-41.
128. Williams, K. R., Analysis of Ethylene-Vinyl Acetate Copolymers: A Combined TGA/FTIR Experiment. *Journal of Chemical Education* **1994**, *71* (8), A195-A196, A198.
129. Wendlandt, W. W., *Thermal Analysis*. 3<sup>rd</sup> ed.; John Wiley Interscience: New York, 1986; p 814.
130. Wiles, K. B.; Bhanu, V. A.; Pasquale, A. J.; Long, T. E.; McGrath, J. E., Monomer Reactivity Ratios for Acrylonitrile-Methyl Acrylate Free-Radical Copolymerization. *Journal of Polymer Science Part A: Polymer Chemistry* **2004**, *42* (12), 2994-3001.
131. Scott, P. J.; Penlidis, A.; Rempel, G. L., Ethylene-Vinyl Acetate Semi-Batch Emulsion Copolymerization: Experimental Design and Preliminary Screening Experiments. *Journal of Polymer Science, Part A: Polymer Chemistry* **1993**, *31* (2), 403-426.
132. Alfrey, T., Jr.; Price, C. C., Relative Reactivities in Vinyl Copolymerization. *Journal of Polymer Science* **1947**, *2* (1), 101-106.
133. Greenley, R. Z., Q and e Values for Free Radical Copolymerizations of Vinyl Monomers and Telogens. In *Polymer Handbook*, 4<sup>th</sup> ed.; Brandrup, J.; Immergut, E. H.; Grulke, E. A., Eds. Wiley: New York, 1999; pp II/309-319.
134. Filley, J.; McKinnon, J. T.; Wu, D. T.; Ko, G. H., Theoretical Study of Ethylene-Vinyl Acetate Free-Radical Copolymerization: Reactivity Ratios, Penultimate Effects, and Relative Rates of Chain Transfer to Polymer. *Macromolecules* **2002**, *35* (9), 3731-3738.
135. Buback, M.; Panten, K., Terpolymerization of Ethene, Acrylonitrile and Vinyl Acetate. *Makromolekulare Chemie* **1993**, *194* (9), 2471-2481.
136. Van der Meer, R.; German, A. L.; Heikens, D., Effect of Pressure on Free-Radical Copolymerization Kinetics. I. A Concept of Additivity of Partial Molar Volumes of Activation. *Journal of Polymer Science: Polymer Chemistry Edition* **1977**, *15* (7), 1765-1772.

137. Buback, M.; Dietzsch, H., High-Pressure Free-Radical Copolymerization of Ethene and Methyl Methacrylate. *Macromolecular Chemistry and Physics* **2001**, *202* (7), 1173-1181.
138. Raetzsch, M.; Schneider, W.; Musche, D., Reactivity of Ethylene in the Radically-Initiated Copolymerization of Ethylene with Vinyl Acetate. *Journal of Polymer Science, Polymer Chemistry Edition* **1971**, *9* (3), 785-790.
139. Plochocka, K., Effect of the Reaction Medium on Radical Copolymerization. *Journal of Macromolecular Science, Reviews in Macromolecular Chemistry* **1981**, *C20* (1), 67-148.
140. Baradie, B.; Shoichet, M. S., Synthesis of Fluorocarbon-Vinyl Acetate Copolymers in Supercritical Carbon Dioxide: Insight into Bulk Properties. *Macromolecules* **2002**, *35* (9), 3569-3575.
141. Lebduska, J.; Snuparek, J., Jr.; Kaspar, K.; Cermak, V., Solution Copolymerization of Styrene and 2-Hydroxyethyl Methacrylate. *Journal of Polymer Science, Part A: Polymer Chemistry* **1986**, *24* (4), 777-791.
142. Poliakoff, M.; Fitzpatrick, M.; Farren, T. R.; Anastas, P., Green Chemistry: Science and Politics of Change. *Science* **2002**, *297* (5582), 807-810.
143. Leitner, W., Green Chemistry - Theory and Practice by Paul T. Anastas and John C. Warner. *Science* **1999**, *284* (5421), 1780-1781.
144. Meunier, B., Catalytic Degradation of Chlorinated Phenols. *Science* **2002**, *296* (5566), 270-271.
145. Service, R. F., Organic Chemistry: New-Model Reactions Skip the Drip. *Science* **2002**, *296* (5574), 1784.
146. Ishihara, K.; Ohara, S.; Yamamoto, H., Direct Condensation of Carboxylic Acids with Alcohols Catalyzed by Hafnium(IV) Salts. *Science* **2000**, *290* (5494), 1140-1142.
147. Chin, G., Editors' Choice. *Science* **2001**, *294* (5545), 1243, 1245.
148. DeSimone, J. M., Practical Approaches to Green Solvents. *Science* **2002**, *297* (5582), 799-803.
149. Long, T. E.; Hunt, M. O., *Solvent-Free Polymerizations and Processes: Minimization of Conventional Organic Solvents*. American Chemical Society: Distributed by Oxford University Press: Washington, DC, 1998; p 292.
150. Charpentier, P. A.; Kennedy, K.; DeSimone, J. M.; Roberts, G. W., Continuous Polymerizations in Supercritical Carbon Dioxide: Chain-Growth Precipitation Polymerizations. *Macromolecules* **1999**, *32* (18), 5973-5975.

151. Reverchon, E., Supercritical-Assisted Atomization to Produce Micro- and/or Nanoparticles of Controlled Size and Distribution. *Industrial & Engineering Chemistry Research* **2002**, *41* (10), 2405-2411.
152. Jung, J.; Perrut, M., Particle Design Using Supercritical Fluids: Literature and Patent Survey. *Journal of Supercritical Fluids* **2001**, *20* (3), 179-219.
153. Henon, F. E.; Carbonell, R. G.; DeSimone, J. M., Effect of Polymer Coatings from CO<sub>2</sub> on Water-Vapor Transport in Porous Media. *AIChE Journal* **2002**, *48* (5), 941-952.
154. Pai, R. A.; Humayun, R.; Schulberg, M. T.; Sengupta, A.; Sun, J.-N.; Watkins, J. J., Mesoporous Silicates Prepared Using Preorganized Templates in Supercritical Fluids. *Science* **2004**, *303* (5657), 507-510.
155. Jordan, J.; Jacob, K. I.; Tannenbaum, R.; Sharaf, M. A.; Jasiuk, I., Experimental Trends in Polymer Nanocomposites - A Review. *Materials Science & Engineering, A: Structural Materials: Properties, Microstructure and Processing* **2005**, *A393* (1-2), 1-11.
156. Pinnavaia, T. J.; Beall, G. W., *Polymer-Clay Nanocomposites*. Wiley: Chichester, England 2000; p 349.
157. Sinha Ray, S.; Okamoto, M., Polymer/layered silicate nanocomposites: a review from preparation to processing. *Progress in Polymer Science* **2003**, *28* (11), 1539-1641.
158. Qian, D.; Dickey, E. C.; Andrews, R.; Rantell, T., Load Transfer and Deformation Mechanisms in Carbon Nanotube-Polystyrene Composites. *Applied Physics Letters* **2000**, *76* (20), 2868-2870.
159. Alexandre, M.; Beyer, G.; Henrist, C.; Cloots, R.; Rulmont, A.; Jerome, R.; Dubois, P., "One-Pot" Preparation of Polymer/Clay Nanocomposites Starting from Na<sup>+</sup> Montmorillonite. 1. Melt Intercalation of Ethylene-Vinyl Acetate Copolymer. *Chemistry of Materials* **2001**, *13* (11), 3830-3832.
160. Kumar, S.; Doshi, H.; Srinivasarao, M.; Park, J. O.; Schiraldi, D. A., Fibers from Polypropylene/Nano Carbon Fiber Composites. *Polymer* **2002**, *43* (5), 1701-1703.
161. Wagenknecht, U.; Kretschmar, B.; Reinhardt, G., Investigations of Fire Retardant Properties of Polypropylene-Clay-Nanocomposites. *Macromolecular Symposia* **2003**, *194* (1), 207-212.
162. Rana, P. K.; Swain, S. K.; Sahoo, P. K., Synthesis, Characterization, and Properties of Intercalated Poly(2-ethyl hexylacrylate)/Silicate Nanocomposites: XRD, TEM, IR, TGA, Superabsorbency, Pressure-Sensitive Adhesion, and Biodegradation. *Journal of Applied Polymer Science* **2004**, *93* (3), 1007-1011.



163. Yu, Y.-Y.; Chen, C.-Y.; Chen, W.-C., Synthesis and Characterization of Organic–Inorganic Hybrid Thin Films from Poly(acrylic) and Monodispersed Colloidal Silica. *Polymer* **2003**, *44* (3), 593-601.
164. Sinha Ray, S.; Yamada, K.; Okamoto, M.; Fujimoto, Y.; Ogami, A.; Ueda, K., New Poly(lactide)/Layered Silicate Nanocomposites. 5. Designing of Materials with Desired Properties. *Polymer* **2003**, *44* (21), 6633-6646.
165. Salahuddin, N.; Akelah, A., Synthesis and Characterization of Poly(styrene-maleic anhydride)-Montmorillonite Nanocomposite. *Polymers for Advanced Technologies* **2002**, *13* (5), 339-345.
166. Zhang, X.; Liu, T.; Sreekumar, T. V.; Kumar, S.; Moore, V. C.; Hauge, R. H.; Smalley, R. E., Poly(vinyl alcohol)/SWNT Composite Film. *Nano Letters* **2003**, *3* (9), 1285-1288.
167. Nguyen, V.; Yoshida, W.; Cohen, Y., Graft Polymerization of Vinyl Acetate onto Silica. *Journal of Applied Polymer Science* **2003**, *87* (2), 300-310.
168. Pyun, J.; Jia, S.; Kowalewski, T.; Patterson, G. D.; Matyjaszewski, K., Synthesis and Characterization of Organic/Inorganic Hybrid Nanoparticles: Kinetics of Surface-Initiated Atom Transfer Radical Polymerization and Morphology of Hybrid Nanoparticle Ultrathin Films. *Macromolecules* **2003**, *36* (14), 5094-5104.
169. Sanchez, C.; de Soler-Illia, G. J.; Ribot, F.; Lalot, T.; Mayer, C. R.; Cabuil, V., Designed Hybrid Organic-Inorganic Nanocomposites from Functional Nanobuilding Blocks. *Chemistry of Materials* **2001**, *13* (10), 3061-3083.
170. Zhang, S.-W.; Zhou, S.-X.; Weng, Y.-M.; Wu, L.-M., Synthesis of SiO<sub>2</sub>/Polystyrene Nanocomposite Particles via Miniemulsion Polymerization. *Langmuir* **2005**, *21* (6), 2124-2128.
171. Baradie, B.; Shoichet, M. S.; Shen, Z.; McHugh, M. A.; Hong, L.; Wang, Y.; Johnson, J. K.; Beckman, E. J.; Enick, R. M., Synthesis and Solubility of Linear Poly(tetrafluoroethylene-co-vinyl acetate) in Dense CO<sub>2</sub>: Experimental and Molecular Modeling Results. *Macromolecules* **2004**, *37* (20), 7799-7807.
172. Fink, R.; Hancu, D.; Valentine, R.; Beckman, E. J., Toward the Development of “CO<sub>2</sub>-Philic” Hydrocarbons. 1. Use of Side-Chain Functionalization to Lower the Miscibility Pressure of Polydimethylsiloxanes in CO<sub>2</sub>. *Journal of Physical Chemistry B* **1999**, *103* (31), 6441-6444
173. Nakamoto, K., *Infrared and Raman Spectra of Inorganic and Coordination Compounds*. 5<sup>th</sup> ed.; John Wiley: New York, 1997; Vol. Part B.
174. Moner-Girona, M.; Roig, A.; Molins, E.; Llibre, J., Sol-Gel Route to Direct Formation of Silica Aerogel Microparticles Using Supercritical Solvents. *Journal of Sol-Gel Science and Technology* **2003**, *26* (1/2/3), 645-649.

175. Xu, W. Z.; Charpentier, P. A., Light-Selective Nanofilms of Quantum Dot-Poly(ethylene-co-vinyl acetate) Synthesized Using Supercritical CO<sub>2</sub>. *Journal of Physical Chemistry* **2008**, *Submitted*.
176. Morton, O., Solar Energy: A New Day Dawning? Silicon Valley Sunrise. *Nature* **2006**, *443* (7107), 19-22.
177. Nagami, A. Agricultural Covering Materials with Selective Light Transmittance for Controlling Flowering or Fruiting of Plants. JP 2006191862 A, 2006.
178. Gopalakrishnan, G.; Danelon, C.; Izewska, P.; Prummer, M.; Bolinger, P.-Y.; Geissbuhler, I.; Demurtas, D.; Dubochet, J.; Vogel, H., Multifunctional Lipid/Quantum Dot Hybrid Nanocontainers for Controlled Targeting of Live Cells. *Angewandte Chemie, International Edition* **2006**, *45* (33), 5478-5483.
179. Yao, H.; Zhang, Y.; Xiao, F.; Xia, Z.; Rao, J., Quantum Dot/Bioluminescence Resonance Energy Transfer Based Highly Sensitive Detection of Proteases. *Angewandte Chemie, International Edition* **2007**, *46* (23), 4346-4349.
180. Kukimoto, H., Conductivity Control of Zinc Selenide Grown by MOVPE and its Applications for Blue Electroluminescence. *Journal of Crystal Growth* **1990**, *101* (1-4), 953-957.
181. Peng, X.; Wickham, J.; Alivisatos, A. P., Kinetics of II-VI and III-V Colloidal Semiconductor Nanocrystal Growth: "Focusing" of Size Distributions. *Journal of the American Chemical Society* **1998**, *120* (21), 5343-5344.
182. Yang, C. S.; Awschalom, D. D.; Stucky, G. D., Kinetic-Dependent Crystal Growth of Size-Tunable CdS Nanoparticles. *Chemistry of Materials* **2001**, *13* (2), 594-598.
183. Sheng, W.; Kim, S.; Lee, J.; Kim, S. W.; Jensen, K.; Bawendi, M. G., In-Situ Encapsulation of Quantum Dots into Polymer Microspheres. *Langmuir* **2006**, *22* (8), 3782-3790.
184. Barrelet, C. J.; Wu, Y.; Bell, D. C.; Lieber, C. M., Synthesis of CdS and ZnS Nanowires Using Single-Source Molecular Precursors. *Journal of the American Chemical Society* **2003**, *125* (38), 11498-11499.
185. Trindade, T.; O'Brien, P.; Zhang, X. M., Synthesis of CdS and CdSe Nanocrystallites Using a Novel Single-Molecule Precursors Approach. *Chemistry of Materials* **1997**, *9* (2), 523-530.
186. Crouch, D. J.; O'Brien, P.; Malik, M. A.; Skabara, P. J.; Wright, S. P., A One-Step Synthesis of Cadmium Selenide Quantum Dots from a Novel Single Source Precursor. *Chemical Communications* **2003**, (12), 1454-1455.

187. Hines, M. A.; Guyot-Sionnest, P., Synthesis and Characterization of Strongly Luminescing ZnS-Capped CdSe Nanocrystals. *Journal of Physical Chemistry* **1996**, *100* (2), 468-471.
188. Mattoussi, H.; Radzilowski, L. H.; Dabbousi, B. O.; Fogg, D. E.; Schrock, R. R.; Thomas, E. L.; Rubner, M. F.; Bawendi, M. G., Composite Thin Films of CdSe Nanocrystals and a Surface Passivating/Electron Transporting Block Copolymer: Correlations between Film Microstructure by Transmission Electron Microscopy and Electroluminescence. *Journal of Applied Physics* **1999**, *86* (8), 4390-4399.
189. Peng, X.; Schlamp, M. C.; Kadavanich, A. V.; Alivisatos, A. P., Epitaxial Growth of Highly Luminescent CdSe/CdS Core/Shell Nanocrystals with Photostability and Electronic Accessibility. *Journal of the American Chemical Society* **1997**, *119* (30), 7019-7029.
190. Dabbousi, B. O.; Rodriguez-Viejo, J.; Mikulec, F. V.; Heine, J. R.; Mattoussi, H.; Ober, R.; Jensen, K. F.; Bawendi, M. G., (CdSe)ZnS Core-Shell Quantum Dots: Synthesis and Characterization of a Size Series of Highly Luminescent Nanocrystallites. *Journal of Physical Chemistry B* **1997**, *101* (46), 9463-9475.
191. Kuno, M.; Lee, J. K.; Dabbousi, B. O.; Mikulec, F. V.; Bawendi, M. G., The Band Edge Luminescence of Surface Modified CdSe Nanocrystallites: Probing the Luminescing State. *Journal of Chemical Physics* **1997**, *106* (23), 9869-9882.
192. Youn, H. C.; Baral, S.; Fendler, J. H., Dihexadecyl Phosphate, Vesicle-Stabilized and In Situ Generated Mixed Cadmium Sulfide and Zinc Sulfide Semiconductor Particles: Preparation and Utilization for Photosensitized Charge Separation and Hydrogen Generation. *Journal of Physical Chemistry* **1988**, *92* (22), 6320-6327.
193. Yim, J. H.; Jang, E. J.; Ahn, T. K. Method for Producing Quantum Dot Silicate Thin Film for Light Emitting Device. US Patent 2004266148, 2004.
194. Kim, S.; Bawendi, M. G., Oligomeric Ligands for Luminescent and Stable Nanocrystal Quantum Dots. *Journal of the American Chemical Society* **2003**, *125* (48), 14652-14653.
195. Chan, W. C. W.; Nie, S., Quantum Dot Bioconjugates for Ultrasensitive Nonisotopic Detection. *Science* **1998**, *281* (5385), 2016-2018.
196. Mattoussi, H.; Mauro, J. M.; Goldman, E. R.; Anderson, G. P.; Sundar, V. C.; Mikulec, F. V.; Bawendi, M. G., Self-Assembly of CdSe-ZnS Quantum Dot Bioconjugates Using an Engineered Recombinant Protein. *Journal of the American Chemical Society* **2000**, *122* (49), 12142-12150.
197. Wang, Y. A.; Li, J. J.; Chen, H.; Peng, X., Stabilization of Inorganic Nanocrystals by Organic Dendrons. *Journal of the American Chemical Society* **2002**, *124* (10), 2293-2298.

198. Huang, B.; Tomalia, D. A., Dendronization of Gold and CdSe/cdS (Core-Shell) Quantum Dots with Tomalia Type, Thiol Core, Functionalized Poly(amidoamine) (PAMAM) Dendrons. *Journal of Luminescence* **2005**, *111* (4), 215-223.
199. Skaff, H.; Sill, K.; Emrick, T., Quantum Dots Tailored with Poly(para-phenylene vinylene). *Journal of the American Chemical Society* **2004**, *126* (36), 11322-11325.
200. Landi, B. J.; Castro, S. L.; Ruf, H. J.; Evans, C. M.; Bailey, S. G.; Raffaele, R. P., CdSe Quantum Dot-Single Wall Carbon Nanotube Complexes for Polymeric Solar Cells. *Solar Energy Materials and Solar Cells* **2005**, *87* (1-4), 733-746.
201. Yang, X.; Zhang, Y., Encapsulation of Quantum Nanodots in Polystyrene and Silica Micro-/Nanoparticles. *Langmuir* **2004**, *20* (14), 6071-6073.
202. Li, Y.; Liu, E. C. Y.; Pickett, N.; Skabara, P. J.; Cummins, S. S.; Ryley, S.; Sutherland, A. J.; O'Brien, P., Synthesis and Characterization of CdS Quantum Dots in Polystyrene Microbeads. *Journal of Materials Chemistry* **2005**, *15* (12), 1238-1243.
203. Tekin, E.; Smith, P. J.; Hoepfner, S.; van den Berg, A. M. J.; Susha, A. S.; Rogach, A. L.; Feldmann, J.; Schubert, U. S., Inkjet Printing of Luminescent CdTe Nanocrystal-Polymer Composites. *Advanced Functional Materials* **2007**, *17* (1), 23-28.
204. Yue, B.; Yang, J.; Huang, C.-Y.; Dave, R.; Pfeffer, R., Synthesis of Macroporous PMMA/Silica Nanocomposite Monoliths in Supercritical Carbon Dioxide. *Macromolecular Rapid Communications* **2005**, *26* (17), 1406-1411.
205. Souza, A. G.; Machado, M. C. N.; Helker-Carvalho, L.; Trindade, M. F. S., Kinetic Analysis of the Decomposition of Chelates of Di-alkyldithiocarbamate of Cd(II). *Journal of Thermal Analysis and Calorimetry* **2000**, *59* (3), 633-642.
206. Hursthouse, M. B.; Malik, M. A.; Motevalli, M.; O'Brien, P., Mixed Alkyl Dialkylthiocarbamates of Zinc and Cadmium: Potential Precursors for II/VI Materials. X-ray Crystal Structure of  $[\text{MeZnS}_2\text{CNET}_2]_2$ . *Organometallics* **1991**, *10* (3), 730-732.
207. Lee, J.; Sundar, V. C.; Heine, J. R.; Bawendi, M. G.; Jensen, K. F., Full Color Emission from II-VI Semiconductor Quantum Dot-Polymer Composites. *Advanced Materials* **2000**, *12* (15), 1102-1105.
208. Cao, X.; Li, C. M.; Bao, H.; Bao, Q.; Dong, H., Fabrication of Strongly Fluorescent Quantum Dot-Polymer Composite in Aqueous Solution. *Chemistry of Materials* **2007**, *19* (15), 3773-3779.
209. Sui, R.; Rizkalla, A. S.; Charpentier, P. A., Kinetics Study on the Sol-Gel Reactions in Supercritical CO<sub>2</sub> by Using In Situ ATR-FTIR Spectrometry. *Crystal Growth & Design* **2008**, *8* (8), 3024-3031.

## **Appendices**

**Appendix 1. Examination of the Linear Relationship between Absorbance and Weight of DEPDC in Heptane**

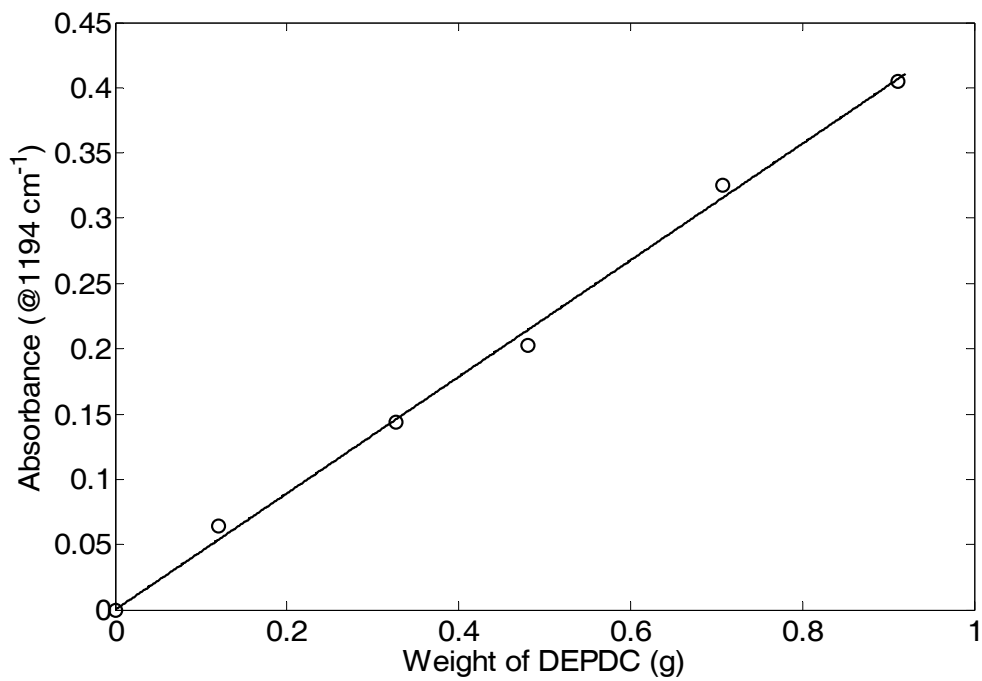


**Figure A.1** Linear curve fit of Absorbance (1194cm<sup>-1</sup>) versus Weight of DEPDC (20°C in 40mL heptane, linear correlation coefficient 0.998)

## Appendix 2. Matlab Program Used for the Calculation of $k_d$ and $E_a$ from $k_d \sim t$ Data

```

function Initiator

% Calculate Activation Energy (Ea) and Pre-exponential Factor (Ad)

% Using Arrhenius Equation "lnkd=lnAd-Ea/(RT)"

T1=40:5:60; % Assign temperature values for reactions in scCO2

T2=[40 45 50 60 70 74];% Assign temperature values for reactions in heptane

T1=T1+273.15; %Convert temperature from Celsius to Kelvin scale

T2=T2+273.15; %Convert temperature from Celsius to Kelvin scale

kd1=[8.7 20 34 70 140]*1e-6; %Assign kd values for reactions in scCO2

kd2=[7.8 29 48 180 520 740]*1e-6; %Assign kd values for reactions inHeptane

Lkd1=log(kd1); RT1=1/8.314./T1; %Calculate lnkd from kd and "1/(RT)" from T

Lkd2=log(kd2); RT2=1/8.314./T2;

AEa0=input('Enter the initial guesses of [Ad Ea]as a vector: ');

AEa0(1)=log(AEa0(1)); %Convert Ad to lnAd

[AEa1 R1 J1]=nlinfit(RT1,Lkd1,@ar,AEa0);

[AEa2 R2 J2]=nlinfit(RT2,Lkd2,@ar,AEa0);

ci1 = nlparci(AEa1,R1,J1); % Calculate 95% confidence interval

ci2 = nlparci(AEa2,R2,J2);

PLkd1=ar(AEa1, RT1) ; %Calculate predicted values of "lnkd" for reactions in scCO2

PLkd2=ar(AEa2, RT2) ; %Calculate predicted values of "lnkd" for reactions in heptane

R1=sqrt(sum((PLkd1-mean(Lkd1)).^2)/sum((Lkd1-mean(Lkd1)).^2)); % Calculate linear

correlation coefficient R for reactions in scCO2

```

```
R2=sqrt(sum((PLkd2-mean(Lkd2)).^2)/sum((Lkd2-mean(Lkd2)).^2)); % Calculate linear correlation coefficient R for reactions in heptane
```

```
disp('Determined Parameters for Decomposition in ScCO2:')
```

```
disp('Ad = '), disp(exp(AEa1(1))) % unit "1/s"
```

```
disp('Lower limit of Ad for 95% confidence interval = '), disp(exp(ci1(1,1)))
```

```
disp('Upper limit of Ad for 95% confidence interval = '), disp(exp(ci1(1,2)))
```

```
disp('Ea = '), disp(AEa1(2)*1e-3) % unit "kJ/mol"
```

```
disp('Lower limit of Ea for 95% confidence interval = '), disp(ci1(2,1)*1e-3)
```

```
disp('Upper limit of Ea for 95% confidence interval = '), disp(ci1(2,2)*1e-3)
```

```
disp(' Linear correlation coefficient R = '), disp(R1)
```

```
disp('Determined Parameters for Decomposition in Heptane:')
```

```
disp('Ad = '), disp(exp(AEa2(1))) % unit "1/s"
```

```
disp('Lower limit of Ad for 95% confidence interval = '), disp(exp(ci2(1,1)))
```

```
disp('Upper limit of Ad for 95% confidence interval = '), disp(exp(ci2(1,2)))
```

```
disp('Ea = '), disp(AEa2(2)*1e-3) % unit "kJ/mol"
```

```
disp('Lower limit of Ea for 95% confidence interval = '), disp(ci2(2,1)*1e-3)
```

```
disp('Upper limit of Ea for 95% confidence interval = '), disp(ci2(2,2)*1e-3)
```

```
disp(' Linear correlation coefficient R = '), disp(R2)
```

```
function y=ar(C,x)
```

```
y=C(1)-C(2).*x;
```

```
return
```



### Appendix 3. NMR Spectra of the Residue from Decomposition of DEPDC in ScCO<sub>2</sub>

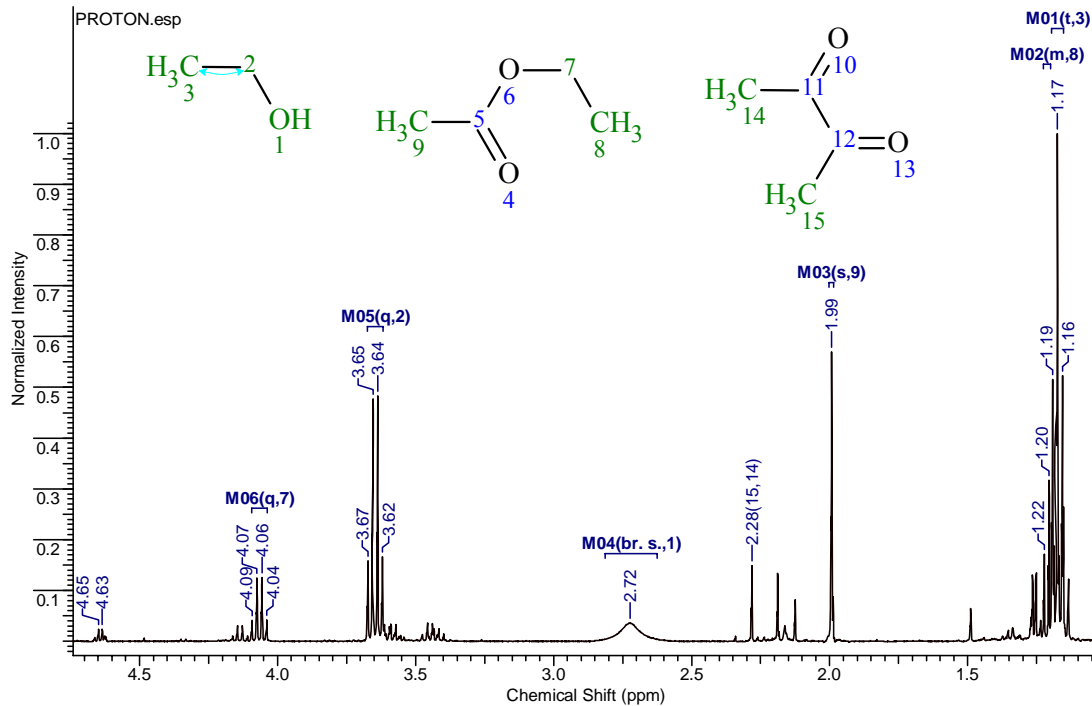


**Figure A.2** <sup>1</sup>H NMR spectrum of the residue from decomposition of DEPDC in scCO<sub>2</sub>

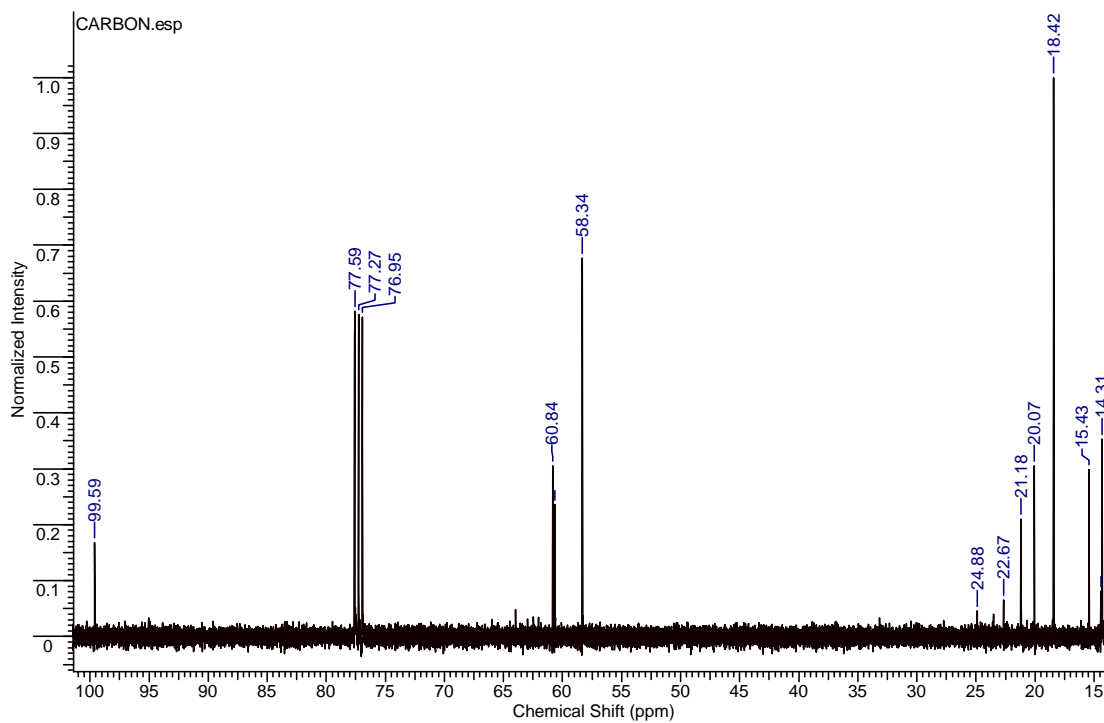


**Figure A.3** <sup>13</sup>C NMR spectrum of the residue from decomposition of DEPDC in scCO<sub>2</sub>

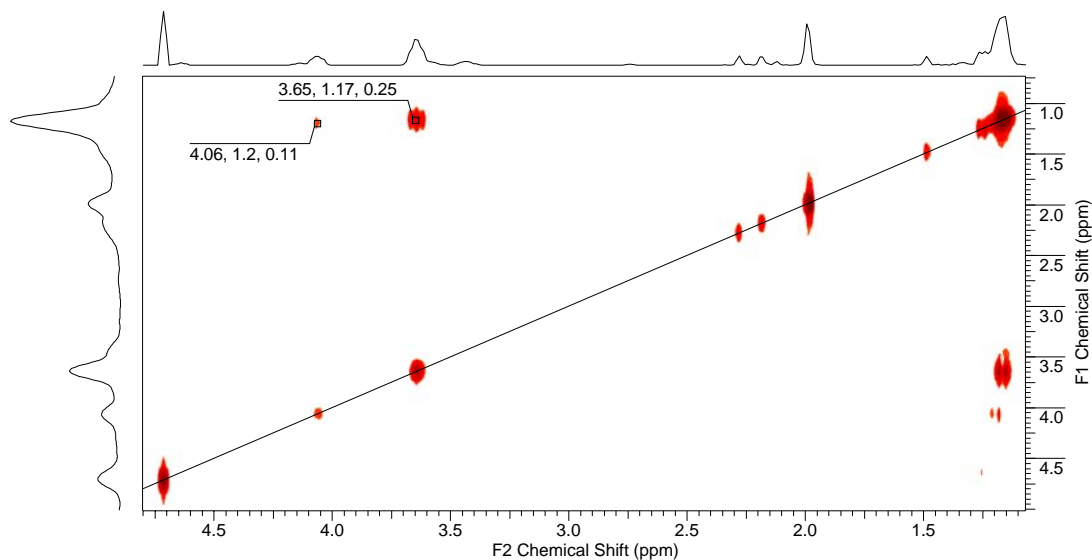


**Figure A.4** gCOSY NMR spectra of the residue from decomposition of DEPDC in  $scCO_2$

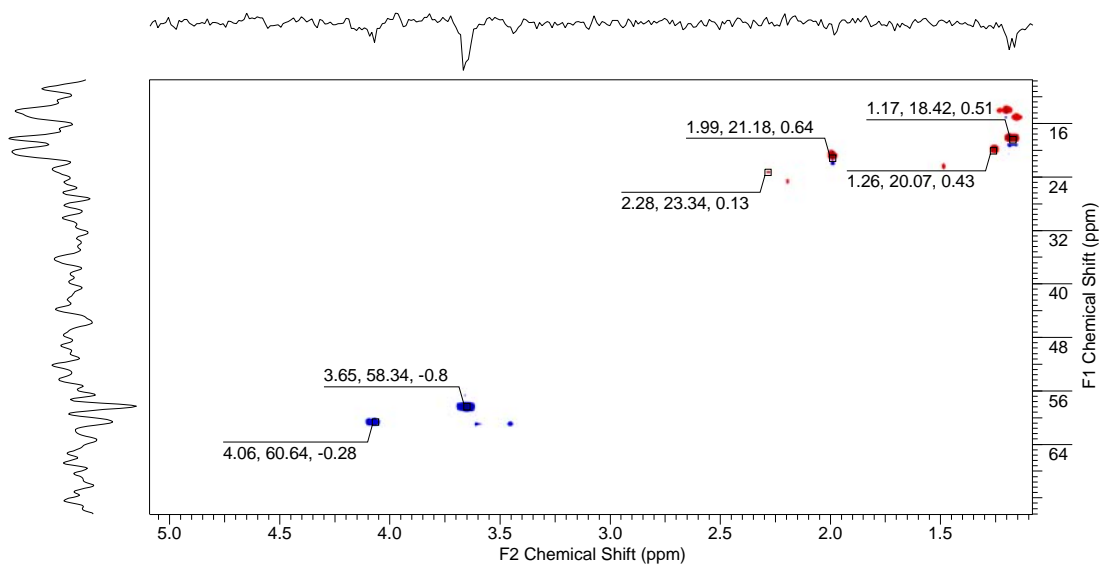


**Figure A.5** gHSQC NMR spectra of the residue from decomposition of DEPDC in  $scCO_2$

**Appendix 4. Data Used for the Calibration of Absorbance Ratio versus VAc Content  
in PEVA Copolymer**

**Table A.1** VAc contents in PEVA copolymer and the corresponding absorbance ratios

VAc wt% of PEVA from $^1\text{H}$ NMR	Abs Ratio $1737\text{cm}^{-1}/2929\text{cm}^{-1}$
5.5	0.02
12.4	0.24
16.8	0.33
18.7	0.37
27.2	0.62
34.7	0.77
41.9	1.05
57.4	1.68
69.3	2.84
86.2	7.47
91.2	10.29
98.1	22.88

## Appendix 5. Linearization Methods for Determining Monomer Reactivity Ratios of Copolymerization

Fineman and Ross<sup>122</sup> developed a linearization method by rearranging the equation (Eqn. 1-2) to

$$G = r_1 H - r_2 \quad (\text{A-1})$$

where  $G = \frac{x(y-1)}{y}$  (A-2)

$$H = \frac{x^2}{y} \quad (\text{A-3})$$

$$x = \frac{[M_1]}{[M_2]} \quad (\text{A-4})$$

$$y = \frac{d[M_1]}{d[M_2]} \quad (\text{A-5})$$

G is plotted against H to yield a straight line with slope  $r_1$  and intercept  $-r_2$ . The experimental composition data are unequally weighted by the Fineman-Ross plot, which can often be manifested as different results are obtained when different monomer is indexed as  $M_1$ .<sup>52</sup>

Kelen and Tudos<sup>123</sup> modified the linearization method by introducing an arbitrary constant  $\alpha$  to the equation so as to spread the data points more evenly.

$$\eta = \left[ r_1 + \frac{r_2}{\alpha} \right] \xi - \frac{r_2}{\alpha} \quad (\text{A-6})$$

where  $\eta = \frac{G}{\alpha + H}$  (A-7)

$$\xi = \frac{H}{\alpha + H} \tag{A-8}$$

The value  $\alpha$  is chosen as  $\alpha = \sqrt{H_m H_M}$  where  $H_m$  and  $H_M$  are the smallest and largest H values, respectively. By plotting  $\eta$  against  $\xi$ , a straight line yields  $-r_2/\alpha$  and  $r_1$  as intercepts on extrapolation to  $\xi=0$  and  $\xi=1$ , respectively.

## Appendix 6. Matlab Program Used for Determining the Monomer Reactivity Ratios of Copolymerization from $f_1 \sim F_1$ data

```
function RRPEVAc

% Calculate monomer reactivity ratios with non-linear least squares and
% the Kelen-Tudos methods from  $f_1 \sim F_1$  data

% For PEVA monomer 1: ethylene, monomer 2: vinyl acetate

f1=input('Enter ethylene mole fraction in feed, f1, [...] as a vector: ');
F1=input('Enter ethylene mole fraction in copolymer, F1, [...] as a vector: ');

% NLLS method

[r res J]=nlinfit(f1,F1,@Reactivity,[1 1]);% Calculate reactivity ratios with NLLS method
ci=nlparci(r,res,J); %Calculate 95% confidence interval

stD_NLLS=sqrt(sum((res).^2)/(length(f1)-1)); %Calculate standard deviation for NLLS
method

disp('Determined Parameters')

disp('r1 = '), disp(r(1))

disp('r2 = '), disp(r(2))

disp('95% confidence interval')

disp('r1_error = +/-'), disp(r(1)-ci(1,1))

disp('r2_error = +/-'), disp(r(2)-ci(2,1))

disp('Standard Deviation = '), disp(stD_NLLS)

%Kelen-Tudos

x=f1./(1-f1);y=F1./(1-F1);H=x.^2./y;G=x.*(y-1)./y; %Fineman-Ross rearrangement

global alpha;
```

```

alpha=sqrt(max(H)*min(H));
eta=G./(alpha+H);xi=H./(alpha+H);%Kelen-Tudos rearrangement
[rKT resKT JKT]=nlinfit(xi,eta,@KT,[1 1]); % Calculate reactivity ratios with KT
method
calres=F1-Reactivity(rKT,f1); %Calculate residual for KT method
stD_KT=sqrt(sum((calres).^2)/(length(f1)-1)); %Calculate standard deviation for KT
method
disp('Determined Parameters by Kelen-Tudos')
disp('r1 = '), disp(rKT(1))
disp('r2 = '), disp(rKT(2))
disp('Standard Deviation = '), disp(stD_KT)
%generate F1~f1 plot
f1g=[0:0.00001:1]; % Generate a vector for f1 from 0 to 1
F1c=Reactivity(r,f1g); % Calculate predicted values of F1 using NLLS
F1cKT=Reactivity(rKT,f1g); % Calculate predicted values of F1 using KT method
plot(f1, F1, 'ko',f1g, F1c,'k-',f1g,F1cKT,'k-',f1g, f1g,'k--')
xlabel('Ethylene mole fraction in feed, f_1')
ylabel('Ethylene mole fraction in copolymer, F_1')
legend('Experimental data', 'Non-linear least squares', 'Kelen-Tudos', 'Ideal
copolymerization')

function f=Reactivity(k,x);
f=(k(1)*x.^2+x.*(1-x))./(k(1)*x.^2+2*x.*(1-x)+k(2)*(1-x).^2);

```

```
return  
function f=KT(k,x)  
global alpha;  
f=(k(1)+k(2)/alpha)*x-k(2)/alpha;  
return
```



**Appendix 7. FTIR and NMR Spectra of the Single-Molecular Precursor  
Bis(diethyldithiocarbamato) Cadmium (II)**

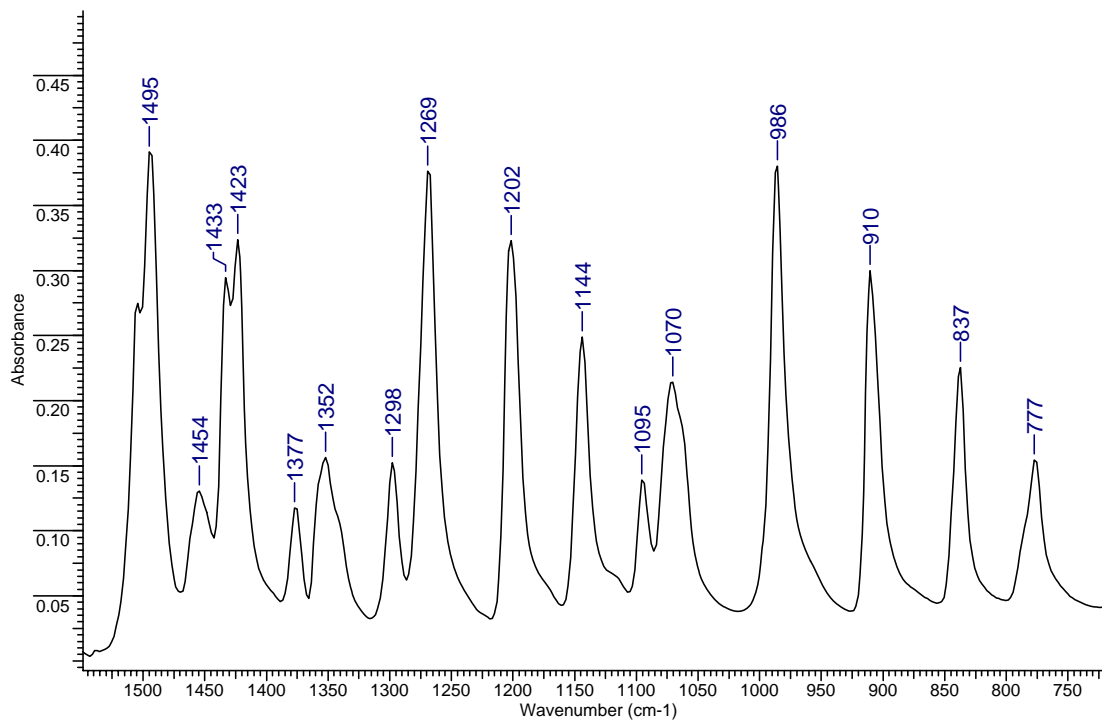


**Figure A.6** FTIR spectrum of bis(diethyldithiocarbamato) cadmium (II)

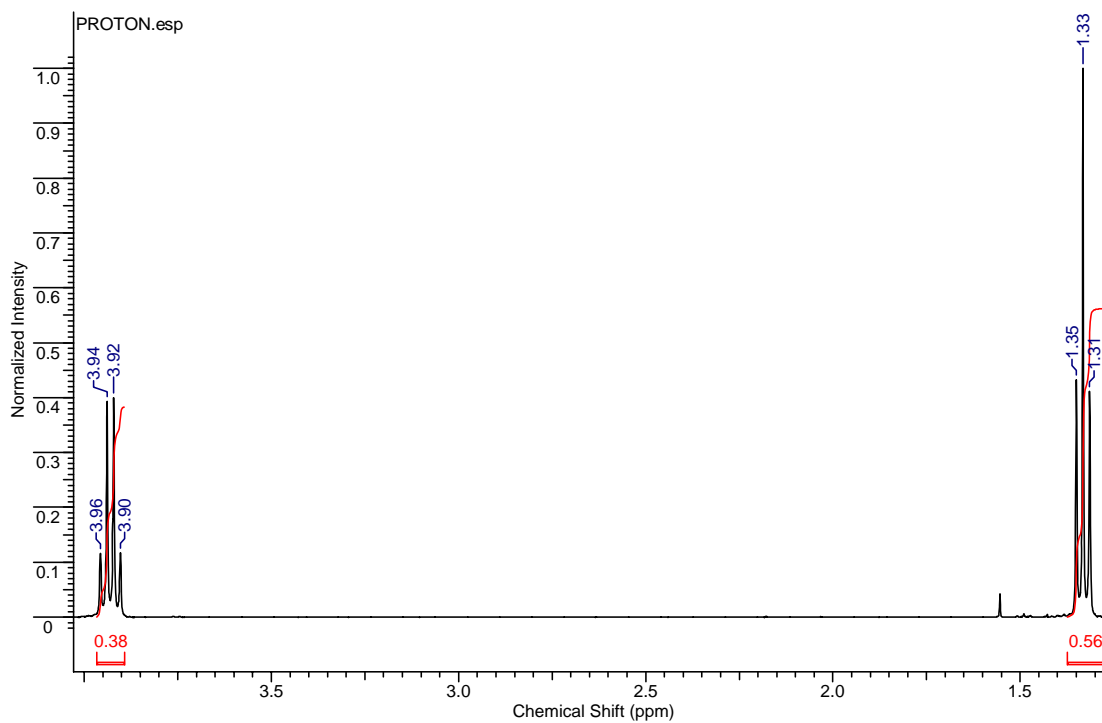


**Figure A.7**  $^1\text{H}$  NMR spectrum of bis(diethyldithiocarbamato) cadmium (II)

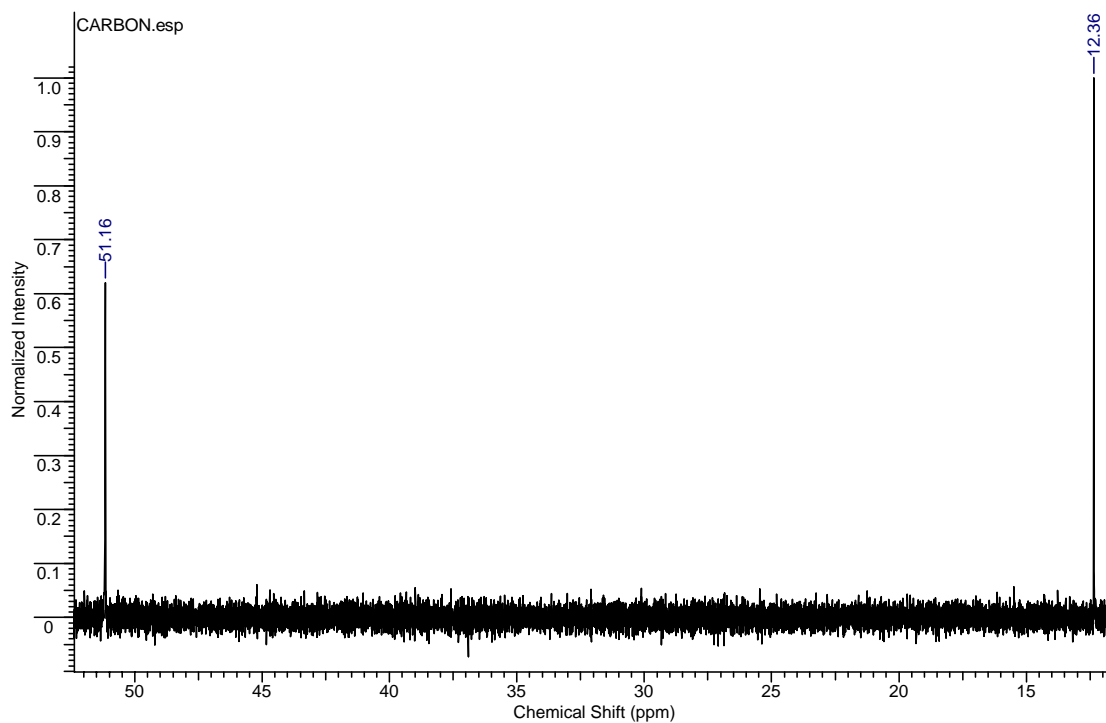


**Figure A.8**  $^{13}\text{C}$  NMR spectrum of bis(diethyldithiocarbamato) cadmium (II)

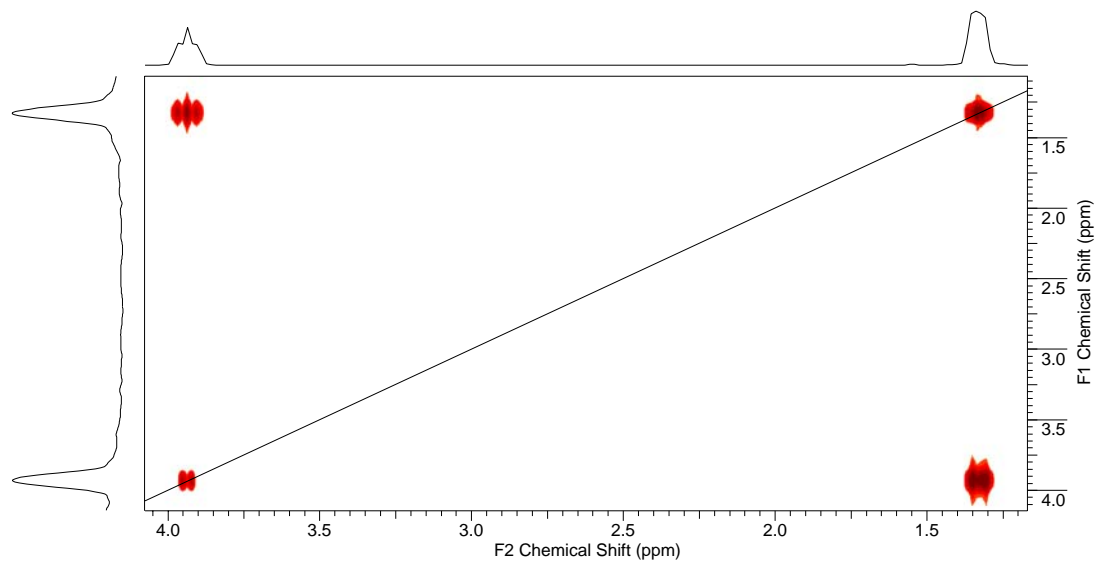


**Figure A.9** gCOSY NMR spectrum of bis(diethyldithiocarbamato) cadmium (II)

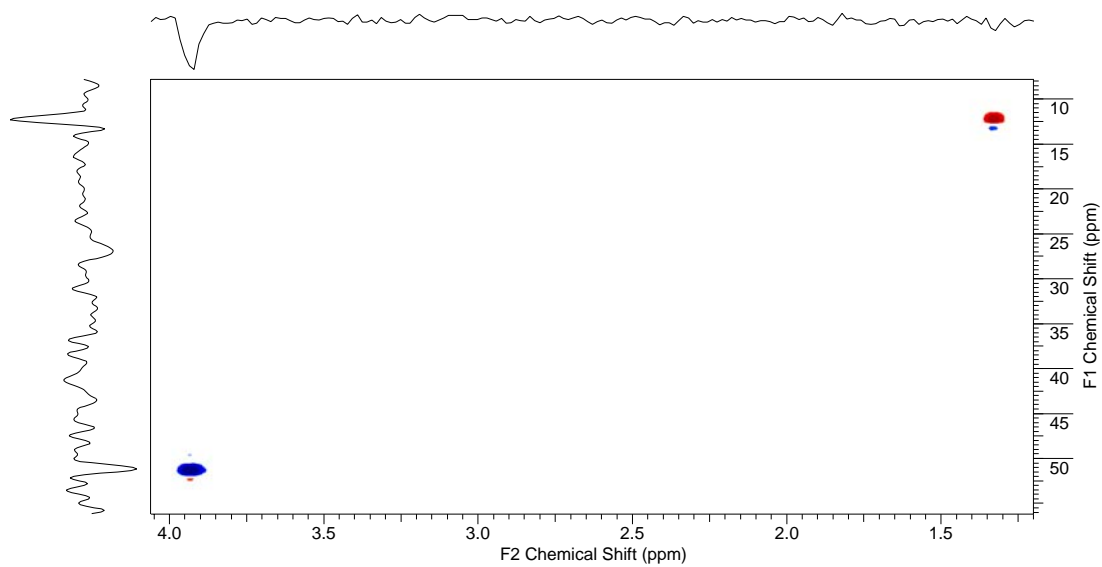


**Figure A.10** gHSQC NMR spectrum of bis(diethyldithiocarbamato) cadmium (II)

## Appendix 8. EDX Plots of the Core-Shell QDs before and after Ligand Exchange

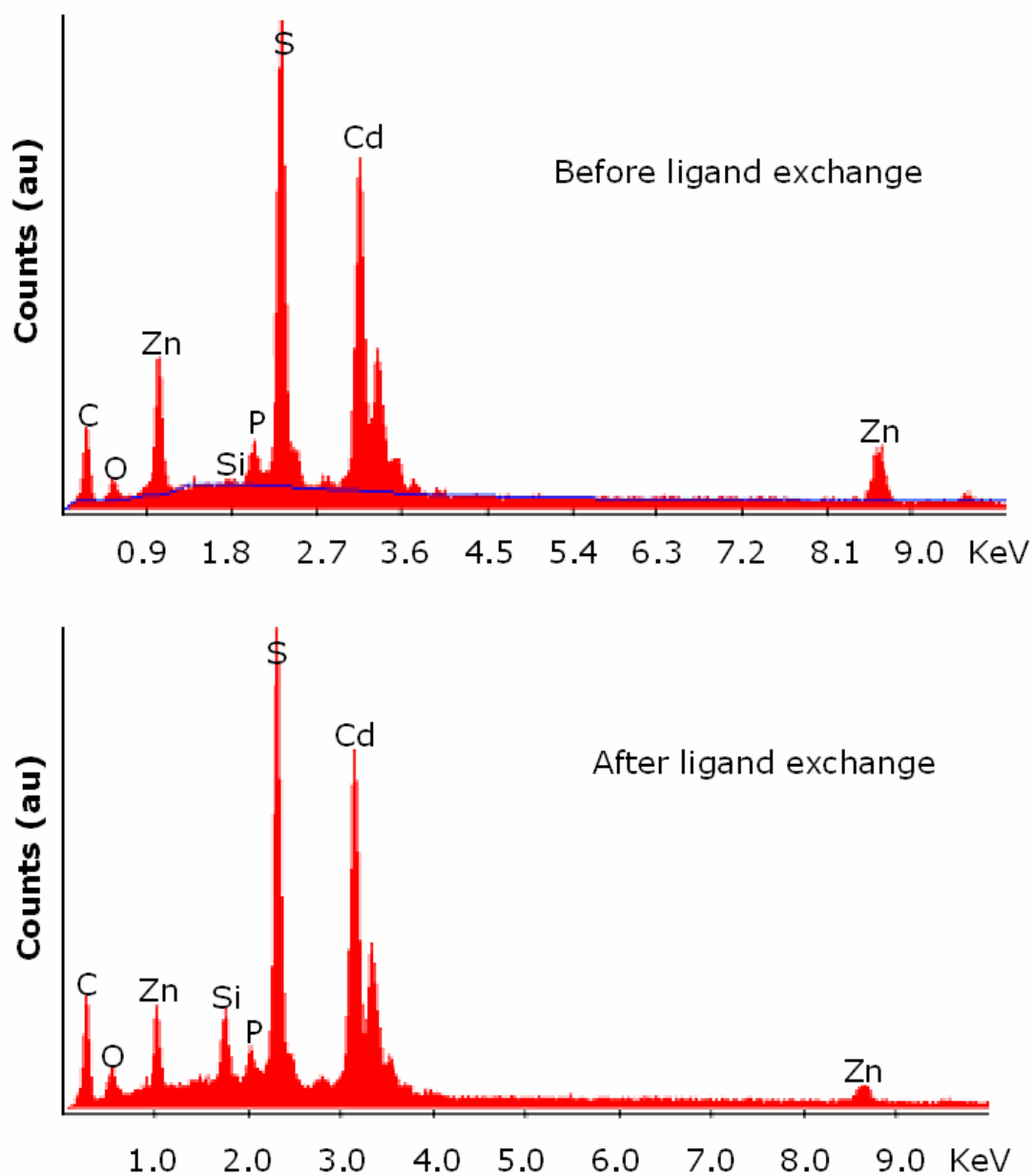


**Figure A.11** EDX plots of the CdS-ZnS core-shell QDs before and after ligand exchange

**Appendix 9. TEM and EDX Elemental Mapping Images of the Synthesized CdS-ZnS QD-PVAc Nanocomposite**

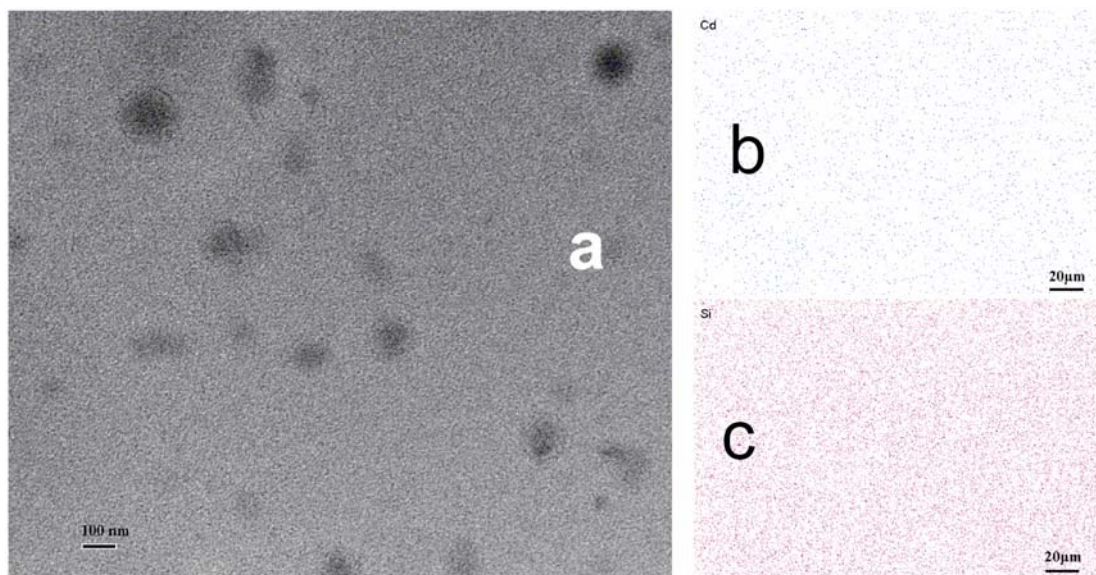


**Figure A.12** TEM image (a), EDX element Cd mapping (b), and EDX element Si mapping (c) of the synthesized CdS-ZnS QD-PVAc nanocomposite.

## Appendix 10. License Agreement with Elsevier Limited

### ELSEVIER LICENSE TERMS AND CONDITIONS

Sep 29, 2008

This is a License Agreement between William Z Xu ("You") and Elsevier ("Elsevier"). The license consists of your order details, the terms and conditions provided by Elsevier, and the payment terms and conditions.

Supplier	Elsevier Limited The Boulevard, Langford Lane Kidlington, Oxford, OX5 1GB, UK
Registered Company Number	1982084
Customer name	William Z Xu
Customer address	
License Number	2038241367385
License date	Sep 29, 2008
Licensed content publisher	Elsevier
Licensed content publication	Polymer
Licensed content title	<i>In situ</i> ATR-FT-IR study of the thermal decomposition of diethyl peroxydicarbonate in supercritical carbon dioxide
Licensed content author	William Z. Xu, Xinsheng Li and Paul A. Charpentier
Licensed content date	23 February 2007
Volume number	48
Issue number	5
Pages	10
Type of Use	Thesis / Dissertation
Portion	Full article
Format	Both print and electronic
You are an author of the Elsevier article	Yes
Are you translating?	No
Purchase order number	
Expected publication date	Nov 2008
Elsevier VAT number	GB 494 6272 12
Permissions price	0.00 USD
Value added tax 0.0%	0.00 USD
Total	0.00 USD
Terms and Conditions	

## INTRODUCTION

1. The publisher for this copyrighted material is Elsevier. By clicking "accept" in connection with completing this licensing transaction, you agree that the following terms and conditions apply to this transaction (along with the Billing and Payment terms and conditions established by Copyright Clearance Center, Inc. ("CCC"), at the time that you opened your Rightslink account and that are available at any time at <<http://myaccount.copyright.com>>).

## GENERAL TERMS

2. Elsevier hereby grants you permission to reproduce the aforementioned material subject to the terms and conditions indicated.

3. Acknowledgement: If any part of the material to be used (for example, figures) has appeared in our publication with credit or acknowledgement to another source, permission must also be sought from that source. If such permission is not obtained then that material may not be included in your publication/copies. Suitable acknowledgement to the source must be made, either as a footnote or in a reference list at the end of your publication, as follows:

“Reprinted from Publication title, Vol /edition number, Author(s), Title of article / title of chapter, Pages No., Copyright (Year), with permission from Elsevier [OR APPLICABLE SOCIETY COPYRIGHT OWNER].” Also Lancet special credit - “Reprinted from The Lancet, Vol. number, Author(s), Title of article, Pages No., Copyright (Year), with permission from Elsevier.”

4. Reproduction of this material is confined to the purpose and/or media for which permission is hereby given.

5. Altering/Modifying Material: Not Permitted. However figures and illustrations may be altered/adapted minimally to serve your work. Any other abbreviations, additions, deletions and/or any other alterations shall be made only with prior written authorization of Elsevier Ltd. (Please contact Elsevier at [permissions@elsevier.com](mailto:permissions@elsevier.com))

6. If the permission fee for the requested use of our material is waived in this instance, please be advised that your future requests for Elsevier materials may attract a fee.

7. Reservation of Rights: Publisher reserves all rights not specifically granted in the combination of (i) the license details provided by you and accepted in the course of this licensing transaction, (ii) these terms and conditions and (iii) CCC's Billing and Payment terms and conditions.

8. License Contingent Upon Payment: While you may exercise the rights licensed immediately upon issuance of the license at the end of the licensing process for the transaction, provided that you have disclosed complete and accurate details of your proposed use, no license is finally effective unless and until full payment is received from you (either by publisher or by CCC) as provided in CCC's Billing and Payment terms and conditions. If full payment is not received on a timely basis, then any license preliminarily granted shall be deemed automatically revoked and shall be void as if never granted. Further, in the event that you breach any of these terms and conditions or any of CCC's Billing and Payment terms and conditions, the license is automatically revoked and shall be void as if never granted. Use of materials as described in a revoked license, as well as any use of the

materials beyond the scope of an unrevoked license, may constitute copyright infringement and publisher reserves the right to take any and all action to protect its copyright in the materials.

9. **Warranties:** Publisher makes no representations or warranties with respect to the licensed material.

10. **Indemnity:** You hereby indemnify and agree to hold harmless publisher and CCC, and their respective officers, directors, employees and agents, from and against any and all claims arising out of your use of the licensed material other than as specifically authorized pursuant to this license.

11. **No Transfer of License:** This license is personal to you and may not be sublicensed, assigned, or transferred by you to any other person without publisher's written permission.

12. **No Amendment Except in Writing:** This license may not be amended except in a writing signed by both parties (or, in the case of publisher, by CCC on publisher's behalf).

13. **Objection to Contrary Terms:** Publisher hereby objects to any terms contained in any purchase order, acknowledgment, check endorsement or other writing prepared by you, which terms are inconsistent with these terms and conditions or CCC's Billing and Payment terms and conditions. These terms and conditions, together with CCC's Billing and Payment terms and conditions (which are incorporated herein), comprise the entire agreement between you and publisher (and CCC) concerning this licensing transaction. In the event of any conflict between your obligations established by these terms and conditions and those established by CCC's Billing and Payment terms and conditions, these terms and conditions shall control.

14. **Revocation:** Elsevier or Copyright Clearance Center may deny the permissions described in this License at their sole discretion, for any reason or no reason, with a full refund payable to you. Notice of such denial will be made using the contact information provided by you. Failure to receive such notice will not alter or invalidate the denial. In no event will Elsevier or Copyright Clearance Center be responsible or liable for any costs, expenses or damage incurred by you as a result of a denial of your permission request, other than a refund of the amount(s) paid by you to Elsevier and/or Copyright Clearance Center for denied permissions.

#### LIMITED LICENSE

The following terms and conditions apply to specific license types:

15. **Translation:** This permission is granted for non-exclusive world **English** rights only unless your license was granted for translation rights. If you licensed translation rights you may only translate this content into the languages you requested. A professional translator must perform all translations and reproduce the content word for word preserving the integrity of the article. If this license is to re-use 1 or 2 figures then permission is granted for non-exclusive world rights in all languages.

16. **Website:** The following terms and conditions apply to electronic reserve and author websites:

**Electronic reserve:** If licensed material is to be posted to website, the web site is to be password-protected and made available only to bona fide students registered on a relevant course if:



This license was made in connection with a course,  
This permission is granted for 1 year only. You may obtain a license for future website posting.

All content posted to the web site must maintain the copyright information line on the bottom of each image,

A hyper-text must be included to the Homepage of the journal from which you are licensing at <http://www.sciencedirect.com/science/journal/xxxxx> or the Elsevier homepage for books at <http://www.elsevier.com> , and

Central Storage: This license does not include permission for a scanned version of the material to be stored in a central repository such as that provided by Heron/XanEdu.

**17. Author website** for journals with the following additional clauses:

This permission is granted for 1 year only. You may obtain a license for future website posting.

All content posted to the web site must maintain the copyright information line on the bottom of each image, and

The permission granted is limited to the personal version of your paper. You are not allowed to download and post the published electronic version of your article (whether PDF or HTML, proof or final version), nor may you scan the printed edition to create an electronic version,

A hyper-text must be included to the Homepage of the journal from which you are licensing at <http://www.sciencedirect.com/science/journal/xxxxx> , or the Elsevier homepage for books at <http://www.elsevier.com> and

Central Storage: This license does not include permission for a scanned version of the material to be stored in a central repository such as that provided by Heron/XanEdu.

**18. Author website** for books with the following additional clauses:

Authors are permitted to place a brief summary of their work online only.

A hyper-text must be included to the Elsevier homepage at <http://www.elsevier.com>

This permission is granted for 1 year only. You may obtain a license for future website posting.

All content posted to the web site must maintain the copyright information line on the bottom of each image, and

The permission granted is limited to the personal version of your paper. You are not allowed to download and post the published electronic version of your article (whether PDF or HTML, proof or final version), nor may you scan the printed edition to create an electronic version,

A hyper-text must be included to the Homepage of the journal from which you are licensing at <http://www.sciencedirect.com/science/journal/xxxxx> , or the Elsevier homepage for books at <http://www.elsevier.com> and

Central Storage: This license does not include permission for a scanned version of the material to be stored in a central repository such as that provided by Heron/XanEdu.

**19. Website** (regular and for author): “A hyper-text must be included to the Homepage of the journal from which you are licensing at <http://www.sciencedirect.com/science/journal/xxxxx> .”

**20. Thesis/Dissertation:** If your license is for use in a thesis/dissertation your thesis may be submitted to your institution in either print or electronic form. Should your thesis be published commercially, please reapply for permission. These requirements include permission for the Library and Archives of Canada to supply single copies, on demand, of the complete thesis and include permission for UMI to supply single copies, on demand, of

the complete thesis. Should your thesis be published commercially, please reapply for permission.

v1.2

**21. Other conditions:**

None

---

---

## Appendix 11. Copyright Permission from the Royal Society of Chemistry

RE: Permission Request Form: William Z. Xu

From: **CONTRACTS-COPYRIGHT (shared)** (Contracts-Copyright@rsc.org)

Sent: September 30, 2008 4:13:41 AM

To:

Dear William Z Xu

The Royal Society of Chemistry (RSC) hereby grants permission for the use of your paper(s) specified below in the printed and microfilm version of your thesis. You may also make available the PDF version of your paper(s) that the RSC sent to the corresponding author(s) of your paper(s) upon publication of the paper(s) in the following ways: in your thesis via any website that your university may have for the deposition of theses, via your university's Intranet or via your own personal website. We are however unable to grant you permission to include the PDF version of the paper(s) on its own in your institutional repository. The Royal Society of Chemistry is a signatory to the STM Guidelines on Permissions (available on request).

Please note that if the material specified below or any part of it appears with credit or acknowledgement to a third party then you must also secure permission from that third party before reproducing that material.

Please ensure that the published article states the following:

*Reproduced by permission of The Royal Society of Chemistry*

and a link is included to the article on the Royal Society of Chemistry's website.

Regards

Gill Cockhead

Contracts & Copyright Executive

Gill Cockhead (Mrs), Contracts & Copyright Executive

Royal Society of Chemistry, Thomas Graham House

Science Park, Milton Road, Cambridge CB4 0WF, UK

Tel +44 (0) 1223 432134, Fax +44 (0) 1223 423623

<http://www.rsc.org>

-----Original Message-----

From:

Sent: 29 September 2008 16:01  
To: CONTRACTS-COPYRIGHT (shared)  
Subject: Permission Request Form: William Z. Xu

Name : William Z. Xu

Address :

Tel :

Fax :

Email :

I am preparing the following work for publication:

Article/Chapter Title : A novel approach to the synthesis of SiO<sub>2</sub>-PVAc nanocomposites using a one-pot synthesis in supercritical CO<sub>2</sub>

Journal/Book Title : Synthesis of light-selective poly(ethylene-co-vinyl acetate) nanofilms in supercritical carbon dioxide

Editor/Author(s) : William Z. Xu

Publisher : Library and Archives Canada

I would very much appreciate your permission to use the following material:

Journal/Book Title : Green Chemistry

Editor/Author(s) : Paul A. Charpentier, William Z. Xu, Xinsheng Li

Volume Number : 9

Year of Publication : 2007

Description of Material : A paper regarding the synthesis of SiO<sub>2</sub>-PVAc nanocomposites

Page(s) : 768-776

Any Additional Comments :

Type of use: Thesis/Dissertation

**DISCLAIMER:**

This communication (including any attachments) is intended for the use of the addressee only and may contain confidential, privileged or copyright material. It may not be relied upon or disclosed to any other person without the consent of the RSC. If you have received it in error, please contact us immediately. Any advice given by the RSC has been carefully formulated but is necessarily based on the information available, and the RSC cannot be held responsible for accuracy or completeness. In this respect, the RSC owes no duty of care and shall not be liable for any resulting damage or loss. The RSC acknowledges that a disclaimer cannot restrict liability at law for personal injury or death arising through a finding of negligence. The RSC does not warrant that its emails or attachments are Virus-free: Please rely on your own screening.

## Appendix 12. Copyright Permission from American Chemical Society

### American Chemical Society's Policy on Theses and Dissertations

If your university requires a signed copy of this letter see contact information below.

Thank you for your request for permission to include **your** paper(s) or portions of text from **your** paper(s) in your thesis. Permission is now automatically granted; please pay special attention to the implications paragraph below. The Copyright Subcommittee of the Joint Board/Council Committees on Publications approved the following:

#### Copyright permission for published and submitted material from theses and dissertations

ACS extends blanket permission to students to include in their theses and dissertations their own articles, or portions thereof, that have been published in ACS journals or submitted to ACS journals for publication, provided that the ACS copyright credit line is noted on the appropriate page(s).

#### Publishing implications of electronic publication of theses and dissertation material

Students and their mentors should be aware that posting of theses and dissertation material on the Web prior to submission of material from that thesis or dissertation to an ACS journal may affect publication in that journal. Whether Web posting is considered prior publication may be evaluated on a case-by-case basis by the journal's editor. If an ACS journal editor considers Web posting to be "prior publication", the paper will not be accepted for publication in that journal. If you intend to submit your unpublished paper to ACS for publication, check with the appropriate editor prior to posting your manuscript electronically.

If your paper has not yet been published by ACS, we have no objection to your including the text or portions of the text in your thesis/dissertation in **print and microfilm formats**; please note, however, that electronic distribution or Web posting of the unpublished paper as part of your thesis in electronic formats might jeopardize publication of your paper by ACS. Please print the following credit line on the first page of your article: "Reproduced (or 'Reproduced in part') with permission from [JOURNAL NAME], in press (or 'submitted for publication'). Unpublished work copyright [CURRENT YEAR] American Chemical Society." Include appropriate information.

If your paper has already been published by ACS and you want to include the text or portions of the text in your thesis/dissertation in **print or microfilm formats**, please print the ACS copyright credit line on the first page of your article: "Reproduced (or 'Reproduced in part') with permission from [FULL REFERENCE CITATION.] Copyright [YEAR] American Chemical Society." Include appropriate information.

**Submission to a Dissertation Distributor:** If you plan to submit your thesis to UMI or to another dissertation distributor, you should not include the unpublished ACS paper in your thesis if the thesis will be disseminated electronically, until ACS has published your paper. After publication of the paper by ACS, you may release the entire thesis (**not the individual ACS article by itself**) for electronic dissemination through the distributor; ACS's copyright credit line should be printed on the first page of the ACS paper.

**Use on an Intranet:** The inclusion of your ACS unpublished or published manuscript is permitted in your thesis in print and microfilm formats. If ACS has published your paper you may include the manuscript in your thesis on an intranet that is not publicly available. Your ACS article cannot be posted electronically on a publicly available medium (i.e. one that is not password protected), such as but not limited to, electronic archives, Internet, library server, etc. The only material from your paper that can be posted on a public electronic medium is the article abstract, figures, and tables, and you may link to the article's DOI or post the article's author-directed URL link provided by ACS. This paragraph does not pertain to the dissertation distributor paragraph above.

Questions? Call +1 202/872-4368/4367. Send e-mail to [copyright@acs.org](mailto:copyright@acs.org) or fax to +1 202-776-8112. 10/10/03, 01/15/04, 06/07/06

## Curriculum Vitae

**Name:** William (Zhiming) Xu

**Post-secondary Education and Degrees:** Nanjing University of Technology  
Nanjing, Jiangsu, China  
1984-1988 B.Eng.

The University of Western Ontario  
London, Ontario, Canada  
2004-2008 Ph.D.

**Honours and Awards:** Nanjing University of Technology  
Outstanding Graduate Scholarship  
1988

American Chemical Society  
Green Chemistry Summer School Scholarship  
2006

American Chemical Society  
Green Chemistry and Engineering Conference  
International Student Scholarship  
2006

Ontario Centers of Excellence (OCE)  
Professional Outreach Award  
2008

Ontario Graduate Scholarship in Science and Technology (OGSST)  
2007-2008, 2008-2009

**Related Work Experience:** Senior Chemical Engineer  
Yuejing Motor (Group) Corporation  
Nanjing, Jiangsu, China  
1988-2002

Production Supervisor  
ARC Glassware (Nanjing) Co., Ltd.  
Nanjing, Jiangsu, China  
2003-2004

Research Assistant  
The University of Western Ontario  
London, Ontario, Canada  
2004-2008

Teaching Assistant  
The University of Western Ontario  
London, Ontario, Canada  
2005-2008

**Publications:**

- (1). **Xu, William Z.**, Li, Xinsheng, and Charpentier, Paul A. (2007). *In situ* ATR-FT-IR study of the thermal decomposition of diethyl peroxydicarbonate in supercritical carbon dioxide. *Polymer*, 48(5), 1219-1228
- (2). Charpentier, Paul A., **Xu, William Z.**, and Li, Xinsheng. (2007). A novel approach to the synthesis of SiO<sub>2</sub>-PVAc nanocomposites using a one-pot synthesis in supercritical CO<sub>2</sub>. *Green Chemistry*, 9(7), 768-776
- (3). **Xu, William Z.** and Charpentier, Paul A. A one-pot route toward light selective quantum dot - polymer nanofilms in scCO<sub>2</sub>. (2008). Abstracts of Papers, 235<sup>th</sup> ACS National Meeting, New Orleans, LA, United States, Apr. 6-10, 2008
- (4). **Xu, William Z.** and Charpentier, Paul A. FTIR study on measuring the monomer reactivity ratios for ethylene-vinyl acetate polymerization in supercritical CO<sub>2</sub>. *Industrial & Engineering Chemistry Research*. Accepted
- (5). **Xu, William Z.** and Charpentier, Paul A. Light-selective nanofilms of quantum dot-poly(ethylene-co-vinyl acetate) synthesized using supercritical CO<sub>2</sub>. *Journal of Physical Chemistry*. Submitted
- (6). **Xu, William Z.** and Charpentier, Paul A. Novel quantum dot-poly(ethylene-co-vinyl acetate) as light-selective nanofilms. Abstracts of Papers, 237<sup>th</sup> ACS National Meeting, Salt Lake City, UT, United States, March 22-26, 2009. Accepted